Probable Maximum Precipitation Study for Maryland
Final Report

Prepared for:

Maryland Department of the Environment under Subcontract to Michael Baker International, Project Number 197361

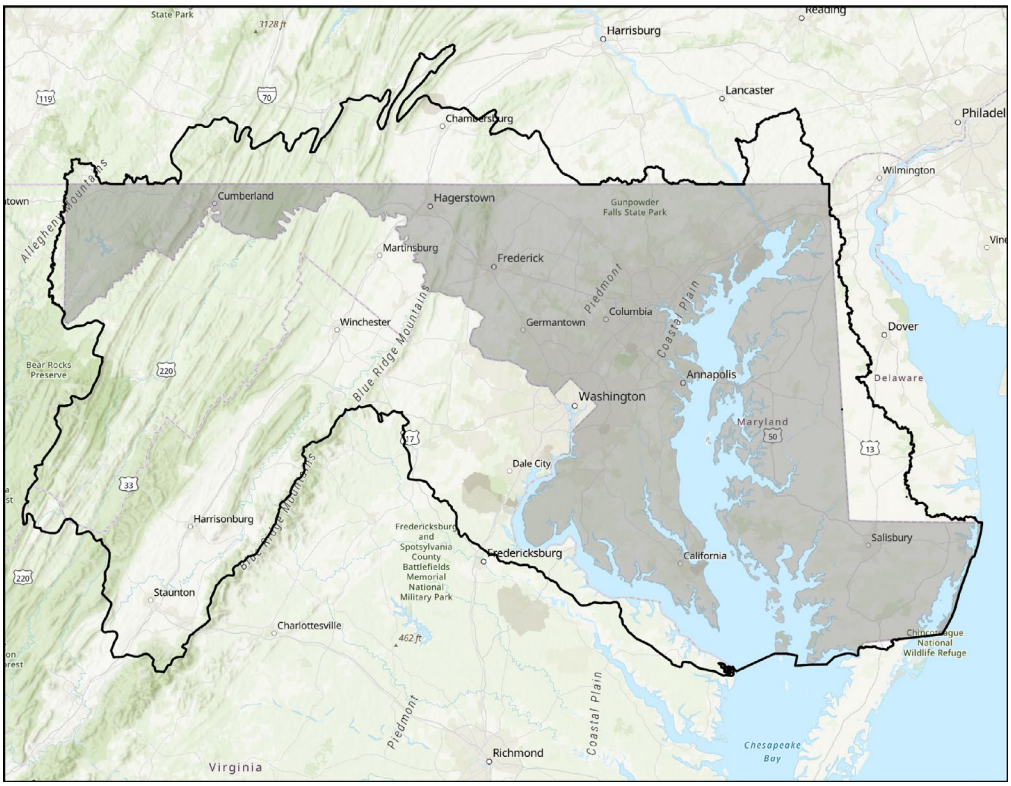

Prepared by:

Applied Weather Associates, LLC
PO Box 175, Monument, CO 80132
(719) 488-4311
www.appliedweatherassociates.com

January 2025

NOTICE

This report was prepared by Applied Weather Associates (AWA). The results and conclusions in this report are based upon best professional judgment using currently available data. Therefore, neither AWA nor any person acting on behalf of AWA can: (a) make any warranty, expressed or implied, regarding future use of any information or method in this report, or (b) assume any future liability regarding use of any information or method contained in this report.

DISCLAIMER

This report is an instrument of service of Applied Weather Associates, LLC (AWA). The report has been prepared for the exclusive use of the Maryland Department of the Environment's (MDE) Stormwater, Dam Safety, and Flood Management Program (Client) for the specific application to provide Probable Maximum Precipitation (PMP) depths and associated meteorological data for any location within the overall PMP domain evaluated in this study, and it may not be relied upon for other purposes by any other party without AWA's or the Client's written consent.

AWA has prepared this report in a manner consistent with the level of care, skill, and diligence ordinarily provided by members of the same profession for projects of similar scope at the time and place the services were rendered. AWA makes no warranty, express or implied.

Use of or reliance upon this instrument of service by the Client is subject to the following conditions:

1. The report is to be read in full, with sections or parts of the report relied upon in the context of the whole report.
2. The Executive Summary is a selection of key elements of the report. It does not include details needed for proper application of the findings and recommendation in the report.
3. The report is based on information provided to AWA by the Client or by other parties on behalf of the Client. AWA has not verified the correctness or accuracy of such information and makes no representations regarding its correctness or accuracy. AWA shall not be responsible to the Client for the consequences of any error or omission contained in Client-supplied information.
4. AWA or the Client should be consulted regarding the interpretation or application of the findings and recommendations in the report.

Bill Kappel, President/Chief Meteorologist, Applied Weather Associates

Credits and Acknowledgements

Applied Weather Associates would like to express sincere appreciation and thanks for the hard work and dedication of all involved in the study, including the members of the Maryland Department of the Environment's Stormwater, Dam Safety, and Flood Management Program Maryland Environmental Service, Michael Baker International, and the entire staff of Applied Weather Associates. We would also like to acknowledge with much appreciation the review and feedback of the study's Review Board and other study observers and participants all of whom provided valuable suggestions, review, and testing of the PMP outputs.

A study of this magnitude and complexity would not have been possible without the involvement and contribution of all involved.

The following staff of Applied Weather Associates participated in this PMP development:

Bill Kappel	Project Manager/Chief Meteorologist
Doug Hultstrand, PhD	Senior Hydrometeorologist
Jake Rodel	GIS Analyst
Geoff Muhlestein	Senior GIS Analyst
Kristi Steinhilber	Staff Meteorologist
Marty Venticinque	Staff Meteorologist
Dan Cheke	Staff Meteorologist
Nicholas Agnoli, P.E.	Senior Risk Analyst

We gratefully acknowledge the assistance of the following individuals for providing project review and information:

Scott Bass	Maryland Dam Safety
John Roche	Maryland Dam Safety
Raymond Bahr	Maryland Dam Safety
Roxanne Sanderson	Maryland Dam Safety
Charles Wallis	Maryland Dam Safety
Christina Lyerly	MDE's Watershed Protection, Restoration, and Planning Program
Michael Manen	Maryland Environmental Service
Victor Siaurusaitis	Michael Baker International
Jeff Blass	AECOM
Jeff Powers	Hazen and Sawyer
Ann Houseman	Hazen and Sawyer
Kate Naughton	Hazen and Sawyer
Arthur DeGaetano	Review Committee
Alfredo Ruiz-Barradas	Review Committee

Table of Contents

Table of Figures

Table of Tables

Appendices

Executive Summary

This study produced gridded PMP values for the project domain covering then entire state of Maryland and immediate surrounding regions which the Maryland Dam Safety Program is responsible for regulating. The PMP grid domain uses a spatial resolution of approximately 2.3-square miles. This spatial resolution captures variations in topography, climate and storm types across the state. A large set of storm data was analyzed for use in developing the PMP depths with numerous storm events evaluated for every region within the overall study domain. In addition to the PMP development, annual exceedance probabilities for the 6- and 24-hour durations were developed over the entire domain and included in the GIS tool. This information provides the recurrence interval of the PMP depths and inputs for risk informed decision making analyses. Finally, climate change projections were evaluated specifically to understand how extreme precipitation may change over the study domain both in magnitude and frequency. The climate change projections demonstrated that the most likely outcome regarding precipitation over the region going forward is that the mean annual and seasonal amount will increase, but the individual extreme events will stay within the range of uncertainty included in the PMP process.

During the course of this study, the National Academy of Science released its recommendations regarding PMP development[1]. These findings recommend the use of probabilistic evaluations in addition to the deterministic storm-based approach. They also recommend accounting for climate change. Then, is the long term (10 years or longer), they recommend the use of numerical weather prediction models as another option for PMP development. Important for this study, AWA already applied these recommendations. As noted, this study develops deterministic PMP depths, then calculates probabilities out to 10^{-10}, which provides the average recurrence interval of the PMP depths and evaluated climate change projections related to PMP and extreme rainfall.

Storm types considered were the local storm, general storm, and tropical storm. These updated PMP depths supersede those provided in Hydrometeorological Reports (HMRs) 33, 51, and 52. PMP type storms are most likely to occur from May through October throughout Maryland when no significant contribution from melting snow would occur. However, heavy rainfall can occur anytime of the year, including when snowpack is on the ground. This is most likely in the central and western portions of Maryland. However, the total runoff from a combined rainfall and snowmelt event is still less than the all-season PMP depths for any of the basins which the the Maryland Dam Safety Program regulates.

Results of this analysis reflect the most current practices used for defining PMP, including comprehensive storm analyses procedures, extensive use of geographical information systems (GIS), explicit quantification of topography and coastal effects, updated maximum dew point and sea surface temperature climatologies for storm adjustments, and improved understanding of the weather and climate related to extreme rainfall throughout the region.

The approach used in this study followed the same philosophy used in the numerous site-specific, statewide, and regional PMP studies that AWA has completed, including regions adjacent to the state and regions encompassing portions of this domain. AWA utilized the storm-based approach

[1] https://www.nationalacademies.org/our-work/modernizing-probable-maximum-precipitation-estimation

which follows the same general procedures used by the National Weather Service (NWS) in the development of the HMRs and the World Meteorological Organization (WMO) Manual on Estimation of PMP (2009). The storm-based approach identified extreme rainfall events that have occurred in regions considered transpositionable to any location within the overall study domain. These are storms that had meteorological and topographical characteristics similar to extreme rainfall storms that could occur over any location within the project domain and were deemed to be PMP-type storm events. Detailed discussions of the storms considered took place with Maryland Dam Safety Program personnel, the review board, and other study participants. This resulted in the list of storms used for PMP development. Each of these storms was analyzed in detail to produce the required outputs for PMP development.

All data, PMP assumptions, and PMP development methods used in this study have been extensively reviewed and accepted as part of PMP studies in the region and again as part of this study. Maryland Dam Safety Program personnel provided significant input and review to ensure data and outputs were specifically relevant to their dam safety requirements. Finally, Maryland Environmental Service, AECOM, and Hazen and Sawyer provided additional feedback as well as detailed testing and hydrologic analyses of the outputs and recommendations.

Although this study produced deterministic PMP depths, it must be recognized that there is some subjectivity associated with the PMP development procedures. Examples of decisions where scientific judgment was involved include determining which storms are used for PMP, determination of storm adjustment factors, and storm transposition limits. For areas where uncertainties in data were recognized, conservative assumptions were applied unless sufficient data existed to make a more informed decision. All data and information supporting decisions in the PMP development process have been documented so that results can be reproduced and verified.

A total of 77 individual storm centers were included for PMP development. This includes 31 tropical storm rainfall centers, 17 general storm rainfall centers, and 26 local storm rainfall centers. Finally, three storm centers exhibited characteristics of more than one storm type, with one utilized for PMP development as both a local and general storm and two utilized for PMP development as both a general and tropical storm.

Each storm center used for PMP development was analyzed using AWA's Storm Precipitation Analysis System (SPAS), which produced several standard products including hourly gridded rainfall depths, depth-area-duration values, storm center mass curves, and total storm isohyetal patterns. Radar outputs from the NWS Next Generation Weather Radar (NEXRAD) were used in storm analyses when available (generally for storms which occurred after the mid-1990's). This added significant detail regarding spatial patterns and temporal accumulation of rainfall.

Standard PMP methods were applied for in-place maximization adjustments (e.g., HMR 51 Section 2.3) in combination with improved techniques and updated datasets to increase accuracy and reliability of the storm adjustments, while adhering to the basic approach used in the HMRs. Updated precipitation frequency analyses data available from the National Oceanic and Atmospheric Administration (NOAA) Atlas 14 were used for this study. These were used to calculate the Geographic Transposition Factors (GTFs) for each storm and were important for

spatial distribution of PMP depths. The GTF procedure provided explicit evaluations of the effects of terrain on rainfall and differences in precipitation process throughout the region and between each storm location and the regions where each storm was utilized. This procedure, through its correlation process, provided quantifiable and reproducible analyses of the differences in precipitation processes between each location including the effects of terrain and coastal convergence processes on rainfall. Results of these factors (in-place maximization and geographic transposition) were applied for each storm at each grid point for each of the area sizes and durations used in this study to define the PMP depths for this study.

Maximization factors were computed for each of the analyzed storm events using updated dew point and sea surface temperature (SST) climatologies representing the maximum moisture equivalent to the 100-year recurrence interval for dew points or +2 sigma for SST that could have been associated with each rainfall event. Note, most of the storms used in this study have been applied in previous PMP studies and therefore the maximization factors have been derived previously. However, these were re-checked and updated dew point and SST climatologies were applied. The maximum process utilizes the average 6-, 12-, and 24-hour 100-year return frequency dew point values and the SST climatology utilizes the +2 sigma values. The most appropriate duration consistent with the duration of the storm rainfall was used for maximization, thereby evaluating storm events by storm type. Hybrid Single Particle Lagrangian Integrated Trajectory (HYSPLIT) model output, which represents model reanalysis fields of air flow in the atmosphere, and NWS synoptic weather maps were used as guidance in identifying the storm representative moisture source regions for each of the storms.

To store, analyze, and produce results from the large datasets developed in the study, the PMP calculation information was stored and analyzed in individual Excel spreadsheets and a GIS database. This combination of Excel and GIS was used to query, calculate, and derive PMP depths for each grid point for each duration for each storm type. The database allowed PMP to be calculated at any area size and/or duration available in the underlying SPAS data from a point location anywhere within the region to the overall region domain.

When compared to previous PMP depths provided in HMR 51 the updated values from this study resulted in a wide range of reductions at most area sizes and durations, with some regions resulting in minor increases. PMP depths are highest near the coast and along the initial ridges of the Appalachians. These regions have exhibited past extreme rainfall accumulations that are the result of both moisture availability, coastal convergence, and topographic enhancement. Minimum values are seen in areas inland but before reaching significant topography.

The contributing watersheds to the majority of dams in Maryland are relatively small in area size, with about 80% of the dams having contributing drainage areas less than 10-square miles. Therefore, a significant amount of emphasis was placed on developing PMP and temporal patterns most relevant for smaller area sizes and quick response basins. This included extensive analysis of short duration, high intensity rainfall accumulation patterns and development of PMP depths for area sizes and durations that are important for these types of basins. Providing PMP depths down to area sizes at 1/3rd-square miles and temporal accumulation patterns at 5-minute increments was a significant improvement for dam safety evaluations in Maryland over what was previously available in the HMRs.

Comparing the PMP depths against HMR 51 PMP across the entire domain, a 13% reduction at 6-hour 10-square miles and a 24% reduction at 24-hour 10-square miles was noted. In general, the largest reductions occurred over the western portions of the study domain, with smaller reductions and slight increases in the eastern regions. For the longer durations, larger area sizes, statewide reductions were 28% at 24-hours, 26% at 72-hours for 200-square miles, 30% at 24-hour, and 16% at 72-hours for 1,000-square miles. Figures E.1-E.4 provide the average percent difference (negative is a reduction) from HMR 51 across the study region for 6-hour 10-square miles, 24-hour 10-square miles, 24-hour 200-square miles, and 72-hours 200-square miles. Tables E.1 and E.2 provide the transposition zone average difference from HMR 51 for 6-hours and 24-hours at 10-square miles and 24-hours and 72-hours at 200 square miles.

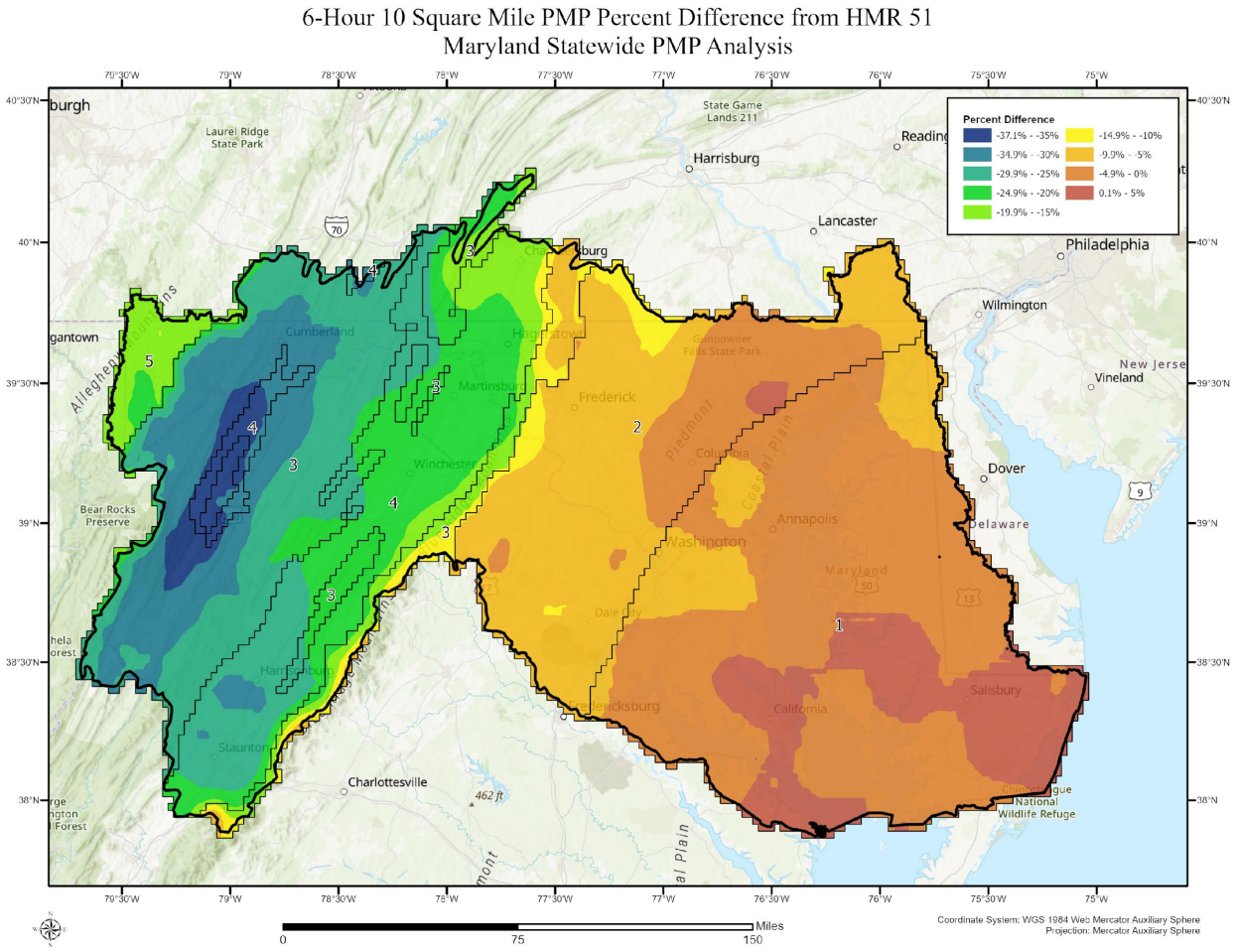

Figure E.1 PMP percent difference from HMR 51 PMP at 6-hour 10-square miles comparing the largest PMP depths regardless of storm type.

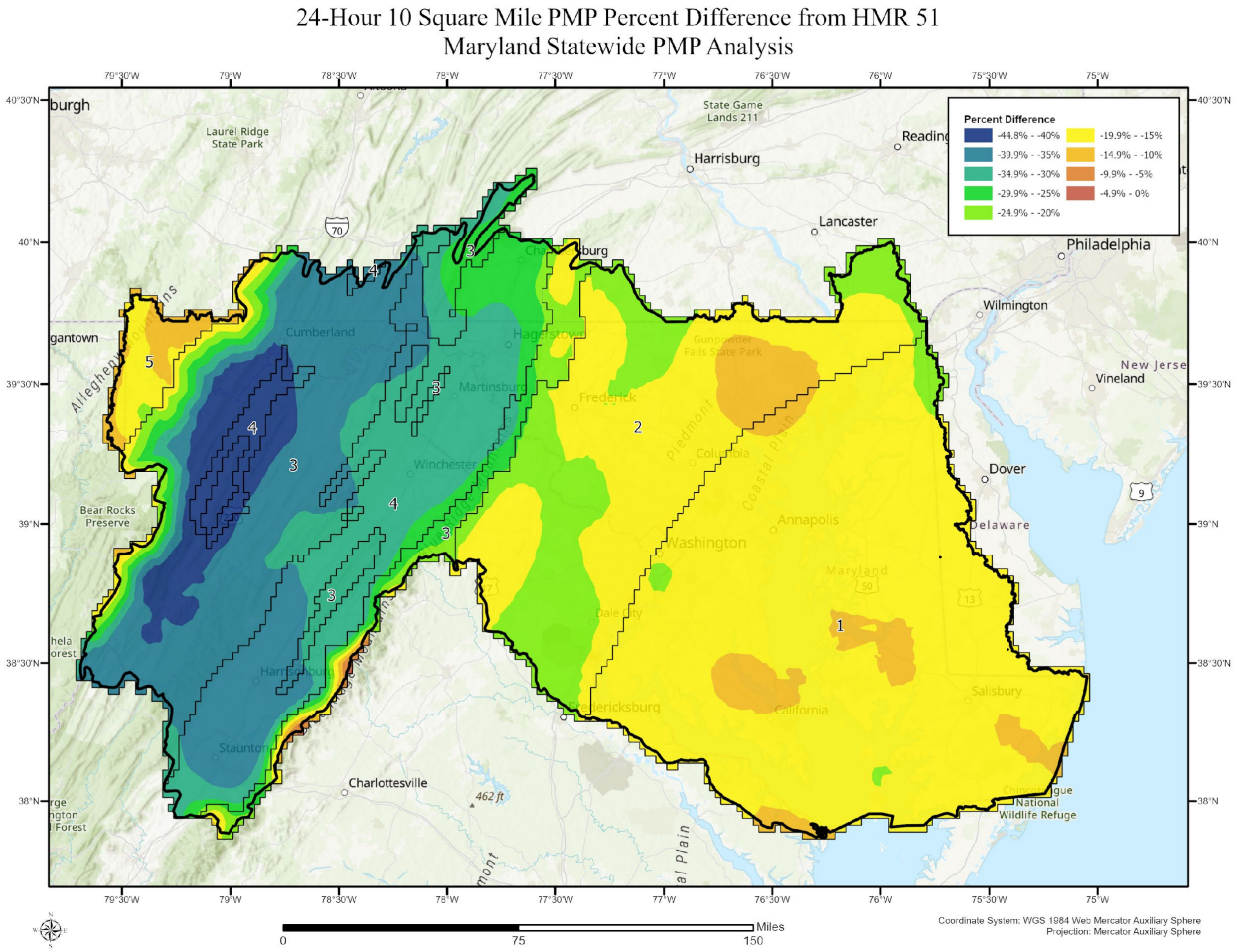

Figure E.2 PMP percent difference from HMR 51 PMP at 24-hour 10-square miles comparing the largest PMP depths regardless of storm type.

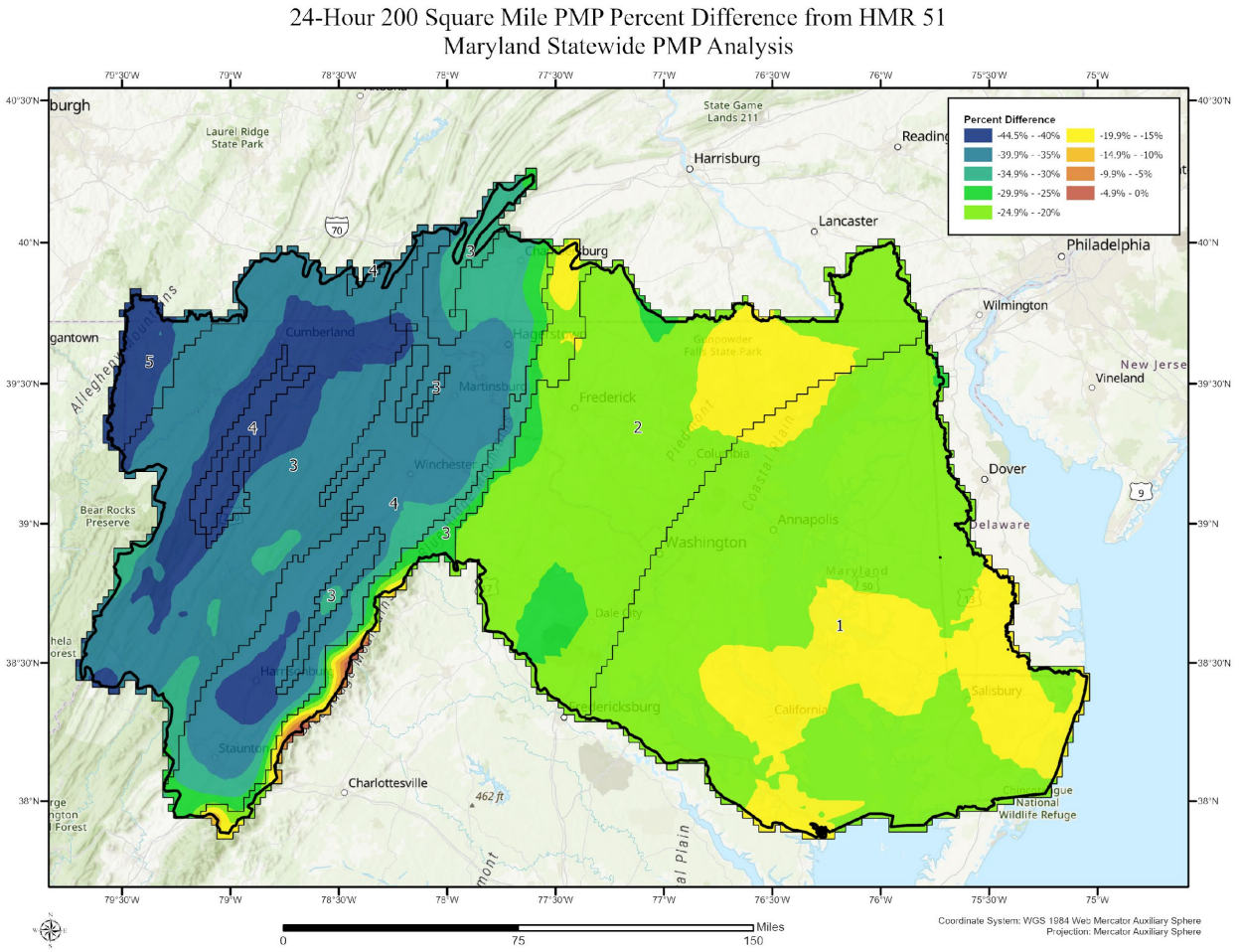

Figure E.3 PMP percent difference from HMR 51 PMP at 24-hour 200-square miles comparing the largest PMP depths regardless of storm type.

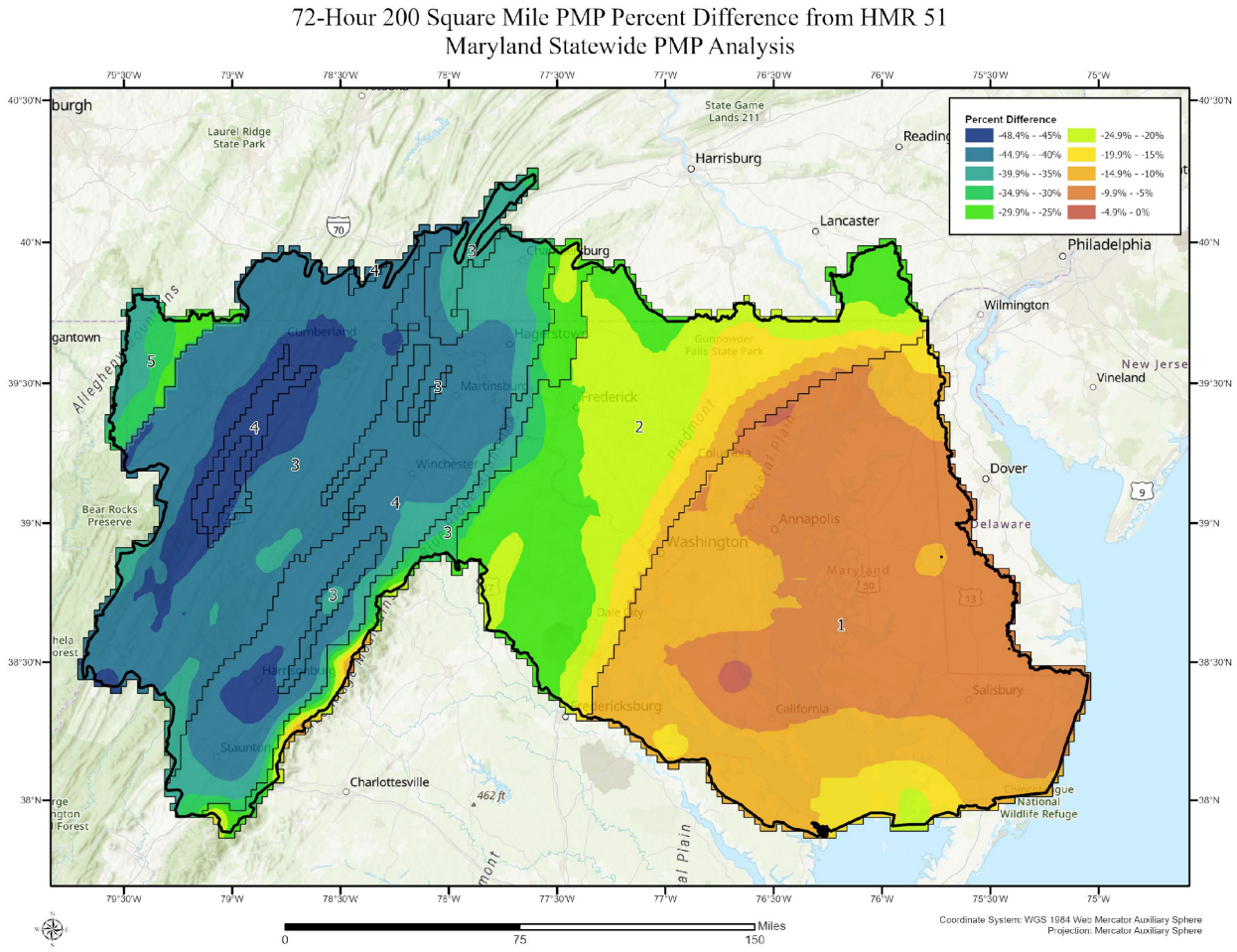

Figure E.4 PMP percent difference from HMR 51 PMP at 72-hour 200-square miles comparing the largest PMP depths regardless of storm type.

Table E.1 PMP percent difference from HMR 51 PMP at 6-hour and 24-hour 10- square miles by transposition zone

10 Square Miles						
ZONE	6-Hour Average PMP	6-Hour HMR 51	Percent Difference from HMR 51	24-Hour Average PMP	24-Hour HMR 51	Percent Difference from HMR 51
1 - Coastal Plain	27.3	27.9	-2.2%	30.6	36.9	-16.9%
2 - Piedmont	25.6	27.4	-6.6%	28.8	35.5	-18.8%
3 - Ridge	20.1	27.4	-26.6%	23.4	35.0	-33.3%
4 - Valley	20.7	27.5	-24.8%	23.3	35.3	-34.0%
5 - Appalachian Plateau	22.2	27.1	-18.1%	29.1	34.3	-15.1%

Table E.2 PMP percent difference from HMR 51 PMP at 24-hour and 72-hour 200- square miles by transposition zone

200 Square Miles						
ZONE	24-Hour Average PMP	24-Hour HMR 51	Percent Difference from HMR 51	72-Hour Average PMP	72-Hour HMR 51	Percent Difference from HMR 51
1 - Coastal Plain	22.0	27.9	-21.0%	29.6	33.0	-10.1%
2 - Piedmont	20.6	26.6	-22.4%	24.3	31.5	-22.7%
3 - Ridge	16.8	26.1	-35.7%	18.4	30.9	-40.6%
4 - Valley	16.8	26.3	-36.3%	18.4	31.2	-41.2%
5 - Appalachian Plateau	14.9	25.4	-41.3%	20.1	30.1	-33.1%

Glossary

Adiabat: Curve of thermodynamic change taking place without addition or subtraction of heat. On an adiabatic chart or pseudo-adiabatic diagram, a line showing pressure and temperature changes undergone by air rising or condensation of its water vapor; a line, thus, of constant potential temperature.

Adiabatic: Referring to the process described by adiabat.

Advection: The process of transfer (of an air mass property) by virtue of motion. In particular cases, advection may be confined to either the horizontal or vertical components of the motion. However, the term is often used to signify horizontal transfer only.

Air mass: Extensive body of air approximating horizontal homogeneity, identified as to source region and subsequent modifications.

Barrier: A mountain range that partially blocks the flow of warm humid air from a source of moisture to the basin under study.

Basin centroid: The point at the exact center of the drainage basin as determined through geographical information systems calculations using the basin outline.

Basin shape: The physical outline of the basin as determined from topographic maps, field survey, or GIS.

Cold front: Front where relatively colder air displaces warmer air.

Convective rain: Rainfall caused by the vertical motion of an ascending mass of air that is warmer than the environment and typically forms a cumulonimbus cloud. The horizontal dimension of such a mass of air is generally of the order of 12 miles or less. Convective rain is typically of greater intensity than either of the other two main classes of rainfall (cyclonic and orographic) and is often accompanied by thunder. The term is more particularly used for those cases in which the precipitation covers a large area as a result of the agglomeration of cumulonimbus masses.

Convergence: Horizontal shrinking and vertical stretching of a volume of air, accompanied by net inflow horizontally and internal upward motion.

Cooperative station: A weather observation site where an unpaid observer maintains a climatological station for the National Weather Service.

Correlation coefficient: The average change in the dependent variable, the orographically transposed rainfall (P_o), for a 1-unit change in the independent variable, the in-place rainfall (P_i).

Cyclone: A distribution of atmospheric pressure in which there is a low central pressure relative to the surroundings. On large-scale weather charts, cyclones are characterized by a system of

closed constant pressure lines (isobars), generally approximately circular or oval in form, enclosing a central low-pressure area. Cyclonic circulation is counterclockwise in the northern hemisphere and clockwise in the southern. (That is, the sense of rotation about the local vertical is the same as that of the earth's rotation).

Depth-Area curve: Curve showing, for a given duration, the relation of maximum average depth to size of area within a storm or storms.

Depth-Area-Duration: The precipitation values derived from Depth-Area and Depth-Duration curves at each time and area size increment analyzed for a PMP evaluation.

Depth-Area-Duration curve: A curve showing the relation between an averaged areal rainfall depth and the area over which it occurs, for a specified time interval, during a specific rainfall event.

Depth-Area-Duration values: The combination of depth-area and duration-depth relations. Also called depth-duration-area.

Depth-Duration curve: Curve showing, for a given area size, the relation of maximum average depth of precipitation to duration periods within a storm or storms.

Dew point: The temperature to which a given parcel of air must be cooled at constant pressure and constant water vapor content for saturation to occur.

Envelopment: A process for selecting the largest value from any set of data. In estimating PMP, the maximum and transposed rainfall data are plotted on graph paper, and a smooth curve is drawn through the largest values.

Explicit transposition: The movement of the rainfall amounts associated with a storm within boundaries of a region throughout which a storm may be transposed with only relatively minor modifications of the observed storm rainfall amounts. The area within the transposition limits has similar, but not identical, climatic and topographic characteristics throughout.

First-order NWS station: A weather station that is either automated or staffed by employees of the National Weather Service and records observations on a continuous basis.

Front: The interface or transition zone between two air masses of different parameters. The parameters describing the air masses are temperature and dew point.

General storm: A storm event that produces precipitation over areas in excess of 500-square miles, has a duration longer than 6 hours, and is associated with a major synoptic weather feature.

Geographic Transposition Factor (GTF): A factor representing the comparison of precipitation frequency relationships between two locations which is used to quantify how rainfall is affected by physical processes related to location and terrain. It is assumed the

precipitation frequency data are a combination of what rainfall would have accumulated without topographic affects and what accumulated because of the topography, both at the location and upwind of the location being analyzed.

Hydrologic Unit: A hydrologic unit is a drainage area delineated to nest in a multi-level, hierarchical drainage system. Its boundaries are defined by hydrographic and topographic criteria that delineate an area of land upstream from a specific point on a river, stream or similar surface waters. A hydrologic unit can accept surface water directly from upstream drainage areas, and indirectly from associated surface areas such as remnant, non-contributing, and diversions to form a drainage area with single or multiple outlet points. Hydrologic units are only synonymous with classic watersheds when their boundaries include all the source area contributing surface water to a single defined outlet point.

HYSPLIT: Hybrid Single-Particle Lagrangian Integrated Trajectory. A complete system for computing parcel trajectories to complex dispersion and deposition simulations using either puff or particle approaches. Gridded meteorological data, on one of three conformal (Polar, Lambert, or Mercator latitude-longitude grid) map projections, are required at regular time intervals. Calculations may be performed sequentially or concurrently on multiple meteorological grids, usually specified from fine to coarse resolution.

Implicit transpositioning: The process of applying regional, areal, or durational smoothing to eliminate discontinuities resulting from the application of explicit transposition limits for various storms.

Isohyets: Lines of equal value of precipitation for a given time interval.

Isohyetal pattern: The pattern formed by the isohyets of an individual storm.

Isohyetal orientation: The term used to define the orientation of precipitation patterns of major storms when approximated by elliptical patterns of best fit. It is also the orientation (direction from north) of the major axis through the elliptical PMP storm pattern.

Jet Stream: A strong, narrow current concentrated along a quasi-horizontal axis (with respect to the earth's surface) in the upper troposphere or in the lower stratosphere, characterized by strong vertical and lateral wind shears. Along this axis it features at least one velocity maximum (jet streak). Typical jet streams are thousands of kilometers long, hundreds of kilometers wide, and several kilometers deep. Vertical wind shears are on the order of 10 to 20 mph per mile of altitude and lateral winds shears are on the order of 10 mph per 100 miles of horizontal distance.

Local storm: A storm event that occurs over a small area in a short time period. Precipitation rarely exceeds 6 hours in duration and the area covered by precipitation is less than 500 square miles. Frequently, local storms will last only 1 or 2 hours and precipitation will occur over areas of up to 200 square miles. Precipitation from local storms will be isolated from general-storm rainfall. Often these storms are thunderstorms.

Low Level Jet stream: A band of strong winds at an atmospheric level well below the high troposphere as contrasted with the jet streams of the upper troposphere.

Mass curve: Curve of cumulative values of precipitation through time.

Mesoscale Convective Complex: For the purposes of this study, a heavy rain-producing storm with horizontal scales of 10 to 1000 kilometers (6 to 625 miles) which includes significant, heavy convective precipitation over short periods of time (hours) during some part of its lifetime.

Mesoscale Convective System: A complex of thunderstorms which becomes organized on a scale larger than the individual thunderstorms, and normally persists for several hours or more. MCSs may be round or linear in shape, and include systems such as tropical cyclones, squall lines, and MCCs (among others). MCS often is used to describe a cluster of thunderstorms that does not satisfy the size, shape, or duration criteria of an MCC.

Mid-latitude frontal system: An assemblage of fronts as they appear on a synoptic chart north of the tropics and south of the polar latitudes. This term is used for a continuous front and its characteristics along its entire extent, its variations of intensity, and any frontal cyclones along it.

Moisture maximization: The process of adjusting observed precipitation amounts upward based upon the hypothesis of increased moisture inflow to the storm.

Observational day: The 24-hour time period between daily observation times for two consecutive days at cooperative stations, e.g., 6:00PM to 6:00PM.

One-hundred year rainfall event: The point rainfall amount that has a one-percent probability of occurrence in any year. Also referred to as the rainfall amount that has a 1 percent chance of occurring in any single year.

Polar front: A semi-permanent, semi-continuous front that separates tropical air masses from polar air masses.

Precipitable water: The total atmospheric water vapor contained in a vertical column of unit cross-sectional area extending between any two specified levels in the atmosphere; commonly expressed in terms of the height to which the liquid water would stand if the vapor were completely condensed and collected in a vessel of the same unit cross-section. The total precipitable water in the atmosphere at a location is that contained in a column or unit cross-section extending from the earth's surface all the way to the "top" of the atmosphere. The 30,000-foot level (approximately 300mb) is considered the top of the atmosphere in this study.

Persisting dew point: The dew point value at a station that has been equaled or exceeded throughout a period. Commonly durations of 12 or 24 hours are used, though other durations may be used at times.

Probable Maximum Flood: The flood that may be expected from the most severe combination of critical meteorological and hydrologic conditions that are reasonably possible in a particular drainage area.

Probable Maximum Precipitation: Theoretically, the greatest depth of precipitation for a given duration that is physically possible over a given size storm area at a particular geographic location at a certain time of the year.

Pseudo-adiabat: Line on thermodynamic diagram showing the pressure and temperature changes undergone by saturated air rising in the atmosphere, without ice-crystal formation and without exchange of heat with its environment, other than that involved in removal of any liquid water formed by condensation.

Rainshadow: The region, on the lee side of a mountain or mountain range, where the precipitation is noticeably less than on the windward side.

Saturation: Upper limit of water-vapor content in a given space; solely a function of temperature.

Shortwave: Also referred to as a shortwave trough, is an embedded kink in the trough / ridge pattern. This is the opposite of longwaves, which are responsible for synoptic scale systems, although shortwaves may be contained within or found ahead of longwaves and range from the mesoscale to the synoptic scale.

Spatial distribution: The geographic distribution of precipitation over a drainage according to an idealized storm pattern of the PMP for the storm area.

Storm transposition: The hypothetical transfer, or relocation of storms, from the location where they occurred to other areas where they could occur. The transfer and the mathematical adjustment of storm rainfall amounts from the storm site to another location is termed "explicit transposition." The areal, durational, and regional smoothing done to obtain comprehensive individual drainage estimates and generalized PMP studies is termed "implicit transposition" (WMO, 1986).

Synoptic: Showing the distribution of meteorological elements over an area at a given time, e.g., a synoptic chart. Use in this report also means a weather system that is large enough to be a major feature on large-scale maps (e.g., of the continental U.S.).

Temporal distribution: The time order in which incremental PMP amounts are arranged within a PMP storm.

Tropical storm: A cyclone of tropical origin that derives its energy from the ocean surface.

Total storm area and total storm duration: The largest area size and longest duration for which depth-area-duration data are available in the records of a major storm rainfall.

Transposition limits: The outer boundaries of the region surrounding an actual storm location that has similar, but not identical, climatic and topographic characteristics throughout. The storm can be transpositioned within the transposition limits with only relatively minor modifications to the observed storm rainfall amounts.

Undercutting: The process of placing an envelopment curve somewhat lower than the highest rainfall amounts on depth-area and depth-duration plots.

Warm front: Front where relatively warmer air replaces colder air.

List of Acronyms

AEP: Annual exceedance probability

AMS: Annual maximum series

ARF: Areal Reduction Factor

ARI: Average Recurrence Interval

AWA: Applied Weather Associates

CDF: Cumulative Distribution Function

DA: Depth-Area

DAD: Depth-Area-Duration

dd: decimal degrees

DND: Drop number distribution

DSD: Drop size distribution

EPRI: Electric Power Research Institute

F: Fahrenheit

FERC: Federal Energy Regulatory Commission

GCM: Global Circulation Models

GCS: Geographical coordinate system

GIS: Geographic Information System

GRASS: Geographic Resource Analysis Support System

GTF: Geographic Transposition Factor

HMR: Hydrometeorological Report

HRRR: High-Resolution Rapid Refresh Model

HYSPLIT: Hybrid Single-Particle Lagrangian Integrated Trajectory Model

IDW: Inverse distance weighting

IPCC: Intergovernmental Panel on Climate Change

IPMF: In-place Maximization Factor

LLJ: Low-level Jet

MADIS: NCEP Meteorological Assimilation Data Ingest System

MAM: Mean Annual Max

mb: millibar

MCC: Mesoscale Convective Complex

MCS: Mesoscale Convective System

MDE: Maryland Department of the Environment

MTF: Moisture Transposition Factor

NCAR: National Center for Atmospheric Research

NCDC: National Climatic Data Center

NCEI: National Centers for Environmental Information

NCEP: National Centers for Environmental Prediction

NEXRAD: Next Generation Radar

NOAA: National Oceanic and Atmospheric Administration

NRC: Nuclear Regulatory Commission

NRCS: Natural Resources Conservation Service

NWS: National Weather Service

PMF: Probable Maximum Flood

PMP: Probable Maximum Precipitation

POR: Period of Record

PRISM: Parameter-elevation Relationships on Independent Slopes

PW: Precipitable Water

QA/QC: Quality Assurance/Quality Control

RAWS: Remote Automated Weather Stations

RCM: Regional Circulation Models

RH: Relative Humidity

RMSE: Root Mean Square Error

SMC: Spatially Based Mass Curve

SPAS: Storm Precipitation and Analysis System

SPP: Significant Precipitation Period

SSM: Storm Separation Method

SSPs: Shared Socioeconomic Pathways

SST: Sea Surface Temperatures

TAF: Total Adjustment Factor

TAR: Total Adjusted Rainfall

USACE: US Army Corps of Engineers

USACE EM: USACE Engineering Manual

USBR: Bureau of Reclamation

USGS: United States Geological Survey

WGS: World Geodetic System

WMO: World Meteorological Organization

1. PMP Development Overview

This study provides Probable Maximum Precipitation (PMP) depths for all drainage basins within Maryland, including regions adjacent to the state that also provide runoff into drainage basins within Maryland (Figure 1.1). PMP depths which would result in the Probable Maximum Flood at a given locations are valid from May through October when significant snowmelt contribution would not occur. Heavy rainfall and flooding can occur outside of this timeframe, but the rainfall depths would less than the full PMP. PMP depths are used in the computation of the Probable Maximum Flood (PMF). PMP depths provided in this study can be used in place of previous design values including those from Hydrometeorological Reports (HMRs) 51 (Schreiner and Riedel, 1978) and HMR 52 (Hansen et al., 1982).

PMP is a deterministic estimate of the theoretical maximum depth of precipitation that can occur over a specified area, at a given time of the year. Parameters to estimate PMP were developed following the storm-based approach as discussed in the HMRs and subsequently refined in the numerous site-specific, statewide, and regional PMP studies completed since the early 1990's.

Methods used to derive PMP for this study included consideration of numerous extreme rainfall events that have been appropriately adjusted to each grid point and represent each PMP-storm type that can occur in the study domain, local, general, and tropical. The process of combining maximized storm events by storm type into a hypothetical PMP design storm resulted in a reliable PMP estimation by combining the worst-case combination of meteorological factors in a physically possible manner. The combination of storm data and storm adjustments provided adequate data from which to derive reasonable PMP depths for use in PMF development and hydrologic evaluations.

During this calculation process, air masses that provide moisture to both the historic storm and the idealized PMP storm were assumed to be saturated through the entire depth of the atmosphere and contain the maximum moisture possible based on the surface dew point or sea surface temperatures (SST) value used to represent the storm environment. The calculation of the saturated atmospheric profile used moist pseudo-adiabatic temperature profiles for both the historic storm and the PMP storm. This method assumed that a sufficient period of record was available to identify rainfall observations over a large region. Further, within that region at least a few storms have been observed which attained or came close to attaining the maximum storm efficiency possible for converting atmospheric moisture to rainfall. The PMP development process assumes that if additional atmospheric moisture had been available, an individual extreme storm would have maintained the same storm efficiency for converting atmospheric moisture to precipitation and hence more precipitation would result. Therefore, the ratio of the maximized precipitation amounts to the actual precipitation amounts would be the same as the ratio of the precipitable water (calculated from the dew point or SST) observed versus the climatological maximum amount in the atmosphere associated with each storm.

Current understanding of meteorology does not support an explicit evaluation of storm efficiency for use in PMP evaluation. To compensate for this, the period of record includes the

entire historic record of rainfall data (200 years for this study), along with an extended geographic region from which to choose storms. By including a long period of record and the large geographic region, it is assumed that one or more of these storms represented storm dynamics that approached the maximum efficiency for rainfall production. Therefore, the assumption is the PMP development process and resulting calculations represent PMP for any given location within the study domain. In essence, the process is trading time for space to capture the PMP processes.

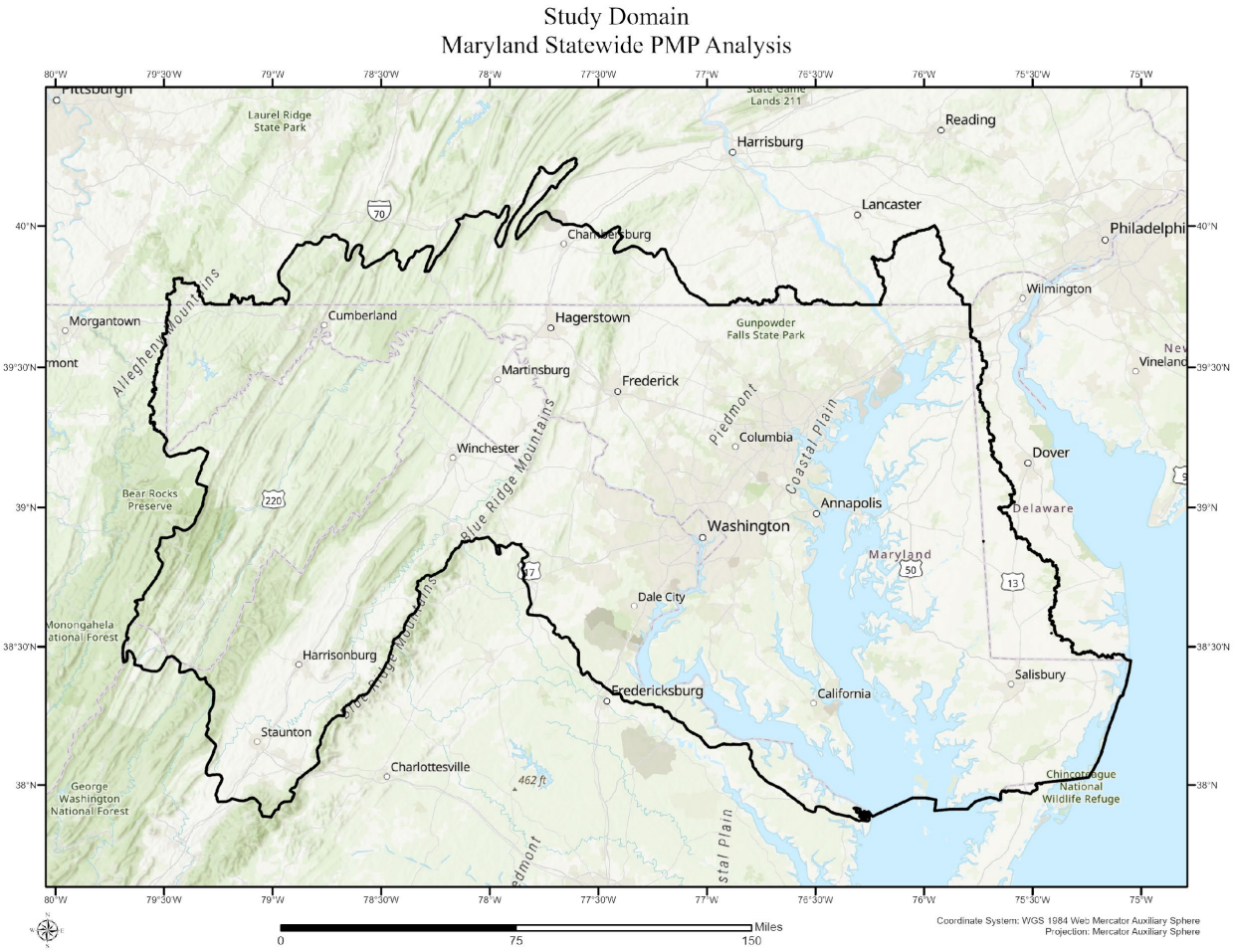

Figure 1.1: Probable Maximum Precipitation study domain utilized for Maryland

1.1 Probable Maximum Precipitation Background

Definitions of PMP are found in most of the HMRs issued by the National Weather Service (NWS). The definition used in the most recently published HMR is "theoretically, the greatest depth of precipitation for a given duration that is physically possible over a given storm area at a particular geographical location at a certain time of the year" (HMR 59, p. 5) (Corrigan et al., 1999). Since the early 1940s, several government agencies have developed methods to calculate PMP for various regions of the United States. The NWS (formerly the U.S. Weather Bureau), the U.S. Army Corps of Engineers (USACE), and the U.S. Bureau of Reclamation (USBR) have been the primary federal agencies involved in this activity. PMP values presented

in their reports are used to calculate the PMF, which in turn, is often used for the design of critical infrastructure and high hazard hydraulic facilities. It is important to remember that the methods used to derive PMP and the hydrological procedures that use the PMP outputs need to adhere to the requirement of being "physically possible." In other words, various levels of conservatism and/or extreme aspects of storms that could not physically co-occur in a PMP storm environment should not be used to produce combinations of storm characteristics that are not physically consistent in determining PMP outputs or for the hydrologic applications of those outputs.

The generalized PMP studies currently in use in the contiguous United States include HMRs 49 (1977) and 50 (1981) for the Colorado River and Great Basin drainage; HMRs 51 (1978), 52 (1982), and 53 (1980) for the U.S. east of the 105th meridian; HMR 55A (1988) for the area between the Continental Divide and the 103rd meridian; HMR 57 (1994) for the Columbia River and Pacific Coast Drainages; and HMRs 58 (1998) and 59 (1999) for California (Figure 1.2). In addition to these HMRs, numerous Technical Papers and Reports deal with specific subjects concerning precipitation (e.g., Technical Paper 1, 1946; Technical Paper 16, 1952; NOAA Tech. Report NWS 25, 1980; and NOAA Tech. Memorandum NWS HYDRO 40, 1984). Topics in these papers include maximum observed rainfall amounts for various return periods and specific storm studies. Climatological atlases (e.g., Technical Paper No. 40, 1961; NOAA Atlas 2, 1973; and NOAA Atlas 14, 2004-current) are available for use in determining precipitation return periods.

Several site-specific, statewide, and regional studies (e.g., Tomlinson et al., 2002-2013; Kappel et al., 2012-2024) augment generalized PMP reports for specific basins or regions included in the areas addressed by the HMRs. Recent site-specific PMP projects completed within the Maryland domain and immediately surrounding regions have updated the storm database and many of the procedures used to estimate PMP depths in the HMRs (e.g. Kappel et al., 2020, Kappel et al., 2023). This study continued that process by applying the most current understanding of meteorology related to extreme rainfall events and updating the storm database through December 2023. PMP results from this study provide values that replace those derived from the various HMRs in the region.

During the course of this study, the National Academy of Science released its recommendations regarding PMP development (National Academy of Sciences, 2024). These findings recommend the use of probabilistic evaluations in addition to the deterministic storm-based approach. They also recommend accounting for climate change. For the long term (10 years and beyond), they recommend the use of numerical weather prediction models as another option to derive PMP depths. As part of the Maryland statewide PMP development, AWA applied the recommendations by including probabilistic evaluations and climate change projections.

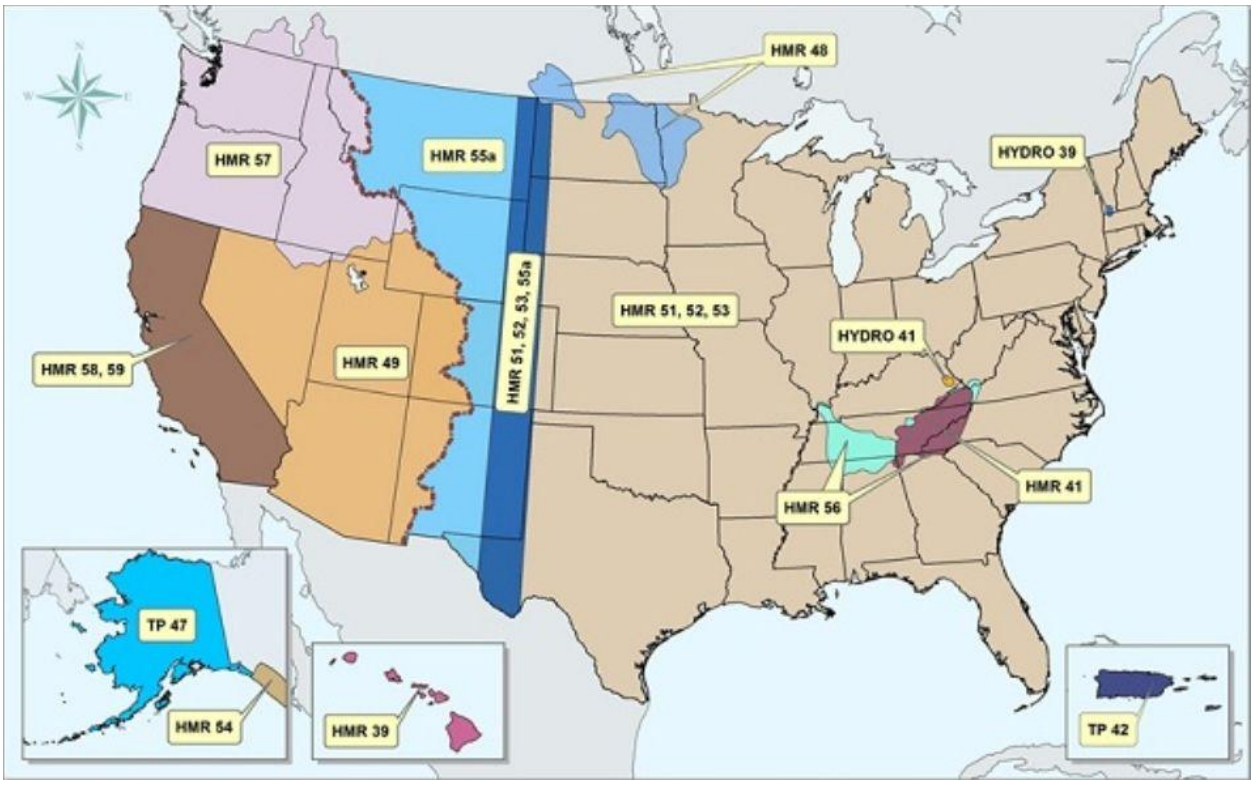

Figure 1.2: Hydrometeorological Report coverages across the United States, from https://www.weather.gov/owp/hdsc_pmp

Maryland is included within the domain covered by HMR 51 and HMR 52. HMR 51 is the most relevant HMR for this study, covering the entire study region. HMR 52 provides background information and hydrologic implementation guidelines for the storm data developed in HMR 51. These HMRs cover diverse meteorological and topographical regions. HMR 51 provides generalized estimates of PMP depths for a large, climatologically diverse area and recognizes that studies addressing PMP over specific regions can incorporate more site-specific considerations and provide improved PMP estimates.

Maryland contains many diverse climatological and physiographic regions (Figure 1.3) where climate and terrain vary, sometimes over short distances. Because of the distinctive climate regions and variations in topography, the development of PMP depths must account for the complexity of the meteorology and terrain throughout the state. Although the HMRs provided relevant data at the time they were published, the understanding of meteorology, including the effects of coastal convergence and terrain on rainfall (orographic effects) have advanced significantly in the subsequent years.

Limitations associated with the HMRs have been explicitly addressed as part of this study. These include updating the storm database from the limited number of analyzed storms utilized in HMR 51 (no storms that have occurred since the early 1970s are included), evaluating of orographic effects, utilizing consistent data and procedures throughout the region, improving documentation describing the PMP development process, and updating procedures and outputs for PMP development and PMF application. This project incorporated the latest methods,

technology, and data to address these complexities. Each of these were addressed and updated where data and current understanding of meteorology allowed.

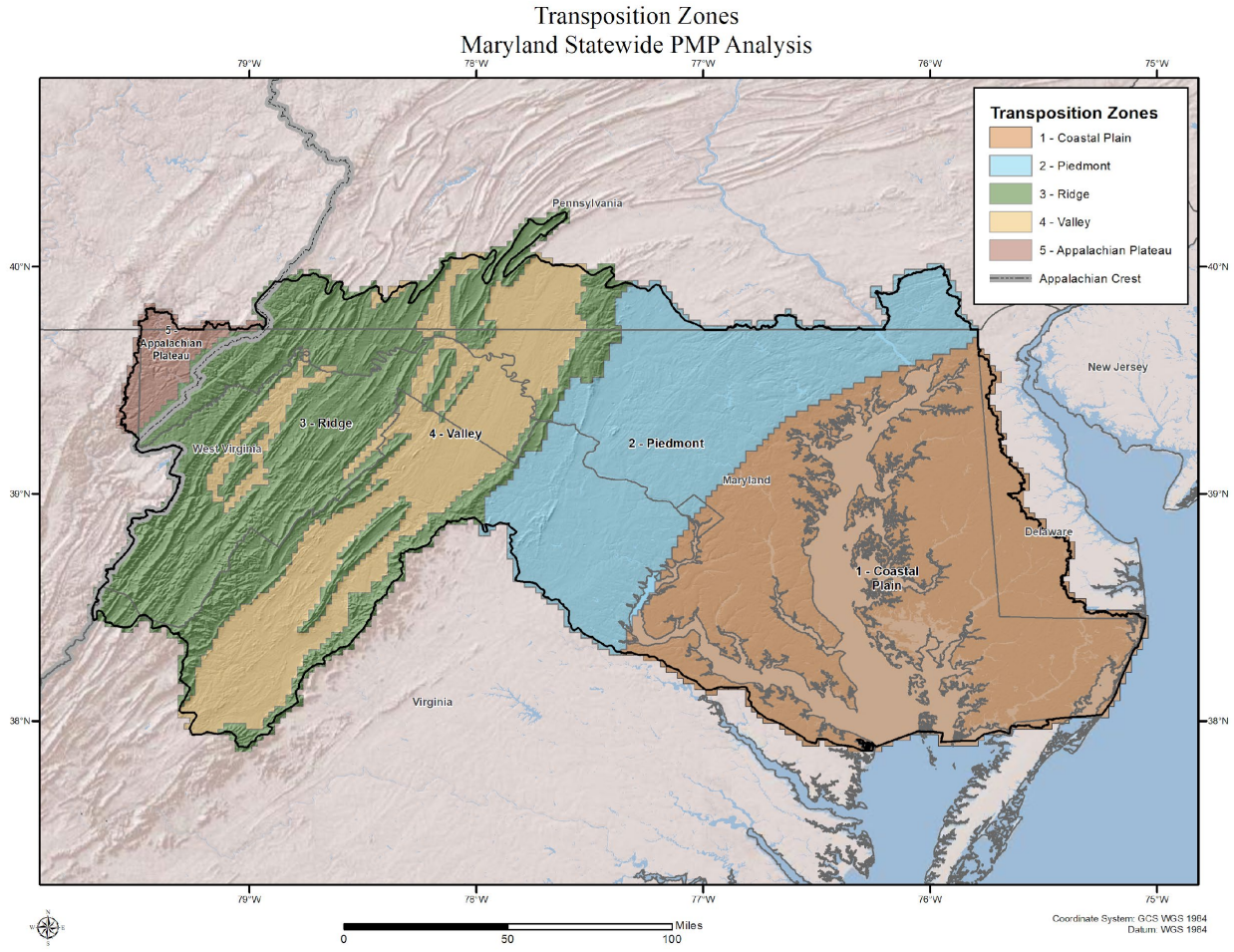

Figure 1.3: Maryland PMP project domain and transposition zones utilized in this study. The overall project domain extends beyond the state boundaries in some areas to ensure all drainage areas are included.

Previous site-specific, statewide, and regional PMP projects completed by AWA provide examples of PMP studies that explicitly consider characteristics of historic extreme storms over meteorologically and topographically similar regions surrounding the area being studied. Most important for this study include the Virginia statewide PMP (2015), the Pennsylvania statewide PMP (2019), the New Jersey statewide PMP (2023), and the North Carolina statewide PMP (ongoing). The procedures incorporate the most up-to-date sets, techniques, and applications to derive PMP. All AWA PMP studies have received extensive review and the results have been used in computing the PMF for various watersheds. This study follows similar procedures employed in those studies while making improvements where advancements in storm data, PMP calculation processes, and storm transposition procedures have become available.

Several PMP studies have been completed by AWA within the region covered by HMR 51 and within Maryland itself, which are directly relevant to this study (Figure 1.4). Each of

these studies provided PMP depths which updated those from HMR 51. These are examples of PMP studies that explicitly consider the meteorology and topography of the study location along with characteristics of historic extreme storms over climatically similar regions. Information, experience, and data from these PMP studies were utilized in this study. These included use of previously analyzed storm events using the SPAS program, previously derived storm lists, previously derived in-place storm maximization factors, climatologies, and explicit understanding of the meteorology of the region.

In addition, comparisons to these previous studies provided sensitivity and context with the results of this study. These regional, statewide, and site-specific PMP studies received extensive review and were accepted by the appropriate regulatory agencies including the Federal Energy Regulatory Commission (FERC), state dam safety regulators, and the Natural Resources Conservation Service (NRCS). This study followed the same procedures used in those studies to determine PMP depths. These procedures, together with the Storm Precipitation Analysis System (SPAS) rainfall analyses (Hultstrand and Kappel, 2017), were used to compute PMP following standard storm-based procedures outlined in HMR 51.

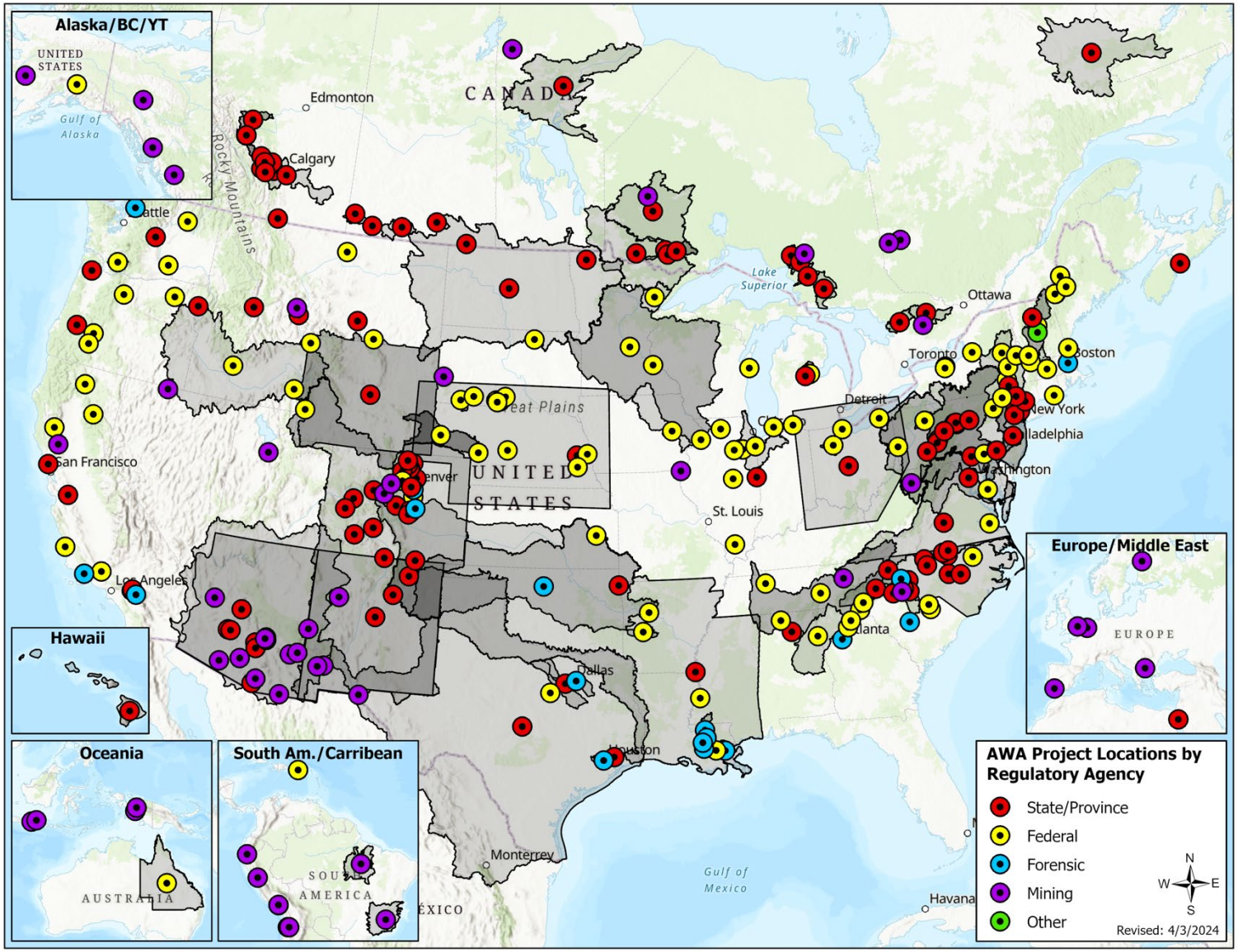

Figure 1.4: Locations of AWA PMP studies as of April 2024

1.2 Objective of this PMP Study

This study determines estimates of PMP depths for use in computing the PMF for various watersheds in the state and within the overall project domain. The most reliable methods and data available were used and updates to methods and data used in HMRs were applied where appropriate. Information is included in this report and the study database so that calculations can be checked and depths can be reproduced and updated in the future.

1.3 PMP Analysis Domain

The project domain was defined to cover all of Maryland as well as watersheds that extended beyond state boundaries for which Maryland Dam Safety (MDE) has responsibility for regulation. This study allows for gridded PMP values to be determined for each grid cell within the project domain. The project domain is shown in Figure 1.1. Discussions with MDE, FERC, NRCS, review board members, and private consultants involved in the study helped refine the analysis region beyond state boundaries to fully incorporate all potential sites that may affect Maryland.

1.4 PMP Analysis Grid Setup

A uniform grid covering the PMP project domain provides a spatial framework for the analysis. The PMP grid resolution for this study was 0.025 x 0.025 decimal degrees (dd), or 90 arc-seconds, using the Geographic Coordinate System (GCS) spatial reference with the World Geodetic System of 1984 (WGS 84) datum. This resulted in 10,957 grid cells with centroids within the domain. Each grid cell represents an approximate area of 2.3-square miles. The grid network placement is essentially arbitrary. However, the placement was oriented in such a way that the grid cell centroids are centered over whole number coordinate pairs and then spaced evenly every 0.025 dd. For example, there is a grid cell centered over 37.875° N and 79° W with the adjacent grid point to the west at 37.875°N and 79.025°W. The PMP analysis grid over the PMP domain is shown in Figure 1.5.

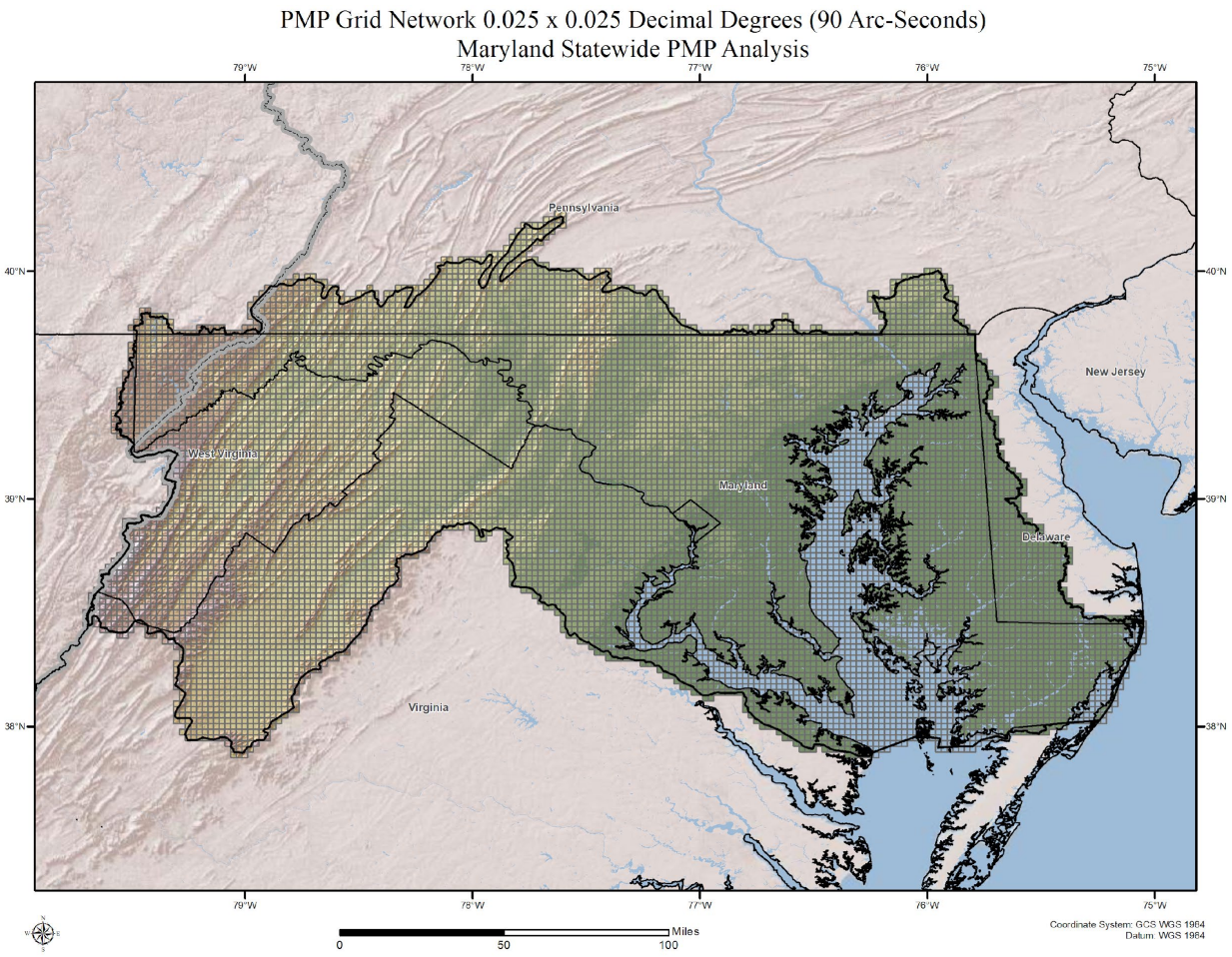

Figure 1.5: PMP analysis grid placement over the PMP domain

2. PMP Development Methodology

The storm-based approach used in this study is consistent with many of the procedures that were used in the development of the HMRs and as described in the World Meteorological Organization PMP documents (WMO, 2009), with updated procedures implemented where appropriate. Methodologies reflecting the current standard of practice were applied in this study considering the unique meteorological and topographical interactions within the region as well as the updated scientific data and procedures available. Updated procedures are described in detail later in this report. Figure 2.1 provides the general steps used in deterministic PMP development utilizing the storm-based approach. Terrain characteristics are addressed as they specifically affect precipitation patterns spatially, temporally, and in magnitude.

This study identified major storms that occurred within the region and areas where those storms were considered transpositionable within the study region. Each of the PMP storm types capable of producing PMP-level rainfall were identified and investigated. The PMP storm types included local storms, general storms, and tropical storms. The "short list" of storms was extensively reviewed, quality controlled, and accepted as representative of all storms that could potentially affect PMP depths at any location or area size within the overall study domain. This short list of storms was utilized to derive the PMP depths for all locations.

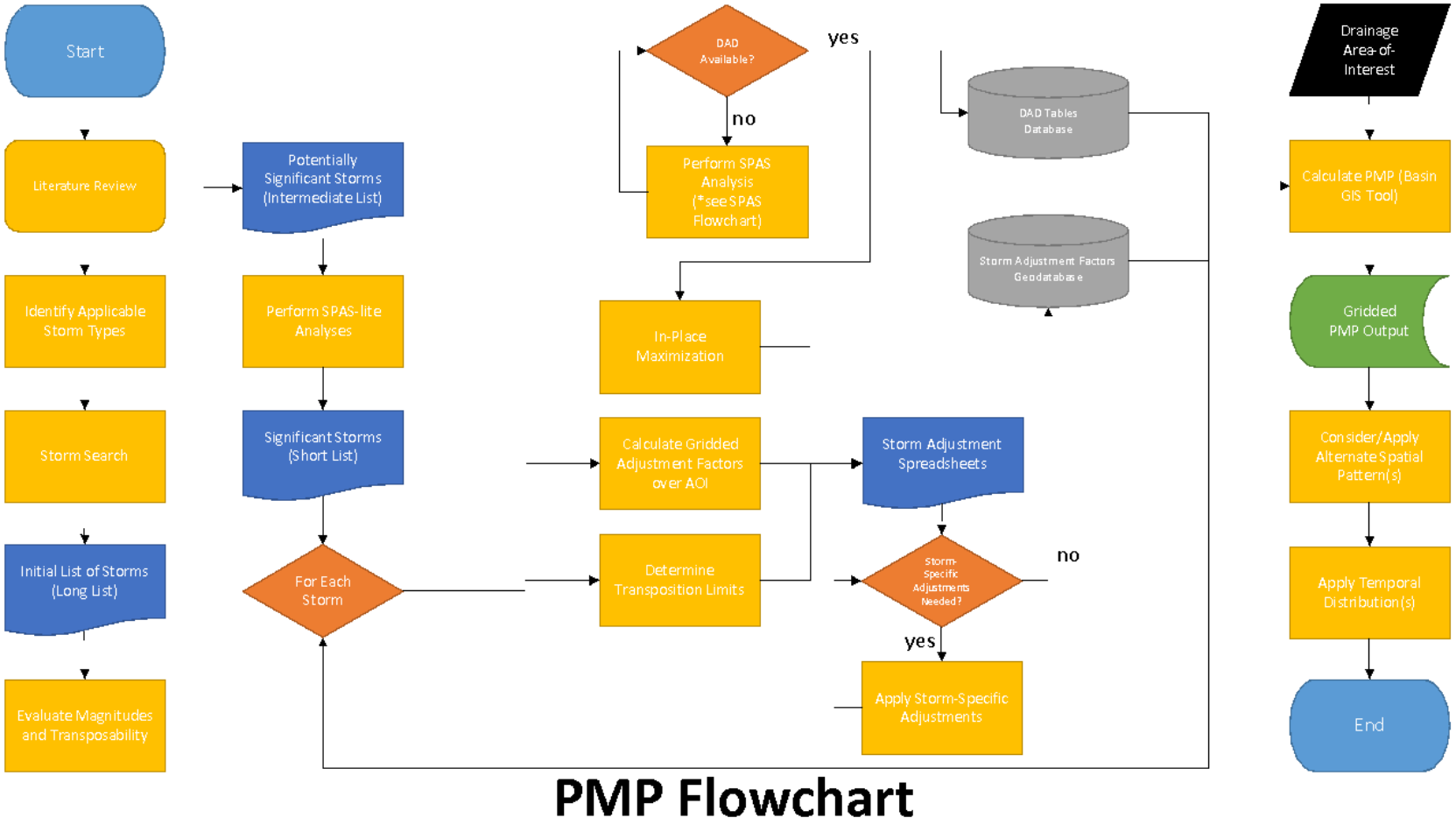

Figure 2.1: Probable Maximum Precipitation calculation steps

The moisture content of each of the short list storms was maximized to provide worst-case rainfall accumulation for each storm at the location where it occurred (in-place storm location). Storms were then transpositioned to regions with similar meteorological and topographical characteristics. Locations where each storm was transpositioned were determined using meteorological judgment, comparison of adjustment factors, comparisons of PMP depths, comparison against previous transposition limits from HMRs and AWA, discussions with the review board/study participants, and comparisons against precipitation frequency climatologies. Adjustments were applied to each storm as it was transpositioned to each grid point to calculate the amount of rainfall each storm would have produced at each grid point versus what it produced at the original location. These adjustments were combined to produce the total adjustment factor (TAF) for each storm for each grid point.

The TAF is applied to the observed precipitation values at the area size of interest to each storm. The Storm Precipitation Analysis System (SPAS) is utilized to analyze the rainfall associated with each storm used for PMP development. SPAS has been used to analyze more than 950 extreme rainfall events since 2002. SPAS analyses are used in PMP development as well as other meteorological applications. SPAS has been extensively peer reviewed and accepted as appropriate for use in analyzing precipitation accumulation by numerous independent review boards and as part of the Nuclear Regulatory Commission (NRC) software certification process (e.g., Kappel et al. 2015 and Hultstrand Kappel, 2017). Appendix E provides a detailed description of the SPAS program. The TAF is a product of the In-Place Maximization Factor (IPMF) and the Geographic Transposition Factor (GTF).

The governing equation used for computation of the Total Adjusted Rainfall (TAR), for each storm for each grid cell for each duration, is given in Equation 1.

$$TAR_{xhr} = P_{xhr} \times IPMF \times GTF \qquad \text{(Equation 1)}$$

where:

TAR_{xhr} is the Total Adjusted Rainfall value at the x-hour (x-hr) duration for the specific grid cell at each duration at the target location;

P_{xhr} is the x-hour precipitation observed at the historic in-place storm location (source location) for the basin-area size;

In-Place Maximization Factor (*IPMF)* is the adjustment factor representing the maximum amount of atmospheric moisture that could have been available to the storm for rainfall production;

Geographic Transposition Factor (GTF) is the adjustment factor accounting for precipitation frequency relationships between two locations. This is used to quantify all processes that affect rainfall, including terrain, location, and seasonality.

The Moisture Transposition Factor (MTF) was not utilized in this study as previous work has demonstrated that the factor is not necessary and represents a potential double counting of

moisture already capture as part of the GTF process. This is consistent with all AWA studies completed since 2019, including the adjacent Pennsylvania and New Jersey statewide study. A description of why the MTF process is no longer used can be found in Section 9.5 of the Pennsylvania statewide PMP study.

Note, the largest of these values at each duration becomes PMP at each grid point. The data and calculations are run at the area size and duration(s) specified through user input. The PMP output depths are then provided for durations required for Probable Maximum Flood (PMF) analysis at a given location by storm type and provided as a basin average. These data have a spatial pattern and temporal pattern associated with them for hydrologic modeling implementation. The spatial and temporal patterns are based on climatological patterns (spatial) and a synthesis of historic storm accumulation patterns (temporal) used in this study.

3. Weather and Climate of the Region

Warm ocean temperatures associated with the Gulf Stream in the Atlantic Ocean and the Gulf of Mexico provide ample moisture to the atmosphere for storm development and precipitation production. When this moisture is drawn into storm systems and advected into the study domain, significant precipitation events can occur. This can be enhanced by topographic interactions and coastal convergence processes (Figure 3.1). The change in elevation and distance from the Atlantic Ocean and/or Gulf of Mexico helps to create a variety of climate patterns. These interactions influence the final amounts of moisture available for precipitation production over the region as well as the spatial rainfall pattern of individual storms (Gelber, 1992; Thaler, 1996).

The latitude of the study domain, between ~37°N and 40°N, places the region in the path of both the polar and sub-tropical jet streams, allowing fronts and areas of low pressure to traverse the region on a consistent basis throughout the year. Storms originating in the Great Plains, Gulf of Mexico, and Atlantic Ocean can produce significant precipitation over different parts of the overall domain. In general, precipitation is evenly distributed throughout the year, although each storm type exhibits preferred seasonality.

For the majority of the study region east of the Appalachian crest, the main low-level moisture source region is the Atlantic Ocean and specifically the warm water associated with the Gulf Stream Current (Figure 3.2). For the region of Maryland west of the Appalachian crest, significant low-level moisture is also contributed by the Gulf of Mexico moving in from the southwest through the west to the northwest. High levels of atmospheric moisture can be entrained from both of these sources as storm systems move through and continue to develop in the region. Depending on the atmospheric steering currents, the moisture and/or storm can move onshore and over eastern sections of Maryland. This will often result in heavy rainfall, which can then be further enhanced as it encounters the first major ridgelines and elevated terrain.

During the tropical storm season, which extends from June through November in the Atlantic Ocean and Gulf of Mexico, tropical systems (Tropical Depressions, Tropical Storms, and Hurricanes) can move directly into the region or along the coastline and produce heavy rainfall. The moist air moving inland from the Gulf Stream and Gulf of Mexico will provide significant low-level moisture that feeds into developing thunderstorms, most common from late spring through early fall. This can then be enhanced by a front, areas of low pressure, and/or interactions with topography.

Because of the movement and strength of the upper-level winds in the region, storm patterns generally do not stay fixed over the region for long periods. Therefore, the synoptic patterns which produce high levels of atmospheric moisture in the region are generally transient and limit the magnitude of precipitation at any one location. However, PMP-type rainfall occurs during situations where the storm movement is blocked or slowed and allowed to concentrate heavy rainfall for extended durations over the same region. In addition, topography plays a role in the initiation of storms in the region, the magnitude of the rainfall, and the spatial distribution of the rainfall. Higher elevations generally act to enhance rainfall production and therefore exhibit higher rainfall values. Conversely, sheltered valleys and regions in general downwind

locations exhibit lower rainfall values. This effect of topography and distance from the coast is seen in the PMP spatial patterns across the regions, with the highest amounts near the coast and along the Appalachian crest and lower amounts to the east of the Appalachian crest inland from the coastal region.

Figure 3.1: Synoptic weather features associated with moisture from the Gulf of Mexico into the region

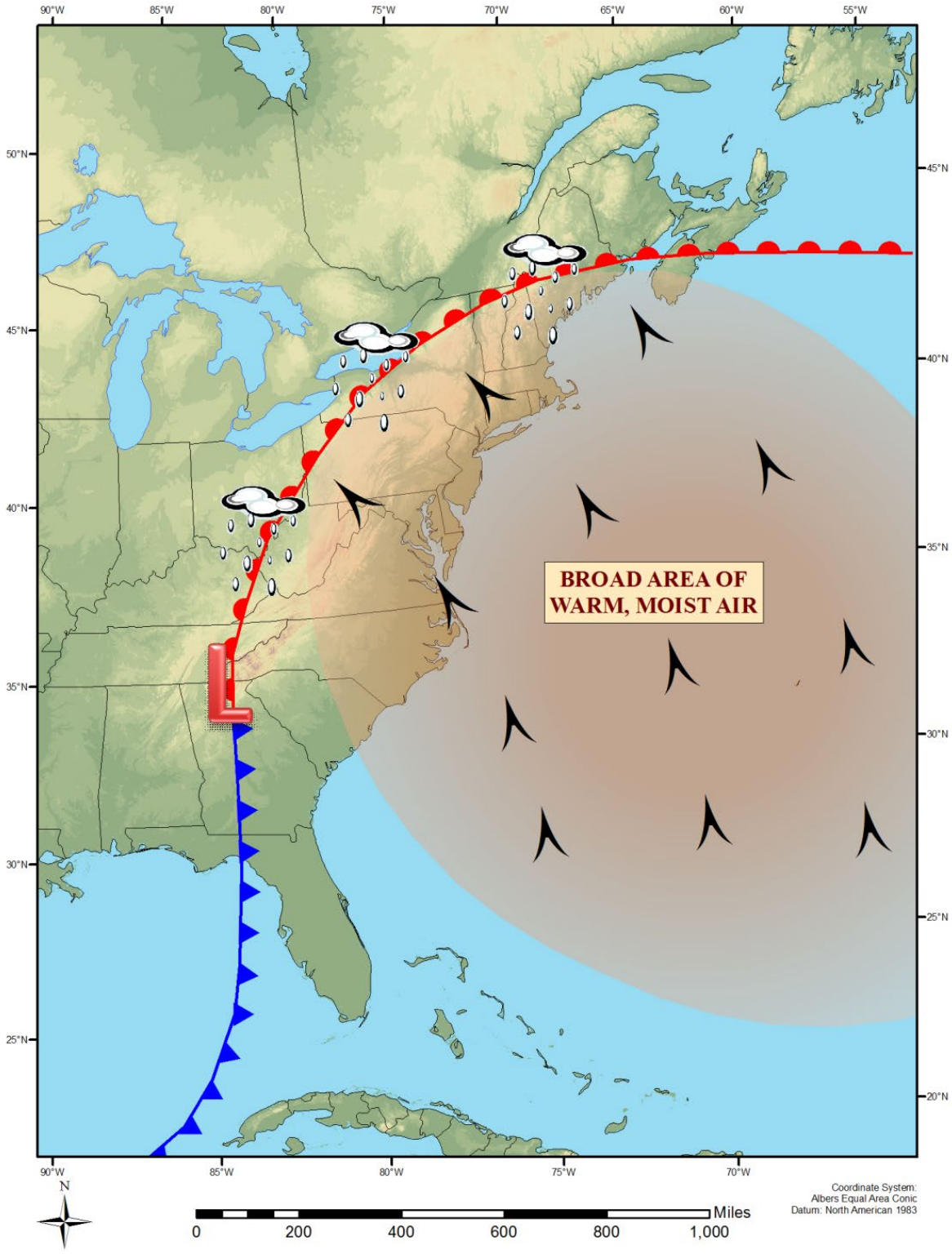

Figure 3.2: Locations of surface features associated with moisture advection from the Atlantic Ocean

In simple terms, precipitation is a product of two processes, rising air motion (lift) and moisture. The lift required to convert atmospheric moisture into precipitation is generated in several ways in and around the region. Synoptic storm dynamics are very effective in converting atmospheric moisture into precipitation. This type of storm environment is most often associated with fronts (boundaries between two different air masses) and areas of low pressure. Fronts can be a focusing mechanism providing upward motion in the atmosphere resulting in heavy precipitation production. In some instances, the pattern can become blocked causing these fronts to stall or move very slowly across the region. This pattern allows heavy rainfall to continue for several days in the same general area, causing widespread flooding.

Another mechanism which creates lift in the region is heating of the lower atmosphere by solar radiation, conduction, and convection. This creates warmer air below colder air resulting in atmospheric instability and leads to rising motions called convection. In unique circumstances, the instability and moisture levels in the atmosphere can reach very high levels and can potentially stay over the same region for an extended period of time. This can lead to intense thunderstorms and very heavy precipitation.

Another common mechanism for heavy precipitation is associated with tropical systems which affect the region every few years during the summer and fall seasons. The lift associated with such storms is a combination of convective process and lift provided by the topography and coastal convergence.

3.1 Climatological Characteristics Affecting PMP Storm Types

Weather patterns in the region are characterized by three main types:

1. Areas of low pressure moving through the region from the west through the southwest or redeveloping along the lee slopes of the Appalachians or over the warm water of the Gulf of Mexico and Gulf Stream (general storms);
2. Direct tropical system or remnant tropical moisture either from the Atlantic Ocean or Gulf of Mexico (tropical storms); and
3. Isolated thunderstorms/Mesoscale Convective Systems (local storms).

General storms which produce PMP-type rainfall are most frequent in the spring and fall. Tropical systems occur from June through November. Local storms which can produce PMP-type rainfall are most active from late spring through early fall, with an increase in activity during the summer (Smith et al., 1996; Smith et al., 2011). General storms associated with frontal systems do occur often in the winter season; however, these sometimes produce snow instead of rain, are associated with lower levels of moisture, and move through relatively quickly. These factors all limit the amount of total precipitation that can occur in the study region. These can produce significant flooding however, with March of 1936 and December of 2023 examples of these types of flooding events.

The PMP storm types investigated during the study were local thunderstorms/Mesoscale Convective Systems (MCS) where the main rainfall occurs over short durations and small area sizes, general storms where main rainfall occurs over large areas sizes and longer durations, and tropical systems which occur less frequently and have accumulation characteristics similar to the general storm type with imbedded short burst of heavy rainfall. The unique temporal patterns

associated with each of these storm types were explicitly investigated and applied to PMP outputs. Numerous discussions and testing of PMP outputs were completed by AECOM and Hazen and Sawyer as part of this study. This was an important aspect of this study, as it allowed for direct application of the PMP depths for hydrologic testing and evaluation. This ensured that the PMP depths and outputs were thoroughly tested and evaluated from a hydrologic application perspective and are appropriate for use in deriving the PMF.

The classification of storm types, and hence PMP development by storm type used in this study, is similar to descriptions provided in several HMRs (e.g., HMR 55A Section 1.5). Storms were classified by rainfall accumulation characteristics, while trying to adhere to previously used classifications. In addition, the storm classifications were cross-referenced with the storm typing completed as part of several other AWA PMP studies in the region (e.g., (Beaver Valley-Kappel et al., 2014; Tennessee Valley Authority-Kappel et al., 2015a; Virginia-Kappel et al., 2015b; Colorado-New Mexico-Kappel et al., 2018; Pennsylvania-Kappel et al., 2019; North Dakota-Kappel et al., 2021; New Jersey-Kappel et al., 2023) to ensure consistency with adjacent studies.

Local storms were defined using the following guidance:

- The main rainfall accumulation period occurred over a 6-hours or less
- Previously classified as a local storm by the USACE, in the HMRs, or adjacent studies
- Not associated with overall synoptic patterns leading to rainfall across large regions
- Exhibited high intensity accumulations over short periods (i.e., 1-hour or less)
- Occurred during the appropriate season, spring through fall

General storms were defined using the following guidance:

- The main rainfall accumulation period lasted for 24 hours or longer
- Occurred with a synoptic environment associated with a low-pressure system, frontal interaction, and/or regional precipitation coverage
- Was previously classified as a general storm by the USACE, in the HMRs, or adjacent studies
- Exhibited lower rainfall accumulation intensities compared to local storms

Tropical storms were defined using the following guidance:

- The rainfall was a direct result of a tropical system, either landfalling or directly offshore and a warm core circulation
- Was previously classified as a tropical storm by the USACE, in the HMRs, or adjacent studies
- Occurred during the appropriate season, June through November

It should be noted that some of the storms exhibit characteristics of more than one storm type and therefore have been included for PMP development as more than one type. These are classified as hybrid storms.

3.1.1 Local Storms

Localized thunderstorms and MCSs can produce extreme amounts of precipitation for short durations and over small area sizes, generally 6 hours or less over area sizes of 500 square miles or less. During any given hour, the heaviest rainfall only covers small areas, generally less than 100 square miles. This is the result of sustained low-level moisture availability combined with atmospheric stability parameters required to create sustained lift through deep layers of the atmosphere. Because these ideal combined factors do not stay over the same location for sustained periods and cover small areas at a given time, limitations are applied to the local storm PMP for hydrologic application. Limitations are based on the DAD values from local storms used for PMP development in this study. For each of these local storms, the rainfall depths decrease rapidly after the 100-square mile area size, demonstrating that the ideal combination of moisture and stability are not maintained above this area size. Therefore, it is recommended that the local storm PMP only be applied to any individual basin of 100-square miles or less. This is consistent with other studies and reflects the PMP rainfall environment associated with local storms in Maryland.

Many of the storms previously analyzed by the USACE and NWS Hydrometeorological Branch, in support of pre-1979 PMP research, have features that indicate they were most likely Mesoscale Convective Complexes (MCCs) or MCSs. However, this nomenclature had not yet been introduced into the scientific literature, nor were the events fully understood. It is important to note that an MCC is a subset of the broader MCS category of mesoscale atmospheric phenomena. Another example of an MCS is the derecho, an organized line of thunderstorms that are notable for strong winds and resultant significant straight-line wind damage. On rare occasions derechos will move through the region generally from west to east and produce significant straight line wind damage and brief heavy rainfall.

For the study domain east of the Appalachian crest the MCC storm type is not common. Instead, these storms take on a different form, which includes interaction with a front or remnant tropical moisture (Letkewicz and Parker, 2010). This is because there is a lack of low-level jet (LLJ) east of the Appalachians. However, the MCS storm type is very important for determining PMP values for small area sizes and short durations.

Separate from MCC and MCS storm types, individual thunderstorms can be isolated from the overall general synoptic weather patterns and fueled by localized moisture sources. The local storm type in the region has a distinct seasonality, occurring during the warm season when the combination of moisture and atmospheric instability is at its greatest, most common from spring through fall. This is the time of the year when convective characteristics and moisture within the atmosphere are adequate to produce lift and instability needed for thunderstorm development and heavy rainfall.

Local storm PMP depths derived in this report are valid from spring through fall when no snowpack would co-occur and can be associated with various synoptic conditions. Local storm PMP depths should not be applied with snowpack on the ground as that would not allow the atmospheric instability and moisture levels to occur in combination that would produce convective initiation and PMP level local storm rainfall. Examples of the local storm type

include Jewell, MD July 1897, Ewan, NJ September 1940, Smethport, PA July 1942, Rapidan, VA June 1995, and Sparta, NJ August 2000.

3.1.2 General Storms

General storms occur in association with frontal systems and along boundaries between sharply contrasting air masses. Precipitation associated with frontal systems is enhanced when the movement of weather patterns slow or stagnates, allowing moisture and instability to affect the same general region for several days. In addition, when there is a larger than normal thermal contrast between air masses in combination with higher than normal moisture, PMP-level precipitation can occur. The processes can be enhanced by the effects of topography, with heavier precipitation occurring along and immediately upwind of upslope regions. Intense regions of heavy rain can also occur along a front as a smaller scale disturbance moving along the frontal boundary, called a shortwave, creating a region of enhanced lift and instability. These shortwaves are not strong enough to move the overall large-scale pattern, but instead add to the storm dynamics and energy available for producing precipitation.

This type of storm will usually not produce the highest rainfall rates over short durations, but instead results in flooding situations as moderate rain continues to fall over the same region for an extended period of time. This storm is not expected to control PMP depths for any basins less than 10-square miles. Therefore, it is recommended that the general storm PMP only be applied to any individual basin larger than 10-square miles.

The seasonality of general storms varies, but the general storm PMP depths produced in this study are assumed to be a rainfall only event where melting snow would not contribute significantly to runoff. Although they can occur at almost any time of the year, they are most likely to produce flooding rainfall during spring and fall. Strong frontal systems do affect many parts of the region in winter. However, most of the precipitation occurs in the form of snow or moves through too quickly to produce PMP level rainfall. Therefore, the full general storm PMP depths should not be used when significant snowpack is present. Instead, an adjustment to the general storm PMP depths should be applied when utilized as a rain-on-snow event. It is suggested that cool-season PMP depths be derived when this is required through a site-specific evaluation or use of HMR 33 (Riedel et al., 1956). It is assumed that rain-on-snow runoff scenarios that would result in a PMF larger than the warm-season general storm PMP/PMF would only occur in very large basins, generally greater than 20,000-mi^2 and therefore do not affect the dams regulated by MDE in the study domain.

3.1.3 Tropical Storms

Tropical systems directly impact the study region on a relatively frequent basis. When these systems move slowly over the area, large amounts of rainfall can be produced both in convective bursts and over longer durations. These types of storms require warm water and proper atmospheric conditions to be in place over the Gulf of Mexico and Atlantic Ocean, and therefore only form from June through November, with August and September being the most common period of tropical storm activity in this region. Significant research is available on past tropical systems affecting the study region including strike probability for a given location per year (e.g., Keim et al., 2007).

3.1.4 Hybrid Storms

Hybrid storms include characteristics of more than one storm type. In this study, three storms were considered hybrid events. One was classified as both a local and tropical storm (Hector, NY July 1935 SPAS 1629) and two storms were classified as general and tropical storms (Big Meadows, VA, October 1942 SPAS 1340 and Montgomery Dam, PA September 2004 SPAS 1275). These were applied as each storm type for PMP development to ensure inclusion for overall PMP development.

4. Topographic Effects on Precipitation

Terrain plays a significant role in precipitation development, magnitudes, and accumulation patterns in time and space. The terrain within the region both enhances and depresses precipitation depending on whether the terrain is forcing the air to rise (upslope effect) or descend (downslope effect). To account for the effect of precipitation by terrain features (called orographic effects) evaluations were performed using precipitation frequency climatologies and investigations into past storm spatial and accumulation patterns across the region. NOAA Atlas 14 precipitation frequency climatologies (Bonin et al., 2004; Perica et al., 2013a; Perica et al., 2013b) were used in this analysis. These climatologies were used to derive the GTF and the spatial distribution of the PMP. This approach is similar to the use of the NOAA Atlas 2 100-year 24-hour precipitation frequency climatologies used in HMRs 55A (Sections 6.3 and 6.4, Hansen et al., 1988), HMR 57 (Section 8.1, Hansen et al., 1994), and HMR 59 (Sections 6.6.1 and 6.6.2, Corrigan et al., 1999) as part of the Storm Separation Method (SSM) to quantify orographic effects in topographically significant regions.

The terrain within the study domain analyzed varies from sea level to elevated terrain in the western regions (Figure 4.1). When incoming air is forced to rise as it encounters elevated terrain, release of conditional instability can occur more effectively and enhance the conversion of moisture in the air to precipitation. These interactions must be considered in the PMP determination procedures including storm adjustment processes and determination of transposition limits.

The quantification of terrain effects was completed by evaluating rainfall depths at the 100-year recurrence interval using the 6-hour duration for local storms and the 24-hour duration for tropical and general storms at both the source (storm center) and target (grid point) location. This comparison produced a ratio that quantified the differences of precipitation processes, including terrain, between the two locations. The assumption is that the precipitation frequency data represent all aspects that have produced precipitation at a given location over time, including the effect of terrain. Therefore, if two locations are compared within regions of similar meteorological and topographical characteristics, the resulting difference of the precipitation frequency climatology should reflect the difference of all precipitation processes between the two locations, including topography, access to moisture, coastal convergence, seasonality, etc.

This relationship between precipitation frequency climatology and terrain is also recognized in the WMO PMP Manual (WMO, 1986 pg. 54) and by the Australian Bureau of Meteorology (Section 3.1.2.3 of Minty et al., 1996). Although the terrain effects at a particular location may vary from storm to storm, the overall effect (or lack thereof) is inherently included in the climatology of precipitation that occurred at that location, assuming that the climatology is based on storms of the same type. In WMO 2009 Section 3.1.4 it is stated "since precipitation-frequency values represent equal probability, they can also be used as an indicator of the effects of topography over limited regions. If storm frequency, moisture availability, and other precipitation-producing factors do not vary, or vary only slightly, over an orographic region, differences in precipitation-frequency values should be directly related to variations in orographic effects." Therefore, by applying appropriate transposition limits, analyzing by storm type, and utilizing the duration for storm typing, it is assumed the storms being compared using

the precipitation frequency data are of similar moisture availability and other precipitation-producing factors.

This assumption was evaluated and determined to be acceptable during the development of PMP in the adjacent statewide studies in Virginia, Pennsylvania, and New Jersey statewide studies and again evaluated in this study. Various sensitivity analyses and discussions with MDE, the review panel, and others involved in this study took place to determine how terrain influenced storm patterns and storm transposition limits.

These included testing of PMP depths from a spatial perspective, comparing the difference of using the single grid at the storm center location versus an area size of several grids around the storm center, and comparing resulting PMP depths against 100-year recurrence interval depths. In previous PMP studies, additional sensitivities and evaluations were completed through numerical modeling applications which included removing/adding topography (Volume IV of the Colorado-New Mexico Regional Extreme Precipitation Study, Kappel et al., 2018).

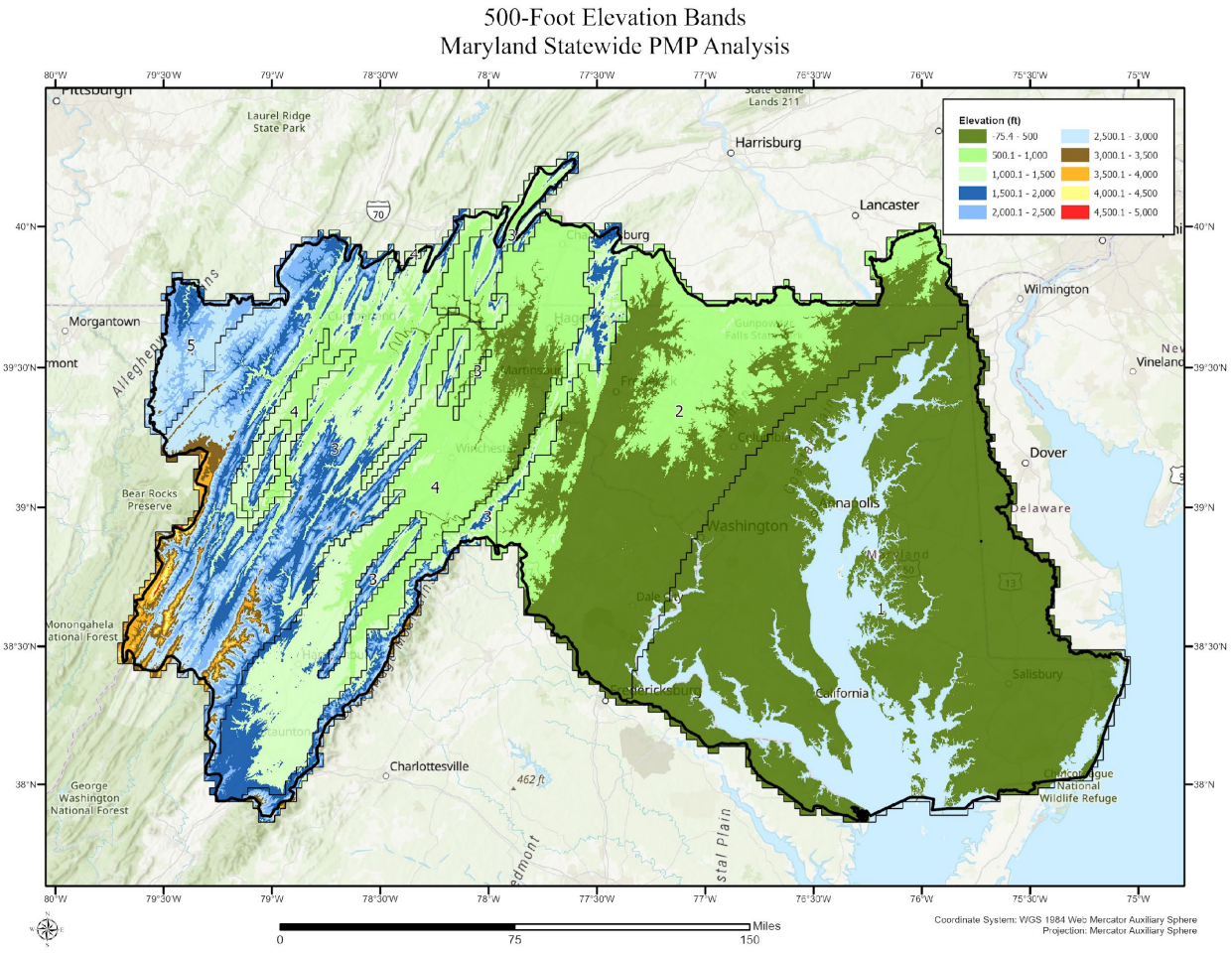

Figure 4.1: Elevation bands at 500-foot intervals over the region analyzed

5. Data Description and Sources

Detailed evaluations of potential storms to use for PMP development were conducted as part of this study. This included investigating the storm lists from previous relevant studies in the region (e.g., statewide studies in Ohio, Virginia, Pennsylvania, and New Jersey, as well as the regional PMP study for the Tennessee Valley Authority, and several site-specific studies within the region). The storm list and the updated storm search completed to augment those previous storm lists utilized data from the sources below:

1. Storm data and meteorological information from various Hydrometeorological Reports (e.g., 1, 33, 40, 51, and 52) each of which can be downloaded from the Hydrometeorological Design Studies Center website at https://www.weather.gov/owp/hdsc_pmp
2. Cooperative Summary of the Day / TD3200. These data are published by the National Centers for Environmental Information (NCEI), previously the National Climatic Data Center (NCDC). These are stored on AWA's database server and can be obtained directly from the NCEI.
3. Hourly Weather Observations published by NCEI, U.S. Environmental Protection Agency, and Forecast Systems Laboratory (now National Severe Storms Laboratory). These are stored on AWA's database server and can be obtained directly from NCEI.
4. NCEI Recovery Disk. These are stored on AWA's database server and can be obtained directly from the NCEI.
5. U.S. Army Corps of Engineers Storm Studies (USACE, 1973).
6. United States Geological Survey (USGS) Flood Reports.
7. Other data published by NWS offices. These can be accessed from the National Weather Service homepage at http://www.weather.gov/.
8. Data from supplemental sources, such as Community Collaborative Rain, Hail, and Snow Network (CoCoRaHS), Weather Underground, Forecast Systems Laboratories, RAWS, and various Google searches.
9. Previous and ongoing PMP and storm analysis work (Tomlinson et al., 2008-2013; Kappel et al., 2013-2023).
10. Peer reviewed journals (e.g., Dwight, 1822; Smith et al., 1996; Keim 1998; Pontrelli et al., 1999; Konrad, 2001; Robinson et al., 2001; Hicks et al., 2005; Keim et al., 2007; Smith et al., 2010; Smith et al., 2011; Keim et al., 2018).

5.1 Use of Dew Point Temperatures for Storm Maximizations

HMR and WMO procedures for storm maximization use a representative storm dew point as the parameter to represent available moisture to a given storm. Prior to the mid-1980s, maps of maximum 12-hour persisting dew point values from the *Climatic Atlas of the United States* (EDS, 1968) were the source for maximum dew point values. This study used the 100-year return frequency dew point climatology, which is periodically updated by AWA. Storm precipitation amounts were maximized using the ratio of precipitable water for the maximum dew point to precipitable water for the storm representative dew point, assuming a vertically saturated atmosphere through 30,000 feet. The precipitable water values associated with each storm representative value were taken from the WMO Manual for PMP Annex 1 (1986).

The use of the 100-year recurrence interval dew point climatology in the maximization process is appropriate because it provides a sufficiently rare occurrence of moisture level when combined with the maximum storm efficiency to produce a combination of rainfall producing mechanisms that could physically occur. Recent research has shown that the assumption of combining the maximum storm efficiency with the maximum dew point value results in the most conservative combination of storm parameters and hence the most conservative PMP depths when considering all the possibilities of PMP development (Ben Alaya et al., 2018).

An envelope of maximum dew point values is no longer used because in many cases the maximum observed dew point values do not represent a meteorological environment that would produce rainfall, but instead often represents a local extreme moisture value that can be the result of local evapotranspiration and other factors not associated with a storm environment and fully saturated atmosphere. Also, data availability increased significantly since the publication of the maximum dew point climatologies used in HMR 51. Hourly dew point observations became standard at all first-order NWS weather stations starting in 1948. This has allowed for a sufficient period of record of hourly data to exist from which to develop the climatologies out to the 100-year recurrence interval. These data were not available in sufficient quantity and period of record during the development of HMR 51.

Maximum dew point climatologies are used to determine the maximum atmospheric moisture that could have been available. Prior to the mid-1980s, maps of maximum dew point values from the *Climatic Atlas of the United States* (EDS, 1968) were the source for maximum dew point values. For the region covered by HMR 49, HMR 50 (Hansen and Schwartz, 1981) provided updated dew point climatologies. HMR 55A contained updated maximum dew point values for a portion of the United States from the Continental Divide eastward into the Central Plains. HMR 57 updated the 12-hour persisting dew points values and added a 3-hour persisting dew point climatology. The regional PMP study for Michigan and Wisconsin produced dew point frequency maps representing the 50-year recurrence interval. The choice to use a recurrence interval and average duration was first determined to be the best representation of the intent of the process during the Electric Power Research Institute (EPRI) Michigan/Wisconsin region PMP study (Section 2-1 and 7, Tomlinson, 1993). That study included original authors of HMR 51 on the review board.

The EPRI study was conducted using an at-site method of analysis with L-moment statistics. The review committee for that study included representatives from NWS, FERC, Bureau of Reclamation, and others. They agreed that the 50-year recurrence interval values were appropriate for use in PMP calculations. For the Nebraska statewide study (Tomlinson et al., 2008), the review committee and FERC Board of Consultants agreed that the 100-year recurrence interval dew point climatology maps were appropriate because their use added a layer of conservatism over the 50-year return period. This has subsequently been utilized in all PMP studies completed by AWA. This study is again using the 100-year recurrence interval climatology constructed using dew point data updated through 2018 (Figure 5.1).

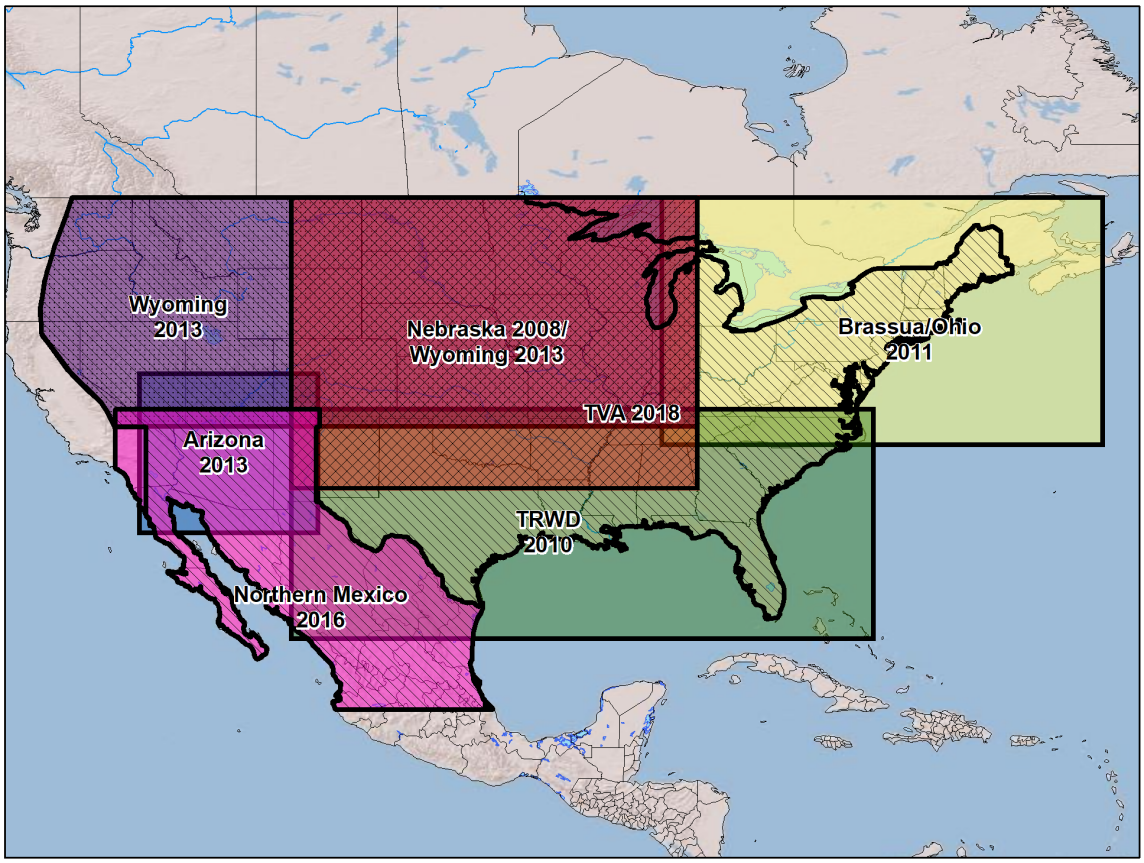

Figure 5.1: Maximum dew point climatology development regions and dates

5.2 Use of Sea Surface Temperatures for Storm Maximizations

Dew point observations for use in storm maximizations are not available over ocean regions. Therefore, when the source region of atmospheric moisture advecting into a rainfall event originates from over the ocean, a substitute for dew points observations is required. The NWS adopted a procedure for using SSTs as surrogates for dew point data (U.S. Navy Marine Climate Atlas, 1981). The value used as the maximum SST in the PMP calculations is determined using the SSTs two standard deviations warmer (+2 sigma) than the mean SST (Worley et al., 2005; Kent et al., 2007; and Reynolds et al., 2007). This provides a value for the maximum SST that has a probability of occurrence of about 0.025 (i.e., about the 40-year recurrence interval value). Use of the mean plus 2-sigma SSTs is consistent with the NWS procedure used in HMRs 57 and 59 (e.g., HMR 57 Section 4.3). These discussions note that SSTs change slowly in time and space when compared to surface-based dew points. In addition, AWA has completed evaluations of the difference between +2 and +3 sigma SSTs in the Atlantic Ocean and Gulf of Mexico. These showed only small differences, less than a 0.5°F. This is well within the rounding error and uncertainty involved in developing the storm representative values. Therefore, we continue to utilize the +2 sigma for consistency with use in the HMRs and all past AWA studies where SST are utilized for storm maximizations.

HYSPLIT model output provides detailed analyses for determining the upwind trajectories of atmospheric moisture that was advected into the storm systems. Using these trajectories as general guidance, the moisture source locations can be investigated. This is especially helpful over ocean regions where surface data are lacking to help with guidance in determining the moisture source region for a given storm. The procedures followed are similar to the approach used in HMR 59. However, by utilizing the HYSPLIT model trajectories, much of the subjectivity is eliminated. Further, details of each evaluation can be explicitly provided, and the results are reproducible. These trajectories extend over cooler coastal ocean currents immediately offshore in New England to the warmer regions of the ocean (over the Gulf Stream) that provide the atmospheric moisture that is later converted to rainfall by the storm system. Use of SSTs for in-place maximization and storm transpositioning follow a similar procedure to that used with land-based surface dew points. Use of the HYSPLIT model provides a significant improvement in determining the inflow wind vectors compared to older methods of extrapolating coastal wind observations and estimating moisture advection from synoptic features over the ocean. This more objective procedure is especially useful for situations where a long distance is involved to reach warmer ocean regions.

Timing is not as critical for inflow wind vectors extending over the oceans since SSTs change very slowly with time compared to dew point values over land. What is important is the changing wind direction, especially for situations where there is curvature in the wind fields. Any changes in wind curvature and variations in timing are inherently captured in the HYSPLIT model re-analysis fields, thereby eliminating another subjective parameter.

The start time of HYSPLIT is determined using the rainfall mass curves from the region of maximum rainfall associated with a given storm event. The location of the storm representative SST was determined by identifying the location where the SSTs are generally changing less than 1-2°F in an approximate 1° x 1° latitude and/or longitude distance following the inflow vector upwind. This is used to identify the homogeneous (or nearly homogeneous) region of SSTs associated with the atmospheric moisture source for the storm being analyzed. The value from the SST daily analysis for that location is used for the storm representative SST. The storm representative SST becomes a surrogate for the storm representative dew point in the maximization procedure.

The value for the maximum SST was determined using the mean +2 sigma (two standard deviations warmer than the mean) SST for that location. SSTs were substituted for dew points in this study for several storms where the inflow vector originated over the Atlantic Ocean. The data presented in Appendix F shows the moisture source region for each storm and whether dew points or SSTs were used in the maximization calculations. For storm maximization, the value for the maximum SST is determined using the mean +2 sigma SST for that location for a date two weeks before or after the storm date (whichever represents the climatologically warmer SST period). Storm representative SSTs and the mean +2 sigma SSTs are used in the same manner as storm representative dew points and maximum dew point climatology values in the maximization and transpositioning procedure.

6. Data Quality Assurance and Quality Control

During the development of the deterministic PMP depths, quality assurance (QA) and quality control (QC) measures were in-place to ensure data used were free from errors and processes followed acceptable scientific procedures. QA/QC procedures were in-place internally from AWA and externally from MDE, the review panel, and other study participants.

Numerous QA/QC checks are part of the SPAS algorithms and are included in each SPAS analysis. These include gauge quality control, gauge mass curve checks, statistical checks, gauge location checks, co-located gauge checks, rainfall intensity checks, observed versus modeled rainfall checks, ZR relationship checks (if radar data are available). These data QA/QC measures help ensure accurate precipitation reports, ensure proper data analysis and compilation of values by duration and area size, and consistent output of SPAS results. For additional information on SPAS, the data inputs, modeled outputs, and QA/QC measures, see Appendix E. For the storm adjustment process, internal QA/QC included validation that all IPMF were 1.00 or greater, that the MTF was set to 1.00, that upper (1.50) and lower (0.50) limits of the GTF were applied, and that any unique GTF limits were appropriate.

Maps of gridded GTF values were produced to cover the PMP analysis domain (Appendix B). These maps serve as a tool to spatially visualize and evaluate adjustment factors. Spot checks were performed at various positions across the domain and calculations were completed via Excel file equations to verify adjustment factor calculations are consistent. Internal consistency checks were applied to compare the storm data used for PMP development against previous PMP studies including Virginia (Kappel et al., 2015), Pennsylvania (Kappel et al., 2019), New Jersey (Kappel et al., 2023), and numerous site-specific studies in the region (Kappel et al., 2014-2022). Comparisons against HMR 51 PMP depths and other data such as NOAA Atlas 14 precipitation depths, and world record rainfall depths were completed.

Maps of each PMP version (see Appendix I for the Version Log notes) were plotted at standard area sizes and durations to ensure proper spatial continuity of PMP depths. Updates were applied to ensure reasonable gradients and depths based on overall meteorological and topographical interactions. The PMP tool utilized in this study employs very few calculations, however, the script utilizes Python's 'try' and 'except' statements to address input that may be unsuitable or incorrect.

MDE, AECOM, and Hazen and Sawyer completed external QA/QC on several important aspects of the PMP development. Each explicitly evaluated storms used for PMP development, the transposition limits of important storms, the storm representative values for each storm, and applied the hydrology to derive the PMF for sample basins across the region.

7. Storm Selection for PMP Calculations

7.1 Storm List Development Process

The initial search began with identifying storms that had been used in other PMP studies in the region covered by the storm search domain (Figure 7.1). These storm lists were combined to produce an initial list of storms for this study. As mentioned in Section 5, previous lists analyzed included the Ohio PMP study (2013), the Virginia PMP study (2015), the Tennessee Valley Authority regional PMP study (2015), the Pennsylvania statewide PMP study (2019), the New Jersey PMP study (2023), and the numerous site-specific PMP studies in the region (see Figure 7.2). The storm search included storms extending from the early 1800's through the course of this study. The oldest storm used in the study was from July 1819, herefore, more than 200 years of storm data were considered which provides a robust database from which to derive PMP-type storms.

These previous storms lists were updated with data through the course of this study and from other reference sources such as HMRs, USGS, USACE, USBR, state climate center reports, and NWS reports. In addition, discussions with MDE and other project participants were reviewed to identify dates with large rainfall amounts for locations within the storm search domain.

Storms from each of these sources were evaluated to see if they occurred within the initial storm search domain shown in Figure 7.1 and were previously important for PMP development. Next, each storm was analyzed to determine whether it was included on the short list for any of the previous studies, whether it was used in the relevant HMRs, and/or whether it produced an extreme flood event. Storms included on the initial storm list all exceeded the 100-year return frequency value for specified durations at the station location.

Each storm was then classified by storm type (e.g., local, general, tropical) based on their accumulating characteristics and seasonality as discussed in Section 2. Storm types were discussed with the review board to ensure concurrence and cross-referenced with previous storm typing to ensure consistency. The storms were then grouped by storm type, storm location, and duration for further analysis to define the final short list of storms used for PMP development. These storms were plotted and mapped using GIS to better evaluate the spatial coverage of the events throughout the region by storm type to ensure adequate coverage for PMP development.

The recommended storm list was presented to MDE, the review panel, and other study participants for discussion and evaluation. The recommended short list of storms was based on the above evaluations and experience with past studies and relevance for this project. The recommended short storm list was discussed in detail during review meetings and subsequently through the end of the project as various iterations of the PMP were developed. A few storms were removed from final consideration because of transposition limits and others were classified as hybrid events when they exhibit rainfall accumulation characteristics of more than one storm type. Iterations of how each storm was used can be found in the PMP Version Log provided in Appendix I.

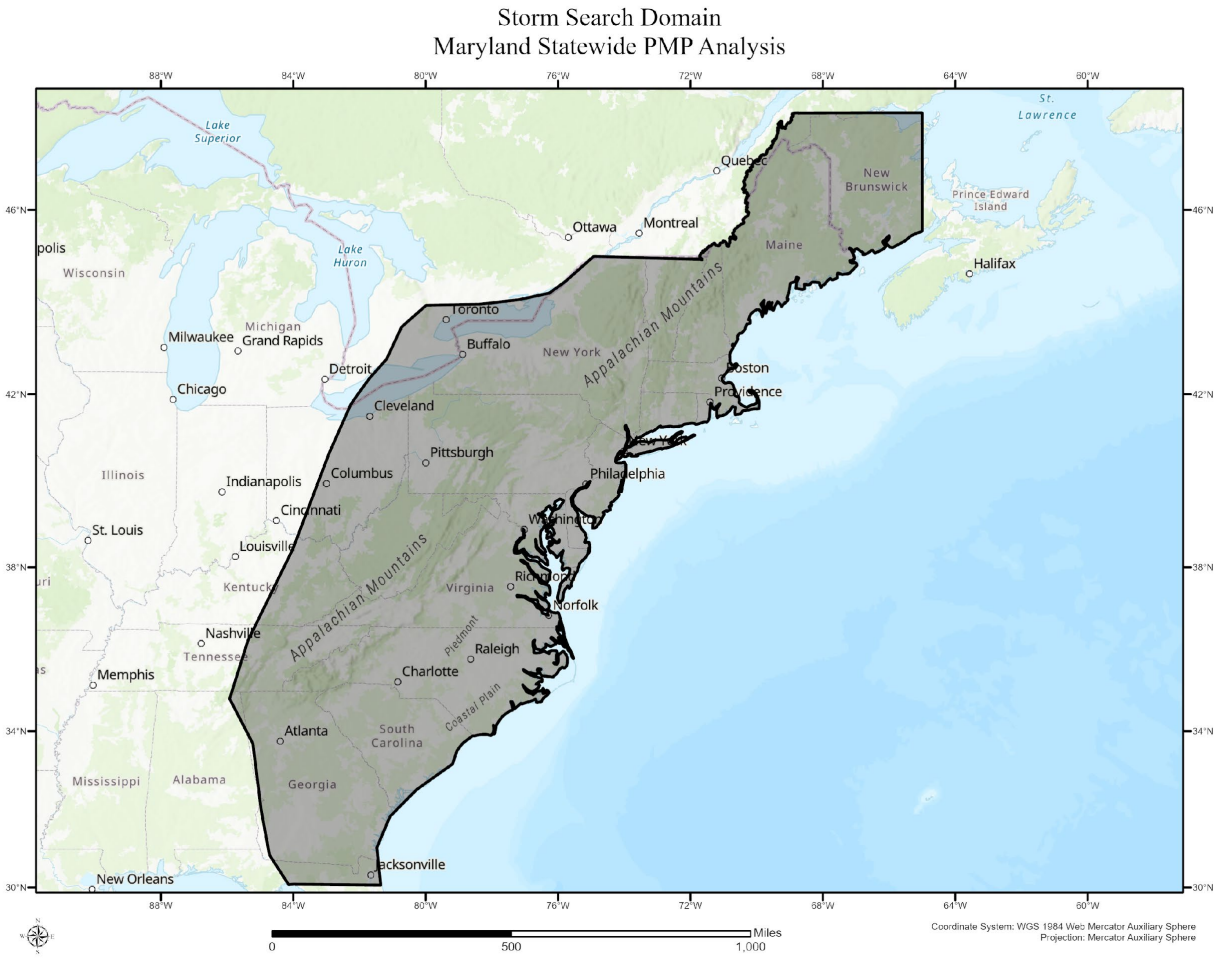

Figure 7.1: Initial storm search domain used for initial storm identification

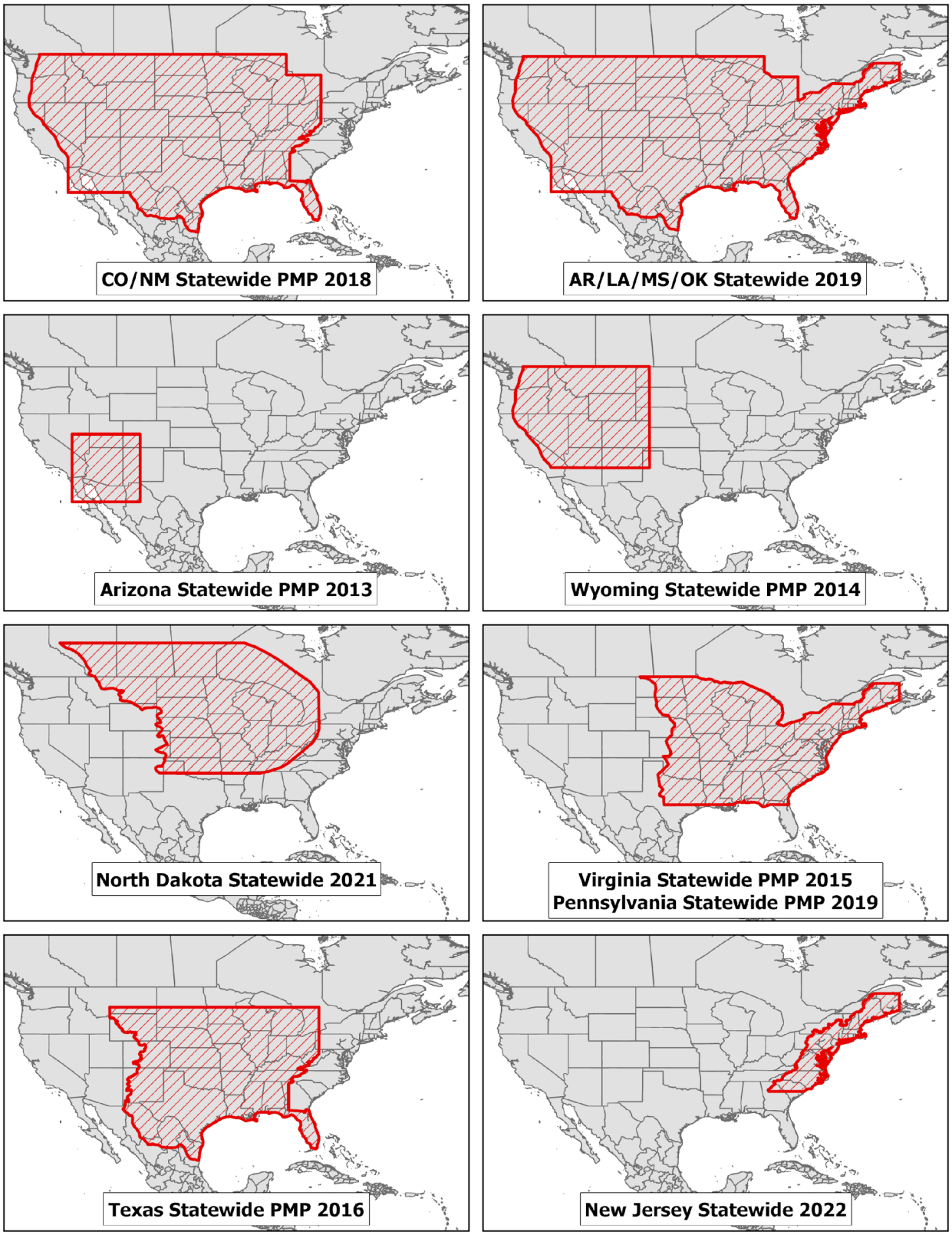

Figure 7.2: Previous AWA Statewide PMP studies storm search domains

From the initial storm list, the storms to be used for PMP development were identified and moved to the recommended short storm list. Each storm was investigated using both published and unpublished references described above and AWA PMP studies to determine its significance in the rainfall and flood history of surrounding regions. These included evaluations and comparisons of the storms, discussions of each storm's effects in the location of occurrence, discussion of storms in regions that were underrepresented, discussion of storms importance for PMF development in previous design analyses, and other meteorological and hydrological relevant topics.

Consideration was given to each storm's transpositionability within the overall domain and each storm's relative magnitude compared to other similar storms on the list and whether another storm of similar storm type was significantly larger. In this case, what is considered is whether after all adjustments are applied a given storm would still be smaller than other storms used. To determine this, several evaluations were completed. These included how a given storm was used of the storm in previous PMP studies, comparison of the precipitation values at area sizes relevant to the basin, and comparison of precipitation values after applying a 50% maximum increase to the observed values.

7.2 Final PMP Storm List Development

The final storm list used to derive PMP depths for this study considered each of the discussions in the previous sections in detail. Each storm on the final short storm list exhibited characteristics that were determined to be possible over some portion of the overall study domain. The storms that made it through these final evaluations were placed on the PMP storm list (Table 7.1 and Figure 7.3). Figure 7.4, Figure 7.5, and Figure 7.6 provide the short list storms by storm type with a callout providing the storm name and date that can be cross-referenced with the information provided in Table 7.1. Each of these storms were fully analyzed in previous PMP studies or as part of this study using the SPAS process (Appendix E). Note, Sparta, NJ SPAS 1674 is an updated analysis of SPAS 1017 used in the Pennsylvania and Virginia statewide studies. Similarly, Wellsboro, PA SPAS 1339 has been updated to include three DAD zones vs the single DAD zone used in the previous studies.

Ultimately, only a subset of the storms on the short list control PMP depths at a given location for a given duration, with most providing support for the PMP depths.

The PMP storm list contains 77 unique SPAS storm Depth-Area-Duration (DAD) zones, far more storms than were ultimately controlling of the PMP depths. This is one of the steps that helps to ensure no storms were omitted which could have affected PMP depths after all adjustment factors were applied. The conservative development of the PMP storm list is completed because the final magnitude of the rainfall accumulation associated with a given storm is not known until all the total adjustment factors have been calculated and applied. In other words, a storm with large point rainfall values may have a relatively small total adjustment factor, while a storm with a relatively smaller but significant rainfall value may end up with a large total adjustment factor. The combination of these calculations may provide a total adjusted rainfall value for the smaller rainfall event that is greater than the larger rainfall event after all adjustments are applied.

Table 7.1Storm list used for PMP developments

SPAS_ID	Storm Name	State	Lat	Lon	Year	Month	Day	Max Rainfall	Elevation	Storm Rep Analysis	Storm Rep Dew Point/SST	Adjusted In Place Max Dew	In Place Max Dew Point/SST	In Place Max Factor	Tdor SST	TD_DATE	Storm Rep Lat	Storm Rep Lon	TYPE
SPAS_1339_1	WELLSBORO	PA	41.7042	-77.2292	1889	5	30	10.11	1842	24	77.00	81.00	80.91	1.21	SST	15-Jun	34.00	-76.00	General
SPAS_1339_2	WELLSBORO	PA	40.9042	-78.5958	1889	5	30	8.99	1562	24	77.00	81.00	80.91	1.21	SST	15-Jun	34.00	-76.00	General
SPAS_1339_3	WELLSBORO	PA	40.3958	-76.9292	1889	5	30	9.19	389	24	77.00	81.00	80.91	1.21	SST	15-Jun	34.00	-76.00	General
SPAS_1566_1	PATERSON	NJ	40.9375	-74.1375	1903	10	8	15.96	60	24	72.50	78.00	78.14	1.30	SST	25-Sep	37.50	-72.50	General
SPAS_1514_1	VADE MECUM	NC	36.3125	-80.2792	1908	8	23	17.97	803	24	82.50	85.00	85.14	1.11	SST	15-Aug	31.00	-78.20	General
SPAS_1195_2	PADDY MOUNTAIN	WV	39.0200	-78.5600	1936	3	16	8.32	2212	24	68.00	72.50	72.25	1.26	SST	1-Apr	34.00	-73.00	General
SPAS_1346_1	BLUE RIDGE DIVIDE	NC	35.0375	-83.0792	1940	8	28	14.09	3267	12	76.00	81.00	81.08	1.29	Td	15-Aug	30.50	-86.50	General
SPAS_1680_1	WEST SHOKAN	NY	42.0042	-74.3958	1955	10	14	20.27	3548	24	78.00	81.50	81.56	1.19	SST	1-Oct	35.00	-71.00	General
SPAS_1312A_2	ROSMAN	NC	35.1458	-82.8042	1964	9	26	17.86	2271	24	74.50	78.00	78.11	1.19	Td	15-Sep	30.65	-82.50	General
SPAS_1380_1	BURTON DAM	GA	34.7958	-83.6958	1967	8	21	18.42	3720	24	73.50	80.00	79.85	1.40	Td	7-Aug	31.00	-85.00	General
SPAS_1362_2	ROBBINSVILLE	VA	35.3208	-83.6875	1977	4	2	9.21	4727	24	72.50	75.50	75.29	1.18	Td	20-Apr	30.00	-89.50	General
SPAS_1533_1	MONTEBELLO	VA	37.8125	-79.1625	1985	11	1	22.56	3892	24	76.50	79.50	79.51	1.17	SST	17-Oct	35.00	-73.00	General
SPAS_1201_1	HALIFAX	VT	42.7699	-72.7500	2005	10	7	15.40	1485	24	80.00	82.50	82.66	1.13	SST	24-Sep	32.00	-67.00	General
SPAS_1047_1	TAMAQUA	PA	41.6750	-75.3750	2006	6	26	12.26	1260	24	70.50	76.00	76.10	1.31	Td	10-Jul	40.10	-74.70	General
SPAS_1350_1	NEW BERN	NC	35.1750	-77.2150	2010	9	27	23.44	39	24	81.50	84.00	84.20	1.11	SST	15-Sep	30.00	-73.00	General
SPAS_1298_1	HARRISBURG	PA	39.9850	-76.4950	2011	9	4	18.32	226	24	81.50	84.00	83.79	1.11	SST	20-Aug	33.00	-74.00	General
SPAS_1564_1	MOUNT PLEASANT	SC	32.8950	-79.7650	2015	10	1	27.97	8	24	83.00	84.30	84.50	1.07	SST	17-Sep	31.00	-76.50	General
SPAS_1629_1	HECTOR	NY	42.5042	-76.7958	1935	7	6	14.27	1828	24	81.00	83.00	82.78	1.11	SST	15-Jul	35.00	-74.75	Hybrid (G/L)
SPAS_1340_1	BIG MEADOWS	VA	38.5458	-78.4042	1942	10	12	19.77	3299	24	78.00	81.50	81.25	1.19	SST	1-Oct	34.00	-70.00	Hybrid (G/T)
SPAS_1275_2	MONTGOMERY DAM	PA	40.6050	-76.4650	2004	9	18	8.80	1602	12	72.00	77.50	77.29	1.32	Td	1-Sep	40.64	-82.30	Hybrid (G/T)
SPAS_1547_1	CATSKILL	NY	42.1842	-73.8688	1819	7	27	18.23	1	6	72.50	78.50	78.28	1.13	Td	15-Jul	40.75	-72.95	Local
SPAS_1944_1	ROCKPORT	WV	39.0625	-81.5375	1889	7	18	21.07	926	6	79.50	81.50	81.50	1.10	Td	15-Jul	38.00	-86.00	Local
SPAS_1489_1	JEWELL	MD	38.7290	-76.5710	1897	7	26	15.88	163	12	71.50	80.50	80.31	1.50	SST	10-Aug	38.00	-73.50	Local
SPAS_1343_1	JOHNSON CITY	TN	36.3042	-82.0625	1924	6	13	16.14	3137	6	77.50	80.50	80.50	1.16	Td	27-Jun	30.70	-88.10	Local
SPAS_1344_1	SIMPSON	KY	38.1042	-83.2958	1939	7	4	20.82	1101	6	75.50	81.00	80.85	1.30	Td	18-Jul	39.83	-84.03	Local
SPAS_1534_1	EWAN	NJ	39.6875	-75.1807	1940	9	1	24.30	103	6	76.00	81.50	81.41	1.29	SST	15-Aug	37.27	-74.47	Local
SPAS_1681_1	SMETHPORT	PA	41.8438	-78.2687	1942	7	17	35.30	1799	6	77.50	80.50	80.45	1.03	Td	15-Jul	42.60	-82.83	Local
SPAS_1681_2	SMETHPORT	PA	41.7188	-78.0812	1942	7	17	26.67	2236	6	77.50	80.50	80.45	1.03	Td	15-Jul	42.60	-82.83	Local
SPAS_1681_3	SMETHPORT	PA	41.9729	-78.1937	1942	7	17	23.93	1571	6	77.50	80.50	80.45	1.03	Td	15-Jul	42.60	-82.83	Local
SPAS_1681_4	SMETHPORT	PA	41.9146	-77.8979	1942	7	17	32.76	2088	6	77.50	80.50	80.45	1.03	Td	15-Jul	42.60	-82.83	Local
SPAS_1681_5	SMETHPORT	PA	42.3563	-77.9479	1942	7	17	25.33	2111	6	77.50	80.50	80.45	1.03	Td	15-Jul	42.60	-82.83	Local
SPAS_1681_6	SMETHPORT	PA	41.6021	-78.5729	1942	7	17	20.41	2045	6	77.50	80.50	80.45	1.03	Td	15-Jul	42.60	-82.83	Local
SPAS_1536_1	GLENVILLE	WV	38.8958	-80.7708	1943	8	4	15.04	1113	6	78.50	80.50	80.44	1.10	Td	22-Jul	39.70	-83.50	Local
SPAS_1546_1	LITTLE RIVER	VA	38.8625	-79.1875	1949	6	17	15.13	2068	24	70.50	76.50	76.60	1.36	Td	30-Jun	38.83	-76.96	Local
SPAS_1402_1	LITTLE BARREN	TN	36.3625	-83.7208	1965	7	24	11.00	1066	6	77.00	81.50	81.28	1.24	Td	8-Aug	38.50	-87.00	Local
SPAS_1402_2	ROSEDALE	TN	36.1792	-84.2292	1965	7	24	13.32	2731	6	77.00	81.50	81.28	1.25	Td	8-Aug	38.50	-87.00	Local
SPAS_1362_1	COEBURN	VA	37.2792	-81.8042	1977	4	2	15.66	2296	24	72.50	75.50	75.29	1.17	Td	20-Apr	30.00	-89.50	Local
SPAS_1550_1	JOHNSTOWN	PA	40.3958	-78.9542	1977	7	18	12.64	2531	12	75.00	78.50	78.61	1.20	Td	15-Jul	39.50	-80.00	Local
SPAS_1406_1	RAPIDAN	VA	38.4150	-78.3350	1995	6	27	28.39	1288	6	82.00	84.00	83.84	1.09	SST	10-Jul	33.50	-77.00	Local
SPAS_1548_1	REDBANK	PA	41.2550	-79.1550	1996	7	19	9.42	1737	12	74.00	78.50	78.60	1.25	Td	15-Jul	40.20	-81.10	Local
SPAS_1818_1	ATLANTIC CITY	NJ	39.5050	-74.4350	1997	8	20	14.28	1	24	78.00	81.50	81.54	1.17	SST	6-Aug	37.00	-75.00	Local
SPAS_1674_1	SPARTA	NJ	41.0300	-74.6400	2000	8	11	16.70	796	12	68.00	77.00	77.07	1.50	Td	15-Aug	41.17	-73.44	Local
SPAS_1040_1	TABERNACLE	NJ	39.8812	-74.6895	2004	7	13	15.63	61	6	74.00	79.50	79.65	1.29	Td	30-Jul	38.34	-75.34	Local
SPAS_1049_1	DELAWARE COUNTY	NY	42.0100	-74.9000	2007	6	19	11.69	2157	6	71.00	77.50	77.34	1.39	Td	1-Jul	41.43	-74.90	Local
SPAS_1415_1	ISLIP	NY	40.8050	-73.0650	2014	8	13	14.23	80	24	76.50	80.00	79.75	1.18	SST	15-Aug	38.50	-73.00	Local
SPAS_1700_1	ELLICOTT CITY	MD	39.2650	-76.7550	2018	5	27	14.22	404	6	73.50	77.00	77.10	1.18	Td	10-Jun	38.41	-77.69	Local
SPAS_1628_1	JEFFERSON	OH	41.8458	-80.8375	1878	9	10	15.01	665	24	72.50	77.00	77.16	1.25	Td	27-Aug	40.00	-84.00	Tropical
SPAS_1565_1	PATERSON	NJ	40.8875	-74.0958	1882	9	20	17.88	52	24	80.00	83.00	82.88	1.15	SST	7-Sep	35.00	-69.00	Tropical
SPAS_1299_1	ALTA PASS	NC	35.8792	-81.8708	1916	7	13	24.90	1968	24	81.50	84.00	83.87	1.13	SST	30-Jul	32.00	-75.00	Tropical
SPAS_1299_2	KINGSTREE	NC	33.6625	-79.8292	1916	7	13	16.79	43	24	81.50	84.00	83.87	1.11	SST	30-Jul	32.00	-75.00	Tropical
SPAS_1516_1	GLENVILLE	GA	31.9458	-81.8875	1929	9	23	20.80	1793	24	82.00	85.00	85.03	1.14	SST	10-Sep	29.00	-79.00	Tropical
SPAS_1516_2	GLENVILLE	GA	34.8208	-84.1542	1929	9	23	20.88	1558	24	82.00	85.00	85.03	1.14	SST	10-Sep	29.00	-79.00	Tropical
SPAS_1517_2	MONCURE	NC	35.6042	-79.0708	1929	9	29	11.55	181	24	80.00	84.50	84.48	1.22	SST	15-Sep	31.00	-78.00	Tropical
SPAS_1517_3	SETTLE	NC	35.9458	-80.6958	1929	9	29	9.97	766	24	80.00	84.50	84.48	1.22	SST	15-Sep	31.00	-78.00	Tropical
SPAS_1490_1	EASTON	MD	38.8625	-76.0708	1935	9	4	17.00	55	24	80.50	83.00	82.91	1.12	SST	20-Aug	35.00	-73.00	Tropical
SPAS_1341_1	BUCK	CT	41.5542	-72.6542	1938	9	17	18.06	126	24	80.00	83.50	83.60	1.17	SST	5-Sep	32.00	-70.00	Tropical
SPAS_1567_1	TUCKERTON	NJ	39.6790	-74.2710	1939	8	19	18.07	19	24	81.00	83.00	82.90	1.09	SST	15-Aug	35.50	-72.50	Tropical
SPAS_1342_1	MT MITCHELL	NC	36.3000	-81.4500	1940	8	10	20.27	3064	24	82.00	84.00	83.90	1.10	SST	15-Aug	33.00	-74.00	Tropical
SPAS_1630_1	BOLTON	ONT	43.8375	-79.9792	1954	10	14	11.23	1250	24	68.00	71.50	71.51	1.19	Td	1-Oct	41.16	-81.35	Tropical
SPAS_1243_1	WESTFIELD	MA	42.1200	-72.7000	1955	8	17	18.93	265	24	75.00	77.00	76.77	1.11	Td	15-Aug	40.20	-74.25	Tropical
SPAS_1679_1	SLIDE MOUNTAIN	NY	42.0208	-74.3958	1955	8	11	15.20	2798	24	73.00	76.00	76.13	1.17	Td	5-Aug	40.80	-73.20	Tropical
SPAS_1312B_2	ROSMAN	NC	35.1375	-82.8375	1964	10	3	17.53	2440	24	75.50	77.50	77.73	1.11	Td	20-Sep	30.65	-82.50	Tropical
SPAS_1491_1	TYRO	VA	37.8125	-79.0042	1969	8	19	27.23	800	12	77.50	79.50	79.68	1.10	Td	5-Aug	36.08	-79.95	Tropical
SPAS_1276_1	WELLSVILLE	NY	42.0375	-78.0708	1972	6	18	18.78	2398	24	72.50	78.00	78.04	1.33	Td	5-Jul	36.50	-79.15	Tropical
SPAS_1276_2	ZERBE	PA	40.5375	-76.6208	1972	6	18	18.79	1617	24	78.00	80.50	80.25	1.12	SST	5-Jul	36.00	-67.00	Tropical
SPAS_1373_1	ANTREVILLE	SC	34.8550	-82.2250	1995	8	26	19.99	733	24	82.50	85.50	85.55	1.13	SST	15-Aug	29.00	-78.00	Tropical
SPAS_1552_1	SOUTHPORT	NC	34.0050	-77.9950	1999	9	14	24.30	31	24	78.00	83.00	82.81	1.25	SST	1-Sep	35.00	-72.00	Tropical
SPAS_1552_2	YORKTOWN	VA	37.2750	-76.5550	1999	9	14	19.22	0	24	78.00	83.00	82.81	1.25	SST	1-Sep	35.00	-72.00	Tropical
SPAS_1552_3	POMPTON LAKE	NJ	40.9950	-74.2850	1999	9	15	14.62	214	24	77.50	82.50	82.34	1.26	SST	1-Sep	36.33	-72.00	Tropical
SPAS_1552_4	CAIRO	NY	42.2950	-74.0050	1999	9	15	11.71	412	24	77.50	82.50	82.34	1.26	SST	1-Sep	36.33	-72.00	Tropical
SPAS_1535_2	UPPER SHERANDO	VA	37.9125	-79.0292	2003	9	17	20.22	2284	24	80.50	83.00	83.23	1.14	SST	3-Sep	36.50	-70.50	Tropical
SPAS_1275_1	MONTGOMERY DAM	PA	40.6450	-80.3850	2004	9	18	8.79	1055	12	72.00	77.50	77.29	1.32	Td	1-Sep	40.64	-82.30	Tropical
SPAS_1551_1	RICHMOND	VA	37.7050	-77.3750	2004	8	30	14.38	182	6	81.00	83.00	83.15	1.09	SST	15-Aug	34.75	-72.50	Tropical
SPAS_1526_1	RALEIGH	NC	34.3350	-81.0050	2006	6	13	9.32	408	24	81.00	83.50	83.60	1.12	SST	29-Jun	29.00	-78.00	Tropical
SPAS_1224_1	MAPLECREST	NY	42.3000	-74.1600	2011	8	27	22.91	2264	12	81.50	83.50	83.32	1.10	SST	15-Aug	34.00	-72.00	Tropical
SPAS_1669_1	EVERGREEN	NC	34.4550	-78.8650	2016	10	6	19.12	103	24	82.50	84.00	84.19	1.07	SST	22-Sep	30.50	-77.00	Tropical
SPAS_1720_1	WRIGHTSVILLE BEACH	NC	34.2350	-77.7650	2018	9	14	43.29	0	24	82.00	83.00	83.23	1.04	SST	31-Aug	33.00	-73.00	Tropical

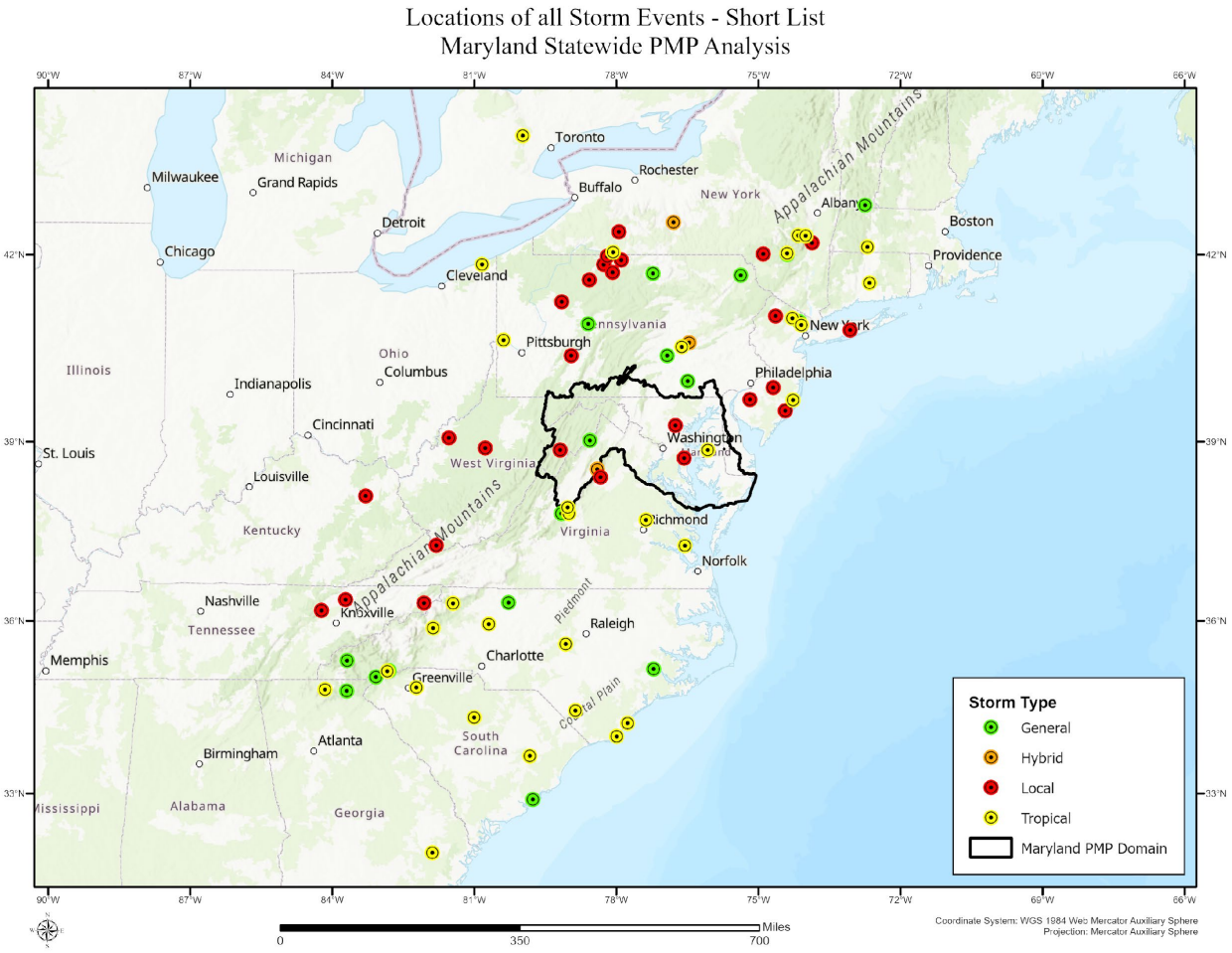

Figure 7.3: Storm list locations, all storms used for PMP development

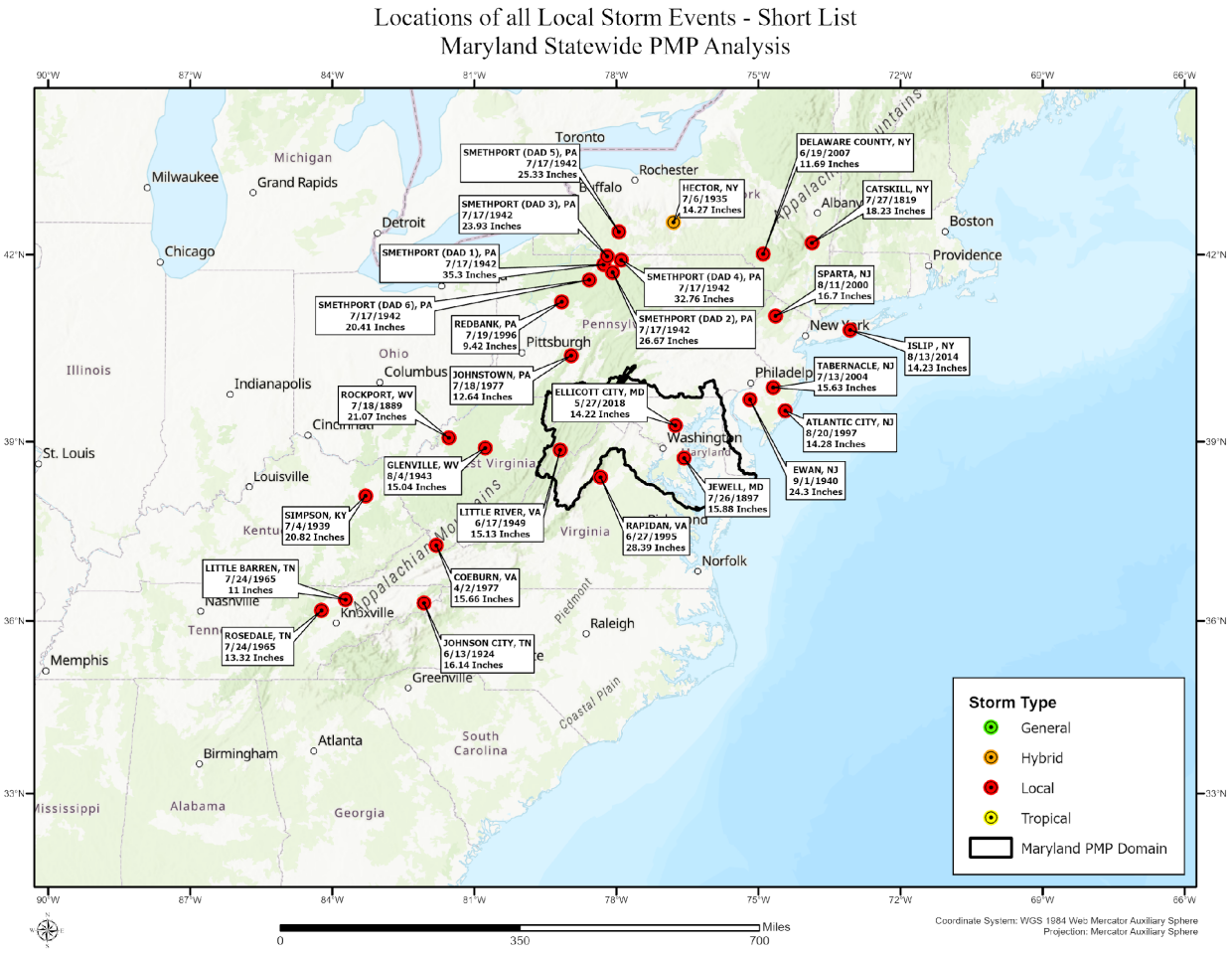

Figure 7.4: Location of local storms on the PMP storm list

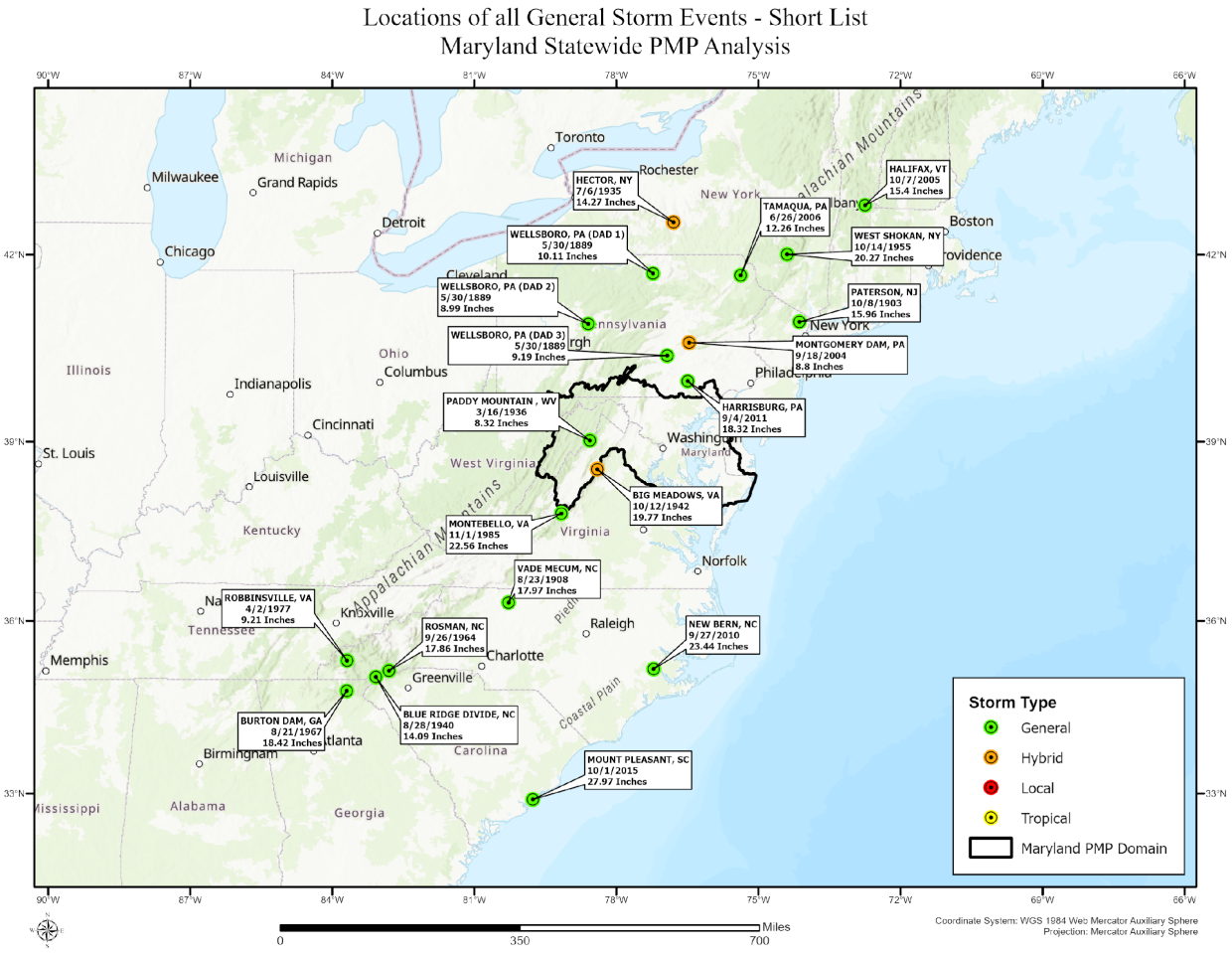

Figure 7.5: Location of general storms on the PMP storm list

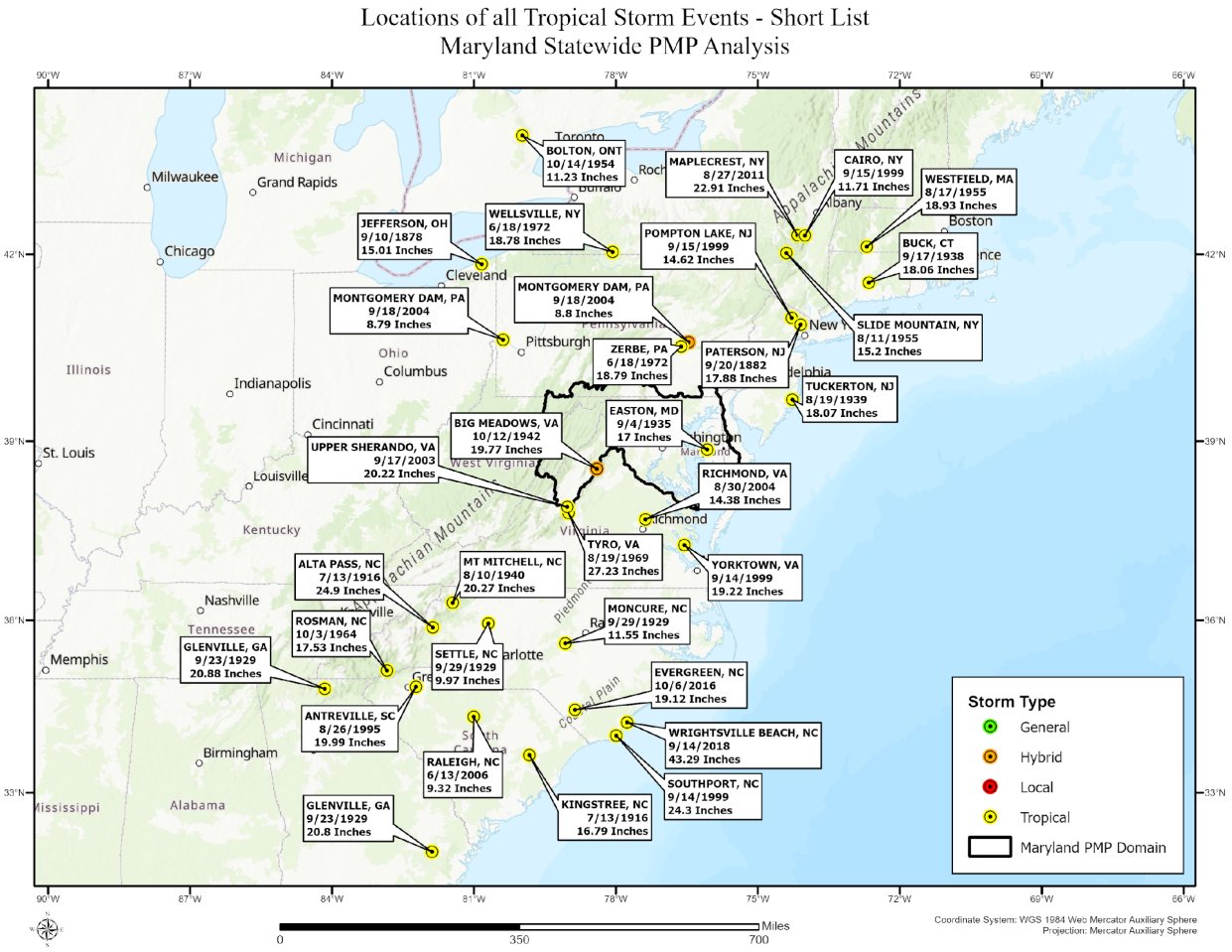

Figure 7.6: Location of tropical storms on the PMP storm list

8. SPAS Analysis Process

For all storms identified as part of this study, DAD data and hourly rainfall accumulation gridded outputs are required for PMP development. These outputs are required for GTF calculations and to calculate PMP depths. SPAS was used to compute DADs for all the storms used in this study. Results of all SPAS analyses used in the study are provided in Appendix F. This Appendix includes the standard output files associates with each SPAS analysis, including the following:

- SPAS analysis notes and description
- Total storm isohyetal
- DAD table and graph
- Storm center mass curve (hourly and incremental accumulation)

There are two main steps in the SPAS DAD analysis: 1) The creation of high-resolution hourly rainfall grids and 2) the computation of Depth-Area (DA) rainfall amounts for various durations, i.e., how the depth of the analyzed rainfall varies with area sizes being analyzed. The reliability of the results from step 2) depends on the accuracy of step 1). Historically, the process has been very labor intensive. SPAS utilizes GIS concepts to create spatially oriented and accurate results in an efficient manner (step 1). Furthermore, the availability of NEXRAD (NEXt generation RADar) data allows SPAS to better account for the spatial and temporal variability of storm precipitation for events occurring since the early 1990s. Prior to NEXRAD, the NWS developed and used a method based on Weather Bureau Technical Paper No. 1 (1946). Because this process has been the standard for many years and holds merit, the DAD analysis process developed for this study attempts to follow the NWS procedure as much as possible. By adopting this approach, some level of consistency between the newly analyzed storms and the hundreds of storms already analyzed by the USACE, USBR, and/or NWS can be achieved. Appendix E provides a detailed description of the SPAS program with the following sections providing a high-level overview of the main SPAS processes.

8.1 SPAS Data Collection

The areal extent of a storm's rainfall is evaluated using existing maps and documents along with plots of total storm rainfall. Based on the storm's spatial domain (longitude-latitude box), hourly and daily rain gauge data are extracted from the database for the specified area, dates, and times. To account for the temporal variability in observation times at daily stations, the extracted hourly data must capture the entire observational period of all extracted daily stations. For example, if a station takes daily observations at 8:00 AM local time, then the hourly data needs to be complete from 8:00 AM local time the day prior. As long as the hourly data are sufficient to capture all of the daily station observations, the hourly variability in the daily observations can be properly addressed.

The daily database is comprised of data from NCDC TD-3206 (pre-1948) and TD-3200 (generally 1948 through present). The hourly database is comprised of data from NCDC TD-3240 and NOAA's Meteorological Assimilation Data Ingest System (MADIS). The daily supplemental database is largely comprised of data from "bucket surveys," local rain gauge networks (e.g., USGS, CoCoRaHS, etc.) and daily gauges with accumulated data.

8.2 SPAS Mass Curve Development

The most complete rainfall observational dataset available is compiled for each storm. To obtain temporal resolution to the nearest hour in the final DAD results, it is necessary to distribute the daily precipitation observations (at daily stations) into hourly bins. In the past, the NWS had accomplished this process by anchoring each of the daily stations to a single hourly station for timing. However, this may introduce biases and may not correctly represent hourly precipitation at locations between hourly observation stations. A preferred approach is to anchor the daily station to some set of nearest hourly stations. This is accomplished using a spatially based approach called the spatially based mass curve (SMC) process (see Appendix E).

8.3 Hourly and Sub-Hourly Precipitation Maps

At this point, SPAS can either operate in its standard mode or in NEXRAD-mode to create high resolution hourly or sub-hourly (for NEXRAD storms) grids. In practice, both modes are run when NEXRAD data are available so that a comparison can be made between the methods. Regardless of the mode, the resulting grids serve as the basis for the DAD computations.

8.4 Standard SPAS Mode Using a Basemap Only

The standard SPAS mode requires a full listing of all the observed hourly rainfall values, as well as the newly created estimated hourly data from daily and daily supplemental stations. This is done by creating an hourly file that contains the newly created hourly mass curve precipitation data (from the daily and supplemental stations) and the "true" hourly mass curve precipitation. If not using a base map, the individual hourly precipitation values are simply plotted and interpolated to a raster with an inverse distance weighting (IDW) interpolation routine in GIS.

8.5 SPAS-NEXRAD Mode

Radar has been in use by meteorologists since the 1960s to estimate rainfall depth. In general, most current radar-derived rainfall techniques rely on an assumed relationship between radar reflectivity and rainfall rate. This relationship is described by the Equation 2 below:

$$Z = aR^b \qquad \text{Equation 2}$$

where Z is the radar reflectivity, measured in units of dBZ, R is the rainfall rate, a is the "multiplicative coefficient" and b is the "power coefficient". Both a and b are related to the drop size distribution (DSD) and the drop number distribution (DND) within a cloud (Martner et al., 2005).

The NWS uses this relationship to estimate rainfall using their network of Doppler radars (NEXRAD) located across the United States.

A standard default Z-R algorithm of $Z = 300R^{1.4}$ has been the primary algorithm used throughout the country and has proven to produce highly variable results. The variability in the results of Z vs. R is a direct result of differing DSD and DND, and differing air mass

characteristics across the United States (Dickens, 2003). The DSD and DND are determined by a complex interaction of microphysical processes in a cloud. They fluctuate hourly, daily, seasonally, regionally, and even within the same cloud (see Appendix E for a more detailed description).

Using the technique described above, also discussed in Appendix E, NEXRAD rainfall depth and temporal distribution estimates are determined for the area in question.

8.6 Depth-Area-Duration Program

The DAD extension of SPAS runs from within a Geographic Resource Analysis Support System (GRASS) GIS environment and utilizes many of the built-in functions for calculation of area sizes and average rainfall depths. The following is the general outline of the procedure:

1. Given a duration (e.g., x-hours) and cumulative precipitation, sum up the appropriate hourly or sub-hourly precipitation grids to obtain an x-hour total precipitation grid starting with the first x-hour moving window.
2. Determine x-hour precipitation total and its associated areal coverage. Store these values. Repeat for various lower rainfall thresholds. Store the average rainfall depths and area sizes.
3. The result is a table of depth of precipitation and associated area sizes for each x-hour window location. Summarize the results by moving through each of the area sizes and choosing the maximum precipitation amount. A log-linear plot of these values provides the depth-area curve for the x-hour duration.
4. Based on the log-linear plot of the rainfall depth-area curve for the x-hour duration, determine rainfall amounts for the standard area sizes for the final DAD table. Store these values as the rainfall amounts for the standard sizes for the x-duration period. Determine if the x-hour duration period is the longest duration period being analyzed. If it is not, analyze the next longest duration period and return to step 1.
5. Construct the final DAD table with the stored rainfall values for each standard area for each duration period.

8.7 Comparison of SPAS DAD Output Versus Previous DAD Results

The SPAS process and algorithms have been thoroughly reviewed as part of many AWA PMP studies. The SPAS program was reviewed as part of the NRC software verification and validation program to ensure that its use in developing data for use in NRC regulated studies was acceptable (Hultstrand and Kappel, 2017). The result of the NRC review showed that the SPAS program performed exactly as described and produced expected results.

As part of this study, comparisons were made of the SPAS DAD tables and previously published DAD tables developed by the USACE and/or NWS. AWA discussed these comparisons for important storms where previous DADs were available that covered the same domain as the SPAS analysis. Table 8.1 provides an example comparison of a SPAS 1566 DAD from the analysis of the Paterson, NJ storm versus the USACE GL 4-9 DAD previously developed. As expected, the differences between SPAS DAD depths and previously published depths varied by area size and duration. The differences were a result of one or more of the following:

- SPAS utilizes a more accurate basemap to spatially distribute rainfall between known observation locations. The use of a climatological basemap reflects how rainfall has occurred over a given region at a given time of the year and therefore how an individual storm pattern would be expected to look over the location being analyzed. Previous DAD analyses completed by the NWS and USACE often utilized simple IDW or Thiessen polygon methods that did not reflect climatological characteristics as accurately. In some cases, the NWS and USACE utilized precipitation frequency climatologies to inform spatial patterns. However, these relied on NOAA Atlas 2 (Miller et al., 1973) patterns and data that are not as accurate as current data from PRISM (Daly et al., 1994 and Daly et al., 1997) and NOAA Atlas 14.
- In some cases, updated sources of data uncovered during the data mining process were incorporated into SPAS that were not utilized in the original analysis. SPAS utilizes sophisticated algorithms to distribute rainfall temporally and spatially. In contrast, the isohyetal maps developed previously were hand drawn. Therefore, they reflected the best guess of the analyst of each storm, which could vary between each analyst's interpretations. Also, only a select few stations were used for timing, which limited the variation of temporal accumulation patterns throughout the overall domain being analyzed. SPAS uses the power of all the rainfall observations that have passed QA/QC measures to inform patterns over the entire domain. These temporal and spatial fits are evaluated and updated on an hourly basis for the entire duration.

Table 8.1: Comparison of SPAS 1566 DAD versus the USACE GL 4-9 DAD, both representing the Paterson New Jersey October 1903 storm event

Percent Difference ((SPAS 1566 - GL 4-9)/GL 4-9) MAXIMUM AVERAGE DEPTH OF PRECIPITATION (INCHES)									
areasqmi	6-hr	12-hr	18-hr	24-hr	36-hr	48-hr	72-hr	96-hr	Total
10	-2%	5%	1%	1%	5%	4%	6%	2%	2%
100	-4%	9%	4%	3%	8%	7%	5%	5%	5%
200	-5%	5%	4%	2%	5%	4%	3%	2%	4%
500	-5%	0%	4%	1%	4%	4%	1%	1%	2%
1,000	-1%	1%	4%	0%	3%	2%	1%	1%	2%
2,000	1%	0%	5%	-2%	0%	-1%	-3%	1%	2%
5,000	3%	-6%	-1%	-10%	1%	-2%	-2%	1%	2%
10,000	10%	-1%	-3%	-6%	1%	-1%	3%	2%	3%
20,000	11%	0%	-2%	-10%	4%	0%	3%	2%	4%

9. Storm Adjustments

9.1 In-Place Maximization Process

Maximization was accomplished by increasing surface dew points (or SST when the storm representative location is over the ocean) to a climatological maximum and calculating the enhanced rainfall amounts that could potentially be produced if the climatological maximum moisture had been available during the observed storm period. Additionally, the climatological maximum dew point/SST for a date 15 days towards the warm season is selected with higher amounts of moisture from the date that the storm occurred. This procedure assumes that the storm could have occurred with the same storm dynamics two weeks towards the time in the year when maximum dew points occur.

This assumption follows HMR guidance and is consistent with procedures used to develop PMP depths in all the current HMR documents (e.g., HMR 51 Section 2.3), the WMO Manual for PMP (WMO, 2009), as well as in all prior AWA PMP studies. The storm data in Appendix F provides the individual analysis maps used for each storm adjustment process including the HYSPLIT model output, the surface dew point/SST observations, the storm center location, the storm representative location, and the IPMF for each storm.

Each storm used for PMP development was thoroughly evaluated in adjacent studies and again during this study to confirm the reasonableness of the storm representative value and location used. As part of this process, AWA provided and discussed all the information used to derive the storm representative value for review, including the following:

- Hourly surface dew point observations
- Daily SST observations
- HYSPLIT model output
- Storm adjustment spreadsheets
- Storm adjustments maps with data plotted

These data allowed for an independent review of each storm. Results of this analysis demonstrated that the values AWA utilized to adjust each storm were reasonable for PMP development.

For storm maximization, average dew point or daily SST values for the appropriate duration that are most representative of the actual rainfall accumulation period for an individual storm (e.g., 6-, 12-, or 24-hour) are used to determine the storm representative value. This value (either dew point or SST) is then maximized using the appropriate climatological value representing the 100-year return interval or +2 sigma SST at the same location moved two weeks towards the season of higher climatological maximum values.

The HYSPLIT model (Draxler and Rolph, 2013; Stein et al., 2015; and Rolph et al., 2017) provides detailed and reproducible analyses for assisting in the determination of the upwind trajectories of atmospheric moisture that was advected into the storm systems. Using these model trajectories, along with an analysis of the general synoptic weather patterns and

available surface dew point temperature data/daily SST data, the moisture source region for candidate storms is determined. The procedure is followed to determine the storm representative location and is similar to the approach used in the HMRs. However, by utilizing the HYSPLIT model, much of the subjectivity found in the HMR analysis process was corrected. Further, details of each evaluation can be explicitly provided, and the HYSPLIT trajectory results based on the input parameters defined are reproducible. Available HYSPLIT model results are provided as part of Appendix F.

The IPMF process results in a ratio of observed moisture compared to climatological maximum moisture. Therefore, this value is always 1 or greater. The intent of the process is to produce a hypothetical storm event that represents the upper limit of rainfall that the storm could have produced if the ideal combination of moisture and maximum storm efficiency (atmospheric processes that convert moisture to precipitation) had occurred during the storm. This assumes that the storm efficiency processes remain constant as more moisture is added to the storm environment. Therefore, an upper limit of 1.50 (50%) is applied to the IPMF with the assumption that increases beyond this amount would change the storm efficiency processes and the storm would no longer be the same storm as observed from an efficiency perspective.

This upper limit is a standard application applied in the HMRs (e.g., HMR 51 Section 3.2.2). During this study the 1.50 upper limit was applied against two storms, Jewell, MD July 1897 (SPAS 1489) and Sparta, NJ August 2000 (SPAS 1017). Note, this upper limit was investigated further during the Colorado-New Mexico REPS study using the Dynamical Modeling Task and the HRRR model interface (Alexander et al., 2015). This explicitly demonstrated that storm efficiency changes as more moisture is added, well before the 50% moisture increase level for the storms investigated (Mahoney, 2016). Therefore, the use of 1.50 as an upper limit is a conservative application.

9.2 Storm Representative Determination Process

For storm maximization using dew point observations, average dew point values for the duration most consistent with the actual rainfall accumulation period for an individual storm (i.e., 3-, 6-, 12-, or 24-hour) were used to determine the storm representative dew point. To determine which time frame was most appropriate, the total rainfall amount was analyzed. The duration closest to when approximately 90% of the rainfall had accumulated was used to determine the duration used, i.e., 6-hour, 12-hour, or 24-hour.

The storm representative dew point was investigated for each of the storm events analyzed in previous studies and re-evaluated in this study. Once the general upwind location was determined, the hourly surface observations were analyzed for all available stations within the vicinity of the inflow vector. From these data, the appropriate durational dew point value was averaged for each station (6-, 12-, or 24-hour depending on the storm's rainfall accumulation). These values were then adjusted to 1,000mb (approximately sea level) and the appropriate storm representative dew point and location were derived. The line connecting this point with the storm center location (point of maximum rainfall accumulation) is termed the moisture inflow vector. The information used and values derived for each storm’s moisture inflow vector are included in Appendix F.

HYSPLIT was used during the analysis of each of the rainfall events included on the short storm list when available (1948-present). Use of a trajectory model provides increased confidence in determining moisture inflow vectors and storm representative dew points. The HYSPLIT trajectories have been used to analyze moisture inflow vectors in other PMP studies completed by AWA over the past several years. During these analyses, the model trajectory results were verified, and the utility explicitly evaluated (e.g., Tomlinson et al., 2006-2012; Kappel et al., 2013-2022).

In determining the moisture inflow trajectories, the HYSPLIT was used to compute the trajectory of the atmospheric moisture inflow associated with the storm's rainfall production, both location and altitude, for various levels in the atmosphere. The HYSPLIT model was run for trajectories at several levels of the lower atmosphere to capture the moisture source for each storm event. These included 700mb (approximately 10,000 feet), 850mb (approximately 5,000 feet), and storm center location surface elevation.

For most of the analyses, a combination of all three levels was determined to be most appropriate for use in evaluation of the upwind moisture source location. It is important to note that the resulting HYSPLIT trajectories are only used as a general guide to evaluate the moisture source for storms in both space and time. The final determination of the storm representative dew point and its location was made following the standard procedures used by AWA in previous PMP studies (e.g., Tomlinson, 1993; Tomlinson et al., 2006-2013; Kappel et al., 2013-2022) and as outlined in the HMRs (e.g., HMR 51 Section 2.3) and WMO Manual for PMP (Section 2.2). HYSPLIT trajectories are run backwards in time for a 72-hour period starting at the storm center location. This is done to determine where the moisture originated from that eventually ended up within the storm systems and produced the observed precipitation. AWA then evaluated the trajectories in relation to the general synoptic weather patterns, likely moisture source regions, storm type(s), and consistency between each level of the atmosphere. In addition, for trajectories that utilize SST as the storm representative location, it is also valuable to see where one or more of the levels reaches the surface at some point during the analysis period. Finally, dew point (or SST) values are then plotted in the large general region around and along the trajectories for analysis.

The process to determine the storm representative values involves deriving the average dew point (or SST) values at all stations with dew point (or SST) data in a large region along the HYSPLIT inflow vectors. Values representing the average 6-, 12-, and 24-hour dew points or daily SST are analyzed in Excel spreadsheets. The appropriate duration representing the storm being analyzed is determined and data are plotted for evaluation of the storm representative dew point (or SST). This evaluation includes an analysis of the timing of the observed dew point (or SST) values to ensure they occurred in a source region where they would be advected into the storm environment at the time of the rainfall period. Several locations are investigated to find values that are of generally similar magnitude (within a degree or two Fahrenheit). Once these representative locations are identified, an average of the values to the nearest half degree is determined and a location in the center of the stations is identified. This becomes the storm representative dew point (or SST) value, and the location provides the inflow vector (direction and distance) connecting that location to the storm center location.

This follows the approach used in HMR 51 Section 2, HMR 55A Section 5, and HMR 57 Section 4, with improvements provided using HYSPLIT and updated maximum dew point and SST climatologies. Appendix F of this report contains each of the HYSPLIT trajectories analyzed as part of this study for each storm (when used). Figure 9.1 is an example map used to determine the storm representative dew point for the Tamaqua, PA June 2006, SPAS 1047 storm event.

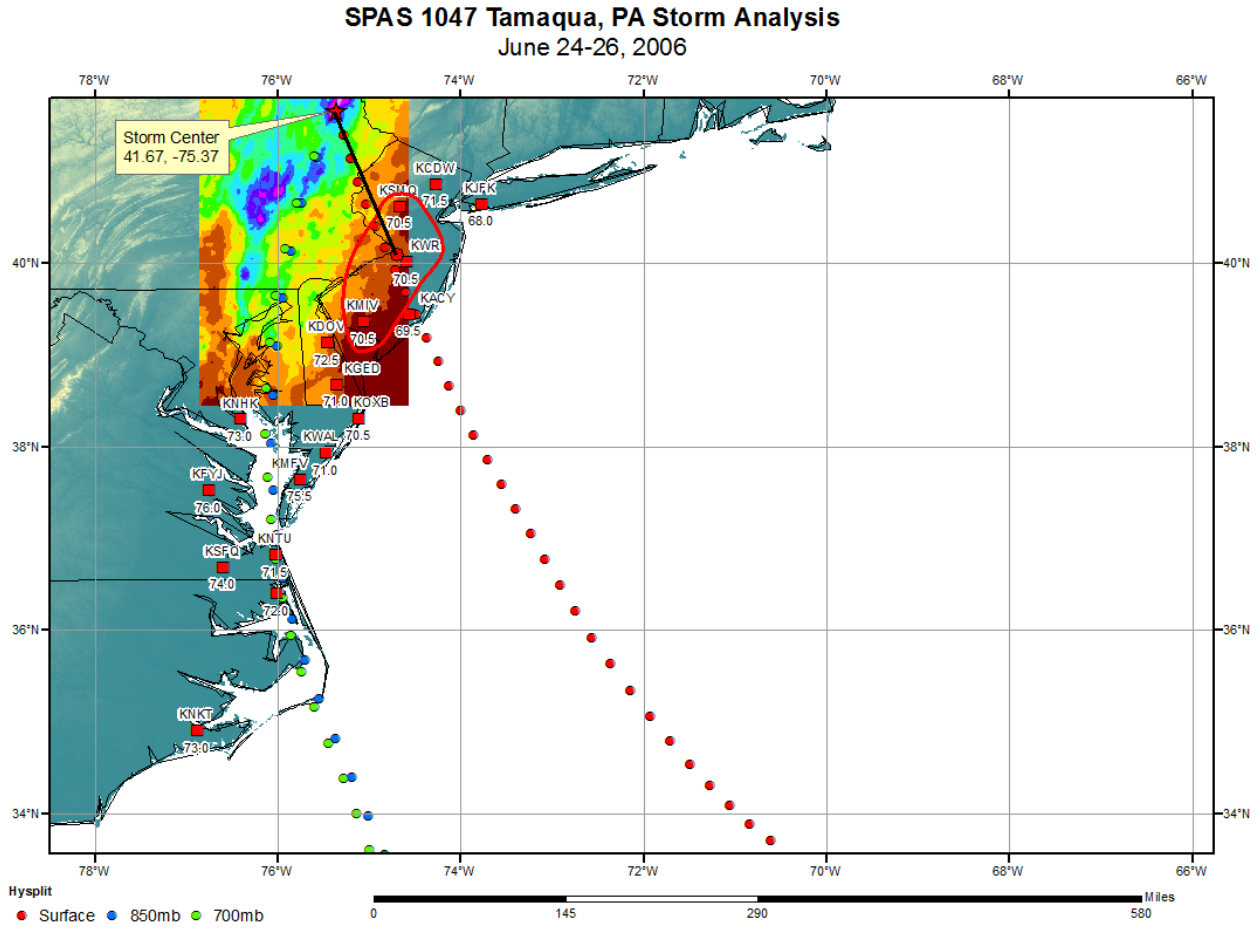

Figure 9.1: Dew point values used to determine the storm representative dew point for Tamaqua, PA June 2006, SPAS 1047 storm event

The value for the maximum SST was determined using the mean +2 sigma (two standard deviations warmer than the mean) SST for that location. SSTs were substituted for dew points in this study for many storms where the inflow vector originated over the Atlantic Ocean. Data presented in Appendix F show the moisture source region for each storm and whether dew points or SSTs were used in the maximization calculations. For storm maximization, the value for the maximum SST was determined using the mean +2 sigma SST for that location for a date two weeks before or after the storm date (which ever represents the climatologically warmer SST period). Storm representative SSTs and the mean +2 sigma SSTs were used in the same manner as storm representative dew points and maximum dew point climatology representing the 15th of the month values in the maximization and transpositioning procedure. Figure 9.2 is an example

of a daily SST map used to determine the storm representative SST for the SPAS 1276 Hurricane Agnes June 1972 storm event.

In this example, the first decision was whether surface dew points were available to derive the storm representative dew point. However, this was not possible for this storm because there was rainfall to the coast, thereby contaminating the dew point readings along the inflow pathway to the Atlantic. Next, SSTs were investigated to determine regions of homogenous temperatures in a region that was appropriate in time and space according to the HYSPLIT trajectories. Several regions were possibilities in this case.

Next, the track of the Hurricane and its relation to moisture advection into the storm center was considered. This better matched the surface (red dots) HYSPLIT trajectory. Finally, sensitivity calculations were performed using several couplets of storm representative SST values versus the +2 sigma climatological maximum values to ensure the range of maximizations was within a reasonable range (i.e., greater than 1.00). After the investigations were completed, the storm representative location of 36.0°N and 67.0°W was chosen. This was an average of several of the SST values within the red circled area of Figure 9.2 on June 18 and June 19, 1972.

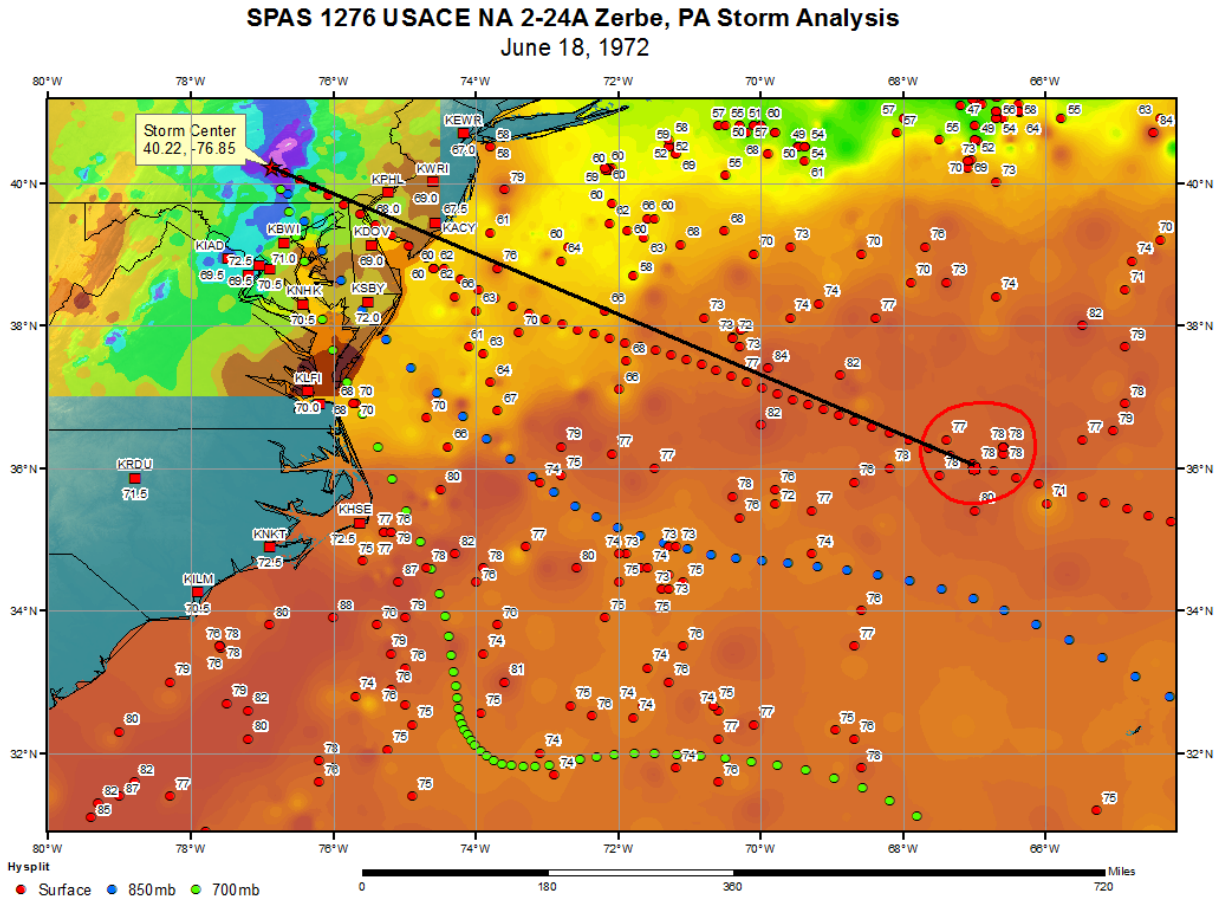

Figure 9.2: Daily SST observations used to determine the storm representative SST value for the SPAS 1276, June 1972 storm event

9.3 In-Place Maximization Factor Calculation

Storm maximization is quantified by the IPMF using Equation 3.

$$IPMF = \frac{W_{p,max}}{W_{p,rep}} \qquad \text{Equation 3}$$

where,

$W_{p,max}$ = precipitable water for maximum dew point (in.)

$W_{p,rep}$ = precipitable water for representative dew point (in.)

The available precipitable water, Wp, is calculated by determining the precipitable water depth present in the atmospheric column (from sea level to 30,000 feet) and subtracting the precipitable water depth that would not be present in the atmospheric column between sea-level and the surface elevation at the storm location using Equation 4.

$$W_p = W_{p,30,000'} - W_{p,elev}$$ Equation 4

where,

W_p	=	precipitable water above the storm location (in.)
$W_{p,30,000'}$	=	precipitable water, sea level to 30,000′ elevation (in.)
$W_{p,elev}$	=	precipitable water, sea level to storm surface elevation (in.)

9.4 Transposition Zones Utilized in PMP Development

PMP-type storm events in regions of similar meteorological and topographic settings surrounding a location are a very important part of the historical evidence on which a PMP estimate is based. Since most locations have a limited period of record for rainfall data, the number of extreme storms that have been observed over a location is limited. Historic storms that have been observed within similar meteorological and topographic regions are analyzed and adjusted to provide information describing the storm rainfall as if that storm had occurred over the location being studied.

Transfer of a storm from where it occurred to a location that is meteorologically and topographically similar is called transposition. The underlying assumption is that storms transposed to the location could have occurred under similar meteorological and topographical conditions. To properly relocate such storms, it is necessary to address issues of similarity as they relate to meteorological conditions, moisture availability, and topography. In this study, adjustment factors used in transpositioning of a storm are quantified by using the GTF.

The regional transposition zones developed for this study were based on the meteorological and topographical characteristics across the PMP study domain along with considerations of moisture source region characteristics, storm types, and seasonality. Initial delineations were developed utilizing information from the National Centers for Environmental Information (formally the National Climatic Data Center) climate regions, USGS physiographic regions, NOAA Atlas 14 precipitation frequency climatologies, and transposition regions used in adjacent/overlapping PMP studies were evaluating in this process. Results of these analyse s were discussed with the review board and MDE to develop final transposition zones.

Figure 9.3 shows the transposition zones utilized in this study. Note, that the zones were used as a general guidance and for initial evaluations. Many storms were ultimately allowed to move between zones and/or were restricted within a given zone for final PMP development.

Transposition zones 1 and 2 represent the coastal and piedmont region where there is direct access to moisture from the Atlantic Ocean and no significant topography. These regions are often affected by tropical systems. Transposition zones 3, 4, and 5 represent the transition from the coastal lowlands to the Appalachians and include the ridge and valley region of Maryland, West Virginia, and Virginia. These regions are orographically influenced regions where rainfall is both enhanced on upwind locations and decreased on downwind locations. In addition, precipitation generally decreases at locations further inland as these are farthest from the low-level moisture source to the east while at the same time low-level moisture is blocked by the Appalachians to the west.

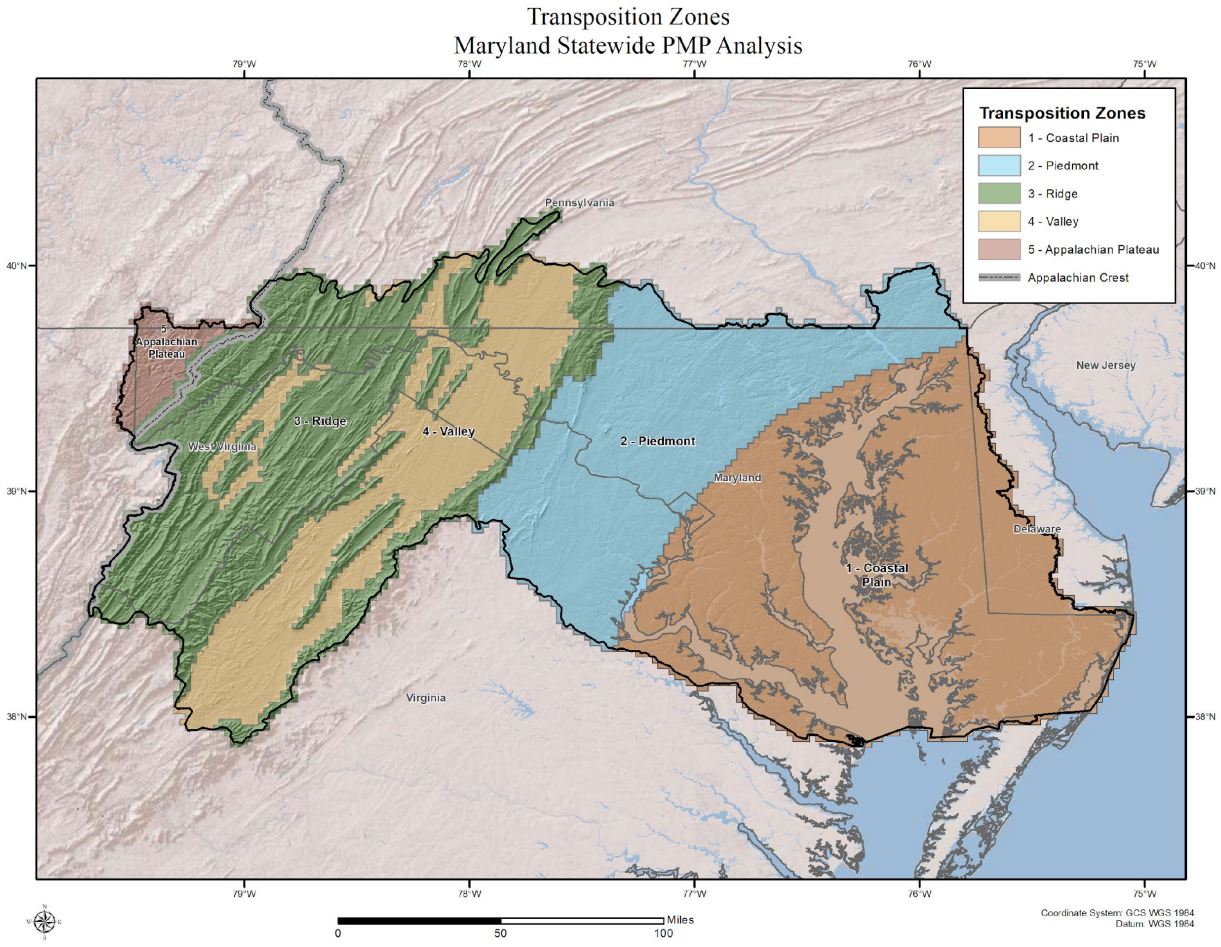

Figure 9.3: Transposition zones utilized for the Maryland PMP study

Initial transposition limits were assigned with the understanding that additional refinements would take place as the data were run through the PMP evaluation process. Numerous sensitivity runs were performed using the PMP database to investigate the results based on the initial transposition limits. Several storms were re-evaluated based on the results that showed inconsistencies and/or unreasonable values, either too high or too low. Examples of inconsistencies and unreasonable values include areas where gradients of PMP depths between adjacent grid points were significantly different and not specifically related to a similar meteorological or topographical change. When these occur because of excessive GTF values or because a storm was likely moved beyond reasonable transposition limits, adjustments are applied.

Although somewhat subjective, decisions to adjust the transposition limits for a storm were based on the understanding of the meteorology which resulted in the storm event, similarity of topography between the two locations, access to moisture source, seasonality of occurrence by storm type, and comparison to other similar storm events. Appendix I provides a description of

the iterations and adjustments that were applied during each PMP version to arrive at the final values via the PMP Version Log.

For all storms, the IPMF does not change during this process. The GTF changes as a storm is moved from its original location to a new location. The spatial variations in the GTF were useful in making decisions on transposition limits for many storms. As described previously, values larger than 1.50 for a storm's maximization factor exceed limits that would no longer produce the same storm as the originally observed event. In these situations, changing a storm by this amount is likely also changing the original storm characteristics so that it can no longer be considered the same storm at the new location. The same concept applies to the GTF. GTF values greater than 1.50 indicate that transposition limits have most likely been exceeded. In addition, a lower limit of 0.50 was applied for the same reason, but this inherently affects a much more limited set of storms and regions. Therefore, storms were re-evaluated for transpositionability in regions which results in a GTF greater than 1.50.

The transposition process is one of the most important aspects of PMP development. This step also contains subjectivity as the processes utilized to define transposition limits are difficult to quantify and based on meteorological judgment. General guidelines are provided in the HMRs (e.g., HMR 51 Section 2.4.1 and HMR 55A Section 8.2). AWA utilized these guidelines as well as updated procedures and data sets developed during the many PMP studies completed in the region since the HMRs were published. General AWA guidelines included:

- Investigation of previous NWS transposition limit maps
- Experience and understanding of extreme rainfall processes in the study region and how those factors vary by location, storm type, and season
- Understanding of topographical interactions and how those affect storms by location, storm type, and season
- Previously applied transposition limits from adjacent statewide PMP studies
- Limiting transposition to east or west of the Appalachian crest
- Use of GTF values as sensitivity
- Spatial continuity of PMP depths
- Comparisons against NOAA Atlas 14 precipitation frequency climatology
- Discussions with the review board, MDE, and others involved in the study

An important aspect of this study was the involvement of the review board and MDE in evaluating and reviewing individual storm transposition limits of controlling storms. They had initial input in helping to define the overall transposition zones used in the study shown in Figure 9.3. Once initial transposition limits were applied to each storm, the resulting GTF values were reviewed during the review meetings. These were most focused on the controlling storms.

The PMP Version Log provided in Appendix I provides the numerous iterations of PMP development and the various transposition limit adjustments that were applied to storms during the PMP development process. In some cases, storms originally considered for a given location were removed after evaluation and in other cases transposition limits were adjusted within a given transposition zone. The red hatch area on the GTF maps contained in Appendix B indicate the final transposition limits applied to each storm.

9.4.1 Updated Transposition Limits for the Smethport, PA and Simpson, KY Storms

PMP depths derived from the Smethport, PA and Simpson, KY storms resulted in significant gradients between locations where they were used and not used. These boundaries create artificial gradients that do not accurately represent the meteorologically based transitions that occur naturally in a storm environment. Extensive discussions took place between AWA, MDE, and other study participants to determine the best way to address these gradients. The goal was to produce more realistic transitions across the boundaries and still represent the intent of the process while producing appropriately conservative PMP depths.

These discussions resulted in applying a smoothing component to the edges of the original transposition limits which utilized distance and PMP depths to create a more realistic transition from the edges of the original transposition limits to the adjacent grids. These storms were allowed to go to east of the Appalachian crest, but 10 one-mile buffers were created around the original transposition zone. This same process applies to similar local storms which occurred west of the Appalachian crest, including Rockport, WV July 1889 and Glenville, WV August 1943. Finally, an additional adjustment factor was applied to each buffer zone that would reduce the PMP values by 3% until those storms were no longer a controlling storm 10 miles out from the original limits. Figure 9.4 displays the smoothed transposition limits for the local storm 6-hour 1-mi^2 PMP map.

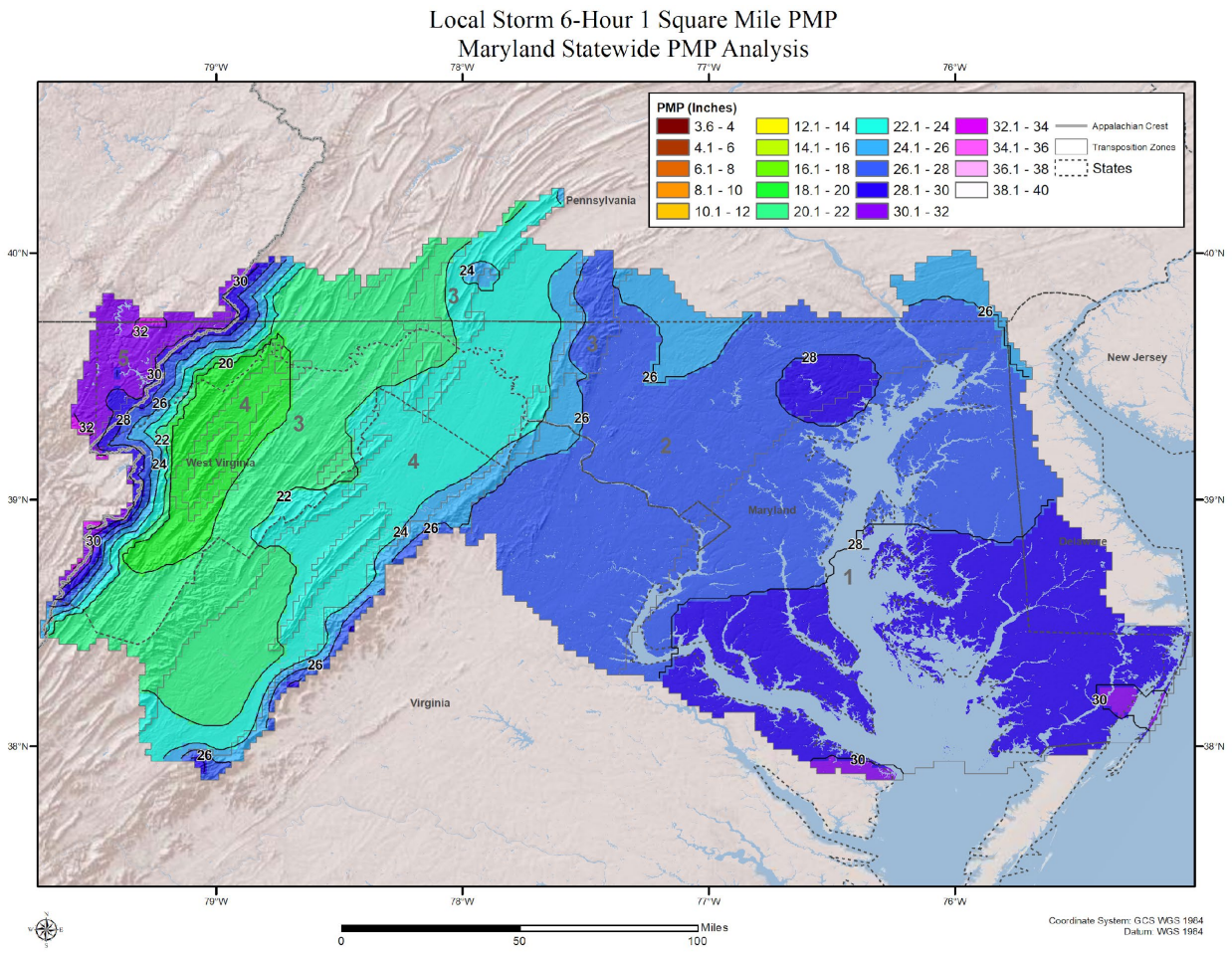

Figure 9.4: Example PMP depths with the customized transposition limits and smoothing of the Smethport, PA July 1942 and Simpson, KY July 1939 storms

9.5 Geographic Transposition Factor

The GTF process is used to capture all processes that result in precipitation reaching the ground at one location versus another location, including the effects of terrain. The GTF is a mathematical representation of the ratio of the precipitation frequency climatology at one location versus another location. The precipitation frequency climatology is derived from observed precipitation events which produced amounts used to identify the Annual Maximum Series (AMS) at a given station. An upper limit of 1.50 and a lower limit of 0.50 were applied to the GTF as described in Section 9.4. This was done to ensure the storm being adjusted was not exceeding reasonable limits when moving a storm from one location to another. The intent was to ensure the original storm characteristics could occur at the new location in a manner as the original location and therefore that would violate the PMP process assumptions related to storm transposition.

GTF values were calculated utilizing NOAA Atlas 14 precipitation frequency data at the 100-year recurrence interval, volumes 2 and 10 (Bonnin et al., 2006 and Perica et al., 2015). These data were used to ensure consistency in the climatological datasets and to ensure required coverage for all storm locations within the overall storm search domain. The storms used in

NOAA Atlas 14 represent observed precipitation events that resulted in an AMS accumulation. Therefore, they represent all precipitation producing processes that occurred during a given storm event. In HMR terms, the resulting observed precipitation represents both the convergence-only component and any orographic component. The NOAA Atlas 14 gridded precipitation frequency climatology was produced using gridded mean annual maxima (MAM) grids that were developed with the PRISM (Daly et al., 1994). PRISM utilizes geographic information such as elevation, slope, aspect, distance from coast, and terrain weighting for weighting station data at each grid location. As noted, use of the precipitation frequency climatology grids should be reflective of all precipitation producing processes. Further, the use of the gridded precipitation climatology at the 100-year recurrence interval represents an optimal combination of factors, including representing extreme precipitation events equivalent to the level of rainfall utilized in AWA's storm selection process, and providing the most robust statistics given the period of record used in the development of the precipitation frequency climatologies.

Therefore, the GTF represents the difference in topographic effects between two locations, but also represents the difference in all precipitation processes between two locations. This is one reason it is very important to apply appropriate transposition limits to each storm during the PMP development process.

Effects of terrain and coastal convergence on precipitation production is well known. However, there are many orographic processes and interactions that are not well understood or quantified. Therefore, observed data (precipitation accumulations represented in the precipitation frequency data) are used as a proxy, where it is assumed that the observed precipitation represents all the precipitation processes associated with a storm event. This follows guidance provided by the WMO 2009, Section 3.1.4 and discussed in Section 4 of this document. Best professional judgment indicates that observed precipitation at a given location represents a combination of all factors that produced the precipitation, including what would have occurred without any terrain influence and what actually occurred because of the terrain influence. Judgement is inherent when determining transposition limits because the process of quantifying similar regions of meteorology and topography is highly subjective. As part of the GTF process, the following assumptions are applied:

- NOAA Atlas 14 precipitation frequency climatologies represent all precipitation producing factors that have occurred at a location. This is based on the fact that the data are derived from AMS values at individual stations that were the result of an actual storm event. That actual storm event included both the amount of precipitation that would have occurred without topography and the amount of precipitation that occurred because of topography (if any).
- If it is accepted that the precipitation frequency climatology is representative of all precipitation producing processes for a given location, then comparing the precipitation frequency climatology at one point to another will produce a ratio that shows how much more or less efficient the precipitation producing processes are between the two locations. This ratio is called the GTF.
- If there is no orographic influence at either location being compared or between the two locations, then the differences should be a function of (1) storm precipitation

producing processes in the absence of topography (thermodynamic and dynamic), (2) how much more or less moisture is available from a climatological perspective, and/or (3) elevation differences at the location.

9.6 Geographic Transposition Factor Calculation

The GTF is calculated by taking the ratio of transposed 100-year rainfall to the in-place 100-year rainfall.

$$GTF = \frac{R_t}{R_s} \qquad \text{Equation 6}$$

where,

R_t = climatological 100-year rainfall depth at the target location

R_s = climatological 100-year rainfall depth at the source storm center

The in-place climatological precipitation (R_s) was determined at the grid point located at the SPAS-analyzed total storm maximum rainfall center location. The corresponding transposed climatological precipitation (R_t) was taken at each grid point in the study region. The 100-year precipitation was used for each transposed location and also for the in-place location for storm centers. For this region, the 6-hour precipitation frequency climatologies were used for the local storm type. Conversely, the 24-hour precipitation frequency climatologies are used for the general and tropical storm types based on accumulation characteristics associated with each storm type.

9.7 Total Adjustment Factor Calculation

The TAF is a product of the IPMF and GTF, which represent the combination of increased moisture and differences in precipitation processes of a given storm from where it occurred versus the transpositioned location.

$$TAF_{xhr} = P_{xhr} \times IPMF \times GTF \qquad \text{(from Equation 1)}$$

The TAF, along with the other storm adjustment factors, is exported and stored within the storm's adjustment factor feature class to be accessed by the GIS PMP tool as described in the following section. These are also stored within an Excel file unique to each storm, via the TAF spreadsheet.

10. Development of PMP Values

10.1 PMP Calculation Process

To calculate PMP, the TAF for each storm must be applied to the storm's SPAS analyzed DAD value for the area size and duration of interest to yield a total adjusted rainfall value. The storm's total adjusted rainfall value is then compared with the adjusted rainfall values of every storm in the database transposable to the target grid point. The largest adjusted rainfall depth becomes the PMP for that point at a given duration. This process must be repeated for each of the grid cells intersecting the input drainage basin for each applicable duration and storm type. The gridded PMP is averaged over the drainage basin of interest to derive a basin average and the accumulated PMP depths are temporally distributed.

A GIS-based PMP calculation tool was developed to automate the PMP calculation process. The PMP tool is a Python scripted tool that runs from a Toolbox in the ArcGIS desktop environment. The tool accepts a basin polygon feature or features as input and provides gridded, basin average, and temporally distributed PMP depths as output. These PMP output elements can be used with hydrologic runoff modeling simulations for PMF calculations. Full documentation of the PMP tool usage and structure is found in Appendix G.

The PMP tool can be used to calculate PMP depths for the following durations.

Local Storm PMP Durations:
1-, 2-, 3-, 4-, 5-, 6-, 12-, and 24-hour

General/Tropical Storm PMP Durations:
1-, 2-, 3-, 4-, 5-, 6-, 12-, 24-, 48-, and 72-hour

The PMP tool provides depths representing an areal average for the drainage basin area size, grid points, or other combinations of grid points or sub basins. This area can be overwritten with a specific user-defined area-size within the tool dialogue.

10.1.1 Sample Calculations

The following sections provide sample calculations for the storm adjustment factors for the Rapidan, VA of June 1995 (SPAS 1406) local storm event when transposed to randomly chosen grid point at 37.90°N, 79.05°W (grid point ID #10). Table 10.1 highlights the adjustment factors in the Storm Adjustment Factor feature class table for the storm at this target grid point location. The target location is about 67 miles southeast of the storm location at an elevation of 2,865 feet in the southwestern part of the PMP domain in transposition zone 3 (Figure 10.1).

Table 10.1: Sample transposition of Rapidan, VA 1995 (SPAS 1406) to grid point #10

ID	STORM	LON	LAT	ZONE	ELEV	IPMF	MTF	GTF	TAF	TRANS
10	1406_1	-79.05	37.90	3	2,865	1.09	1.00	1.04	1.14	1

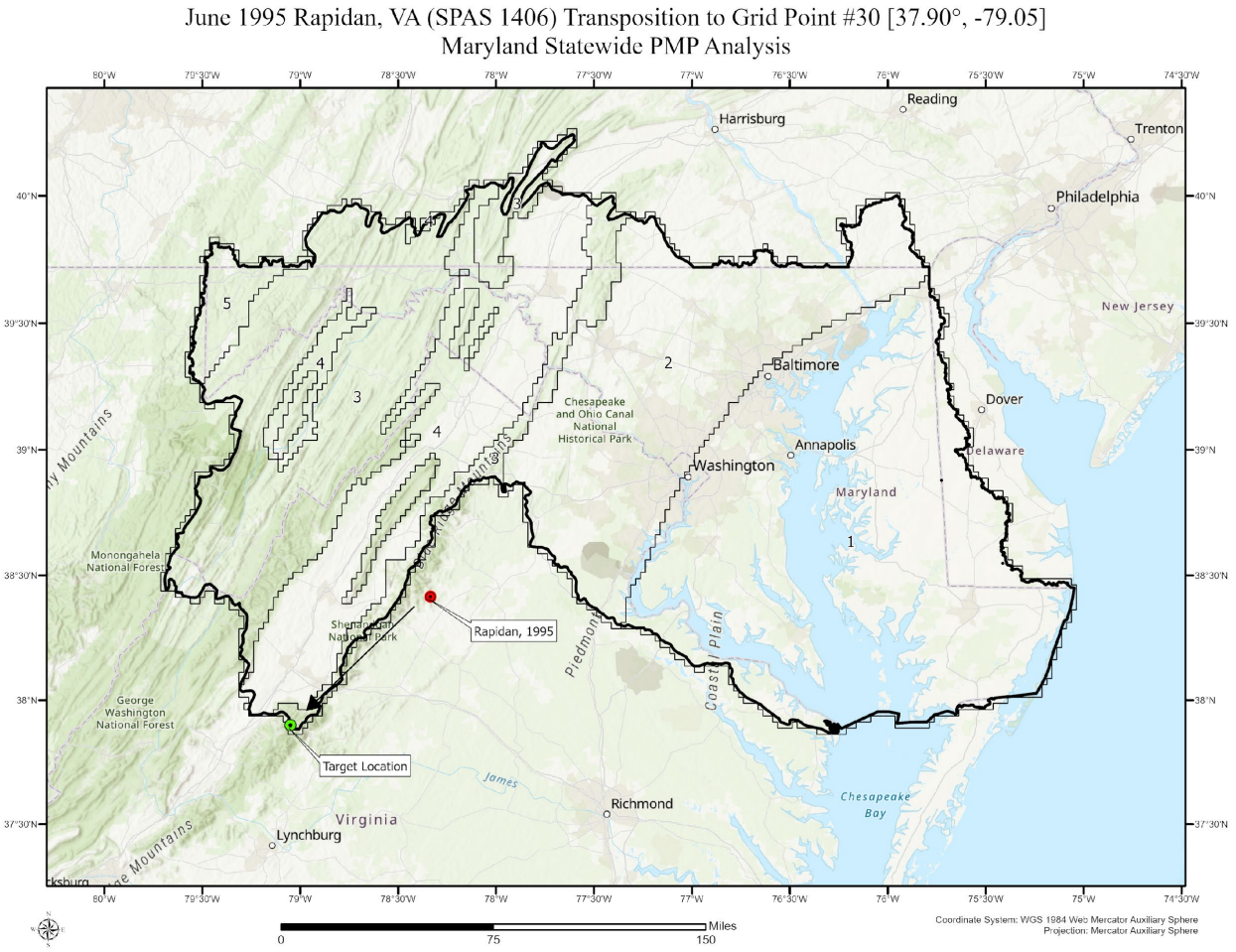

Figure 10.1: Sample transposition of Rapidan, VA 1995 (SPAS 1406) to grid point #10

10.1.2 Sample Precipitable Water Calculation

Using the storm representative sea surface temperature (SST) and storm center elevation as input, the precipitable water lookup table returns the depth, in inches, used in Equation 4. The storm representative SST temperature is 82°F at the storm representative SST location 350 miles southeast of the storm center (see Appendix F for the detailed storm maximization and analysis information). The storm center elevation is approximated at 1,300 feet at the storm center location of 38.415°N, 78.335°W. The storm representative available moisture ($W_{p,\ rep}$) is calculated using Equation 4:

$$W_{p,rep} = W(@82°)_{p,30,000'} - W(@82°)_{p,1,300'}$$

or,

$$W_{p,rep} = 3.95" - 0.39"$$

$$W_{p,rep} = 3.56"$$

The late June storm was adjusted 15 days toward the warm season to a temporal transposition date of July 10th. A weighted average of the June and July +2 sigma sea surface temperatures was used for the July 10th temporal transposition date. The June +2 sigma SST at

the storm representative SST location is 81.85°F and the July is 84.24°F. The two monthly temperatures are averaged (weighted toward July 10th) and rounded to the nearest ½ degree to a climatological maximum SST temperature of 84°F. The in-place climatological maximum available moisture ($W_{p,\,max}$) is calculated.

$$W_{p,max} = W(@84°)_{p,30,000'} - W(@84°)_{p,1,300'}$$

$$W_{p,max} = 4.3" - 0.42"$$

$$W_{p,max} = 3.88"$$

10.1.3 Sample IPMF Calculation

In-place storm maximization is applied for each storm event using the methodology described in Section 7.2. Storm maximization is quantified by the IPMF using Equation 3:

$$IPMF = \frac{W_{p,max}}{W_{p,rep}}$$

$$IPMF = \frac{3.88"}{3.56"}$$

$$IPMF = 1.09$$

10.1.4 Sample GTF Calculation

The ratio of the 100-year 6-hour climatological precipitation depth at the target grid point #10 location to the Rapidan, 1995 storm center was evaluated to determine the storm's GTF at the target location. The 6-hour rainfall depth (R_t) of 5.62" was extracted at the grid point #10 location from the 100-year 6-hour NOAA Atlas 14 precipitation frequency climatology.

$$R_t = 5.62"$$

Similarly, the 6-hour rainfall depth (R_s) of 5.39" was extracted at the storm center location from the 100-year 6-hour NOAA Atlas 14 precipitation frequency climatology.

$$R_s = 5.39"$$

Equation 6 provides the climatological precipitation ratio to determine the GTF.

$$GTF = \frac{R_t}{R_s}$$

$$GTF = \frac{5.62"}{5.39"}$$

$$GTF = 1.04"$$

The GTF at grid #10 is 1.04, or a 4% rainfall increase from the storm center location due to the orographic effects captured within the precipitation climatology. The GTF is then considered to be a temporal constant for the spatial transposition between that specific source/target grid point pair, for that storm only, and can be applied to the other durations for that storm.

10.1.5 Sample TAF Calculation

$$TAF = IPMF \times GTF \text{ (from Equation 1)}$$

$$TAF = 1.09 \times 1.04$$

$$TAF = 1.14$$

The TAF for Rapidan, VA 1995 when moved to the grid point at 37.90°N, -79.05°W, representing storm maximization and transposition, is 1.14. This is an overall increase of 14% from the original SPAS analyzed in-place rainfall. The TAF can then be applied to the DAD value for a given area size and duration to calculate the total adjusted rainfall. If the total adjusted rainfall is greater than the depth for all other transposable storms, it becomes the PMP depth at that grid point for that duration.

11. PMP Tool Outputs

The PMP tool provides basin-specific PMP based for the area-size of the basin. For each storm type analyzed, the tool provides output in ESRI file geodatabase raster format. The output also includes a basin average PMP table. If the sub-basin average option was checked, the tool provides averages for each sub-basin. The depths are calculated for the area-size of the basin, so no further areal reduction should be applied. The tool also provides a point feature class containing PMP depths and controlling storms listed by SPAS ID. There are also temporally distributed accumulated rainfall tables for each temporal pattern applied to the basin described in Section 12.

Spatial patterns of PMP follow the precipitation frequency climatologies patterns. However, other spatial patterns are possible. In general, for basins less then 500-square miles, alternative spatial patterns do not affect the PMF elevation. For basins larger than 500-square miles, alternative spatial pattern may produce high water surface elevations and therefore should be investigated. These can be derived from observed storm patterns that have occurred over the basin or from patterns of storms in the region that are moved over the basin. These can then be that are redistributed over a given basin so that the final basin average PMP depths are the same, but the spatial pattern is representative of observed storm patterns.

Finally, a basin average PMP depth-duration chart in the .png image format is also included in the output folder. An example depth-duration chart is shown in Figure 11.1. Detailed output information is included in the PMP tool documentation in Appendix G.

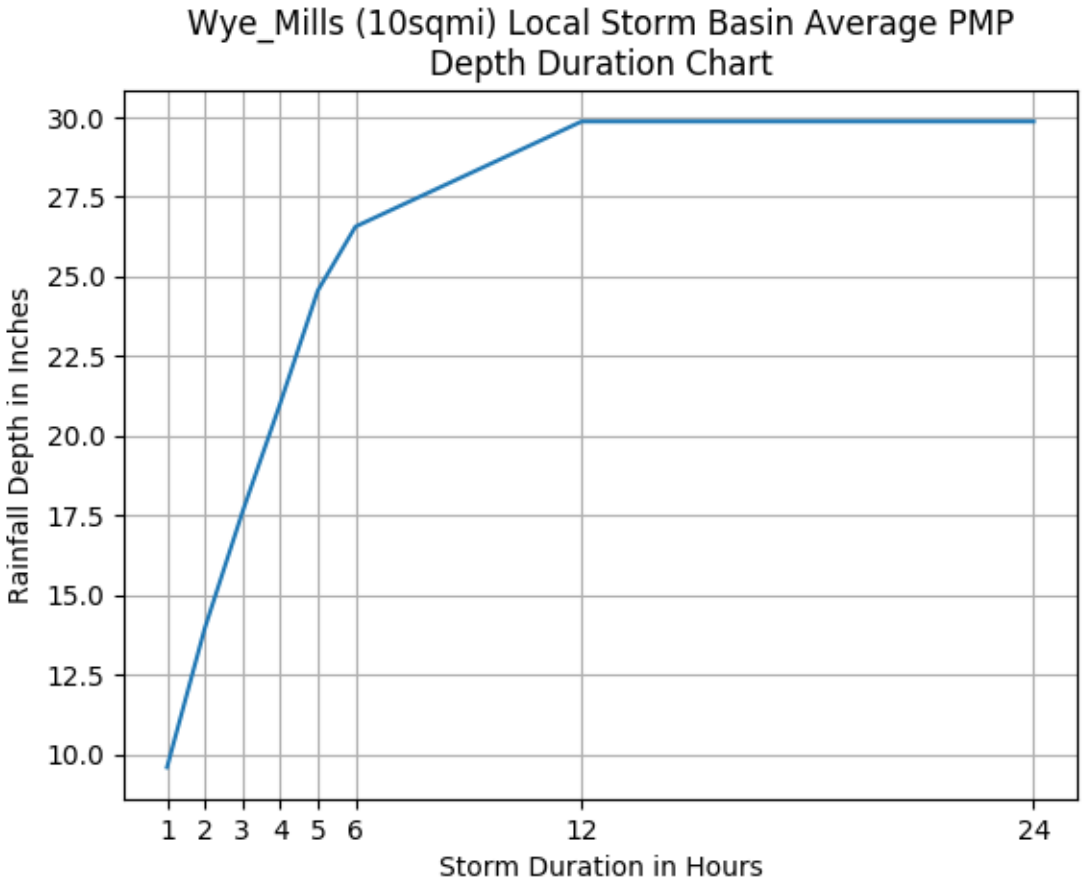

Figure 11.1: Sample PMP depth-area chart image provided in output folder

Gridded PMP depths were calculated for the entire study region at various index area-sizes for several durations as a visualization aid. The maps in Appendix A illustrate the depths for 1-, 10-, and 100-square mile area sizes for local storm PMP for 1-, 6-, and 24-hour durations and 10-, 100-, and 1,000-square mile area sizes for general and tropical storm PMP at 6-, 24-, and 72-hour durations.

12. Development of Temporal Distribution for Use in Runoff Modeling

Site-specific temporal patterns were developed which reflect the rainfall accumulation characteristics of the storm used for PMP in this basin. These temporal patterns were investigated and developed as part of adjacent studies, including the Virginia, Pennsylvania, and New Jersey studies. Storm temporal patterns were developed by storm type (local, general, and tropical) and through frequency analysis following Huff curve methods applied in NOAA Atlas 14 (e.g., Bonnin et al., 2006 and Perica et al., 2019).

In terms of storm types, local storms are characterized by short duration (6-hours or less) and small area size high intensity rainfall accumulations. They are often not associated with large scale weather patterns and can be influenced by local moisture sources. General storms produce precipitation over longer durations (greater than 6-hours) and cover larger areas with comparatively lower intensity rainfall accumulations. General storms are produced by large scale synoptic patterns generally associated with areas of low pressure and frontal systems. These are most common during the fall, winter, and spring seasons. Tropical storms rely on warm water from the Gulf of Mexico and the Gulf Stream in the Atlantic just off the East Coast along with supporting synoptic and upper-level weather patterns which occur from June through November. When these storms move slowly over a region, large amounts of rainfall can be produced both in convective bursts and over longer durations. Some storms exhibit characteristics of both the local and general storm or local and tropical rainfall accumulation patterns. For PMP analysis in this study, these are termed hybrid storms and are evaluated for PMP as more than one storm type.

The result of these methods produces several possible temporal patterns that were applied to the PMP depths. These included the 10^{th} percentile, 90^{th} percentile, synthetic, critically stacked, and controlling storms distributions. The development of each of these patterns are detailed below.

These outputs were provided for detailed testing and evaluation as part of the adjacent New Jersey statewide PMP study and again applied in the test basins evaluated in this study. This provided confirmation that the final set of temporal patterns applied the PMP tool represented PMP storm patterns by storm type for this study. In the final PMP tool, all temporal patterns evaluated in this study are available for use as needed.

12.1 Temporal Curve Development Methodology

Hourly gridded rainfall data were used for all SPAS analyzed storms. The maximum rain accumulations were based on rainfall at the storm center. The rainfall mass curve at the storm center were used for the temporal calculations. The steps used to derive the synthetic curves are described below.

12.1.1 Standardized Timing Distribution by Storm Type

The Significant Precipitation Period (SPP) for each storm was selected by excluding relatively small rainfall accumulations at the beginning and end of the rainfall duration. Accumulated rainfall (R) amounts during the SPP were used in the analysis for the hourly storm rainfall. The total rainfall during the SPP was used to normalize the hourly rainfall amounts. The time scale (T_S) was computed to describe the time duration when half of the rainfall accumulated (R). The procedures used to calculate these parameters are listed below.

12.1.2 Temporal Analysis Parameters Evaluated

SPP - Significant Precipitation Period when the majority of the rainfall occurred
R - Accumulated rainfall at the storm center during the SPP
R_n - Normalized R
T - Time when R occurred
T_s – Time when 50% accumulation occurs, value is set to zero. Negative time values precede the time to 50% rainfall, and positive values follow
T50 - Time when $R_n = 0.5$

12.1.3 Procedures used to calculate parameters

Below are the steps utilized to investigate the rainfall accumulation patterns from each storm used in the PMP development. Each of these were applied to the SPAS analyzed mass curves by storm type.

1. Determine the SPP. Inspect each storm's rainfall data for "inconsequential" rainfall at either the beginning and/or the end of the records. Remove these "tails" from calculations. Generally, AWA used a criterion of less than 0.1 inches/hour intensity to eliminate non-intense periods. No internal rainfall data were deleted.
2. Recalculate the accumulated rainfall records for R. This yields the SPP.
3. Plot the SPAS rainfall and R mass curves and inspect for reasonableness.
4. Normalize the R record by dividing all values by the total R to produce R_n for each hour, R_n ranges from 0.0 to 1.0.
5. Determine T50 using the time when $R_n = 0.5$.
6. Calculate T_s by subtracting T50 from each value of T. Negative time values precede the time to 50% rainfall, and positive values follow.
7. Determine maximum 24-hour and maximum 6-hour precipitation, convert accumulations into a ratio of the cumulative rainfall to the total accumulated rainfall for that duration.
8. Visually inspect resulting data to determine a best fit of the curves. This includes both the intensity (steepness) of accumulation and whether most of the accumulations are exhibiting a front, middle, or back loaded accumulation.

Graphs were prepared of a) R vs T, b) R_n vs T, c) R_n vs T_s, and d) maximum point precipitation for General (24-hour), Local (6-hour), and Tropical (24-hour) storm events. Evaluations of the resulting rainfall accumulation curves individually and in relation to each other were completed by visually inspecting the data. From these investigations, a rainfall accumulation pattern that represented a significant majority of the patterns with a steep intensity was utilized as the synthetic pattern. This process is subjective. The objective is to produce a synthetic pattern that captures the majority of the worst-case runoff scenarios for most basins and represents a physically possible temporal accumulation pattern. However, it is not possible for a single synthetic curve to capture all of the worst-case runoff scenarios for all basins.

12.1.4 Examples of Temporal Pattern Analyses from Adjacent Studies

Following the procedures and description from the previous section, results are presented as three graphs. The graphs are a) R vs T, b) R_n vs T, and c) R_n vs T_s for local, general, tropical, and hybrid storm types. Figure 12.1 to Figure 12.12 show these graphs for SPAS storm events east of the Appalachian Mountains which are relevant to this study.

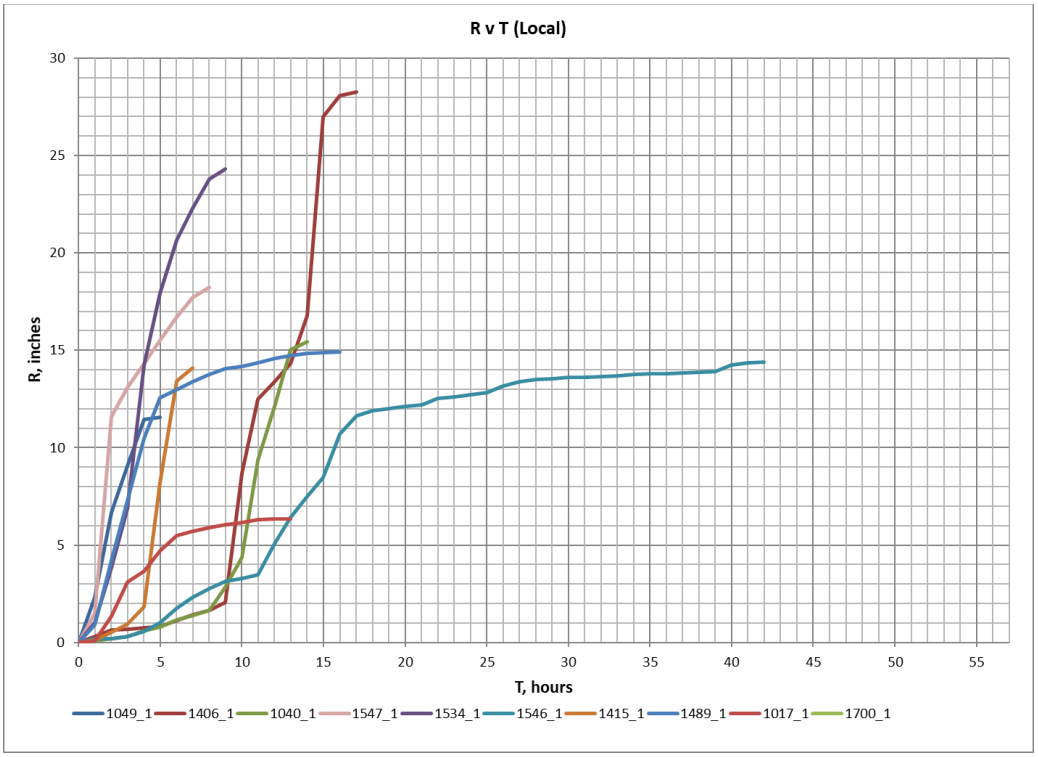

Figure 12.1: SPAS Rainfall (R) versus time (T) for Local Type Storm East of the Appalachians

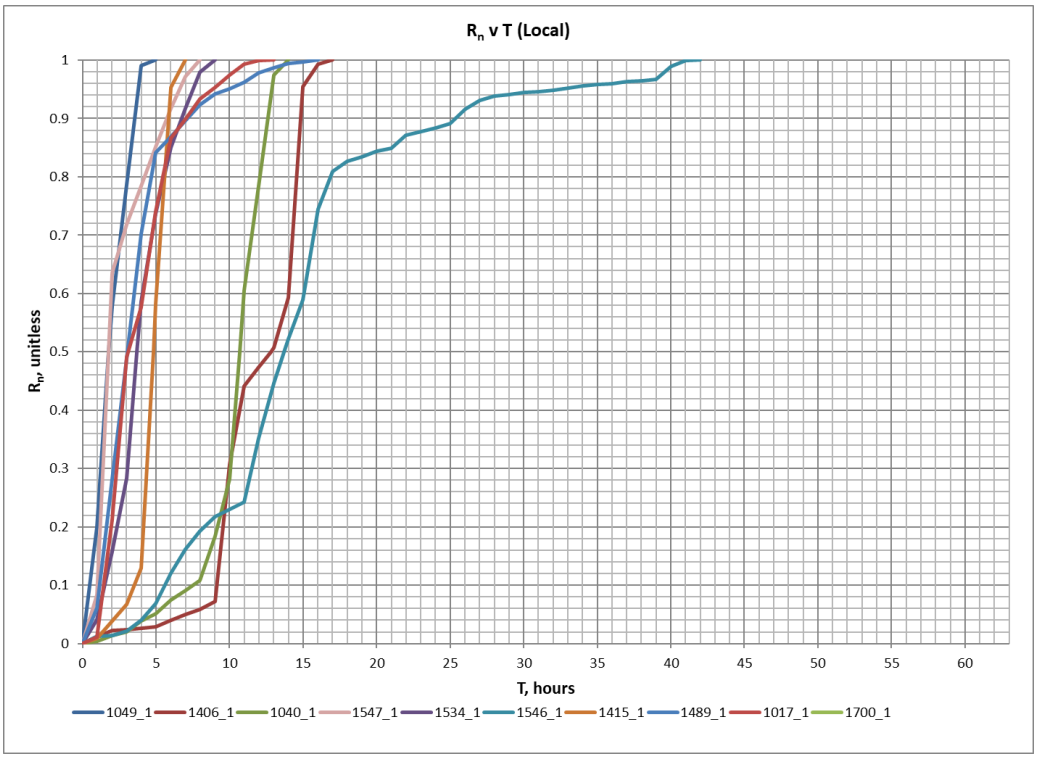

Figure 12.2: Normalized R (Rn) versus time (T) for Local Type Storm East of the Appalachians

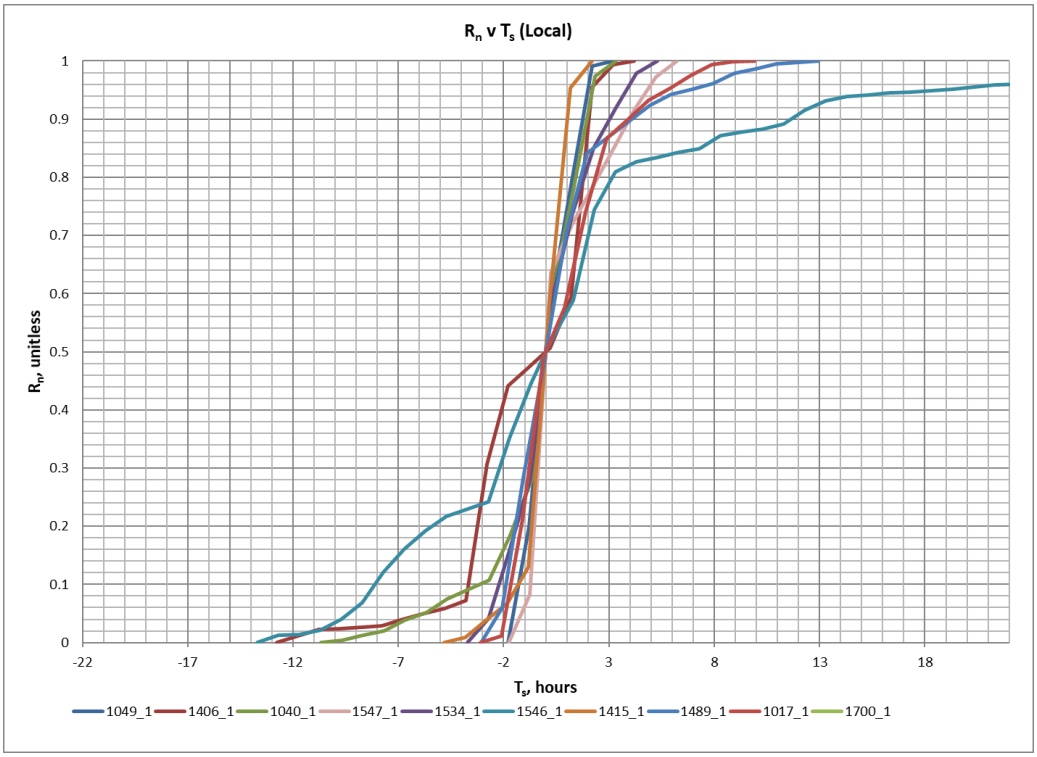

Figure 12.3: Normalized R (Rn) versus shifted time (Ts) for Local Type Storm East of the Appalachians

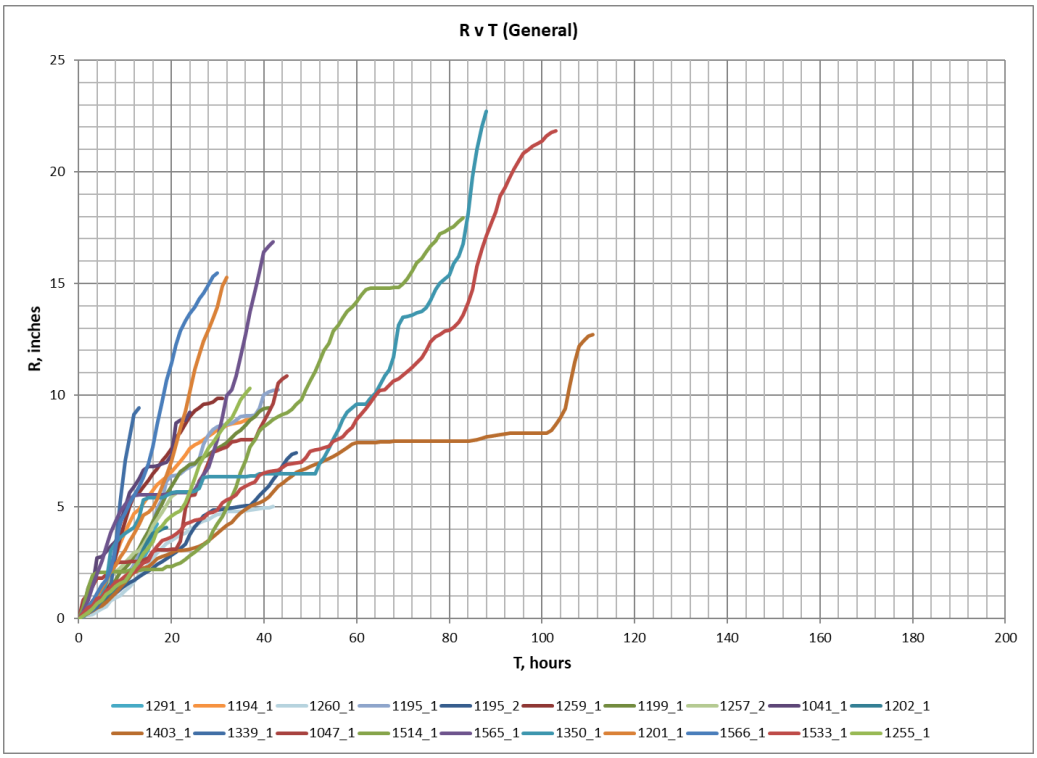

Figure 12.4: SPAS Rainfall (R) versus time (T) for General Type Storm East of the Appalachians

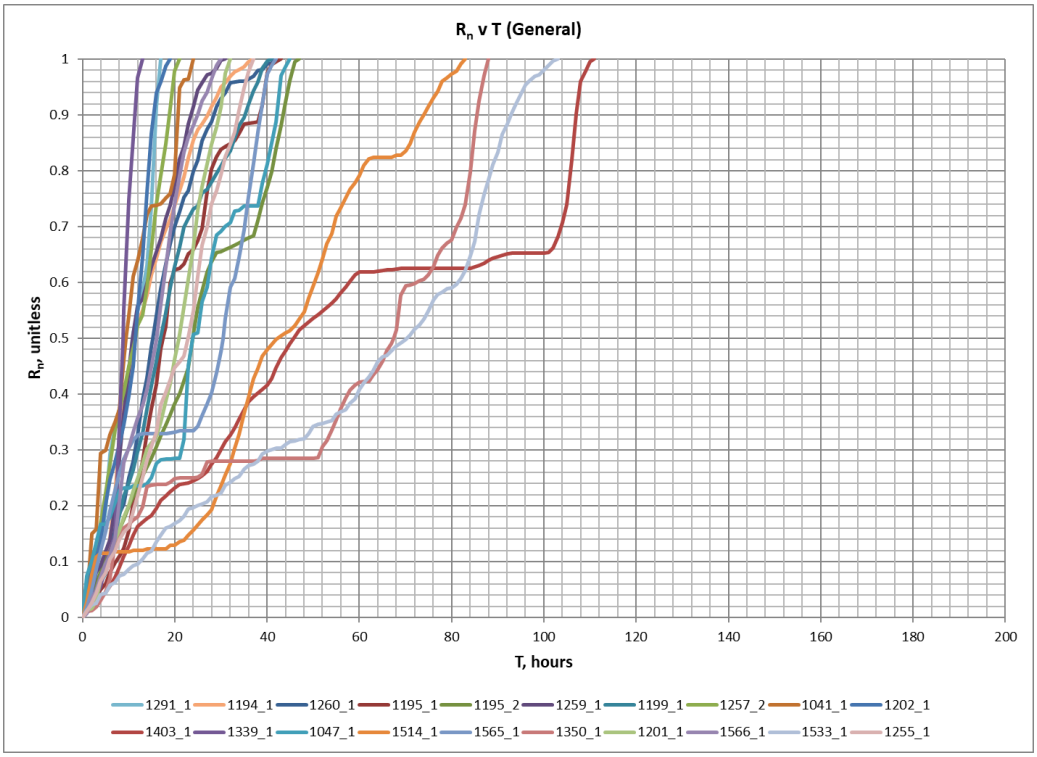

Figure 12.5: Normalized R (Rn) versus time (T) for General Type Storm East of the Appalachians

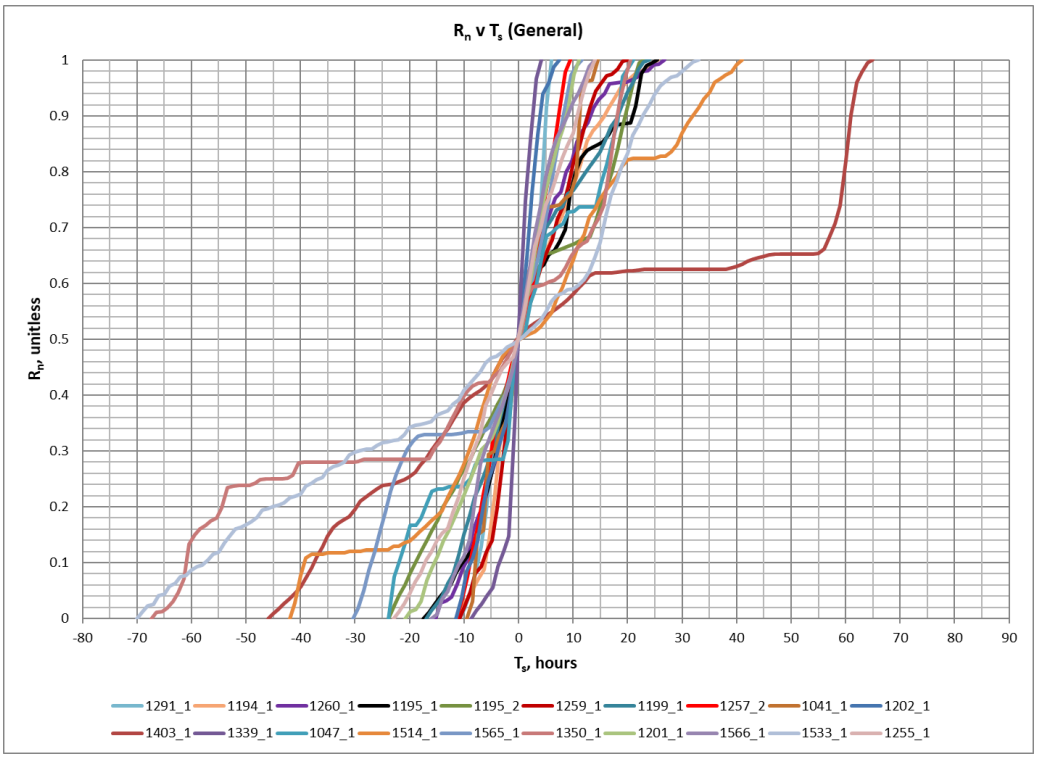

Figure 12.6: Normalized R (Rn) versus shifted time (Ts) for General Type Storm East of the Appalachians

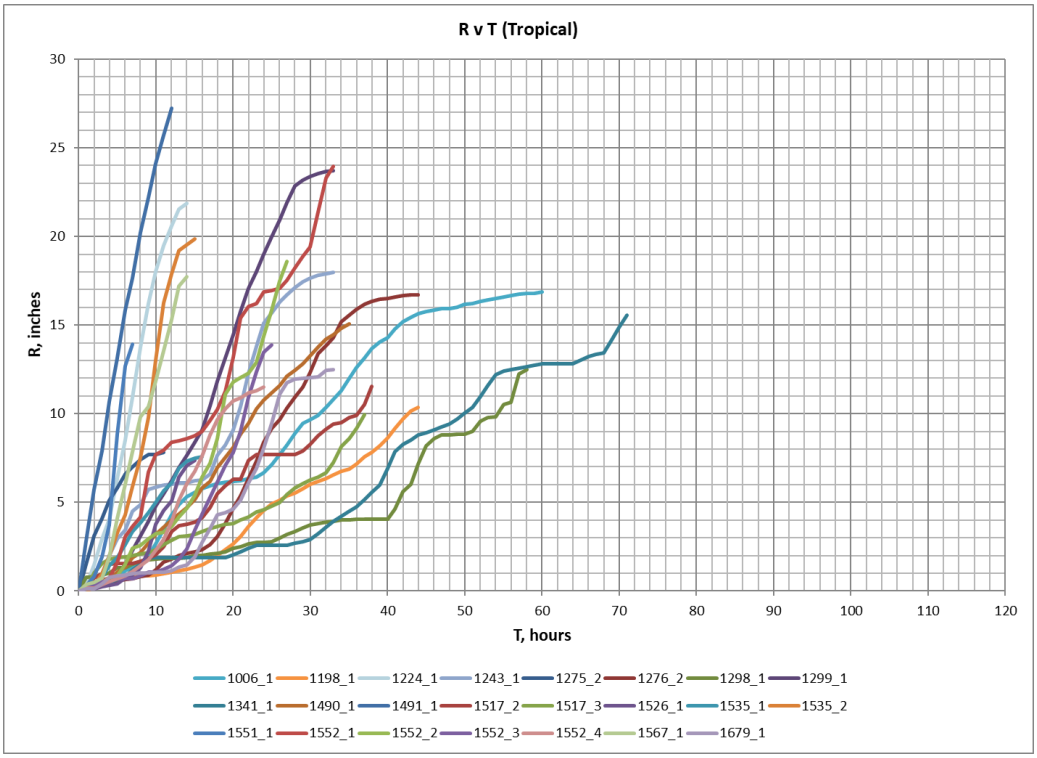

Figure 12.7: SPAS Rainfall (R) versus time (T) for Tropical Type Storm East of the Appalachians

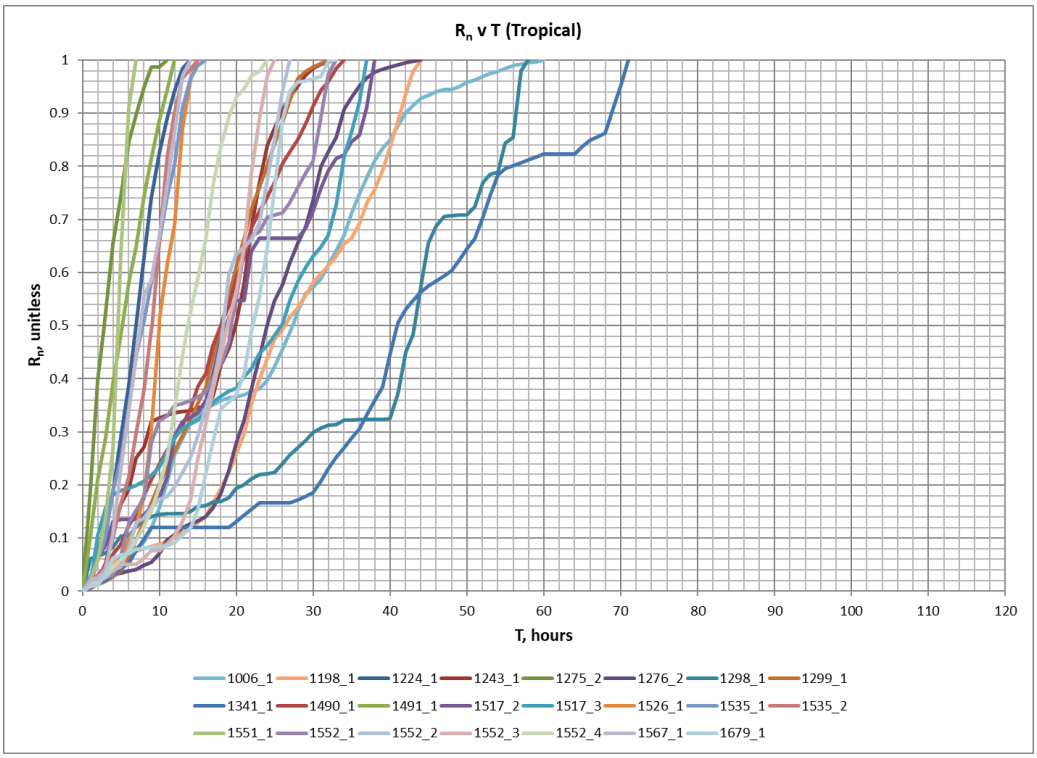

Figure 12.8: Normalized R (Rn) versus time (T) for Tropical Type Storm East of the Appalachians

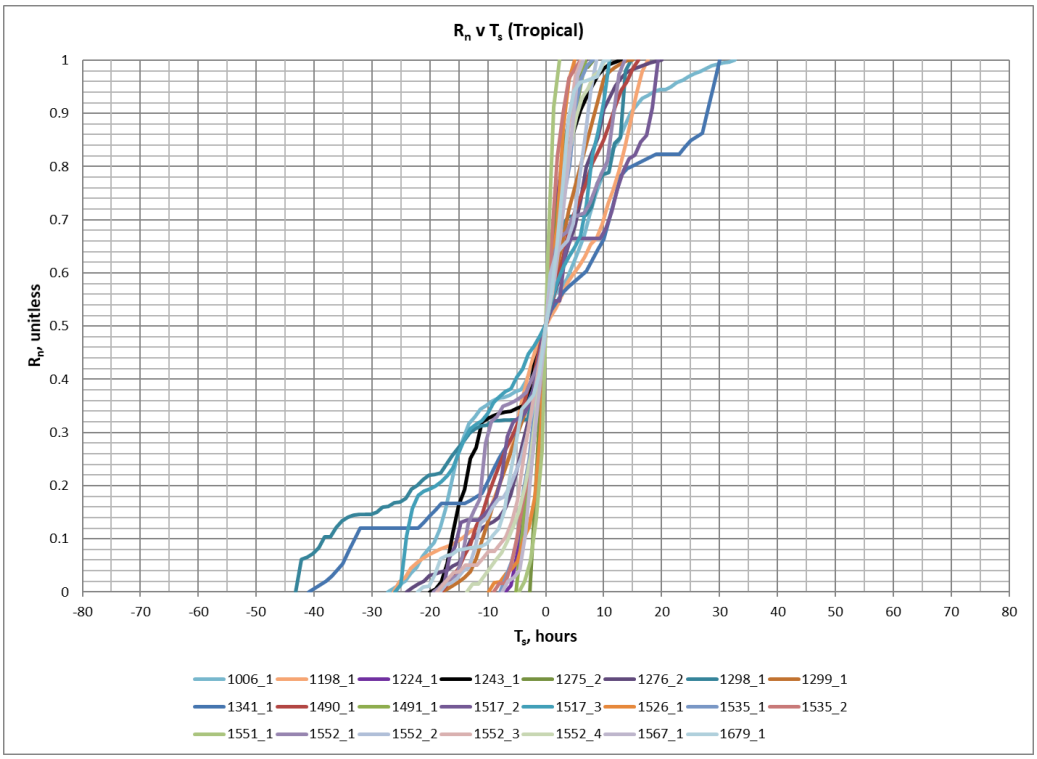

Figure 12.9: Normalized R (Rn) versus shifted time (Ts) for Tropical Type Storm East of the Appalachians

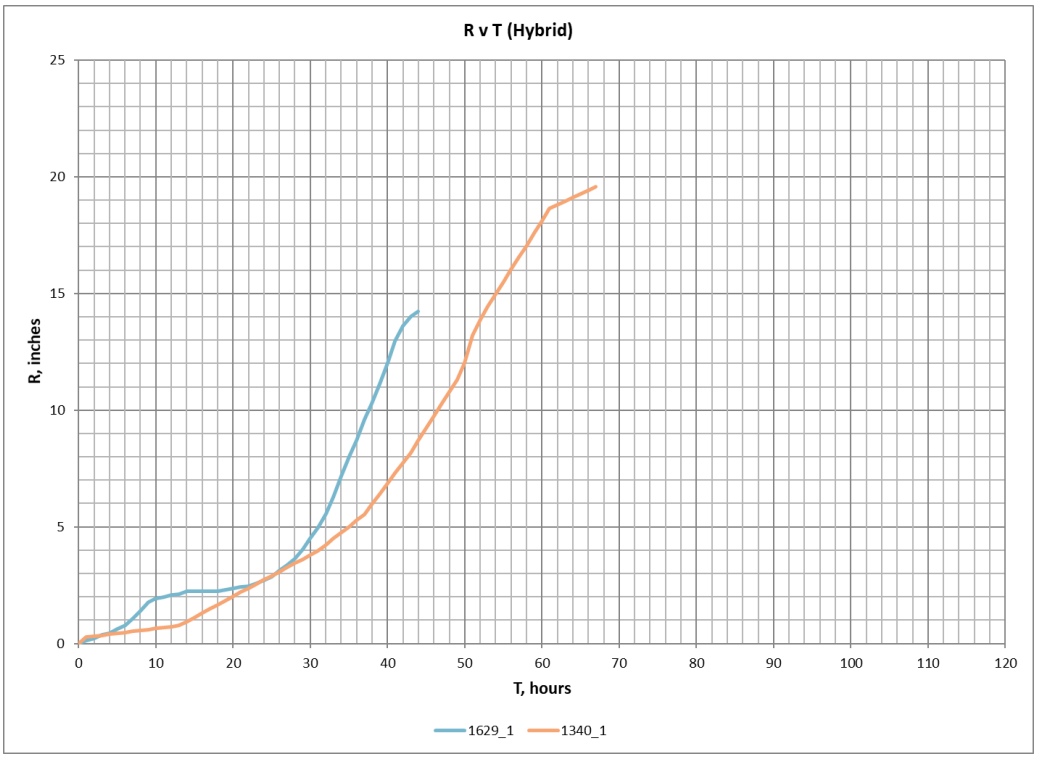

Figure 12.10: SPAS Rainfall (R) versus time (T) for Hybrid Type Storm East of the Appalachians

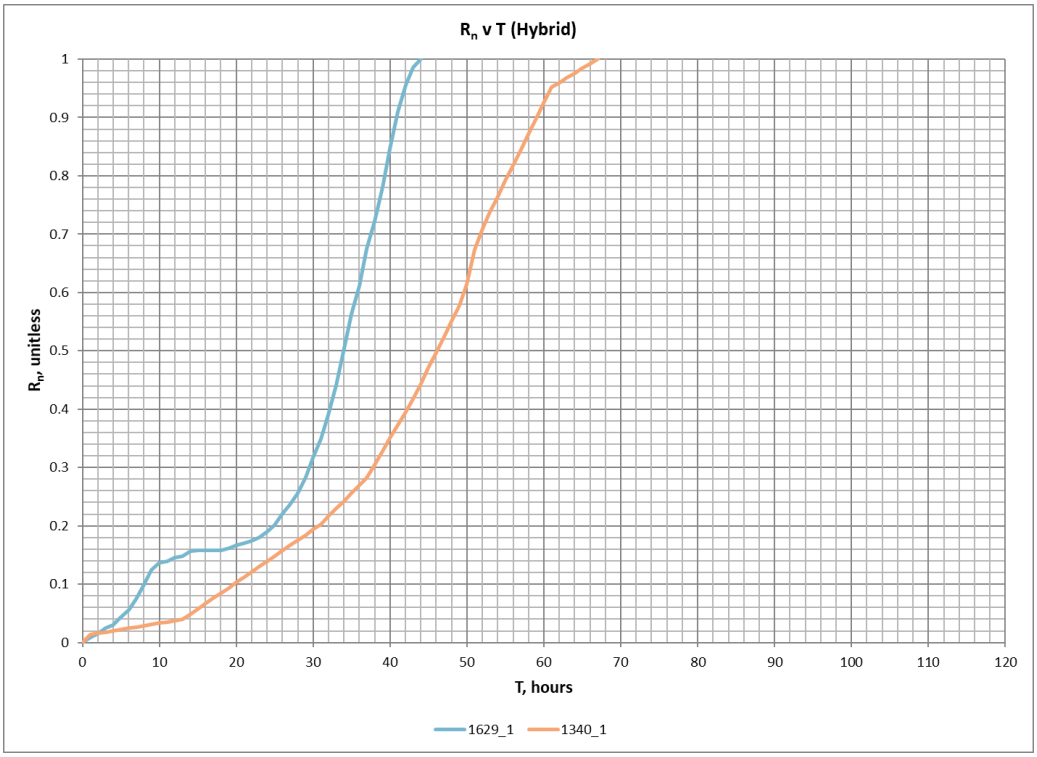

Figure 12.11: Normalized R (Rn) versus time (T) for Hybrid Type Storm East of the Appalachians

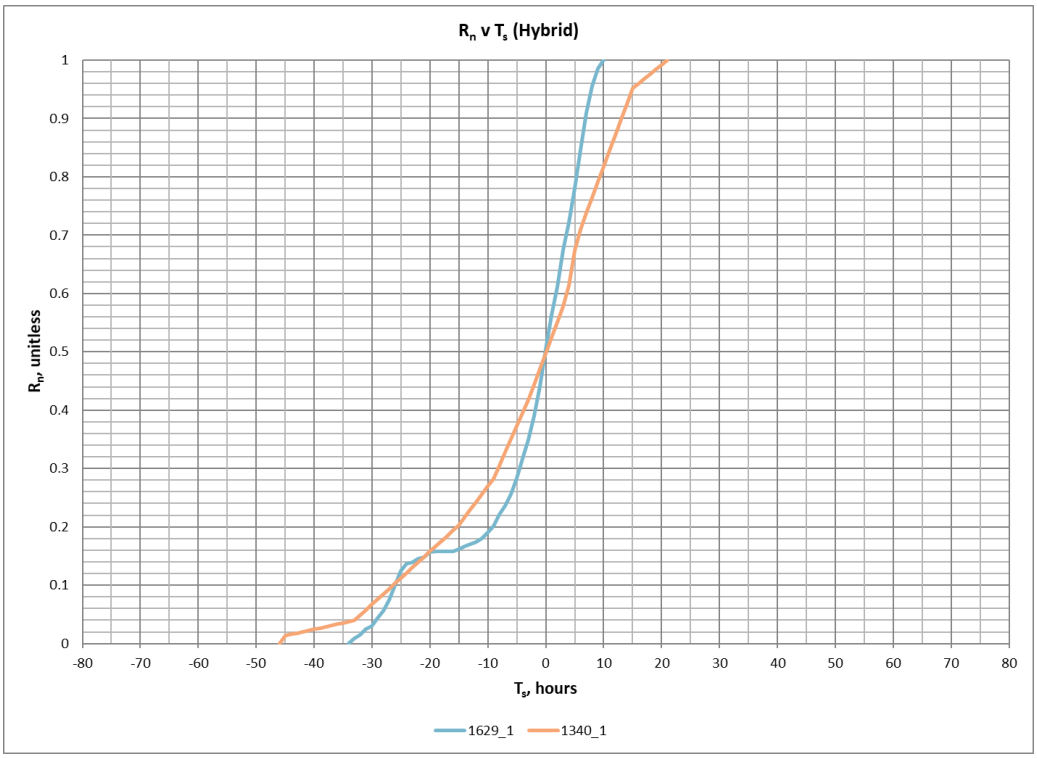

Figure 12.12: Normalized R (Rn) versus shifted time (Ts) for Hybrid Type Storm East of the Appalachians

12.2 Huff Curve Methodology

Huff curves provide a method of characterizing storm mass curves. They are a probabilistic representation of accumulated storm depths for corresponding accumulated storm durations expressed in dimensionless form. The development of Huff curves is described in detail in Huff (1967) and Bonta (2003), a summary of the steps is listed below.

For each SPAS storm center mass curve, the core cumulative precipitation amounts (R, noted in above section) were identified, the core cumulative rainfall were non-dimensionalized and converted into percentages of the total precipitation amount at one hour time steps. The non-dimensionalized duration values were interpolated and extracted at 0.02 increments from 0 to 1. Storms were grouped by storm type: local, general, tropical, and hybrid. The uniform incremental storm data (by duration and location) were combined and probabilities of occurrence were estimated at each 0.02 increment. Probabilities were estimated as 0.1 increments. The raw recommended curves (90^{th} and 10^{th}) were smoothed using a non-linear regression. Smoothing of the raw curves is performed to account for statistical noise in the analysis (Huff, 1967; Bonta, 2003).

The curves generated in this study can be generically described as:

- 90^{th} curve - the 90th curve indicates that 10% of the corresponding SPAS storms had distributions that fell above and to the left of the 90^{th} curve (front-loaded)
- 50^{th} curve - the 50th curve indicates that 50% of the corresponding SPAS storms had distributions that fell above and below the 50^{th} curve (mid-loaded)

- 10^{th} curve - the 10th curve indicates that 10% of the corresponding SPAS storms had distributions that fell below and to the right of the 10^{th} curve (back-loaded)

The raw data results are presented below (Figures 12.13-12.16); the final curves selected for use were smoothed using non-linear regression and data were provided at 5-minute (local storms) and 15-minute (general, hybrid, tropical) time steps from the non-linear regression equation (data were extracted from the non-linear equation). Some of the Huff curves result in accumulated precipitation at time zero, this is a result of front-loaded storms that generate a significant portion of their precipitation in the first hour, the analysis that was performed on hourly data, and the interpolation method that did not force the curve to zero. The final set of Huff curves were set to zero at time zero. The NRCS Type II curve (also known as the SCS curve) is considered a standard temporal pattern for design purposes in many regions of the country; see Section 12.7 for additional description (NRCS, 2005). The Type II curve is added to figures in its native state for comparison (Type II).

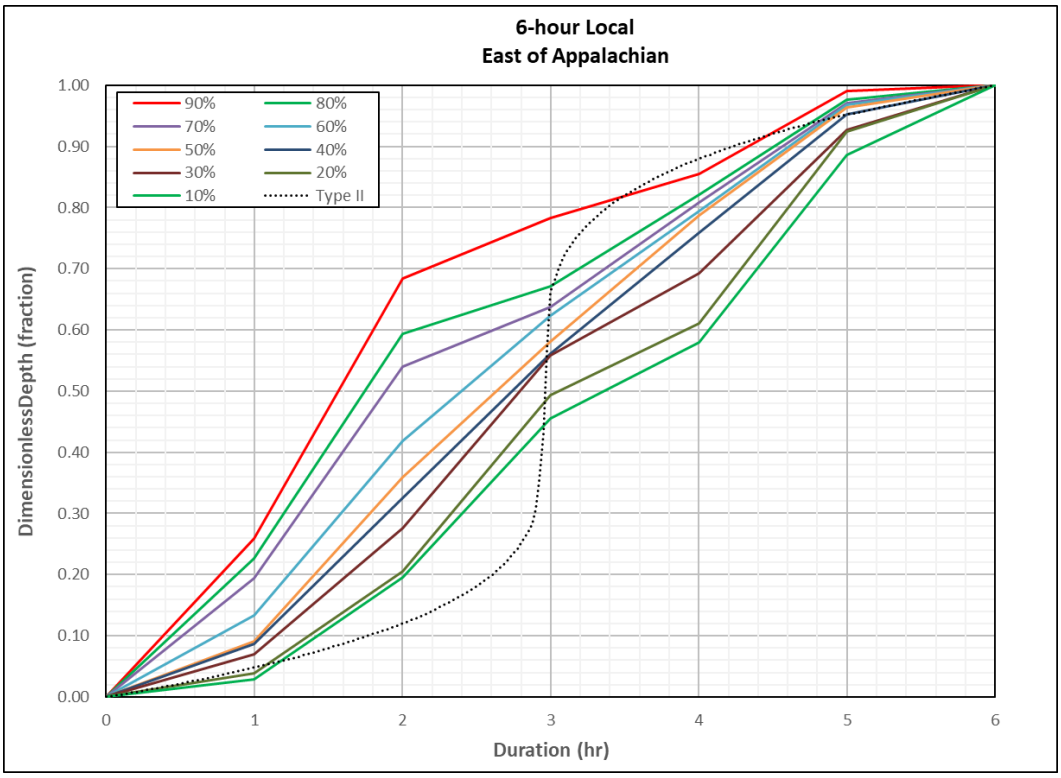

Figure 12.13: Raw Huff temporal curves for 6-hour Local storms East of the Appalachians

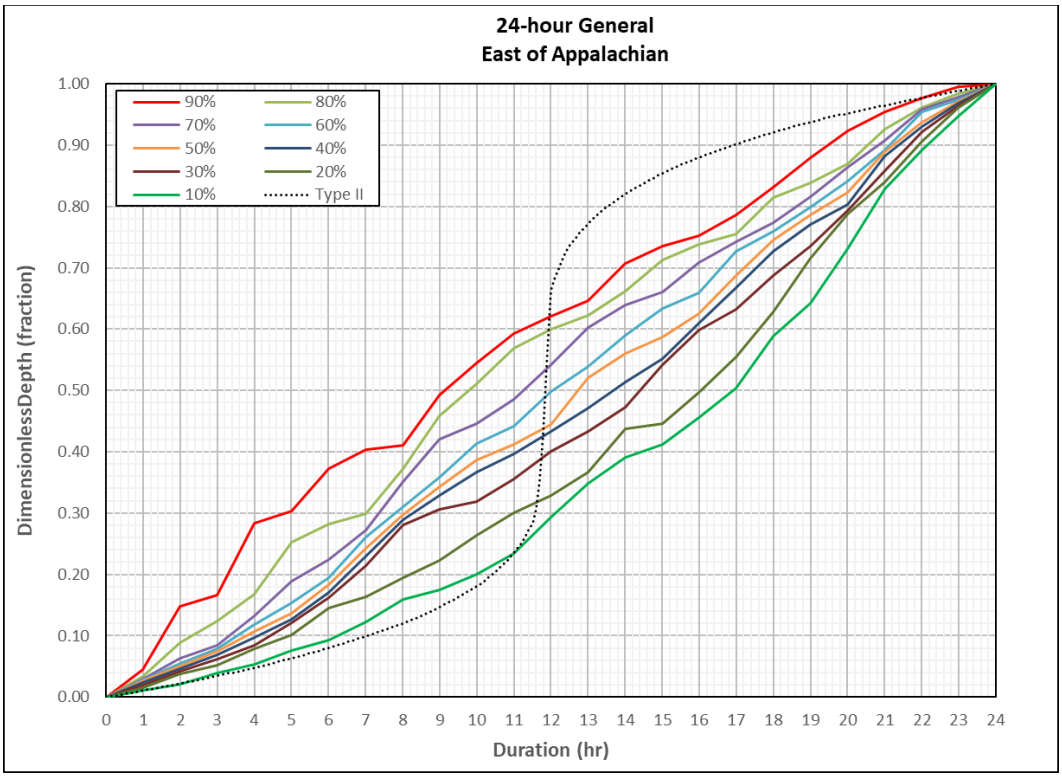

Figure 12.14: Raw Huff temporal curves for 24-hour General storms East of the Appalachians

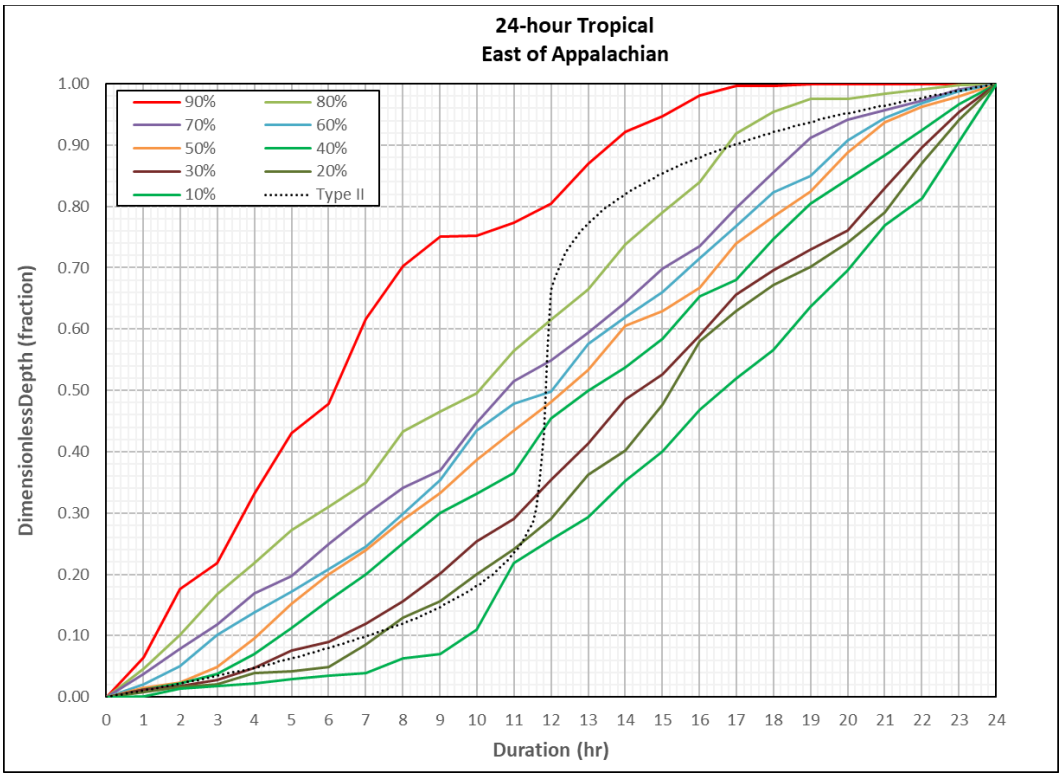

Figure 12.15: Raw Huff temporal curves for 24-hour Tropical storms East of the Appalachians

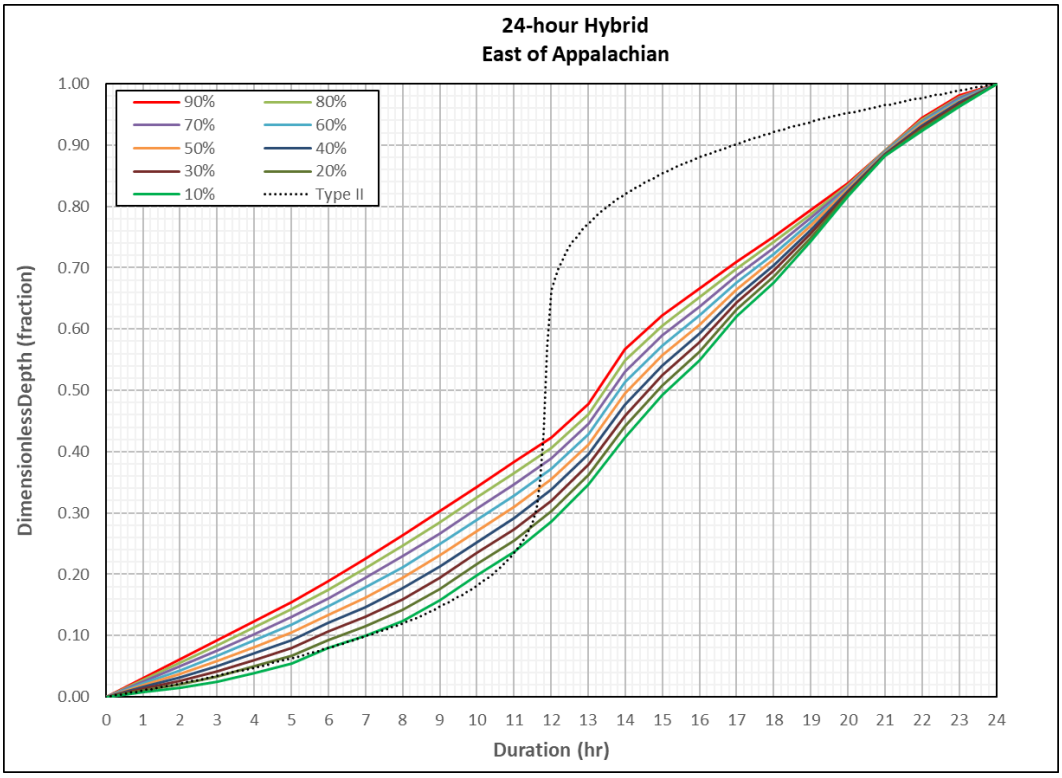

Figure 12.16: Raw Huff temporal curves for 24-hour Hybrid storms East of the Appalachians

12.3 Alternating Block (Critically Stacked) Pattern

Based on HMR 52 (Hansen et al., 1982) procedures and the USBR Flood Hydrology Manual (Cudworth, 1989) a "critically stacked" temporal distribution was developed as a synthetic rainfall distribution. The critically stacked temporal pattern yields a significantly different distribution than actual distributions associated with the storms used for PMP development in this study and in similar analysis of adjacent PMP studies (e.g., Ohio and Virginia). The critically stacked pattern imbeds PMP depths by duration within one another, i.e., the one-hour PMP is imbedded within the 3-hour, which is imbedded within the 6-hour, which is in turn imbedded in the 24-hour PMP. Figure 12.17 provides a graphical illustration of a critically stacked pattern. The critically stacked procedure has often been chosen in the past for runoff modeling because it represents a worst-case design scenario and ensures PMP depths are equaled at all durations.

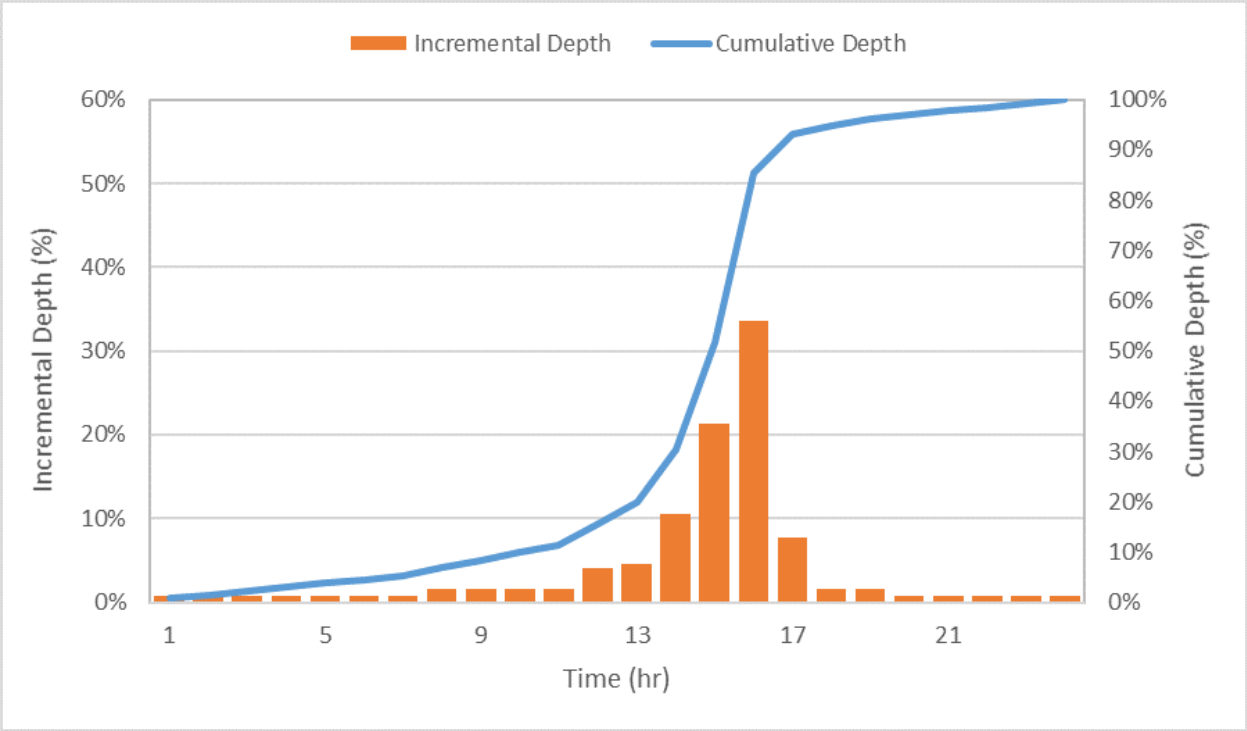

Figure 12.17: Graphical representation of the critically stacked temporal pattern

12.4 Sub-hourly Timing and 2-hour Local Storm Timing

AWA evaluated the 5-minute incremental rainfall accumulations patterns for thirty-six storms from the PMP type that had been analyzed with SPAS-NEXRAD to identify events that could be used to derive site-specific sub hourly accumulation guidance. This SPAS-NEXRAD 5-minute data were used to derive ratios of the greatest 15-, 30-, and 45-minute accumulations during the greatest 1-hour rainfall accumulation. Data from 36 local storm events allowed a specific evaluation of the sub-hourly rainfall patterns to be considered for the PMP study region.

HMR 55A provided recommended temporal patterns to be applied to the Maryland PMP to estimate sub-hourly timing. It is important to note that the 15-minute incremental

accumulation ratios derived for the local PMP storm in HMR 55A is based on very limited (almost none) sub-hourly data. HMR 55A made reference to the limited amount of available data and suggested using HMR 49 information instead (HMR 55A Section 12.7).

Table 12.1 displays the results of this analysis. The largest difference between HMR 55A and this study occurs during the greatest 15-minute increment, where HMR 55A provides a value of 68% (see HMR 55A Table 12.4), while the actual storm data have an average of 38% and a maximum of 64%. HMR55A is used for comparison because that is the only HMR where an evaluation of sub hourly rainfall was completed.

AWA completed additional sensitivity analysis by comparing the sub hourly ratio data to similar data developed during the Arizona statewide PMP study (Kappel et al., 2013) and the Colorado-New Mexico statewide study (Kappel et al., 2018). The results from the Arizona and Colorado-New Mexico statewide PMP analyses and the EM 1-hour percentages are provided in Table 12.1 for comparison with the results. The 2-hour local storm temporal pattern was developed to account for local storms that are less than 2-hours. The 2-hour local storm temporal pattern utilized the stacked 5-min sub-hourly ratio data for the first hour and the second hour was evenly distributed. For example, if a storm event had 8-inches in the first hour and 1-inch in the second hour for a total storm of 9-inches, the accumulation pattern is shown in Figure 12.18.

Table 12.1: Sub-hourly ratio data from HMR 55A and evaluated again during the Pennsylvania study

Duration (hr)	Duration (min)	HMR 55A Table 12.4	MD PMP Local Storms	EM	CO/NM	AZ
0.083	5	-	16%	21%	15%	-
0.167	10	-	28%	38%	28%	-
0.25	15	68%	38%	46%	39%	34%
0.50	30	86%	64%	67%	65%	61%
0.75	45	94%	83%	85%	84%	82%
1.00	60	100%	100%	100%	100%	100%

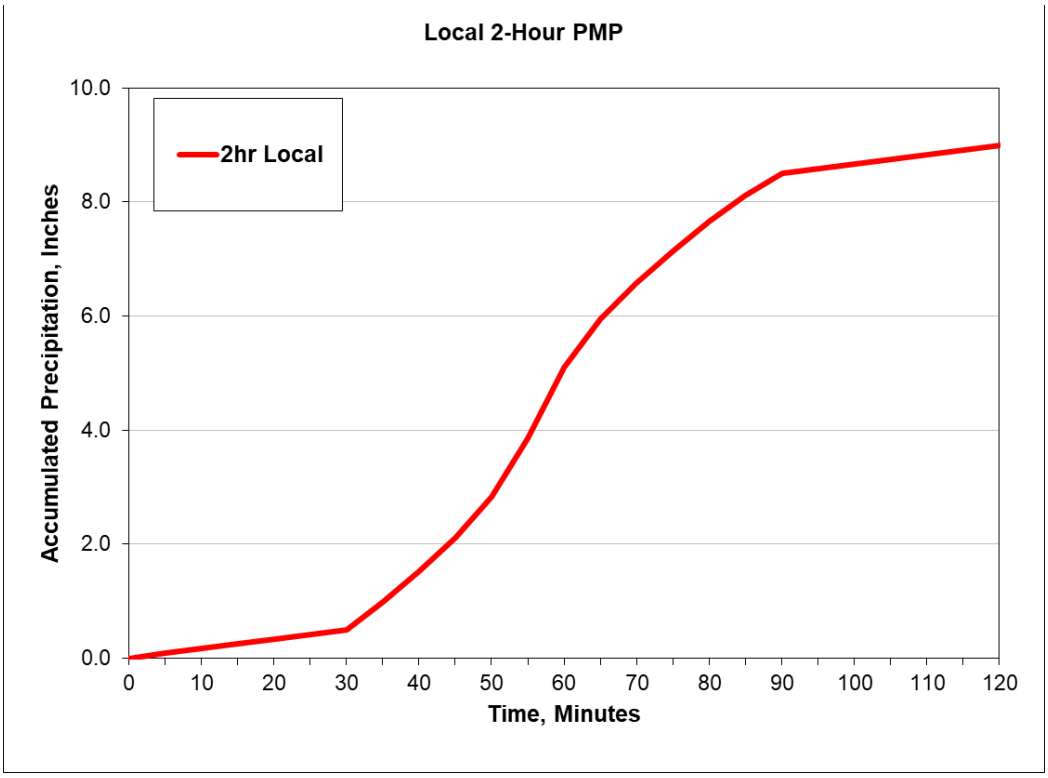

Figure 12.18: Hypothetical 2-hour local storm distribution

12.5 Application of Temporal Patterns

Each of the temporal patterns were derived through visual inspection, meteorological analyses, and comparisons with similar work. Analysis was completed after separating each event by storm type (e.g., general, local, tropical, hybrid). The temporal patterns reflect the meteorological conditions that produce each storm type. These represent observed extreme rainfall accumulation characteristics. It is assumed that similar patterns would occur during a PMP event. Therefore, it is recommended that the PMP temporal patterns included in the tool be used as they represent Maryland specific temporal patterns derived from extreme rainfall events used in this study.

In the PMP tool, there are a number of temporal patterns that can be applied. It is recommended that only patterns which "pass" the interim PMP depth test be used for a given basin per storm type. In addition, for basins larger than 100-square miles, the local storm PMP may not be required. In those situations, the alternating block pattern can be applied to confirm that storm type does not control PMP as this pattern represents the worst-case temporal pattern and therefore it it does not control, no additional local storm PMP runs would be required. Similarly, for basins less than 10-square miles, the tropical and general storm types are unlikely to control the PMP depths. In those cases, the alternating block (critically stacked) pattern can be run to confirm and if those don't control with that temporal pattern, no additional tropical or general storm runs would be required.

13. PMP Depth Sensitivities and Comparisons

In the process of deriving PMP depths, various assumptions and meteorological judgments were made within the framework of state-of-the-practice processes. These parameters and derived values are standard to the PMP development process; however, it is of interest to assess the sensitivity of PMP values to assumptions that were made and to the variability of input parameter values.

PMP depths and intermediate data produced for this study were rigorously evaluated throughout the process. ArcGIS was used as a visual and numerical evaluation tool to assess gridded values to ensure they fell within acceptable ranges and met test criteria. Several iterations of maps were produced as visual aids to help identify potential issues with calculations, transposition limits, DAD values, or storm adjustment values. The maps also helped to define storm characteristics and transposition limits, as discussed previously. Over the entire PMP analysis domain, different storms control PMP values at different locations for a given duration and area size.

In some instances, a discontinuity of PMP depths between adjacent grid point locations resulted. This occurs as a result of the binary transposition limits applied to the controlling storms, with no allowance for gradients of transpositionability. Therefore, different storms are affecting adjacent grids and may result in a shift in values over a short distance. In reality, there would be some transition for a given storm, but the process and definition of transpositionability does not allow for this. It is important to note that these discontinuities make little difference in the overall basin average PMP depths when applied for hydrologic analysis purposes for most basins. The discontinuities are only seen when analyzing data at the highest resolution (e.g., individual grid points). The non-meteorological discontinuities were addressed by adjusting transposition limits.

13.1 Comparison of PMP Depths Against HMR 51

This study employs a variety of improved methods when compared to previous HMR studies. These methods include:

- A far more robust storm analysis system with a higher temporal and spatial resolution
- Improved dew point/SST and precipitation climatologies that provide an increased ability to maximize and transpose storms
- Gridded PMP calculations which result in higher spatial and temporal resolutions
- A greatly expanded storm record

Unfortunately, working papers and notes from the HMRs are not available in most cases. Therefore, direct PMP comparisons between the HMRs and the values from this study are somewhat limited. Furthermore, due to the generalization of the regionally-based HMR studies, comparisons to the detailed gridded PMP of this study can vary greatly over short distances. However, comparisons were made for sensitivity purposes where data allowed. The PMP values in this study resulted in a wide range of both reductions and increases as compared to the HMRs.

Gridded index PMP depths were available for HMR 51 allowing a direct gridded comparison with the depths produced for this study. A gridded percent change was calculated for the area-sizes and durations common with the HMR index PMP maps. The maximum PMP depth from the general storm, tropical storm, or local storm types were used for the HMR 51 comparisons to account for differences in storm typing between this study and HMR 51. Table 13.1 shows the PMP depth comparisons made to HMR 51 by comparing the 10 square mile 6- and 24-hour PMP for each transposition zone.

Table 13.1: Average gridded percent change from HMR 51 to 10sqmi PMP depths

10 Square Miles						
ZONE	6-Hour Average PMP	6-Hour HMR 51	Percent Difference from HMR 51	24-Hour Average PMP	24-Hour HMR 51	Percent Difference from HMR 51
1 - Coastal Plain	27.3	27.9	-2.2%	30.6	36.9	-16.9%
2 - Piedmont	25.6	27.4	-6.6%	28.8	35.5	-18.8%
3 - Ridge	20.1	27.4	-26.6%	23.4	35.0	-33.3%
4 - Valley	20.7	27.5	-24.8%	23.3	35.3	-34.0%
5 - Appalachian Plateau	22.2	27.1	-18.1%	29.1	34.3	-15.1%

13.2 Comparison of PMP Depths with Precipitation Frequency

The ratio of the PMP to 100-year return period precipitation amounts is generally expected to range between two and four, with values as low as 1.7 and as high as 5.5 for regions east of 117°W found in HMR 57 and HMR 59 (Hansen et al., 1994; Corrigan et al., 1999). Further, as stated in HMR 59 "…*the comparison indicates that larger ratios are in lower elevations where short-duration, convective precipitation dominates, and smaller ratios in higher elevations where general storm, long duration precipitation is prevalent*" (Corrigan et al., 1999, p. 207).

For this study, the maximum 24-hour 1-square mile PMP was compared directly to the 100-year 24-hour rainfall-only values on a grid-by-grid basis for the entire analysis domain using GIS. The comparison was presented as a ratio of PMP to 100-year rainfall, and it was determined for each grid point. Figures 13.1-13.2 illustrate the PMP to 100-year rainfall ratios for 6-hour, and 24-hour PMP, respectively. The PMP to 100-year return period rainfall ratios vary from 3.5 to 8, after combining all storm types (local, general, and tropical). The values are in reasonable proportion expected for the study area and demonstrate the PMP values are at appropriately rare levels.

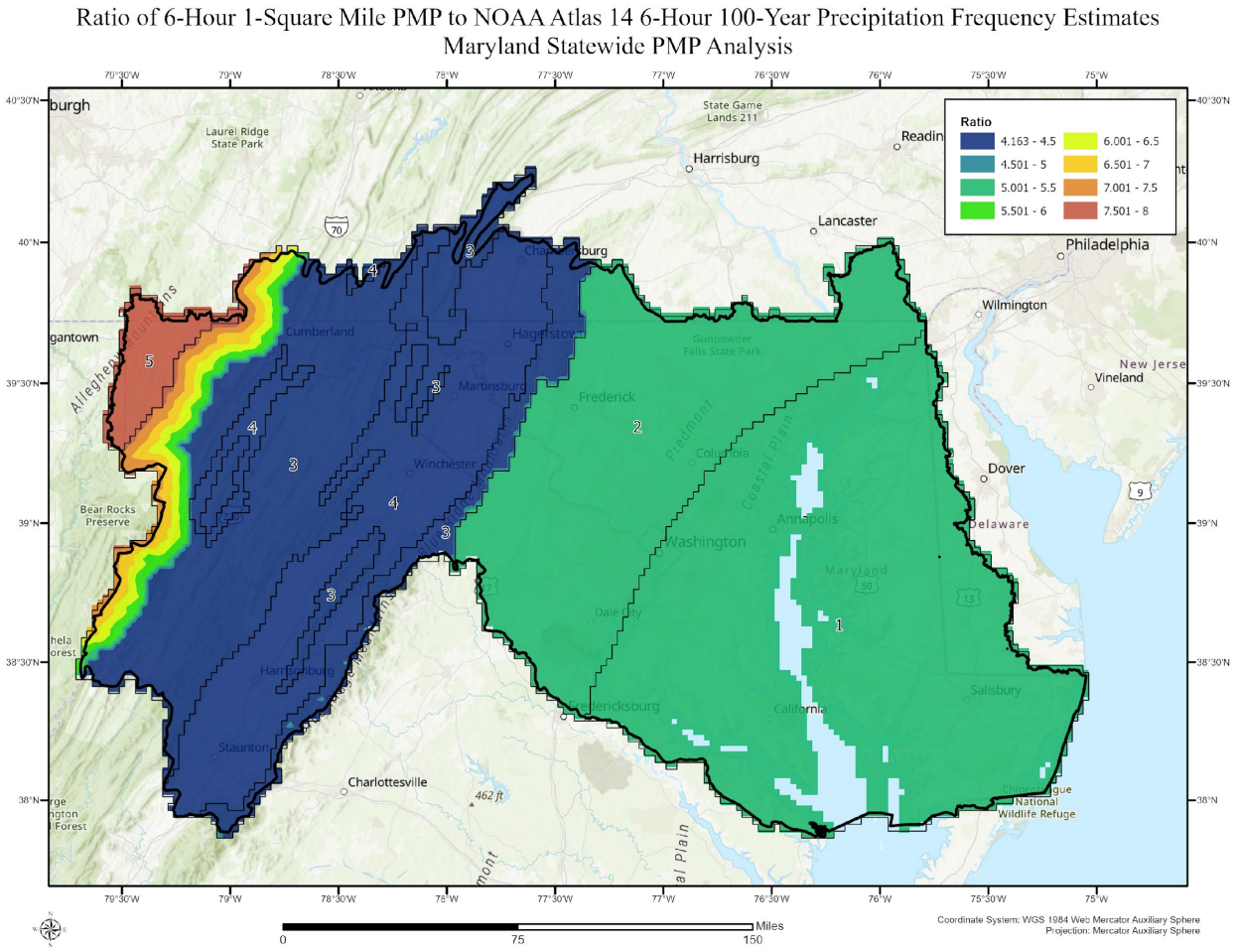

Figure 13.1: Ratio of 6-hour 1-square mile PMP to 100-year precipitation

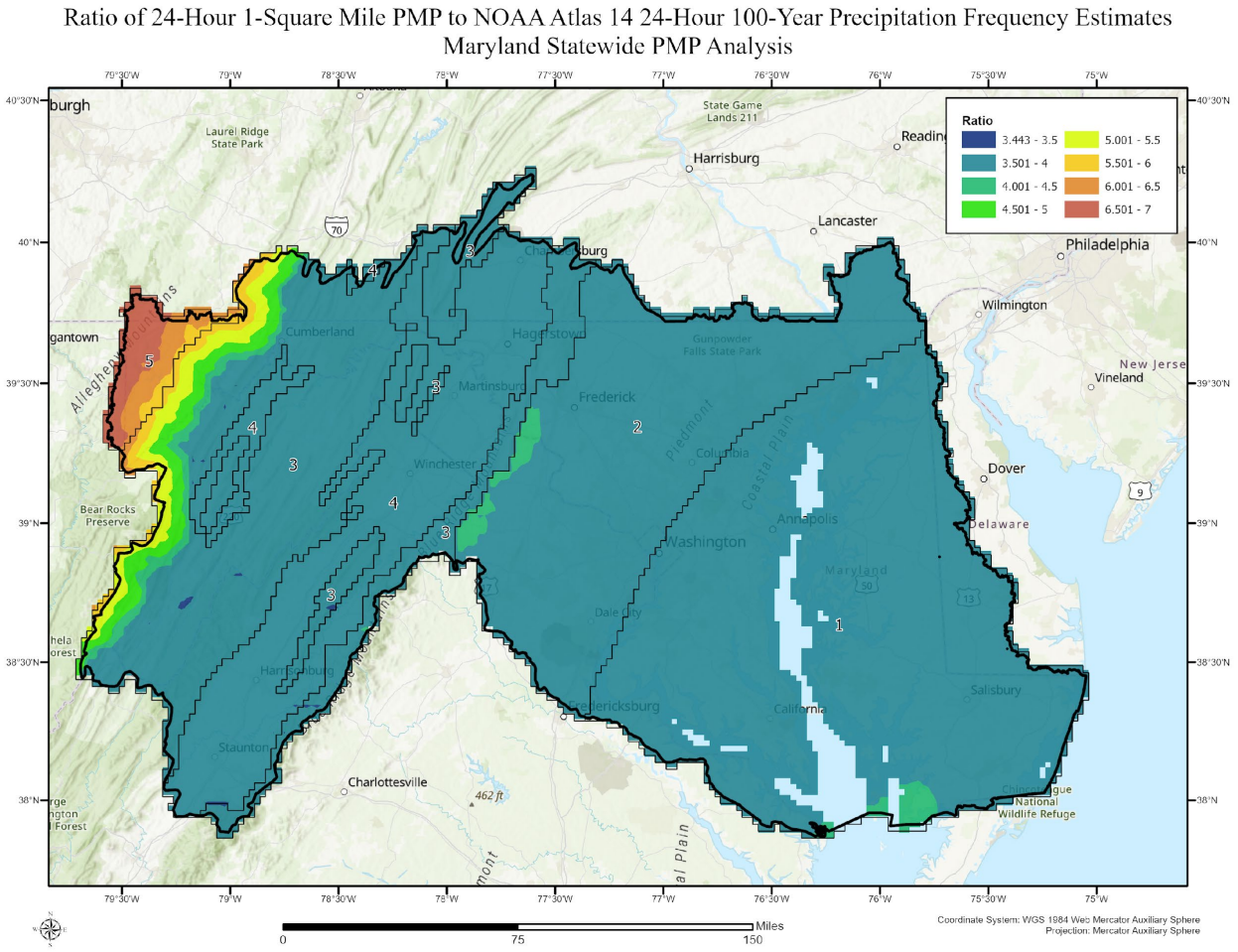

Figure 13.2: Ratio of 24-hour 1-square mile PMP to 100-year precipitation

13.3 Comparison of PMP Against Virginia and Pennsylvania Studies

Some areas of the Maryland Statewide study domain overlap previous statewide studies for Virginia (2015) and Pennsylvania (2019). Differences were expected due to updated datasets and procedures since the completion of those studies, but direct comparisons were made for all 3 storm types where overlap occurred for reference. Figures 13.3 through 13.8 show the percent difference from the previous PMP versions by storm type at relevant are sizes. A negative value indicates a decrease from the previous study and a positive value an increase. In areas where there is overlap, the Maryland PMP values represent the most current at the time of this publication and should be used by Maryland Dam Safety in areas of overlap. The main reasons for the differences between he studies include the following:

- Updated Dew Point Climatology Datasets used for storm maximizations where the climatological dew points have increase slightly in some storm maximizations
- Updated storm transposition limits were applied representing updated information specific related to the Maryland study domain

- Additional storms were used in the Maryland study that were not used in the Virginia or Pennsylvania study because they occurred subsequent to those studie
- The Virginia Study used a moisture transposition factor (MTF) in the total adjustment factor (TAF) calculations, which is not used in this study
- The Virginia study used trendline along a series of return frequencies to calculate the GTF, where the GTF currently applied the 100-year recurrence interval
- In the Virginia study, the Smethport July 1942 storms was only used on the west side of the Appalachian crest. In Pennsylvania and Maryland, it was allowed to cross the crest
- Variable smoothing factors were applied to the Smethport July 1942 when moving it across the Appalachian Crest in the Maryland study vs the Pennsylvania study

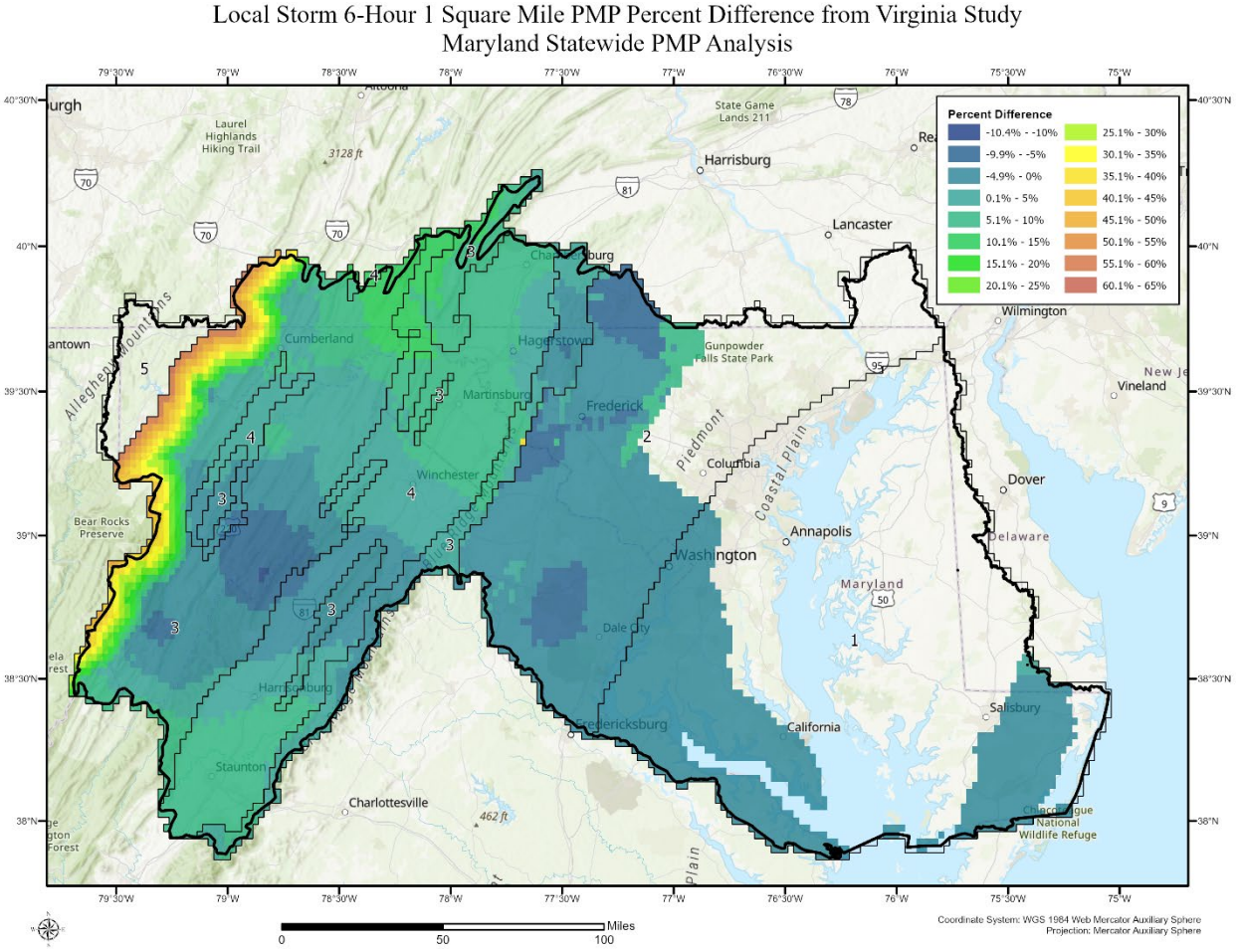

Figure 13.3: Percent difference for Local storm 6 hour 1 square mile PMP from Virginia Study

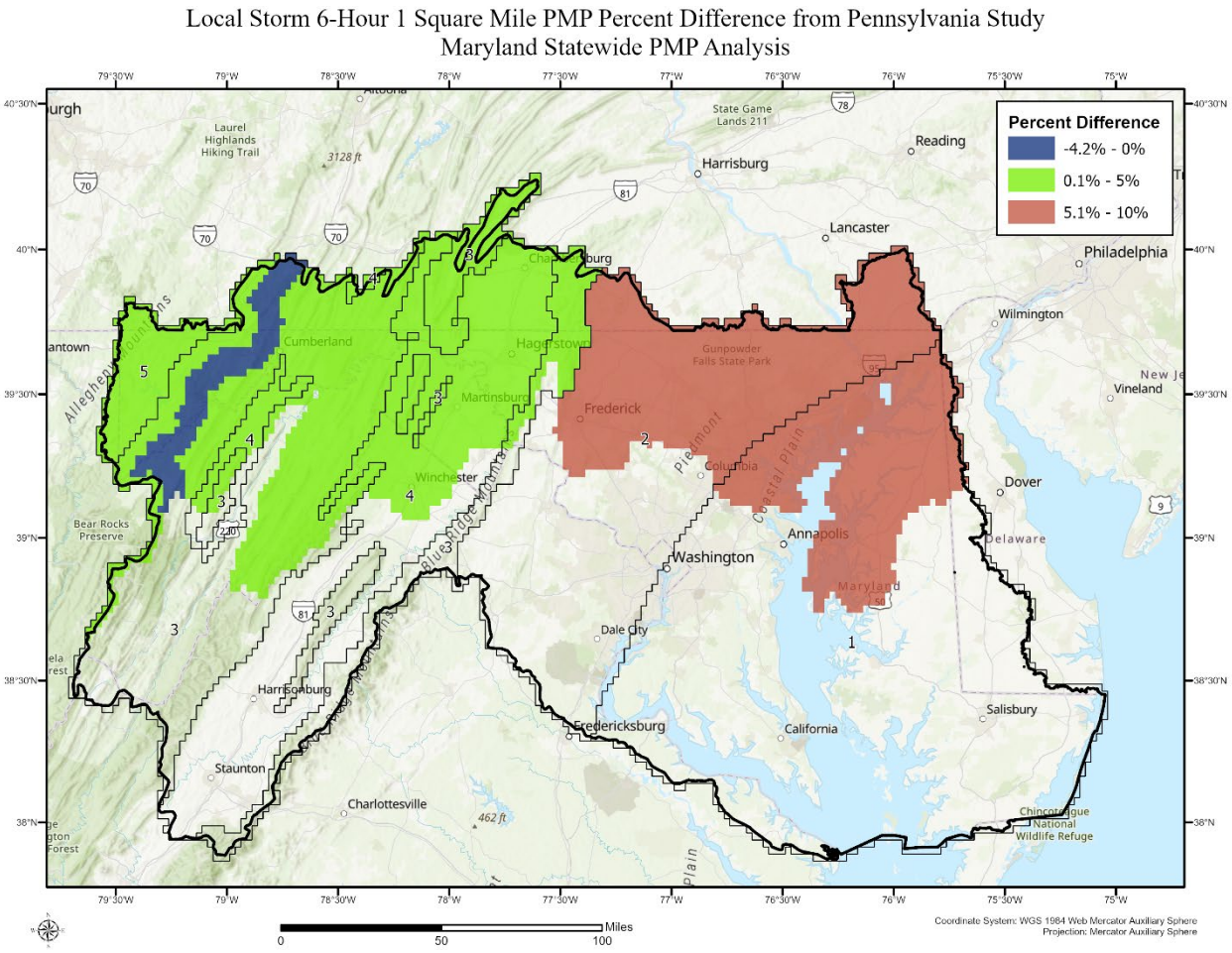

Figure 13.4: Percent difference for Local storm 6 hour 1 square mile PMP from Pennsylvania Study

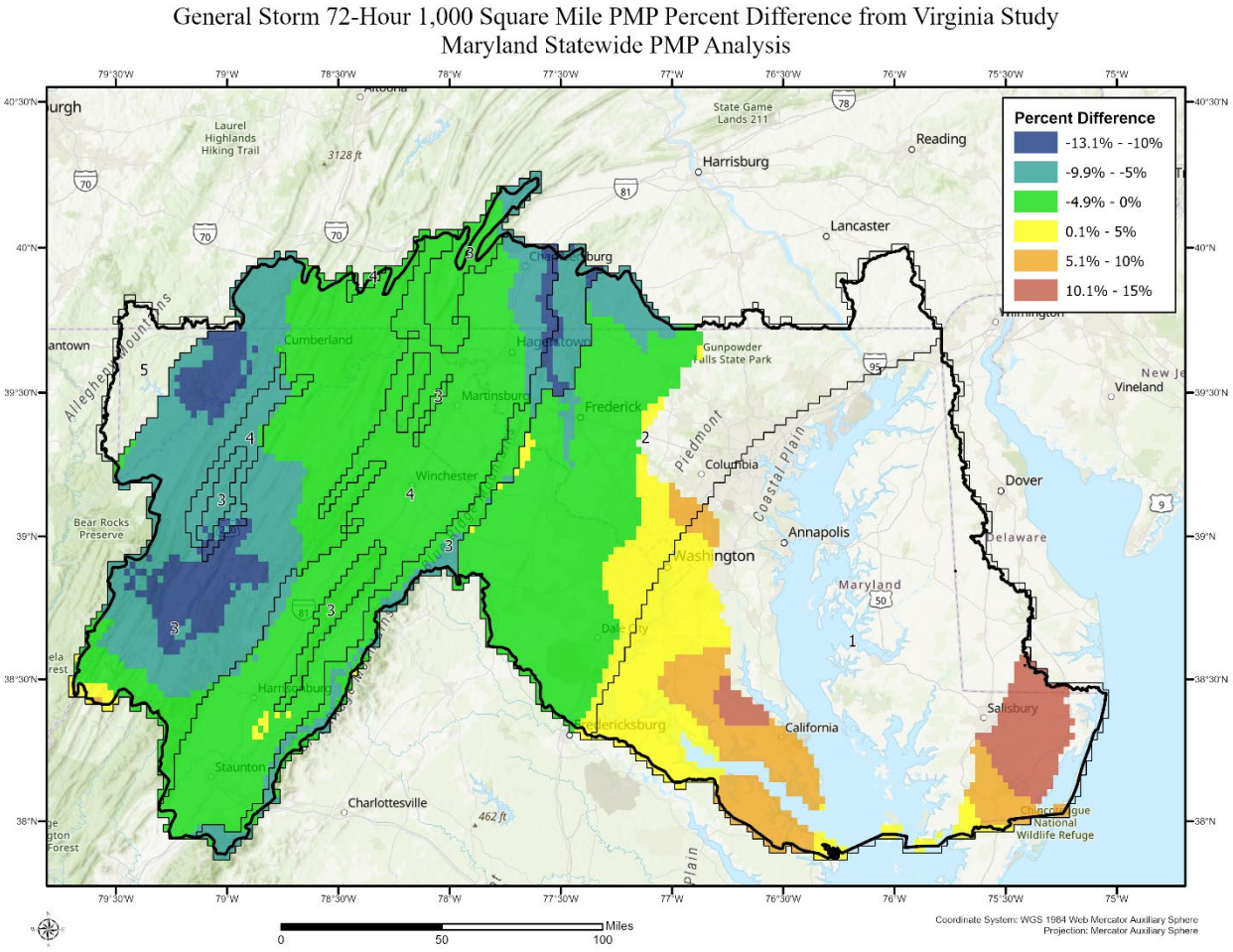

Figure 13.5: Percent difference for General storm 72 hour 1,000 square mile PMP from Virginia Study

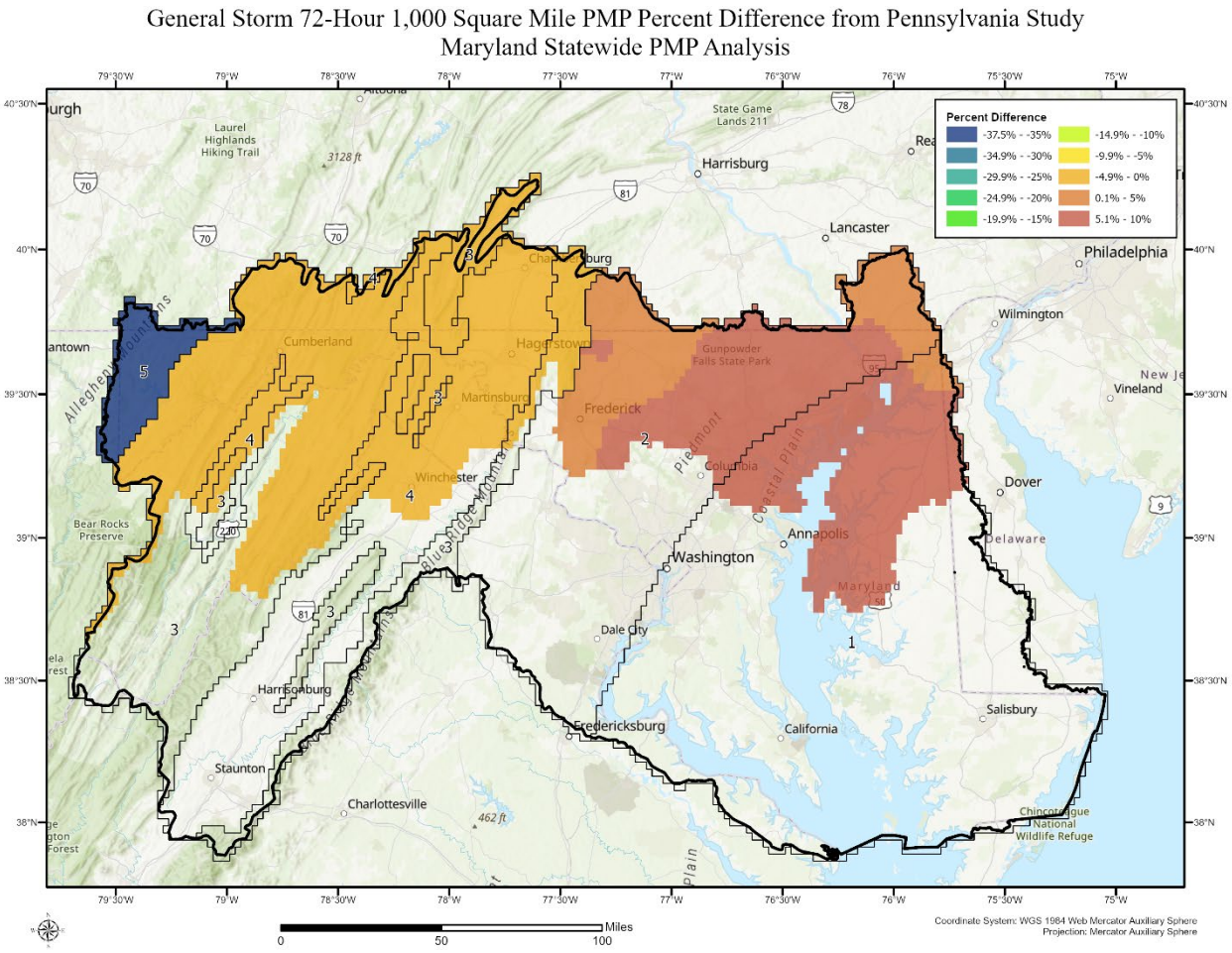

Figure 13.6: Percent difference for General storm 72 hour 1,000 square mile PMP from Pennsylvania Study

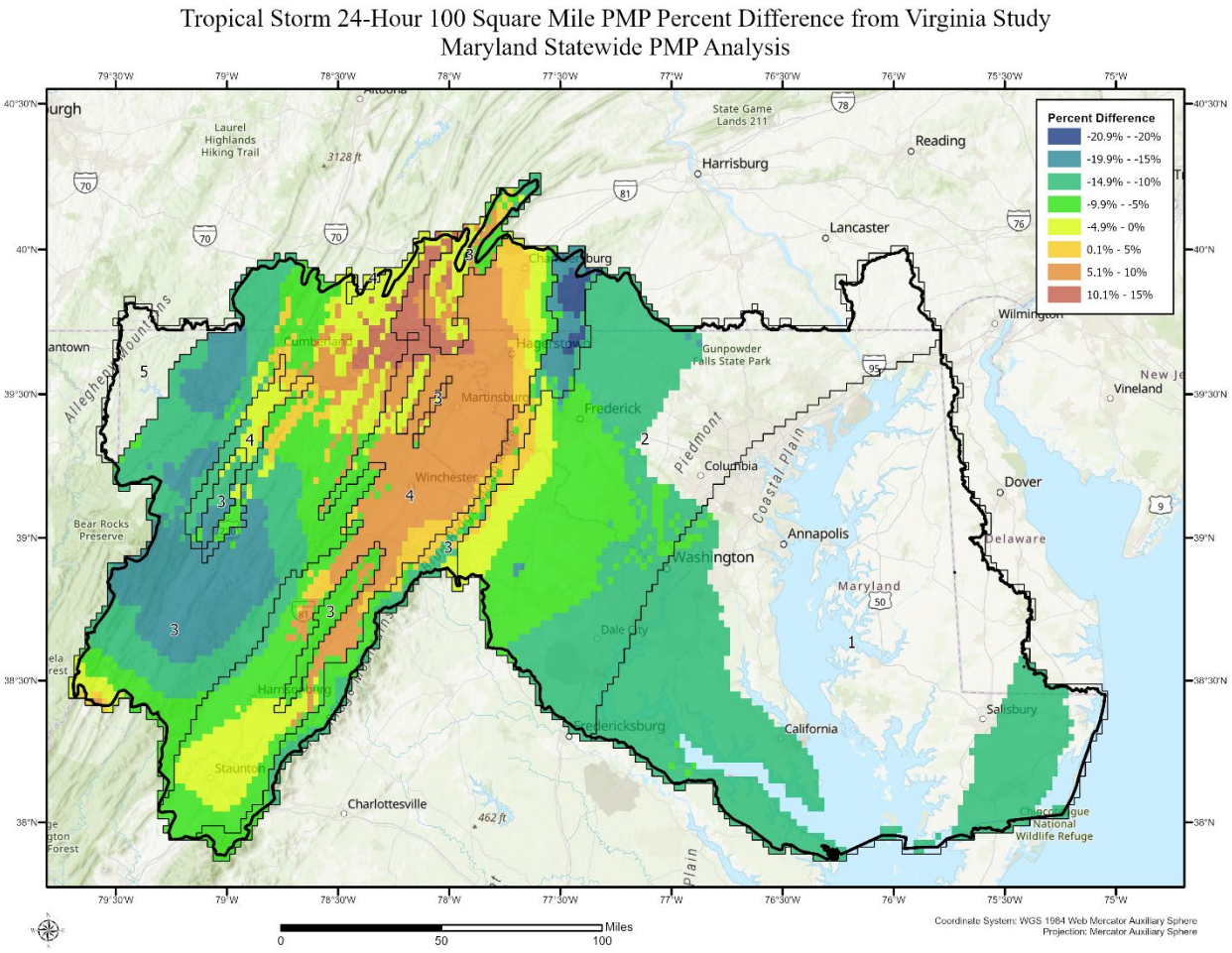

Figure 13.7: Percent difference for Tropical storm 24 hour 100 square mile PMP from Virginia Study

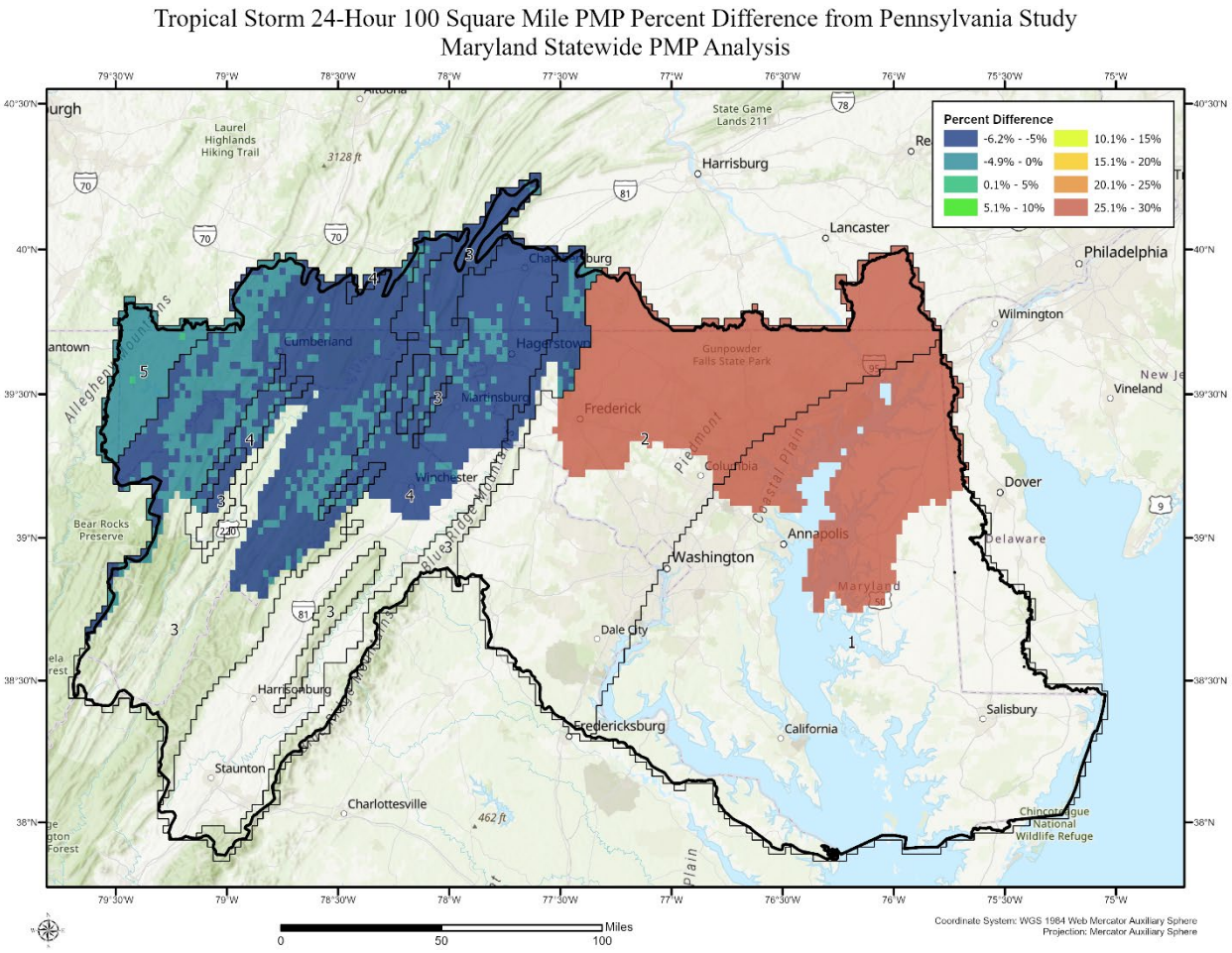

Figure 13.8: Percent difference for Tropical storm 24 hour 100 square mile PMP from Virginia Study

14. Annual Exceedance Probability Analysis of PMP Depths

Precipitation-frequency relationships were analyzed by AWA to derive the Annual Exceedance Probability (AEP) for the 6-hour and 24-hour PMP throughout the state (Figure 14.1). A regional L-moment analysis based on methods described in Hosking and Wallis (1997) and utilizing the R-statistical software packages lmom and lmomRFA developed by Hosking (Hosking 2015a, and Hosking 2015b) conducted.

14.1 Regional Frequency Analysis

A regional frequency analysis approach utilizes L-moment statistics instead of product moment statistics, which decreases the uncertainty of rainfall frequency estimates for more rare events and dampens the influence of outlier precipitation amounts from extreme storms (Hosking and Wallis, 1997). The basis of a regional frequency analysis is that data from sites within a homogeneous region can be pooled to improve the reliability of the magnitude-frequency estimates for all sites. A homogeneous region may be a geographic area delineated by meteorological climatologies or may be a collection of sites having similar characteristics pertinent to the phenomenon being investigated. The data and methods used are listed in the following sub-sections.

14.2 Precipitation Data and Annual Maximum Series Data

A search to identify individual stations in the region was conducted using precipitation data sources from official NWS stations, Remote Automated Weather Stations (RAWS), and USGS stations. Each station's period of record (POR) was evaluated to determine which stations were appropriate for use in the final regional analysis.

The term "annual maximum" refers to a single 6-hour and 24-hour precipitation maximum being selected for each precipitation gauge for each year of record. Several procedures were required for assembly of the precipitation annual maximum series (AMS) dataset. Figure 14.1 shows the extent of the study area and the stations used in the analysis after the completion of these procedures and all subsequent quality checks. Regional L-moment statistics (Hosking and Wallis, 1997) were computed for the annual maximum data for stations used in the analysis. A total of 265 hourly stations were used in the analysis with an average period of record of 37-years with a maximum record length of 115-years. A total of 606 daily stations were used in the analysis with an average period of record of 63-years with a maximum record length of 172-years.

- **Hourly Data Extraction** – Precipitation data from hourly gauges were applicable to the 6-hour and 24-hour duration. Precipitation annual maxima for hourly gauges were identified for each year. In the case of the 6-hour and 24-hour durations, a 6-hour and 24-hour window was examined and precipitation for the given 6-hour and 24-hour period were considered as a candidate annual maximum.

- **Daily Data Extraction** – Precipitation data from daily gauges were applicable to the 24-hour duration. Precipitation annual maxima for daily gauges were identified for each year. In the case of the 24-hour duration, each 1-day window was examined and

precipitation for the given 1-day period was considered as a candidate annual maximum.

- **Identification of Duplicate Gauges** – "Duplicate" gauge is the term given to the situation where two or more gauges are either co-located at a given site or closely located and have overlapping years of record. Closely located gauges were considered to be gauges within about 5 miles of each other and within about a hundred feet of elevation. The AMS of candidate pairs were scrutinized for having duplicate data before determining which gauge to be excludes as a duplicate. Generally, the longer record was retained for analysis as appropriate. Duplicate gauges were marked and not considered in regional frequency analysis to avoid double-counting.

- **Observational Period Adjustments** – Precipitation annual maxima for continuous durations are desired for regional precipitation-frequency analysis. This can be visualized as having continuous precipitation measurements and sliding a window of time for the desired duration through the continuous data to determine the precipitation maximum for the climatic year. However, daily precipitation is reported on fixed time intervals and not on a continuous basis. For example, at a daily gauge where measurements are taken each day at 7 AM, it is easy to imagine situations where part of a continuous 24-hour precipitation event is reported on day 1 (the first calendar day) and the remainder on day 2 (the second calendar day) during a 24-hour period that overlaps midnight. In this example, the maximum 1-day measurement underestimates the continuous 24-hour measurement, 3-day versus 72-hour measurements suffer the same issue, but with less underestimation, and 5-day versus 120-hour measurements suffer the same issue, also with less underestimation. Standard practice is to use an Observational Period Adjustment (Weiss, 1964; Young and McEnroe, 2003)) to adjust the sample statistics for the mean and standard deviation from fixed interval measurements to be representative of continuous measurements. For these adjustments a value of 1.13 13 (Young and McEnroe, 2003) was applied to the 1-day observational period and a value of 1.01 was applied to the 6-hour observational period, these adjustments are similar to other frequency studies (Hershfield, 1961; Young and McEnroe, 2003; Bonin et al., 2011). The observational period adjustment was applied to sample at-site mean values for precipitation gauges and durations (Hosking and Wallis, 1997). No adjustments are needed for dimensionless sample L-Moment ratio statistics for L-Cv, L-Skewness and L-Kurtosis.

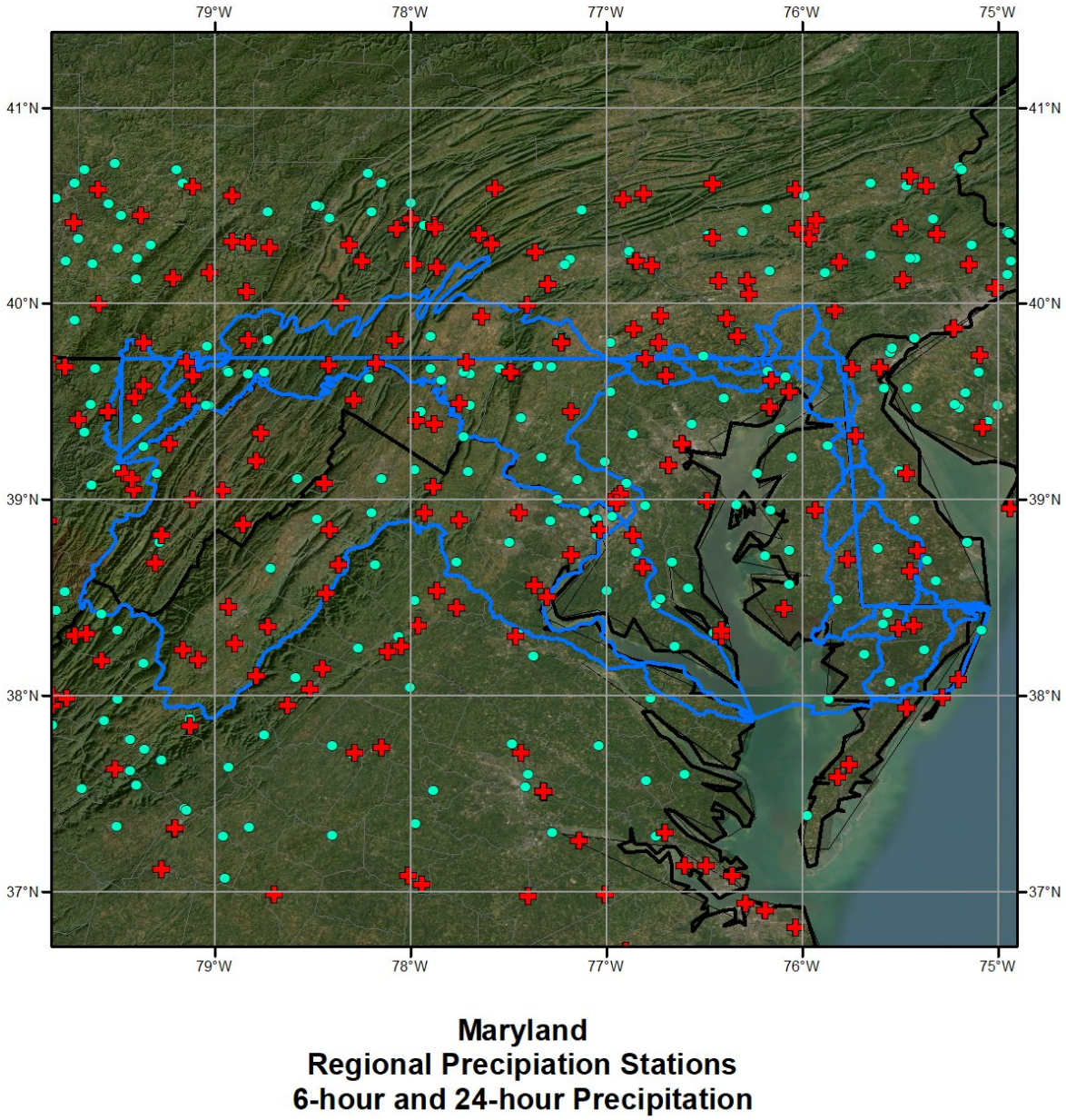

Figure 14.1: Locations of stations used for regional frequency analysis, red plus symbols are hourly stations and light green circles are daily stations

14.3 Regional L-moments

Key steps in the regional precipitation-frequency analysis included: i) extraction and quality control (QC) of annual maximum data, ii) calculation of an areal reduction factor used to relate point precipitation to areal/basin precipitation, iii) determination of homogeneous regions, iv) calculation of goodness-of-fit measurements, v) calculation of regional frequency curves, vi) estimation of the at-site mean (scaling factor) at any location in a region, and vii) derivation of uncertainly bounds.

The definition of a homogeneous region is the condition that all sites can be described by one probability distribution having common distribution parameters after the site data are rescaled by their at-site mean (Hosking and Wallis, 1997; Schaefer et al., 2006). The at-site mean is calculated as the mean value of the AMS data. All sites within a homogeneous region have a common regional magnitude-frequency curve, termed as a regional growth curve, that becomes site-specific after scaling by the at-site mean of the data. Quantile estimates at a given site, *i*, are estimated by:

$$Q_i(F) = u_i q(F) \qquad \text{Equation 6}$$

where $Q_i(F)$ is the at-site inverse Cumulative Distribution Function (CDF), u_i is the index flood, taken as the estimate of the at-site mean, and $q(F)$ is the regional growth curve, or regional inverse CDF. This method is often called an index-flood approach to regional frequency analyses (Hosking and Wallis, 1997). Regional L-moment statistics (Hosking and Wallis, 1997) were computed for the annual maximum data for stations in the basin of interest using R-statistical software packages lmom and lmomRFA developed by Hosking (Hosking, 2015a, and Hosking, 2015b). Figure 14.2 provides a graphical example of a regional growth curve that would be scaled to the at-site mean annual maximum (MAM) value (Equation 6).

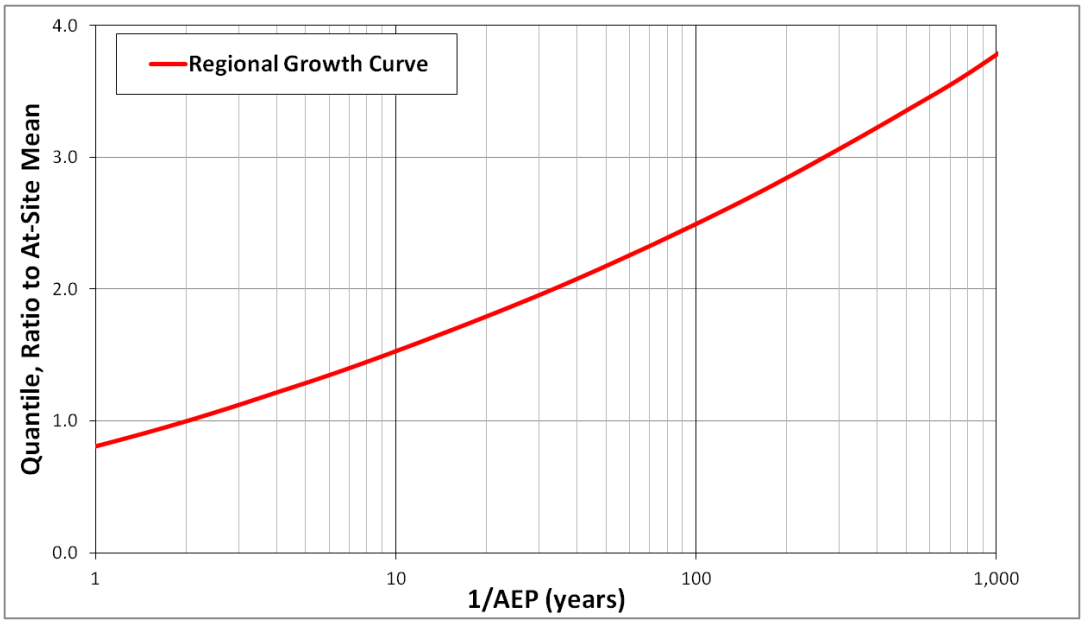

Figure 14.2: Example of regional growth curve

14.4 Areal Reduction Factor: Point to Areal Precipitation

AWA calculated storm centered areal reduction factors (ARFs) using a storm centered depth-area approach based on gridded hourly rainfall data from SPAS. The storm centered ARF does not have a fixed area in which rain falls but changes dynamically with each storm event (NOAA Atlas 2, 1973; Guo, 2012). Instead of the representative point being an average, the representative point is the center of the storm, defined as the point of maximum rainfall. Storm centered ARFs are calculated as the ratio of areal storm rainfall enclosed between isohyets equal

to or greater than the isohyet value to the maximum point rainfall at the storm center. A storm centered ARF is calculated as:

$$ARF_{center} = \frac{\overline{R}_i}{R_{center}} \qquad \text{Equation 7}$$

where $\underline{R_i}$ is the areal storm rainfall enclosed between isohyets equal to or greater than the isohyets, and R_{center} is the maximum point rainfall at the storm center.

The SPAS DAD program was used to derive 6-hour and 24-hour depth-area values based on a set of SPAS storms analyzed and used as part of the PMP development. The point maximum (1-mi^2) 6-hour and 24-hour rainfall (within each SPAS DAD zone) was selected as the storm center. The maximum 6-hour and 24-hour rainfall depth for standard area sizes (1-, 10-, 25-, 50-, 100-, 150-, 200-, 250-, 300-, 350-, 400-, 450-, 500-, 700-, 1000-, 2000-, and 5000-mi^2) were calculated. The point maximum and maximum areal averages depths were used to calculate each event's specific ARFs. The ARFs for the basins were determined by linear interpolation using the two bounding area sizes. A three-parameter log-logistic function with an upper limit of 1 was used to estimate the average, maximum, and minimum ARF by area size following:

$$ARF_x = c + \frac{1-c}{1+exp\,(b(LN(x)-LN(e)))} \qquad \text{Equation 8}$$

where *x* is area size, and *c, b*, and *e* are fitting coefficients. The maximum, average, and minimum ARF curves, based on each event from the short list, are shown in Figures 14.3 and 14.4. For this study, the average storm event ARF were applied for the point to basin area conversion of the 6-hour and 24-hour precipitation data. Several test basins within the Maryland PMP domain are selected, some of the basins' relatively small area size produced very little difference from the point values to the areal values shown in Table 14.1. This was expected but the use of the site-specific ARF information provides a more accurate representation of the AEP across the region.

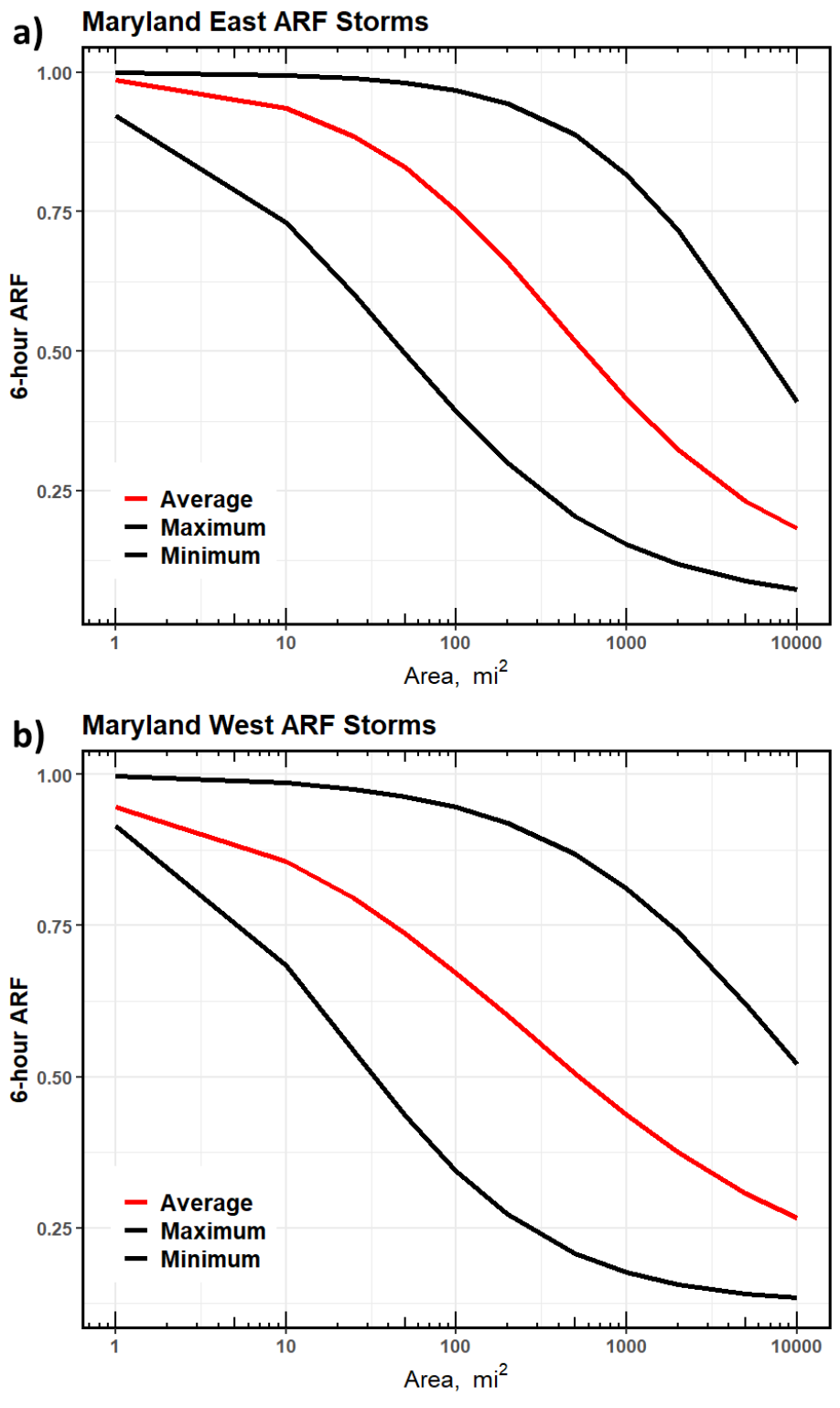

Figure 14.3: Maryland storm short-list specific ARF values for 6-hour duration: a) east of Appalachian crest, and b) west of Appalachian crest

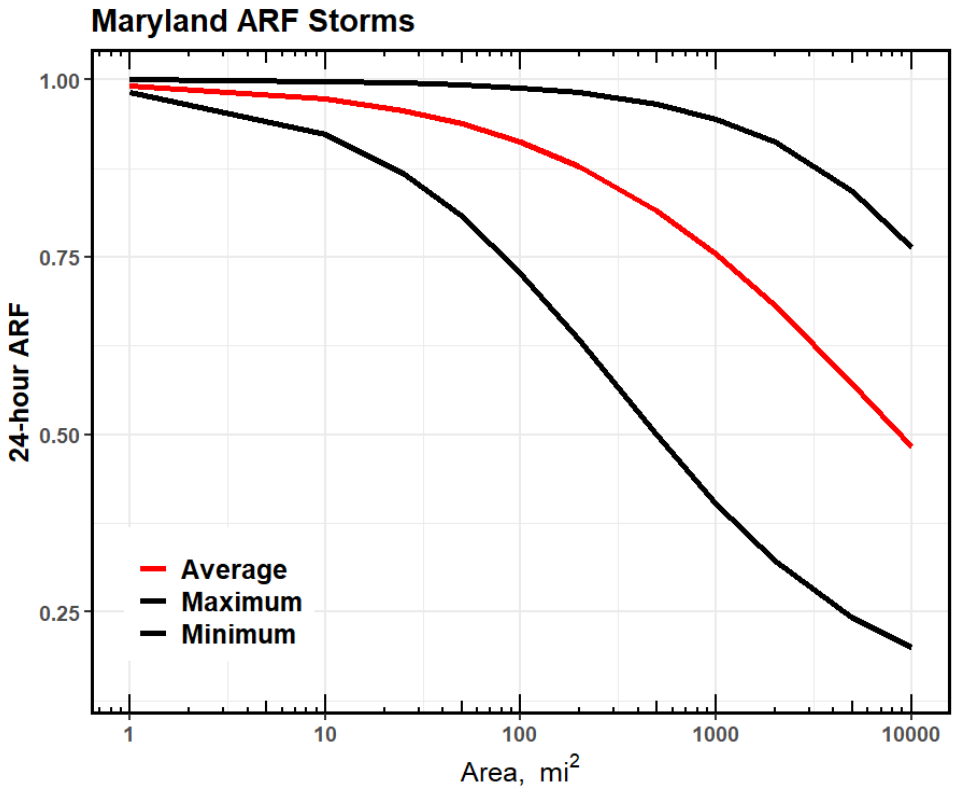

Figure 14.4: Maryland storm short-list specific ARF values for 24-hour duration

Table 14.1: Basin specific ARF values used to convert point precipitation to areal precipitation

Basin Name	Area (mi^2)	6-hour ARF (Min, Ave, Max)			24-hour ARF (Min, Ave, Max)		
Lake Linganore	80.9	0.423	***0.779***	0.973	0.754	***0.921***	0.990
Blairs Valley	3.4	0.844	***0.967***	0.998	0.961	***0.984***	0.999
Seneca Creek	2.9	0.858	***0.971***	0.998	0.965	***0.986***	0.999
Elk Neck	0.3	0.964	***0.994***	1.000	0.992	***0.996***	1.000
Hunting Creek	6.8	0.776	***0.949***	0.996	0.939	***0.978***	0.998
Rocky Gap	8.6	0.751	***0.941***	0.996	0.930	***0.975***	0.998
Wye Mills	9.8	0.734	***0.936***	0.995	0.924	***0.973***	0.998
Lake Merle	0.6	0.944	***0.990***	1.000	0.988	***0.994***	1.000

14.5 Homogenous Regions

The regional analysis approach is based on the concept that at-site data can be pooled within regions that are "homogeneous." In this context, homogeneous is taken to mean that probability distributions and their resultant frequency curves for at-site data are identical, except for a site-specific scaling factor, at all sites in a region. The at-site station mean MAM value is commonly used as the scaling factor in regional analyses. It was initially assumed that one homogeneous region was represented by all stations within close proximity to the basin location. This assumption is reasonable and justifiable to make for a small local region prior to performing heterogeneity measures. Heterogeneity measures were computed for the annual maximum data for stations within the region. Hosking and Wallis (1997) developed heterogeneity measures to help indicate the level of heterogeneity or homogeneity in the L-moment ratios for a group of stations representing a sub-region. The statistics H1 and H2 denote the relative variability of observed L-Cv and L-Skewness respectively for stations within a sub-region. The H1 and H2 measures compare the observed variability to that which is expected from a large sample drawn from a homogeneous region based on the Kappa distribution. The 6-hour duration passed the homogeneity criteria (H1<3) while the 24-hour duration was slightly greater than the homogeneity criteria (H1<3) but was still deemed homogeneous (Hosking and Wallis, 1997). Although Hosking and Wallis (1997) recommend homogenous regions screening of the H1 statistic to be less than three, numerous studies have claimed homogenous regions with H1 values to be larger than three. For example, England et al., (2014) deemed one basin in New Mexico to be homogeneous with an H1 value of 7.73. The heterogeneity tests and three parameter distribution that are statistically significant for the region are shown in Table 14.2.

Table 14.2: Heterogeneity statistics for the region

Duration	H1	H2	Distribution
6-hour	2.32	0.17	GEV
24-hour	3.04	1.48	GEV

14.6 Discordancy Test

Even among homogeneous regions, some stations may be considered grossly inconsistent from the region as a whole. Such stations are identified using a test, which resulted in a discordancy measure. The discordancy measure provided an important indicator of stations that should be moved to a different region and/or contained data errors in their AMS. However, by nature of the L-moment approach, an erroneous individual annual maximum at this early stage in the analysis will have a limited negative impact on the results. For the final set of stations utilized in this study, all passed the discordancy tests (D<3) (Hosking and Wallis, 1997).

14.7 Identification of Probability Distribution

Regional L-moment statistics were computed for annual maximum data for each site at the homogenous region discussed above. Goodness of fit measures were evaluated for five candidate distributions: generalized logistic (GLO), generalized extreme value (GEV), generalized normal (GNO), Pearson type III (PE3), and generalized Pareto (GPA). An L-Moment Ratio Diagram was prepared based on L-Skewness and L-Kurtosis pairs for the

collection of stations in each homogenous region for each duration (Figure 14.5 and Figure 14.6). The regional weighted-average L-Skewness and L-Kurtosis pairing were found to be very near the GEV and GLO distributions.

The GEV distribution was selected over the GNO for frequency estimates because: i) the GEV distribution was ranked statistically higher, ii) NOAA Atlas 14 precipitation frequency studies in the region us this distribution, iii) the GEV was identified in goodness-of-fit measures and used for frequency estimates nearby AWA studies, and iv) using the same distribution among frequency studies ensures a direct comparison to more rare values of the frequency curve (Kappel et al., 2018, Kappel et al., 2023). The GEV is a general mathematical form that incorporates Gumbel's Extreme Value (EV) type I, II, and III distributions for maxima. The parameters of the GEV distribution are the ξ (location), α (scale), and k (shape). The Gumbel EV type I distribution is obtained when $k = 0$. For $k > 0$, the distribution has finite upper bound at $\xi + \alpha / k$ and corresponds to the EV type III distribution for maxima that are bounded above. For $k < 0$, this corresponds to the Gumbel EV type II distribution.

Regional growth curves were created for the homogenous region based on a GEV distribution and quantiles for eighteen return periods (1, 2, 5, 10, 25, 50, 100, 200, 500, 1,000, 5,000, 10,000, 100,000, 1,000,000, 10,000,000, 100,000,000, 1,000,000,000, and 10,000,000,000 years) were calculated for the 6-hour and 24-hour durations.

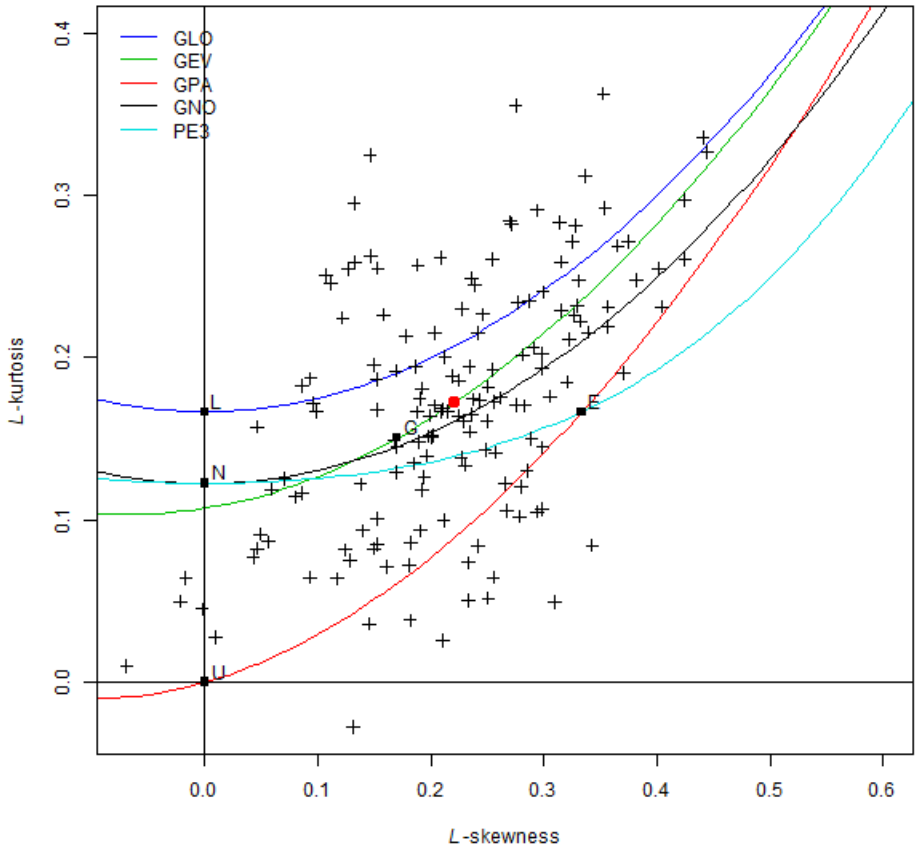

Figure 14.5: 6-hour L-moment ratio diagram for stations used in the regional analysis

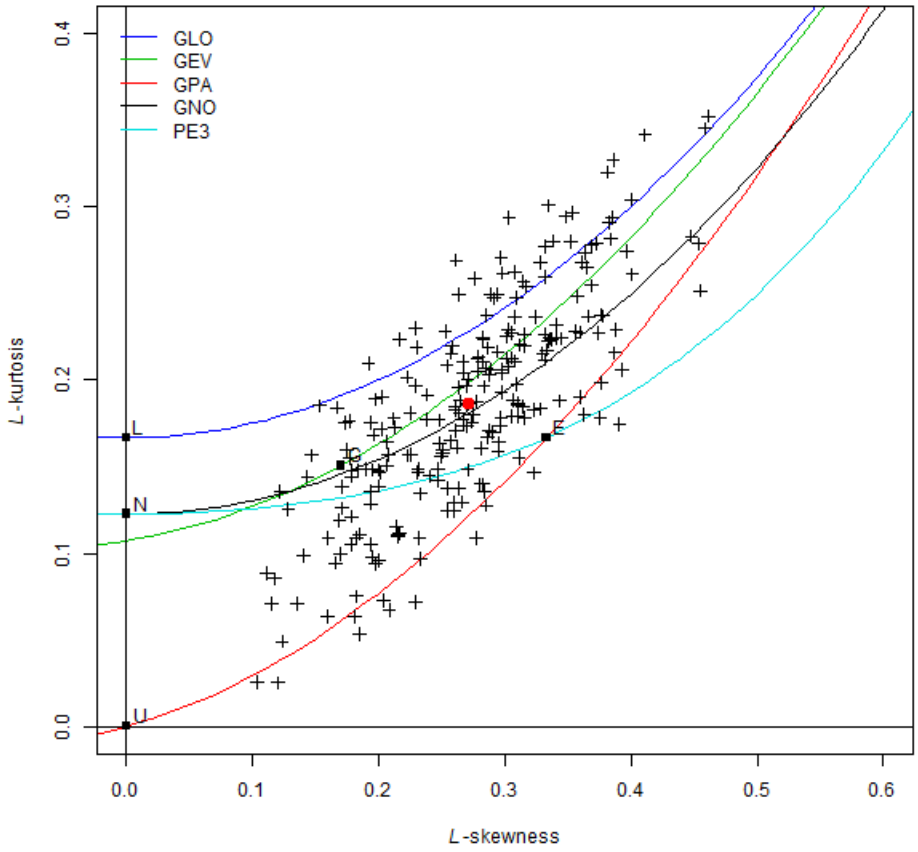

Figure 14.6: 24-hour L-moment ratio diagram for stations used in the regional analysis

14.8 Derivation of Uncertainty Bounds

The uncertainty analysis for deriving the frequency curve and uncertainty bounds were conducted as follows. The frequency distributions at the site were randomly permuted, and data were simulated from the selected frequency distribution. The procedure is described in Hosking and Wallis (1997) and Hosking (2015b), except that the permutation of frequency distributions is a later modification, intended to give more realistic sets of simulated data (Hosking, 2015b). From each permutation, the sample mean values and estimates of the quantiles of the regional growth curve for non-exceedance probabilities are saved. From the simulated values, for each quantile specified the relative root mean square error (relative RMSE) is computed as in Hosking and Wallis (1997). The error bounds are sample quantiles of the ratio of the estimated regional growth curve to the true at-site growth curve or of the ratio of the estimated to the true quantiles at individual sites (Hosking, 2015b).

14.9 Spatial Mapping of At-Site Scaling Factor

The at-site mean or MAM L-moment statistics were spatially mapped for development of frequency grids. Typically, explanatory variables and associated predictor equations are used to map at-site MAM using existing continuous gridded variables. Explanatory variables considered

included climatic and location indices such as PRISM mean annual precipitation (Daly et al., 1997). Spatial mapping of at-site MAM involved a three-step process:

1. Determine a predictor equation that describes the regional behavior of the at-site means across the study area.
2. Compute a best-estimate of the at-site mean at a given station using a weighted average of the regionally-predicted at-site mean (step 1 above) and the sample at-site MAM.
3. Adjust the resulting at-site means to account for spatial coherence of the error residuals (observed-predicted values) in a given locality.

At-site MAM have been well-predicted by climate indicators such as PRISM precipitation. Review of the behavior of at-site means like this allowed for the development of regression relationships for the prediction of at-site means for spatial mapping. Best estimates of the at-site MAMs at the stations were obtained using an Empirical Bayes Approach (Kuczera, 1982) as a weighted average of the values predicted from the regression relationship and the sample value of the station at-site MAM (Step 2 above). Greater weight was given to the sample value of the at-site mean as the record length at a station increased. Residuals were defined as the difference between the weighted-average at-site mean and the regression-predicted at-site mean. Adjustments were then made to the predicted estimates of the at-site means to account for coherence in the spatial distribution of residuals, where the residuals in some geographic areas were not random, but rather systematically over-estimated or under-estimated the at-site mean relative to the regression prediction (Step 3 above); this was done by interpolating standardized residuals and summing the residual grid with the at-site mean grid developed in Step 1.

The estimated at-site MAMs for the study area are compared to the unadjusted observed values. A reduction in the predictive error for the estimated at-site MAMs and better statistical fit were found (e.g. 24-hour initial MAM $r^2 = 0.7208$; final MAM $r^2 = 0.7867$). This is a result of accounting for both regional information (regional predictive equation), local information (station at-site mean) and accounting for the spatial coherence of residuals. The final (mapped) values of the at-site MAM are judged to be the best-estimates achievable from the collection of regional and at-site information. Figure 14.7 and Figure 14.8 depict the final mapped MAM values of the 6-hour and 24-hour at-site MAM.

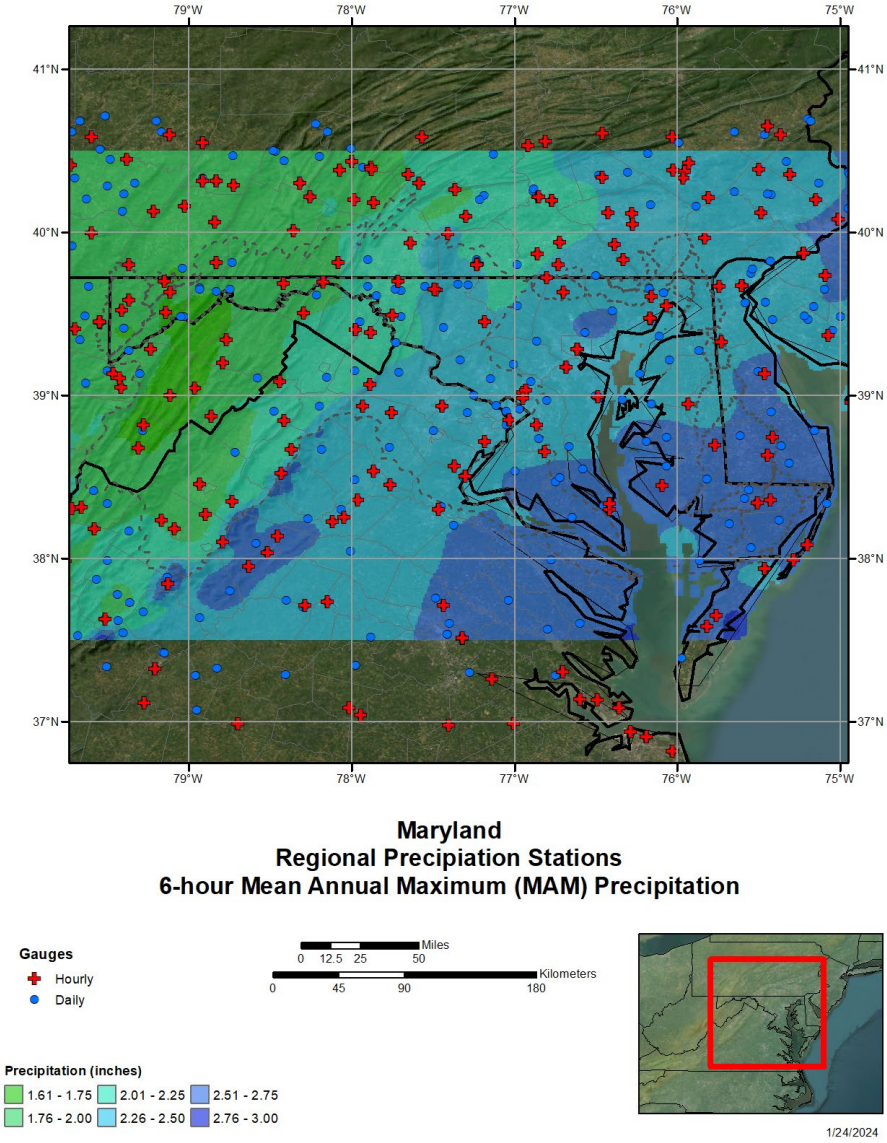

Figure 14.7: Spatially mapped at-site MAM values for 6-hour duration

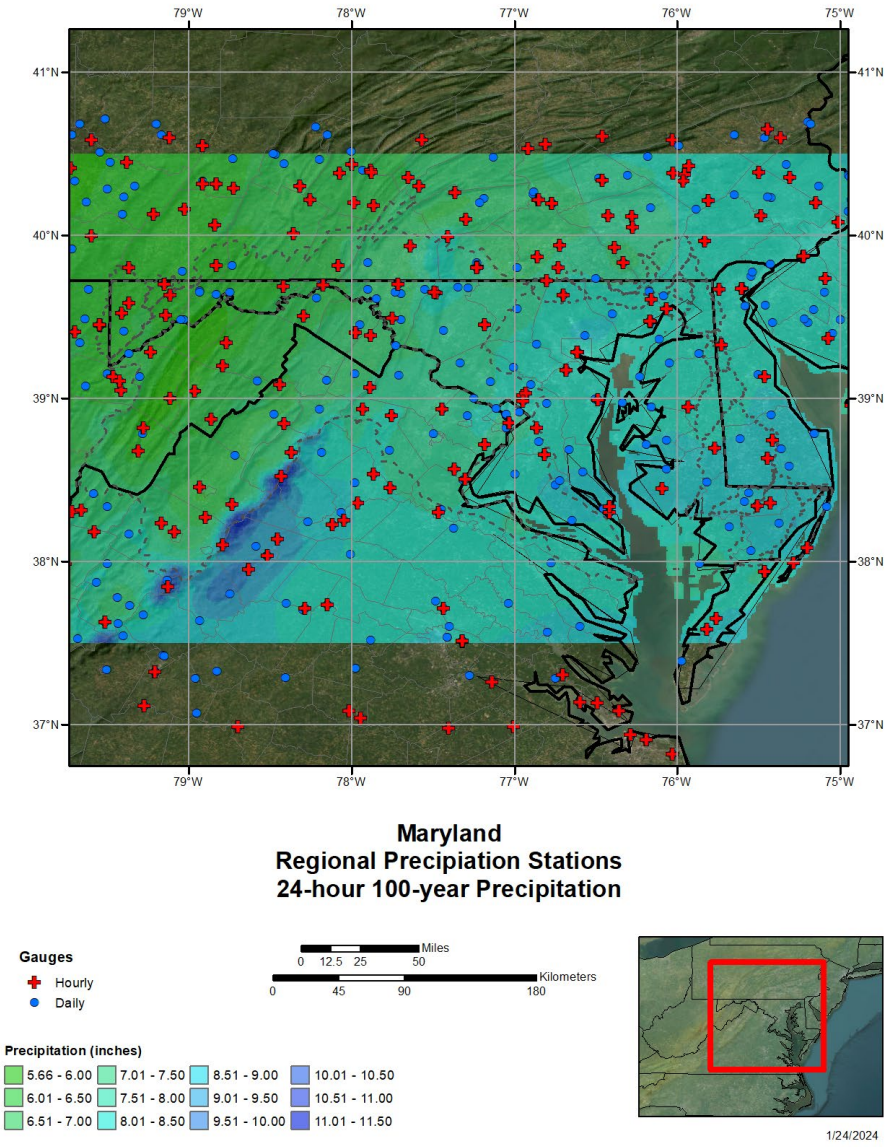

Figure 14.8: Spatially mapped at-site MAM values for 24-hour duration with the test basins shown

14.10 Gridded Precipitation Frequency Estimates

The gridded datasets for the at-site MAM statistics described in the above sections were then used to scale the GEV distribution regional curve for each duration (Equation 6) on a grid-cell by grid-cell basis. This allowed spatial mapping of precipitation-frequency estimates for selected recurrence intervals for the durations of 6-hour and 24-hour. Eighteen average recurrence interval (ARI) grids per duration were prepared from this information for point precipitation maxima for 1, 2, 5, 10, 25, 50, 100, 200, 500, 1,000, 5,000, 10,000, 100,000, 1,000,000, 10,000,000, 100,000,000, 1,000,000,000, and 10,000,000,000 years. The final 6-hour 100-year ARI and 24-hour 100-year ARI are shown in Figure 14.9 and Figure 14.10. Point frequency grids were converted to basin average precipitation using the site-specific ARF discussed above.

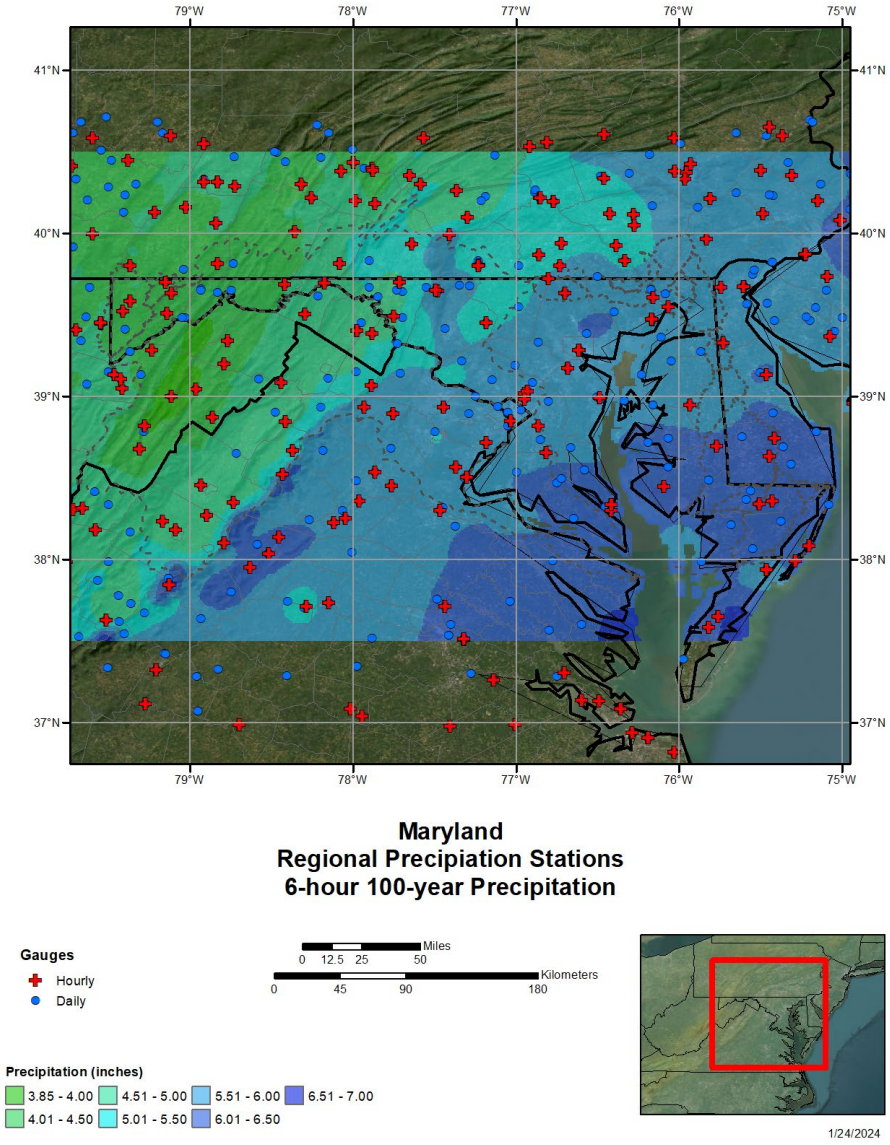

Figure 14.9: Spatially mapped 6-hour 100-year precipitation

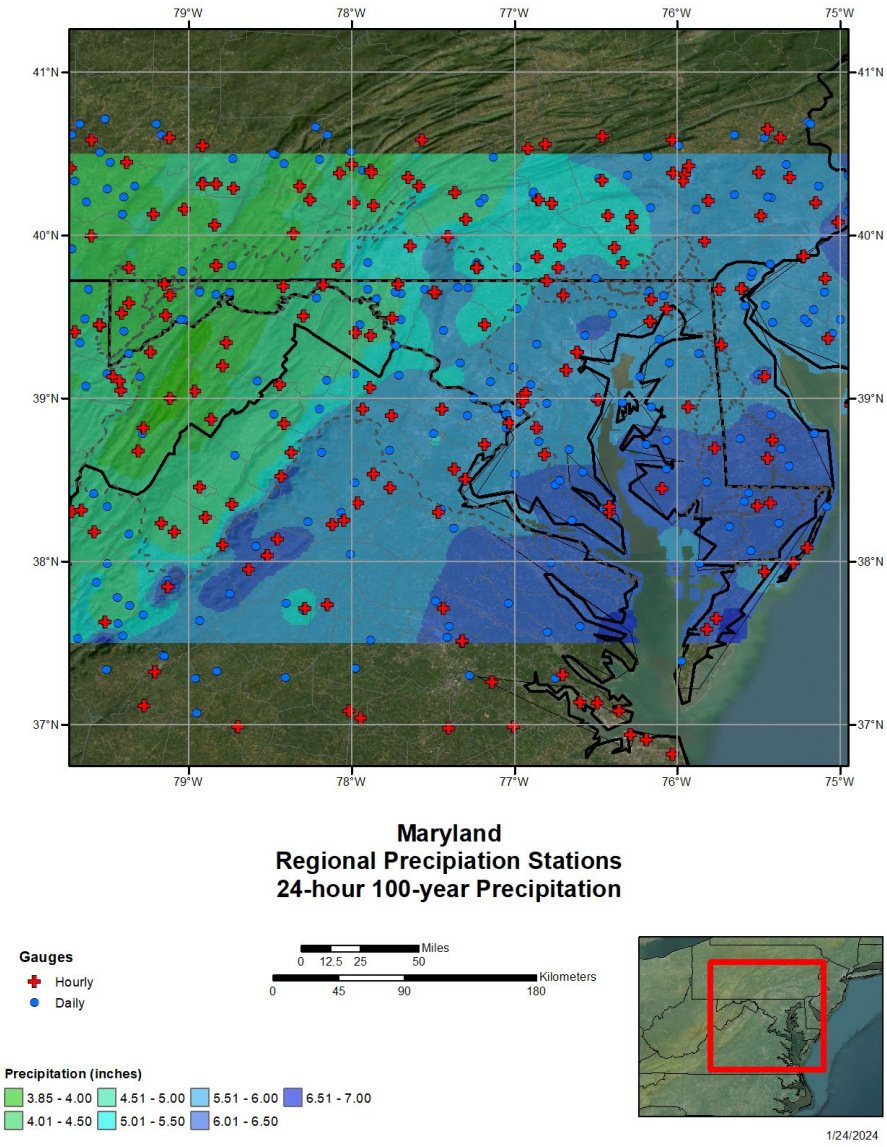

Figure 14.10: Spatially mapped 24-hour 100-year precipitation

14.11 Annual Exceedance Probability Table

Annual Exceedance Probability grids for the 6-hour and 24-hour were used to extract the 1-sq mi AEPs and the eight test basin's average AEPs, the point frequency estimates converted to a basin average precipitation based on ARF, and then estimating the average AEP from all grids within the defined basin (Table 14.3 and Figure 14.11). The 6-hour and 24-hour 1-sqmi AEP of PMP are illustrated in Figure 14.12 and Figure 14.13. The 6-hour and 24-hour basin average AEP values for the eight test basins are provided in Table 14.4 through Table 14.11 and illustrated in Figure 14.14 through Figure 14.21. The eight test basins 6-hour PMP have AEP estimates of 10^{-8} while the eight test basins 24-hour PMP have AEP estimates of 10^{-8} (Table 14.12). For temporal pattern guidance, the information developed for this study as discussed in Section 12 should be applied.

Table 14.3: Eight test basins used to evaluate the 6-hour and 24-hour AEP of PMP

Basin Name	Area (mi^2)	PMP (in) 6-hour; 24-hour	
Lake Linganore	80.9	21.3	23.3
Blairs Valley	3.4	22.5	25.4
Seneca Creek	2.9	26.4	30.0
Elk Neck	0.3	27.3	31.3
Hunting Creek	6.8	25.6	28.8
Rocky Gap	8.6	19.1	21.5
Wye Mills	9.8	26.6	29.9
Lake Merle	0.6	26.4	30.1

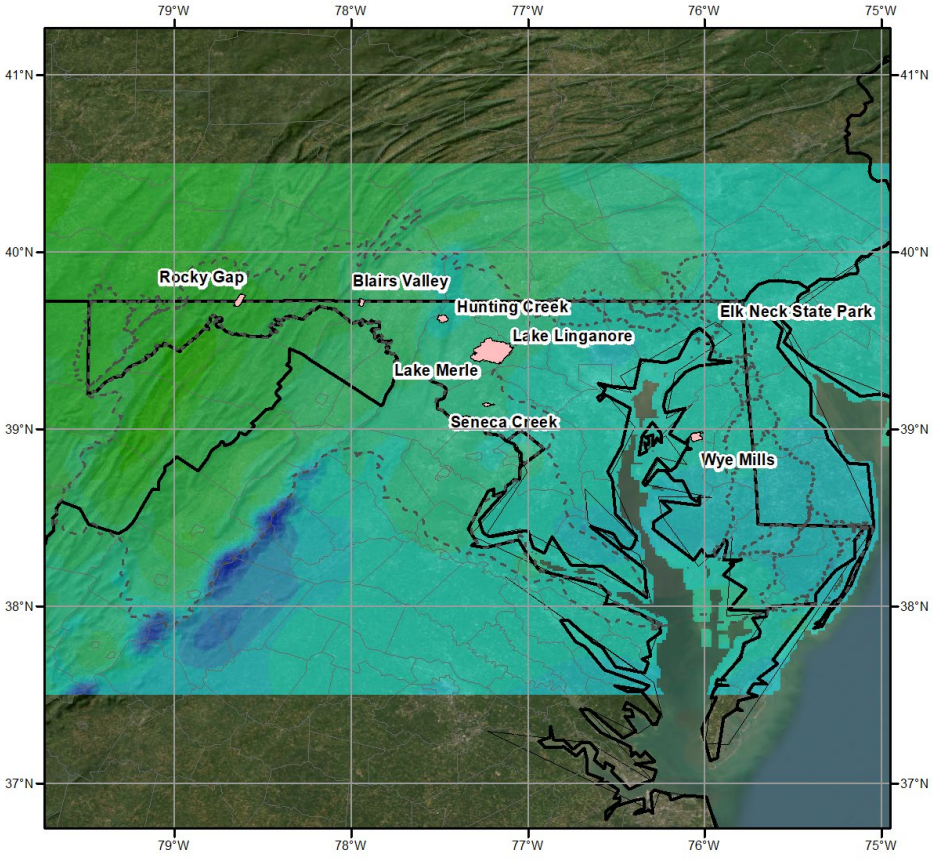

Figure 14.11: Spatial location of eight test basins used to evaluate the 6-hour and 24-hour AEP of PMP

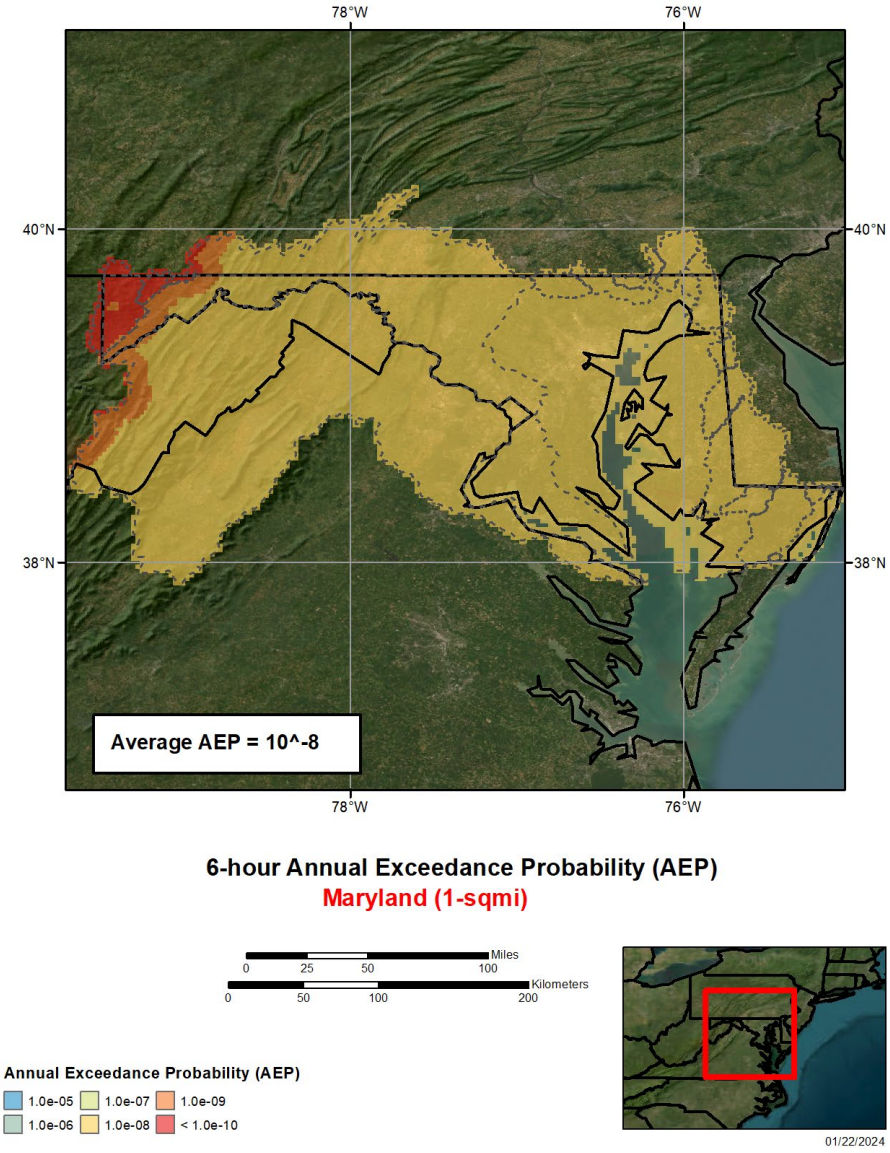

Figure 14.12: Spatially mapped 1-sqmi AEP of 6-hour PMP

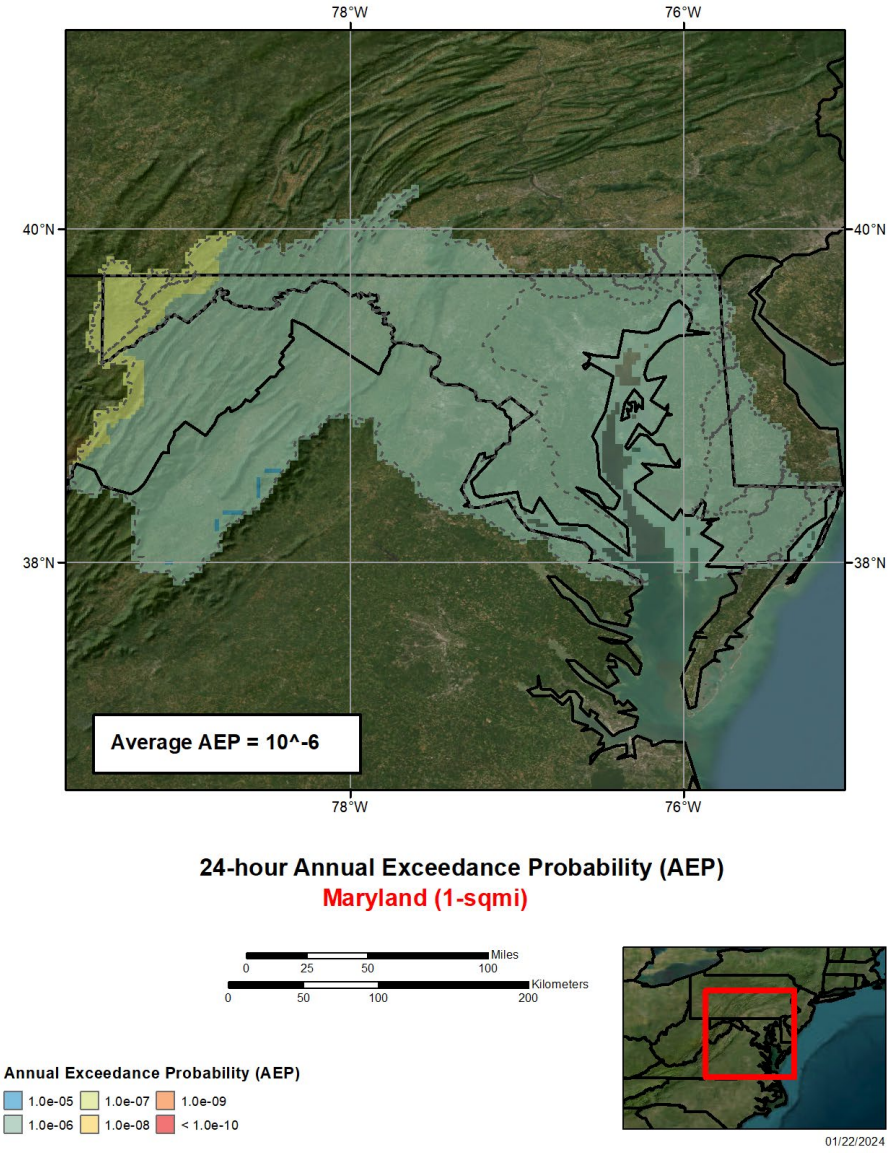

Figure 14.13: Spatially mapped 1-sqmi AEP of 24-hour PMP

Table 14.4: Lake Linganore Basin AEP for 6-hour and 24-hour PMP

Lake Linganore (80.9 mi^2)		6-hour			24-hour		
ARI	AEP	50%	5%	95%	50%	5%	95%
1	$9.9x10^{-1}$	***0.7***	0.6	0.8	***1.4***	1.2	1.6
2	$5.0x10^{-1}$	***1.6***	1.5	1.8	***2.7***	2.4	3.0
5	$2.0x10^{-1}$	***2.2***	2.0	2.5	***3.6***	3.3	4.0
10	$1.0x10^{-1}$	***2.7***	2.4	2.9	***4.4***	4.0	4.8
25	$4.0x10^{-2}$	***3.3***	2.9	3.6	***5.4***	4.8	5.9
50	$2.0x10^{-2}$	***3.7***	3.3	4.1	***6.2***	5.5	6.9
100	$1.0x10^{-2}$	***4.2***	3.7	4.7	***7.1***	6.3	8.0
200	$5.0x10^{-3}$	***4.8***	4.1	5.4	***8.2***	7.1	9.2
500	$2.0x10^{-3}$	***5.5***	4.7	6.2	***9.6***	8.2	10.9
1,000	$1.0x10^{-3}$	***6.1***	5.1	7.0	***10.9***	9.2	12.5
5,000	$2.0x10^{-4}$	***7.6***	6.2	8.9	***14.3***	11.7	16.7
10,000	$1.0x10^{-4}$	***8.3***	6.7	9.9	***16.0***	12.9	19.0
100,000	$1.0x10^{-5}$	***11.1***	8.4	13.9	***23.1***	17.6	29.1
1,000,000	$1.0x10^{-6}$	***14.3***	10.4	19.3	***32.8***	23.7	44.0
10,000,000	$1.0x10^{-7}$	***18.3***	12.5	26.3	***46.0***	31.4	66.0
100,000,000	$1.0x10^{-8}$	***23.1***	14.8	35.6	***64.2***	41.1	98.9
1,000,000,000	$1.0x10^{-9}$	***29.0***	17.4	48.0	***89.2***	53.5	147.8
10,000,000,000	1.010^{-10}	***36.0***	20.3	64.3	***123.4***	69.4	220.3

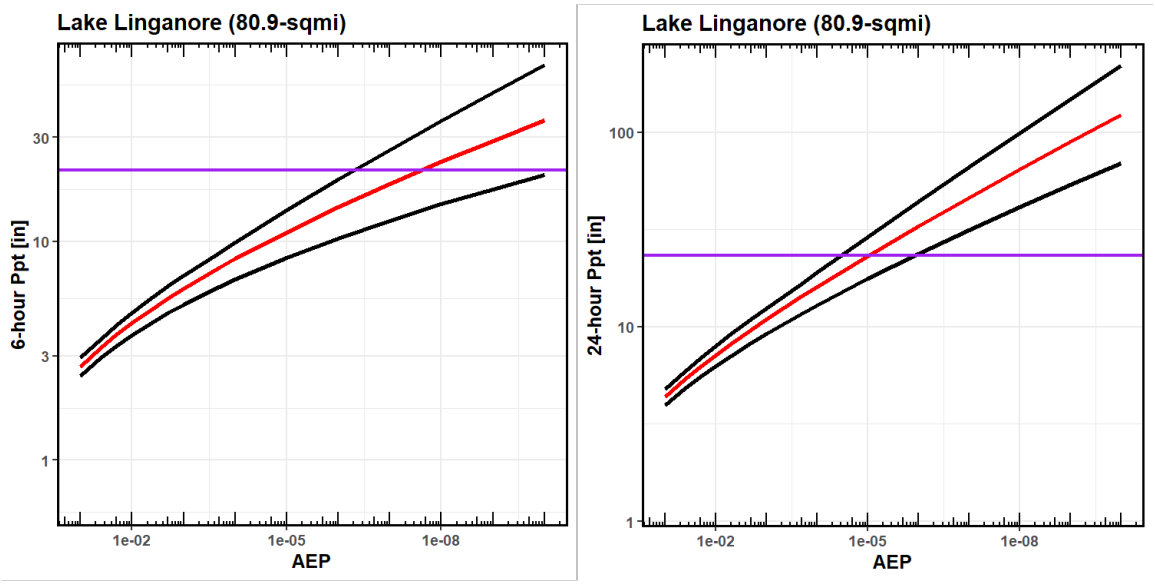

Figure 14.14: Lake Linganore Basin regional L-moment frequency curve (red line) and uncertainty bounds (black line) with basin average PMP (purple line)

Table 14.5: Blairs Valley Basin AEP for 6-hour and 24-hour PMP

Blairs Valley (3.4 mi^2)		6-hour			24-hour		
ARI	AEP	50%	5%	95%	50%	5%	95%
1	$9.9x10^{-1}$	***0.8***	0.7	0.9	***1.4***	1.2	1.6
2	$5.0x10^{-1}$	***1.9***	1.7	2.1	***2.7***	2.5	3.0
5	$2.0x10^{-1}$	***2.6***	2.4	2.9	***3.7***	3.4	4.1
10	$1.0x10^{-1}$	***3.1***	2.8	3.4	***4.4***	4.0	4.8
25	$4.0x10^{-2}$	***3.8***	3.4	4.1	***5.4***	4.9	5.9
50	$2.0x10^{-2}$	***4.3***	3.8	4.8	***6.3***	5.6	6.9
100	$1.0x10^{-2}$	***4.9***	4.3	5.5	***7.2***	6.3	8.0
200	$5.0x10^{-3}$	***5.5***	4.8	6.2	***8.2***	7.2	9.3
500	$2.0x10^{-3}$	***6.4***	5.4	7.2	***9.8***	8.3	11.1
1,000	$1.0x10^{-3}$	***7.0***	5.9	8.1	***11.0***	9.3	12.6
5,000	$2.0x10^{-4}$	***8.8***	7.2	10.2	***14.5***	11.8	16.8
10,000	$1.0x10^{-4}$	***9.6***	7.7	11.4	***16.2***	13.0	19.2
100,000	$1.0x10^{-5}$	***12.8***	9.8	16.1	***23.4***	17.8	29.4
1,000,000	$1.0x10^{-6}$	***16.6***	12.0	22.3	***33.2***	23.9	44.6
10,000,000	$1.0x10^{-7}$	***21.2***	14.4	30.4	***46.6***	31.7	66.8
100,000,000	$1.0x10^{-8}$	***26.7***	17.1	41.1	***65.0***	41.6	100.0
1,000,000,000	$1.0x10^{-9}$	***33.5***	20.1	55.5	***90.2***	54.2	149.5
0 10,000,000,000	1.010^{-10}	***41.6***	23.4	74.3	***124.8***	70.2	222.9

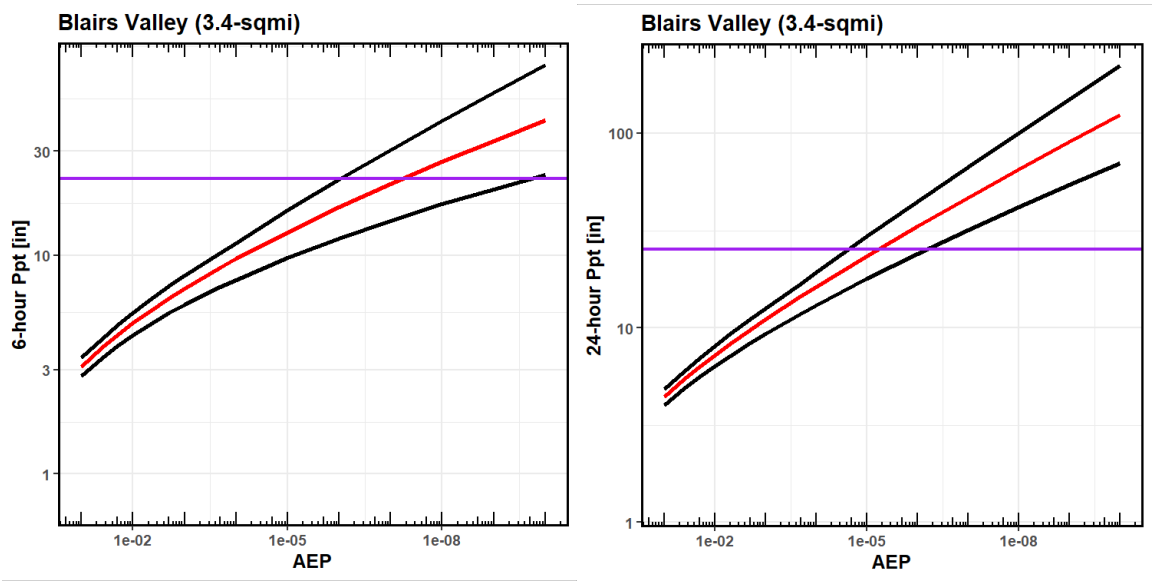

Figure 14.15: Blairs Valley Basin regional L-moment frequency curve (red line) and uncertainty bounds (black line) with basin average PMP (purple line)

Table 14.6: Seneca Creek Basin AEP for 6-hour and 24-hour PMP

Seneca Creek (2.9 mi^2)		6-hour			24-hour		
ARI	AEP	50%	5%	95%	50%	5%	95%
1	$9.9x10^{-1}$	***0.9***	0.8	1.0	***1.5***	1.3	1.7
2	$5.0x10^{-1}$	***2.1***	1.9	2.3	***2.9***	2.6	3.2
5	$2.0x10^{-1}$	***2.9***	2.6	3.2	***3.9***	3.6	4.3
10	$1.0x10^{-1}$	***3.4***	3.1	3.8	***4.7***	4.3	5.2
25	$4.0x10^{-2}$	***4.2***	3.7	4.6	***5.8***	5.2	6.3
50	$2.0x10^{-2}$	***4.8***	4.2	5.3	***6.7***	6.0	7.4
100	$1.0x10^{-2}$	***5.4***	4.7	6.0	***7.7***	6.8	8.6
200	$5.0x10^{-3}$	***6.1***	5.3	6.8	***8.8***	7.6	9.9
500	$2.0x10^{-3}$	***7.0***	6.0	8.0	***10.4***	8.9	11.8
1,000	$1.0x10^{-3}$	***7.8***	6.5	8.9	***11.8***	9.9	13.5
5,000	$2.0x10^{-4}$	***9.7***	7.9	11.3	***15.4***	12.6	18.0
10,000	$1.0x10^{-4}$	***10.6***	8.5	12.6	***17.3***	13.9	20.5
100,000	$1.0x10^{-5}$	***14.1***	10.8	17.7	***24.9***	19.0	31.4
1,000,000	$1.0x10^{-6}$	***18.3***	13.2	24.6	***35.3***	25.5	47.5
10,000,000	$1.0x10^{-7}$	***23.4***	15.9	33.5	***49.6***	33.8	71.2
100,000,000	$1.0x10^{-8}$	***29.5***	18.9	45.4	***69.3***	44.3	106.6
1,000,000,000	$1.0x10^{-9}$	***36.9***	22.2	61.2	***96.2***	57.7	159.3
10,000,000,000	1.010^{-10}	***45.9***	25.8	82.0	***133.0***	74.8	237.6

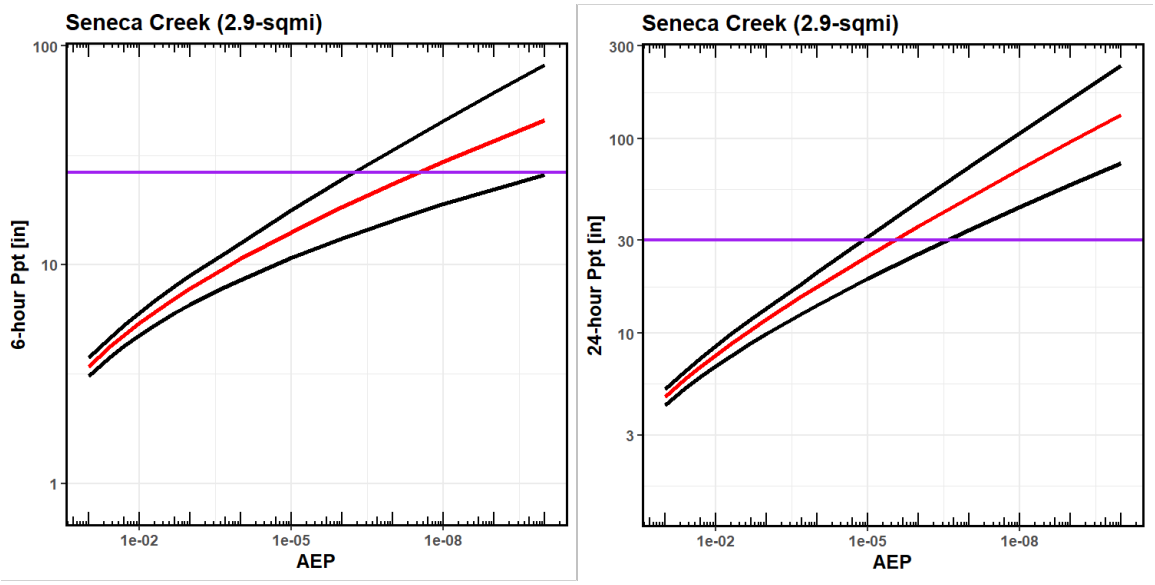

Figure 14.16: Seneca Creek Basin regional L-moment frequency curve (red line) and uncertainty bounds (black line) with basin average PMP (purple line)

Table 14.7: Elk Neck Basin AEP for 6-hour and 24-hour PMP

Elk Neck (0.3 mi^2)		6-hour			24-hour		
ARI	AEP	50%	5%	95%	50%	5%	95%
1	$9.9x10^{-1}$	***1.0***	0.9	1.1	***1.6***	1.4	1.8
2	$5.0x10^{-1}$	***2.2***	2.0	2.5	***3.1***	2.8	3.4
5	$2.0x10^{-1}$	***3.1***	2.8	3.4	***4.2***	3.8	4.6
10	$1.0x10^{-1}$	***3.7***	3.3	4.0	***5.0***	4.5	5.5
25	$4.0x10^{-2}$	***4.5***	4.0	4.9	***6.2***	5.5	6.7
50	$2.0x10^{-2}$	***5.1***	4.6	5.7	***7.1***	6.3	7.9
100	$1.0x10^{-2}$	***5.8***	5.1	6.5	***8.2***	7.2	9.1
200	$5.0x10^{-3}$	***6.5***	5.7	7.4	***9.3***	8.1	10.5
500	$2.0x10^{-3}$	***7.6***	6.5	8.6	***11.0***	9.4	12.5
1,000	$1.0x10^{-3}$	***8.4***	7.1	9.6	***12.5***	10.5	14.3
5,000	$2.0x10^{-4}$	***10.5***	8.5	12.2	***16.4***	13.4	19.1
10,000	$1.0x10^{-4}$	***11.5***	9.2	13.6	***18.4***	14.8	21.8
100,000	$1.0x10^{-5}$	***15.2***	11.6	19.1	***26.5***	20.2	33.3
1,000,000	$1.0x10^{-6}$	***19.7***	14.2	26.5	***37.6***	27.1	50.5
10,000,000	$1.0x10^{-7}$	***25.2***	17.2	36.1	***52.8***	35.9	75.7
100,000,000	$1.0x10^{-8}$	***31.8***	20.4	49.0	***73.6***	47.1	113.3
1,000,000,000	$1.0x10^{-9}$	***39.8***	23.9	66.0	***102.2***	61.4	169.4
10,000,000,000	1.010^{-10}	***49.5***	27.9	88.5	***141.4***	79.5	252.5

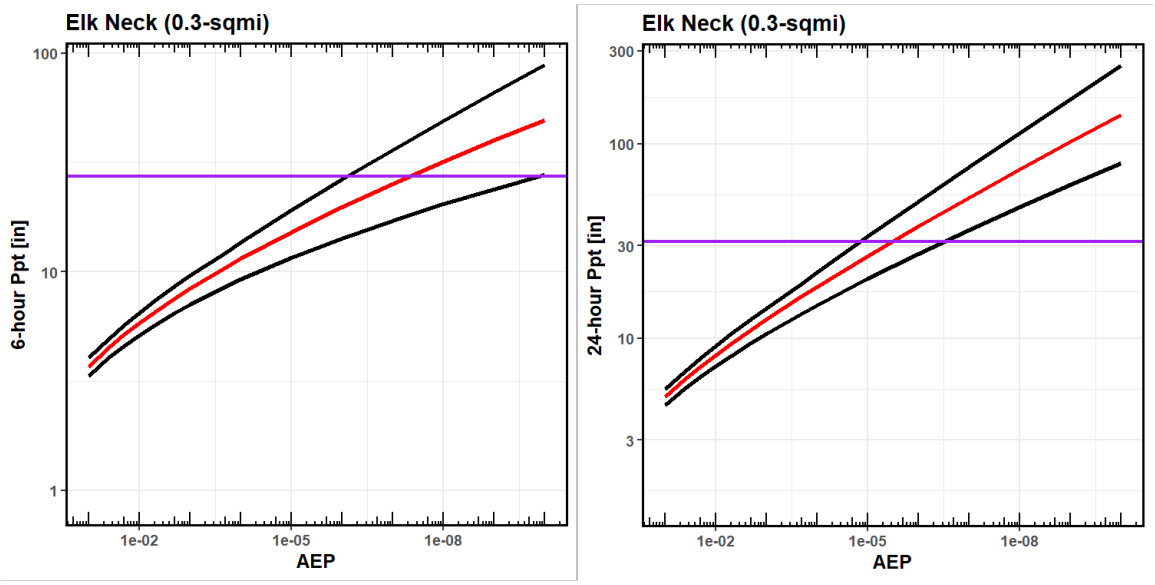

Figure 14.17: Elk Neck Basin regional L-moment frequency curve (red line) and uncertainty bounds (black line) with basin average PMP (purple line)

Table 14.8: Hunting Creek Basin AEP for 6-hour and 24-hour PMP

Hunting Creek (6.8 mi^2)		6-hour			24-hour		
ARI	AEP	50%	5%	95%	50%	5%	95%
1	$9.9x10^{-1}$	***0.9***	0.8	1.0	***1.6***	1.4	1.8
2	$5.0x10^{-1}$	***2.1***	1.9	2.3	***3.0***	2.8	3.4
5	$2.0x10^{-1}$	***2.8***	2.6	3.1	***4.1***	3.8	4.6
10	$1.0x10^{-1}$	***3.4***	3.1	3.7	***4.9***	4.5	5.4
25	$4.0x10^{-2}$	***4.1***	3.7	4.5	***6.1***	5.5	6.7
50	$2.0x10^{-2}$	***4.7***	4.2	5.2	***7.0***	6.2	7.8
100	$1.0x10^{-2}$	***5.4***	4.7	6.0	***8.1***	7.1	9.0
200	$5.0x10^{-3}$	***6.0***	5.2	6.8	***9.2***	8.0	10.4
500	$2.0x10^{-3}$	***7.0***	6.0	7.9	***10.9***	9.3	12.4
1,000	$1.0x10^{-3}$	***7.7***	6.5	8.9	***12.3***	10.4	14.1
5,000	$2.0x10^{-4}$	***9.7***	7.9	11.2	***16.2***	13.2	18.9
10,000	$1.0x10^{-4}$	***10.6***	8.5	12.5	***18.2***	14.6	21.5
100,000	$1.0x10^{-5}$	***14.0***	10.7	17.7	***26.1***	20.0	32.9
1,000,000	$1.0x10^{-6}$	***18.2***	13.1	24.5	***37.1***	26.8	49.9
10,000,000	$1.0x10^{-7}$	***23.2***	15.8	33.3	***52.1***	35.5	74.7
100,000,000	$1.0x10^{-8}$	***29.4***	18.8	45.2	***72.7***	46.5	111.9
1,000,000,000	$1.0x10^{-9}$	***36.8***	22.1	60.9	***100.9***	60.6	167.2
10,000,000,000	1.010^{-10}	***45.7***	25.7	81.6	***139.6***	78.5	249.4

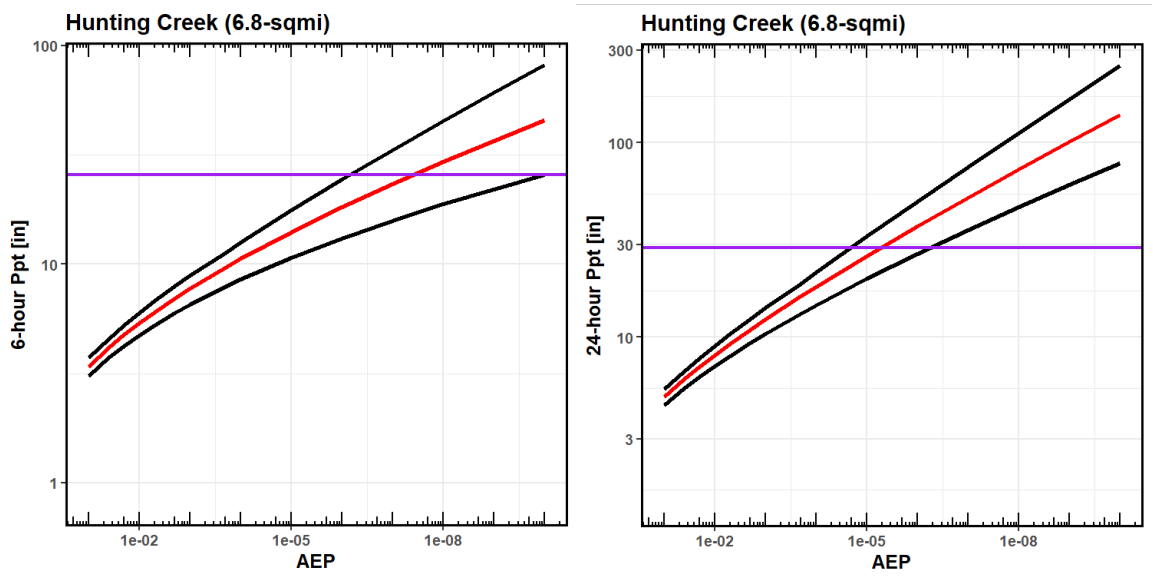

Figure 14.18: Hunting Creek Basin regional L-moment frequency curve (red line) and uncertainty bounds (black line) with basin average PMP (purple line)

Table 14.9: Rocky Gap Basin AEP for 6-hour and 24-hour PMP

Rocky Gap (8.6 mi^2)		6-hour			24-hour		
ARI	AEP	50%	5%	95%	50%	5%	95%
1	$9.9x10^{-1}$	***0.7***	0.6	0.8	***1.2***	1.0	1.3
2	$5.0x10^{-1}$	***1.6***	1.4	1.7	***2.3***	2.1	2.6
5	$2.0x10^{-1}$	***2.1***	2.0	2.4	***3.1***	2.8	3.4
10	$1.0x10^{-1}$	***2.6***	2.3	2.8	***3.7***	3.4	4.1
25	$4.0x10^{-2}$	***3.1***	2.8	3.4	***4.6***	4.1	5.0
50	$2.0x10^{-2}$	***3.6***	3.2	4.0	***5.3***	4.7	5.9
100	$1.0x10^{-2}$	***4.1***	3.6	4.5	***6.1***	5.4	6.8
200	$5.0x10^{-3}$	***4.6***	4.0	5.1	***7.0***	6.1	7.8
500	$2.0x10^{-3}$	***5.3***	4.5	6.0	***8.3***	7.0	9.4
1,000	$1.0x10^{-3}$	***5.8***	4.9	6.7	***9.3***	7.9	10.7
5,000	$2.0x10^{-4}$	***7.3***	6.0	8.5	***12.3***	10.0	14.3
10,000	$1.0x10^{-4}$	***8.0***	6.4	9.5	***13.7***	11.0	16.3
100,000	$1.0x10^{-5}$	***10.6***	8.1	13.4	***19.8***	15.1	24.9
1,000,000	$1.0x10^{-6}$	***13.8***	9.9	18.5	***28.1***	20.3	37.7
10,000,000	$1.0x10^{-7}$	***17.6***	12.0	25.2	***39.4***	26.8	56.5
100,000,000	$1.0x10^{-8}$	***22.2***	14.2	34.2	***55.0***	35.2	84.6
1,000,000,000	$1.0x10^{-9}$	***27.8***	16.7	46.1	***76.3***	45.8	126.5
10,000,000,000	1.010^{-10}	***34.6***	19.4	61.7	***105.6***	59.4	188.6

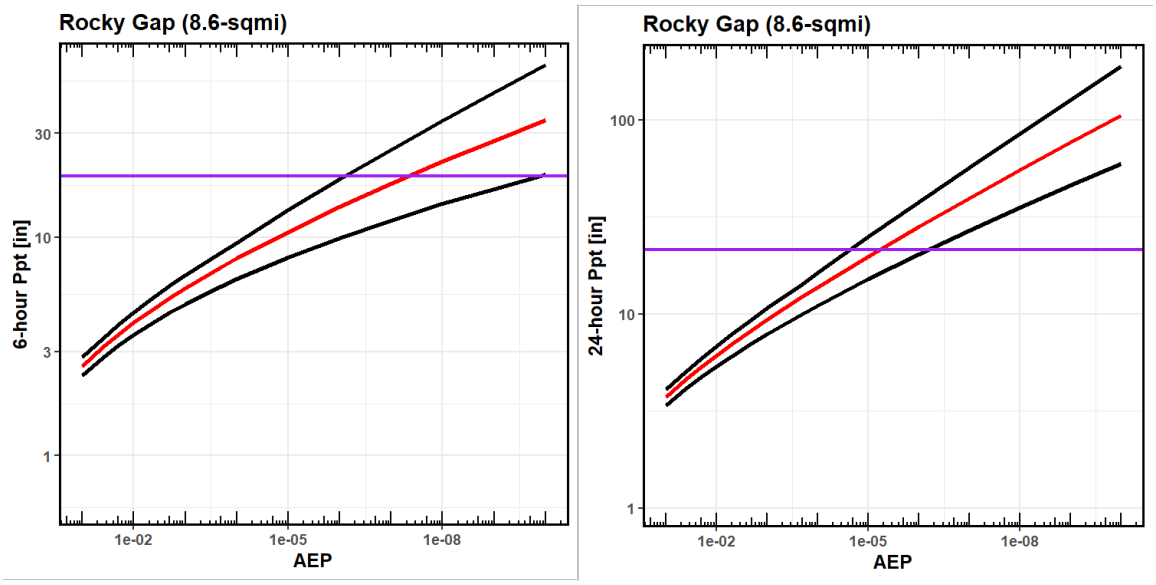

Figure 14.19: Rocky Gap Basin regional L-moment frequency curve (red line) and uncertainty bounds (black line) with basin average PMP (purple line)

Table 14.10: Wye Mills Basin AEP for 6-hour and 24-hour PMP

Wye Mills (9.8 mi^2)		6-hour			24-hour		
ARI	AEP	50%	5%	95%	50%	5%	95%
1	$9.9x10^{-1}$	***0.9***	0.8	1.0	***1.6***	1.4	1.8
2	$5.0x10^{-1}$	***2.1***	1.9	2.3	***3.0***	2.8	3.4
5	$2.0x10^{-1}$	***2.9***	2.7	3.2	***4.1***	3.8	4.5
10	$1.0x10^{-1}$	***3.5***	3.2	3.8	***4.9***	4.5	5.4
25	$4.0x10^{-2}$	***4.3***	3.8	4.7	***6.1***	5.5	6.7
50	$2.0x10^{-2}$	***4.9***	4.3	5.4	***7.0***	6.2	7.8
100	$1.0x10^{-2}$	***5.5***	4.8	6.1	***8.1***	7.1	9.0
200	$5.0x10^{-3}$	***6.2***	5.4	7.0	***9.2***	8.0	10.4
500	$2.0x10^{-3}$	***7.1***	6.1	8.1	***10.9***	9.3	12.4
1,000	$1.0x10^{-3}$	***7.9***	6.7	9.1	***12.3***	10.4	14.1
5,000	$2.0x10^{-4}$	***9.9***	8.1	11.5	***16.2***	13.2	18.8
10,000	$1.0x10^{-4}$	***10.8***	8.7	12.8	***18.1***	14.6	21.5
100,000	$1.0x10^{-5}$	***14.4***	11.0	18.1	***26.1***	20.0	32.9
1,000,000	$1.0x10^{-6}$	***18.7***	13.5	25.1	***37.1***	26.7	49.8
10,000,000	$1.0x10^{-7}$	***23.8***	16.2	34.2	***52.1***	35.4	74.7
100,000,000	$1.0x10^{-8}$	***30.1***	19.3	46.3	***72.6***	46.5	111.8
1,000,000,000	$1.0x10^{-9}$	***37.7***	22.6	62.4	***100.8***	60.5	167.1
10,000,000,000	1.010^{-10}	***46.8***	26.3	83.7	***139.5***	78.4	249.1

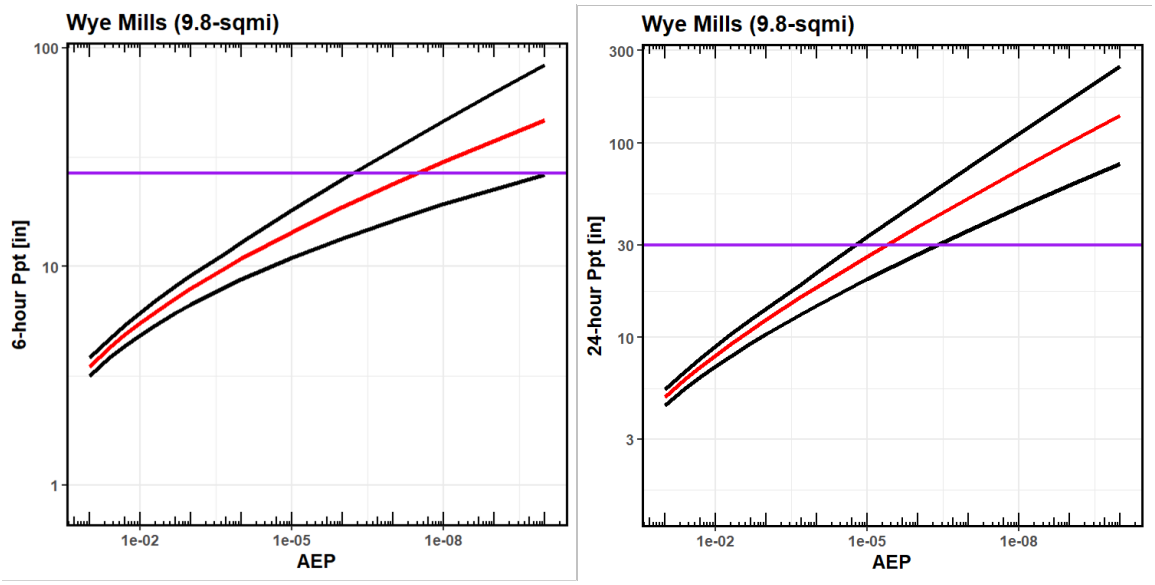

Figure 14.20: Wye Mills Basin regional L-moment frequency curve (red line) and uncertainty bounds (black line) with basin average PMP (purple line)

Table 14.11: Lake Merle Basin AEP for 6-hour and 24-hour PMP

Lake Merle (0.6 mi^2)		6-hour			24-hour		
ARI	AEP	50%	5%	95%	50%	5%	95%
1	$9.9x10^{-1}$	***0.9***	0.8	1.0	***1.5***	1.3	1.6
2	$5.0x10^{-1}$	***2.1***	1.9	2.1	***2.9***	2.6	3.0
5	$2.0x10^{-1}$	***2.9***	2.6	2.9	***4.0***	3.6	4.0
10	$1.0x10^{-1}$	***3.4***	3.1	3.5	***4.7***	4.3	4.8
25	$4.0x10^{-2}$	***4.2***	3.8	4.3	***5.8***	5.2	6.0
50	$2.0x10^{-2}$	***4.8***	4.3	5.0	***6.8***	6.0	7.1
100	$1.0x10^{-2}$	***5.5***	4.8	5.8	***7.8***	6.8	8.2
200	$5.0x10^{-3}$	***6.1***	5.3	6.6	***8.9***	7.7	9.5
500	$2.0x10^{-3}$	***7.1***	6.0	7.8	***10.5***	9.0	11.5
1,000	$1.0x10^{-3}$	***7.9***	6.6	8.8	***11.8***	10.0	13.2
5,000	$2.0x10^{-4}$	***9.8***	8.0	11.4	***15.6***	12.7	18.1
10,000	$1.0x10^{-4}$	***10.7***	8.6	12.7	***17.4***	14.0	20.7
100,000	$1.0x10^{-5}$	***14.2***	10.9	17.9	***25.1***	19.2	31.6
1,000,000	$1.0x10^{-6}$	***18.5***	13.3	24.8	***35.6***	25.7	47.9
10,000,000	$1.0x10^{-7}$	***23.6***	16.1	33.9	***50.1***	34.1	71.8
100,000,000	$1.0x10^{-8}$	***29.8***	19.1	45.9	***69.8***	44.7	107.5
1,000,000,000	$1.0x10^{-9}$	***37.3***	22.4	61.8	***96.9***	58.2	160.6
10,000,000,000	1.010^{-10}	***46.4***	26.1	82.9	***134.1***	75.4	239.5

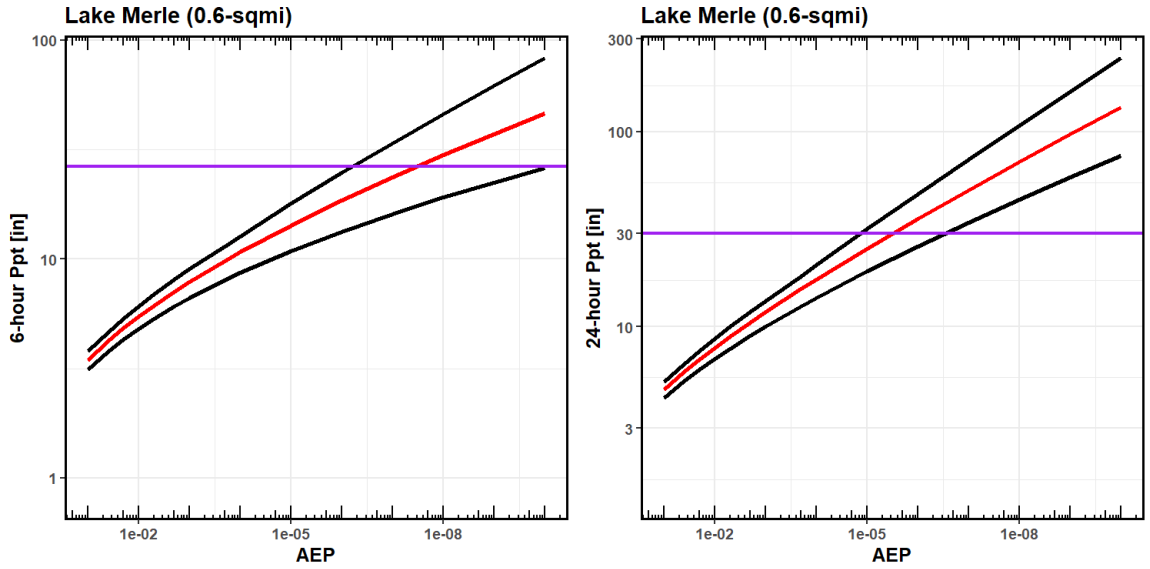

Figure 14.21: Lake Merle Basin regional L-moment frequency curve (red line) and uncertainty bounds (black line) with basin average PMP (purple line)

Table 14.12: Summary of eight test basins AEP of PMP for 6-hour and 24-hour durations. The 50% values represent our best estimate, the 5% and 95% values represent the upper and lower confidence bounds based on Monte-Carlo simulation.

Basin Name	Area (mi^2)	6-hour ARF (50%, 5%, 95%)			24-hour ARF (50%, 5%, 95%)		
Lake Linganore	80.9	***10^{-8}***	$<10^{-10}$	10^{-7}	***10^{-6}***	10^{-6}	10^{-5}
Blairs Valley	3.4	***10^{-8}***	10^{-10}	10^{-7}	***10^{-6}***	10^{-7}	10^{-5}
Seneca Creek	2.9	***10^{-8}***	$<10^{-10}$	10^{-7}	***10^{-6}***	10^{-7}	10^{-5}
Elk Neck	0.3	***10^{-8}***	10^{-10}	10^{-7}	***10^{-6}***	10^{-7}	10^{-5}
Hunting Creek	6.8	***10^{-8}***	10^{-10}	10^{-7}	***10^{-6}***	10^{-7}	10^{-5}
Rocky Gap	8.6	***10^{-8}***	$<10^{-10}$	10^{-7}	***10^{-6}***	10^{-7}	10^{-5}
Wye Mills	9.8	***10^{-8}***	$<10^{-10}$	10^{-7}	***10^{-6}***	10^{-7}	10^{-5}
Lake Merle	0.6	***10^{-8}***	$<10^{-10}$	10^{-7}	***10^{-6}***	10^{-7}	10^{-5}

15. Climate Change Projections Related to PMP

Climate is changing, always has been changing, and always will change as long as the energy received across the Earth's surface is out of balance. Accounting for future changes in climate is important to reduce risk and ensure infrastructure is designed for potential future changes (Kunkel et al., 2013a; Kunkel et al., 2013b; Kunkel and Champion, 2019). Unfortunately, quantification of the amount and rate of change at any given location for any specific meteorological parameter is not explicitly quantifiable and instead has to be modeled based on our incomplete understanding of the Earth climate system. Therefore, model projections that utilize our current understanding of the Earth climate system are developed. The climate projections are based on a physical understanding of various atmospheric parameters and how those affect weather and climate through time and space. However, because our quantification of these parameters is incomplete (and at times inaccurate) and because our understanding of the various interactions and feedbacks is limited, the projections represent possible outcomes (Kappel et al., 2020). None of which can be considered truth.

To overcome these significant limitations, numerous iterations and slight changes in the various parameters are performed so that a suite of ensembles are produced that represent a wide range of potential outcomes. From this output, inferences can be made, with more confidence given when ensemble outcomes converge on a common projection (Mahoney et al., 2013; Ohara et al., 2017). Another layer of uncertainty within the climate change projection process relates to the assumption applied for future emissions scenarios and how those may affect the climate system. Future emissions scenarios have two major areas of uncertainty. First, the assumption that any given emission scenario will occur following a specific path through time is unknown as there are many internal and external factors that can influence the amount of emissions produced through time. Second, the understanding and quantification of how the Earth's climate will respond to any given greenhouse gas emission is limited. Both uncertainties introduce errors into the outcomes of climate projections. Finally, Global Circulation Models (GCMs) are computationally intensive and are therefore run at low resolution both in time and space. In general, the resolution of the GCMs is inadequate to capture the spatial variations. To overcome this, projections from GCMs are downscaled using a statistical process into regional downscaled model projections. The regionally downscaled models are what were utilized for this climate change analysis.

Given all the limitations and uncertainties noted above, it is still useful to evaluate Regional Circulation Models (RCMs) to understand the range of potential outcomes that could occur through time over the basin. To complete this process, AWA investigated Coupled Model Intercomparison Project Phase 6 (CMIP6) output that were newly available over the course of this study.

15.1 Overview of Global Climate Change Models

GCMs produce realizations of the Earth's climate on a generally coarse scale of around 1000 km by 1000 km. Because the scale is so coarse, a single GCM grid may cover vastly differing landscapes (e.g., from very mountainous to flat coastal plains) that have greatly varying potential for floods, droughts, or other extreme events.

15.1.1 Regional Downscaled Climate Change Models

RCMs and Empirical Statistical Downscaling applied over limited areas are done at a much finer resolution. These are therefore able to capture the spatial and temporal variations related to a site-specific region. These downscaling methods are driven by GCMs, where the RCM is nested within the overall GCM and utilizes the GCM to set the initial boundary conditions. The initial boundary conditions are then downscaled using either statistical methodology or the RCM based on a meteorological model interface. The RCM process can provide projections of future climate conditions on a much smaller scale (e.g., < 50km by 50km), which supports more detailed site-specific information and allows for adaptation assessment and planning.

15.2 Climate Change Projections Analysis Methods

The Intergovernmental Panel on Climate Change's (IPCC) sixth assessment report (AR6) contains Shared Socioeconomic Pathways (SSP)s. SSPs are scenarios of projected socioeconomic global changes up to 2100. They are used to derive greenhouse gas emissions scenarios with different climate policies. The SSPs are based on five narratives describing broad socioeconomic trends that could shape future society. These are intended to span the range of plausible futures. These include a world of sustainability-focused growth and equality (SSP1); a "middle of the road" world where trends broadly follow their historical patterns (SSP2); a fragmented world of "resurgent nationalism" (SSP3); a world of ever-increasing inequality (SSP4); and a world of rapid and unconstrained growth in economic output and energy use (SSP5) (IPCC, 2021). The SSPs investigated; SSP1.9, SSP2.6, SSP4.5, SSP7.0, and SSP85; are labeled after a possible range of greenhouse gas emissions scenarios with different climate policies through the year 2100 (Figure 15.1) (IPCC, 2021). SSP-8.5 represents the 95-percentile of all possible ranges of greenhouse gas emissions forcing scenarios through in the year 2100. The IPCC AR6 report does not estimate the likelihoods of the climate scenarios (Masson-Delmotte et al., 2021) but Hausfather and Peters (2020) concluded that SSP5-8.5 was highly unlikely, SSP3-7.0 was unlikely, and SSP2-4.5 was likely. In this assessment, AWA evaluated the projections associated with SSP2-4.5 and SSP5-8.5. These two SSPs were evaluated to be consistent with AWA climate change assessments that utilize the likely scenario and the highly unlikely scenario to bracket various outcomes. In addition, both SSPs provide the parameters needed for the assessments completed by AWA.

The NASA Earth Exchange Global Daily Downscaled Projections (NEX-GDDP-CMIP6) dataset is comprised of thirty-five global downscaled climate scenarios derived from the GCM runs conducted under the Coupled Model Intercomparison Project Phase 6 (CMIP6) and across all of the four "Tier 1" greenhouse gas emissions scenarios. The CMIP6 GCM runs were developed in support of the Sixth Assessment Report of the Intergovernmental Panel on Climate Change (IPCC AR6) (Thrasher et. al, 2021; Thrasher et. al, 2022). The purpose of this dataset is to provide a set of global, high resolution, bias-corrected climate change projections that can be used to evaluate climate change impacts on processes that are sensitive to finer-scale climate gradients and the effects of local topography on climate conditions.

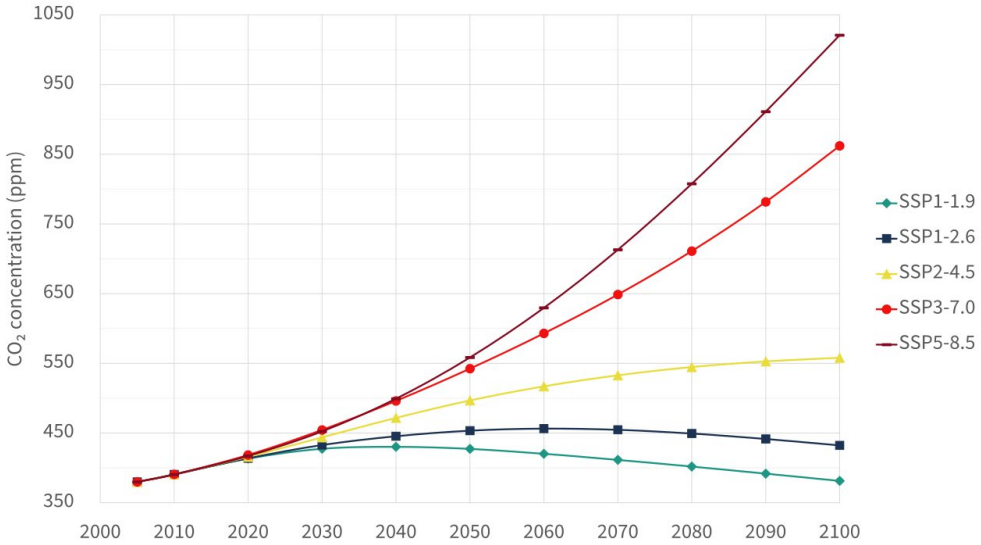

Figure 15.1: Shared Socioeconomic Pathways (SSP) trajectories. Reproduced from IPCC (2021).

The key climate model parameters used in this analysis were precipitation (Ppt), air temperature (Ta), and dew point temperature (Td). The parameters of relative humidity (RH) and Ta were used to derive the estimates of Td. The NEX-GDDP-CMIP6 dataset consists of thirty-five models, of these thirty-five models twenty-six models had the parameters and projections needed for the Maryland climate change analysis (Table 15.1). An example of the modeled climate projection parameters of Ppt, Ta, and Td are shown in Figure 15.2a and Figure 15.2b and the grid resolution covering the four regions is shown in Figure 15.3.

Table 15.1: Subset of twenty-six CMIP6 models and projections of RH, Ppt, and Td utilized

		Relative Humidity (hurs)			*Precipitation (pr)*			*Temperature (tas)*		
Model #	MODEL NAME	HISTORICAL	SSP45	SSP85	HISTORICAL	SSP45	SSP85	HISTORICAL	SSP45	SSP85
1	ACCESS-CM2	1950-2014	2015-2100	2015-2100	1950-2014	2015-2100	2015-2100	1950-2014	2015-2100	2015-2100
2	ACCESS-ESM1-5	1950-2014	2015-2100	2015-2100	1950-2014	2015-2100	2015-2100	1950-2014	2015-2100	2015-2100
4	CanESM5	1950-2014	2015-2100	2015-2100	1950-2014	2015-2100	2015-2100	1950-2014	2015-2100	2015-2100
5	CESM2-WACCM	1950-2014	2015-2100	2015-2100	1950-2014	2015-2100	2015-2100	1950-2014	2015-2100	2015-2100
6	CESM2	1950-2014	2015-2100	2015-2100	1950-2014	2015-2100	2015-2100	1950-2014	2015-2100	2015-2100
7	CMCC-CM2-SR5	1950-2014	2015-2100	2015-2100	1950-2014	2015-2100	2015-2100	1950-2014	2015-2100	2015-2100
8	CMCC-ESM2	1950-2014	2015-2100	2015-2100	1950-2014	2015-2100	2015-2100	1950-2014	2015-2100	2015-2100
9	CNRM-CM6-1	1950-2014	2015-2100	2015-2100	1950-2014	2015-2100	2015-2100	1950-2014	2015-2100	2015-2100
10	CNRM-ESM2-1	1950-2014	2015-2100	2015-2100	1950-2014	2015-2100	2015-2100	1950-2014	2015-2100	2015-2100
11	EC-Earth3-Veg-LR	1950-2014	2015-2100	2015-2100	1950-2014	2015-2100	2015-2100	1950-2014	2015-2100	2015-2100
12	EC-Earth3	1950-2014	2015-2100	2015-2100	1950-2014	2015-2100	2015-2100	1950-2014	2015-2100	2015-2100
13	FGOALS-g3	1950-2014	2015-2100	2015-2100	1950-2014	2015-2100	2015-2100	1950-2014	2015-2100	2015-2100
14	GFDL-CM4_gr1	1950-2014	2015-2100	2015-2100	1950-2014	2015-2100	2015-2100	1950-2014	2015-2100	2015-2100
15	GFDL-CM4_gr2	1950-2014	2015-2100	2015-2100	1950-2014	2015-2100	2015-2100	1950-2014	2015-2100	2015-2100
16	GFDL-ESM4	1950-2014	2015-2100	2015-2100	1950-2014	2015-2100	2015-2100	1950-2014	2015-2100	2015-2100
17	GISS-E2-1-G	1950-2014	2015-2100	2015-2100	1950-2014	2015-2100	2015-2100	1950-2014	2015-2100	2015-2100
21	INM-CM4-8	1950-2014	2015-2100	2015-2100	1950-2014	2015-2100	2015-2100	1950-2014	2015-2100	2015-2100
22	INM-CM5-0	1950-2014	2015-2100	2015-2100	1950-2014	2015-2100	2015-2100	1950-2014	2015-2100	2015-2100
23	IPSL-CM6A-LR	1950-2014	2015-2100	2015-2100	1950-2014	2015-2100	2015-2100	1950-2014	2015-2100	2015-2100
26	MIROC-ES2L	1950-2014	2015-2100	2015-2100	1950-2014	2015-2100	2015-2100	1950-2014	2015-2100	2015-2100
27	MIROC6	1950-2014	2015-2100	2015-2100	1950-2014	2015-2100	2015-2100	1950-2014	2015-2100	2015-2100
28	MPI-ESM1-2-HR	1950-2014	2015-2100	2015-2100	1950-2014	2015-2100	2015-2100	1950-2014	2015-2100	2015-2100
29	MPI-ESM1-2-LR	1950-2014	2015-2100	2015-2100	1950-2014	2015-2100	2015-2100	1950-2014	2015-2100	2015-2100
30	MRI-ESM2-0	1950-2014	2015-2100	2015-2100	1950-2014	2015-2100	2015-2100	1950-2014	2015-2100	2015-2100
33	NorESM2-MM	1950-2014	2015-2100	2015-2100	1950-2014	2015-2100	2015-2100	1950-2014	2015-2100	2015-2100
34	TaiESM1	1950-2014	2015-2100	2015-2100	1950-2014	2015-2100	2015-2100	1950-2014	2015-2100	2015-2100

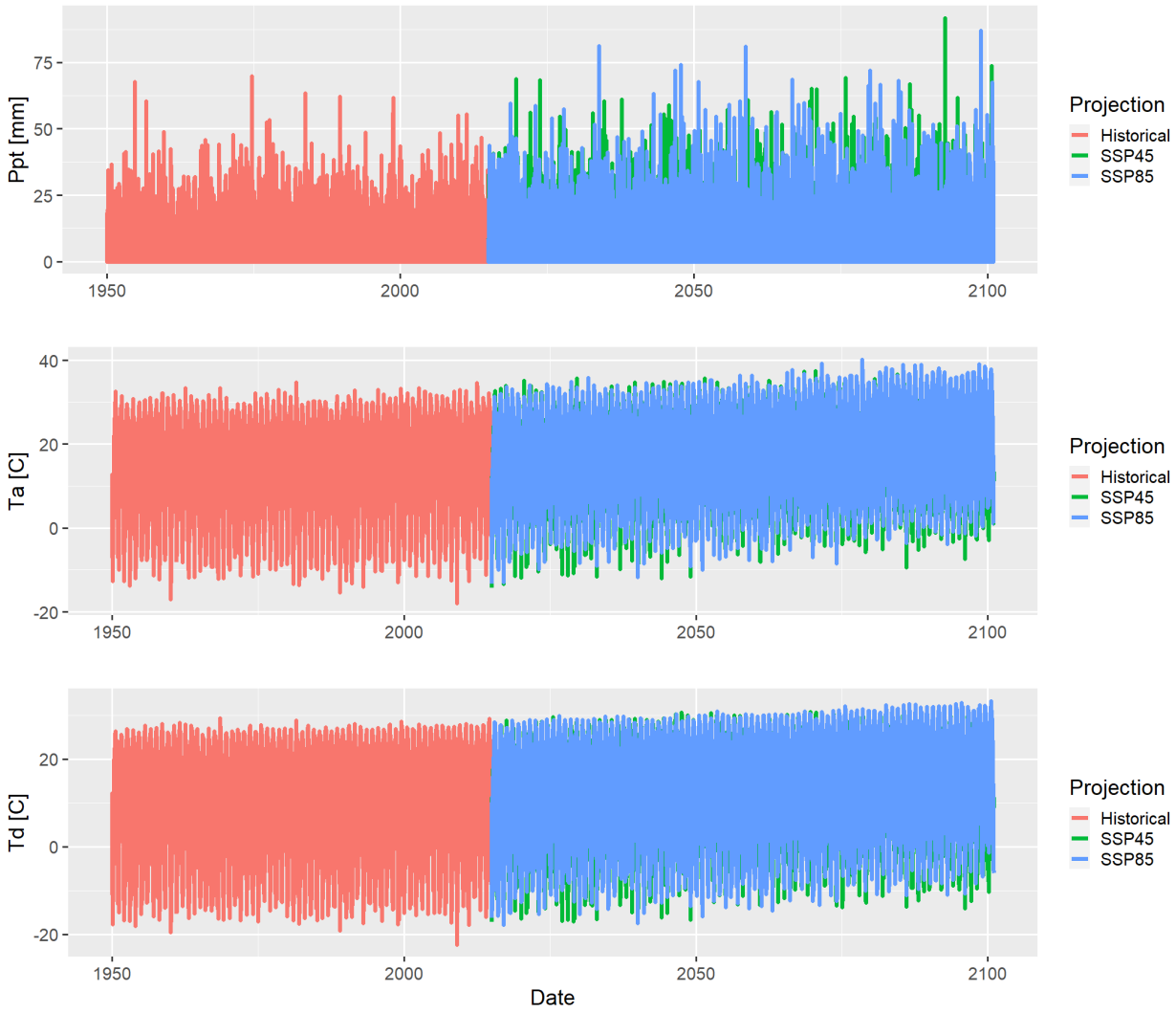

Figure 15.2: (a) Climate projection parameters of Ppt, Ta, and Td from Model 1 Region 1(ACCESS-CM2)

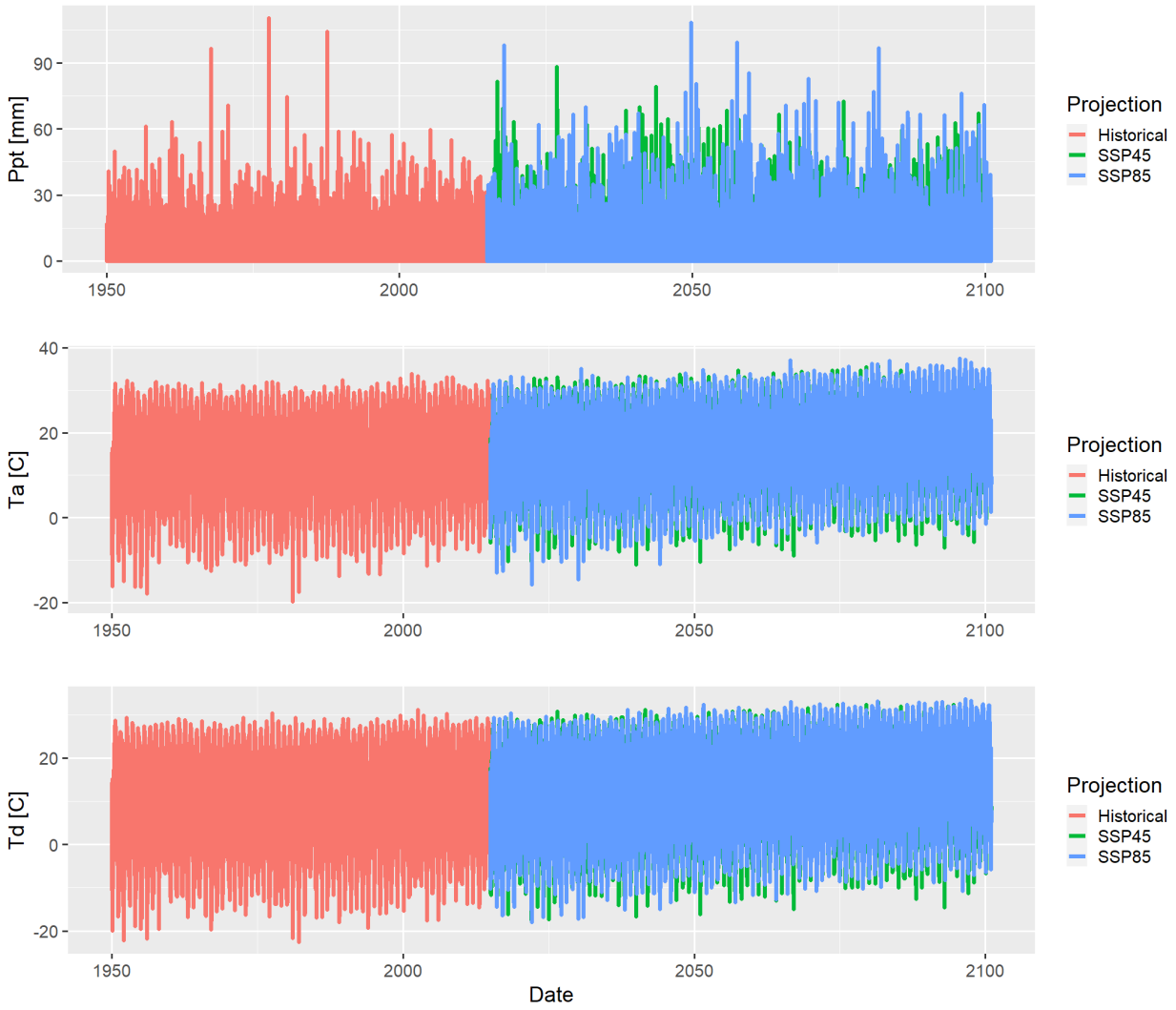

Figure 15.2: (b) Climate projection parameters of Ppt, Ta, and Td from Model 8 Region 1 (CMCC-ESM2)

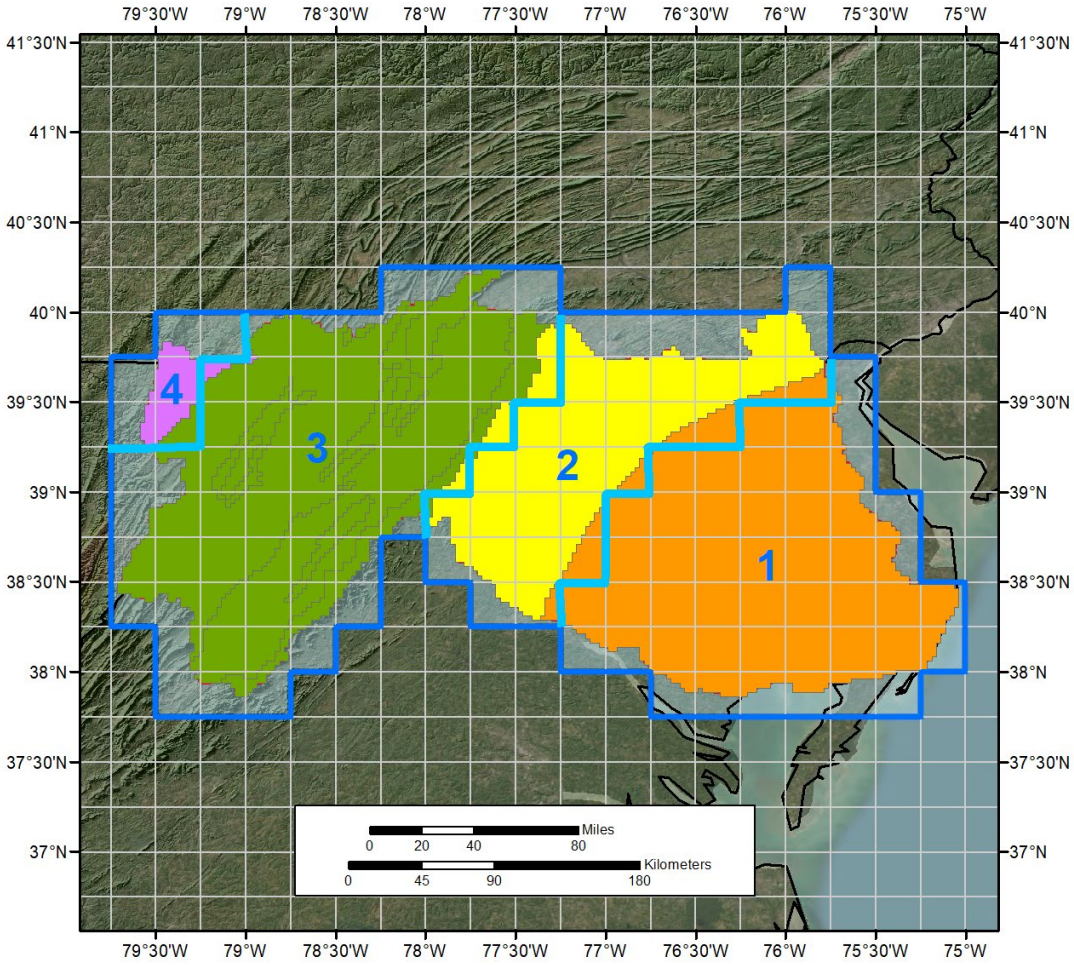

Figure 15.3: CMIP6 climate model grid resolution across the region. The four regions used for the climate change analysis.

15.2.1 Trend Analysis

Mann-Kendall trend analysis (Mann, 1945; Hipel and McLeod, 2005) was performed on twenty-six climate model projections using the three scenarios (historic, SSP2-4.5, SSP5-8.5) for durations of 1-day, 3-day, and annual. Figure 15.4 shows an example of the results for Model 1 Region 1 trend analysis for the historic, SSP-4.5, and SSP-8.5 projections.

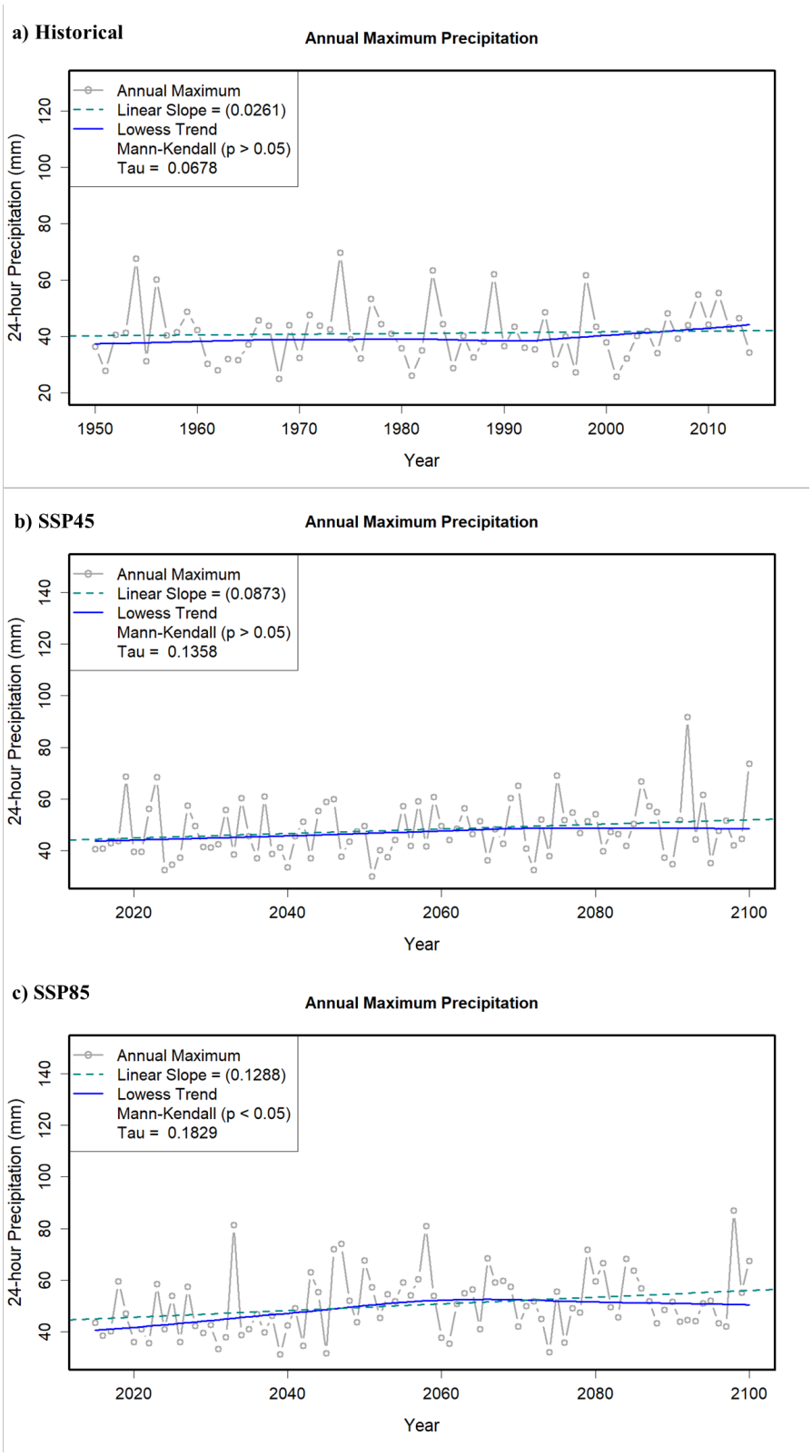

Figure 15.4: Example results for 1-day trend analysis from Model 1 Region 1 (ACCESS-CM2): a) no trend for historical period, b) no trend for SSP45 scenario, and c) increasing trend for SSP85 scenario. Blue line is Lowess trend line, dashed line is a linear trend, and Mann-Kendall p-value shown in lower legend.

15.2.2 Precipitation Frequency Analysis

The precipitation frequency analysis method utilized L-moment statistics instead of product moment statistics, which decrease the uncertainty of rainfall frequency estimates for more rare events and dampen the influence of outlier precipitation amounts from extreme storms (Hosking and Wallis, 1997). Methods to account for non-stationarity in projections were not addressed so the projections were applied assuming stationarity. For the precipitation frequency analysis, AWA utilized the daily climate model projections to perform frequency analysis on the 1-day, 3-day, and annual durations.

AWA identified, extracted, and quality controlled maximum precipitation projections from the NEX-GDDP-CMIP6 dataset for twenty-six CMIP6 models and three projection scenarios. The Annual Maximum Series (AMS) were then subjected to the frequency analysis methods (Hosking and Wallis, 1997). L-moment statistics were computed for annual maximum data for each projection and duration. Goodness of fit measures were evaluated for five candidate distributions: generalized logistic (GLO), generalized extreme value (GEV), generalized normal (GNO), Pearson type III (PE3), and generalized Pareto (GPA). An L-Moment Ratio Diagram was prepared based on L-Skewness and L-Kurtosis pairs for each duration. The weighted-average L-Skewness and L-Kurtosis pairing were found to be near the GEV distribution for all projections.

The GEV distribution was selected because: i) This is the most common distribution used for precipitation frequency studies (e.g., NOAA Atlas 14, Perica, 2015), ii) the GEV was identified on the 1-day, 3-day, and annual goodness-of-fit measures, and iii) using the same distribution ensures a more direct comparison to more rare values of the frequency curve.

In order to separate snow events from rain events the 1-day and 3-day annual maximum were also extracted for the summer season (May - October) and for the winter season (November – April). The summer and winter AMS data were used to perform L-moment frequency analysis methods as described above. Comparisons of percent change were made among model projections for 10-year through 1,000-year recurrence intervals, beyond this the uncertainty in probability distributions estimates is large. Figure 15.5 shows an example of the results for Model 1 Region 1 1-day precipitation frequency analysis for all seasons, the summer season, and the winter season for the historic, SSP-4.5, and SSP-8.5 projections.

*** 1-Day Precipitation

	10yr	50yr	100yr	500yr	1000yr	Pct Change					Average
Historical	54.7	67.3	72.4	83.9	88.7	-	-	-	-	-	
SSP45	62.6	76.6	82.5	96.0	101.8	14%	14%	14%	14%	15%	**14%**
SSP85	66.8	81.1	86.9	99.5	104.6	22%	21%	20%	19%	18%	**20%**

*** 1-Day Summer

	10yr	50yr	100yr	500yr	1000yr	Pct Change					Average
Historical	41.0	63.2	75.9	116.0	139.1	-	-	-	-	-	
SSP45	50.1	77.2	92.3	139.0	165.4	22%	22%	22%	20%	19%	**21%**
SSP85	47.5	61.0	66.5	79.1	84.4	16%	-4%	-12%	-32%	-39%	**-14%**

*** 1-Day Winter

	10yr	50yr	100yr	500yr	1000yr	Pct Change					Average
Historical	52.3	64.3	69.2	80.1	84.7	-	-	-	-	-	
SSP45	57.3	67.5	71.6	80.4	84.0	10%	5%	3%	0%	-1%	**3%**
SSP85	66.2	81.8	88.2	102.7	108.8	27%	27%	28%	28%	28%	**28%**

Figure 15.5: Example results for 1-day precipitation frequency analysis for climate projection from Model 1 Region 1 (ACCESS-CM2)

15.3 Results of Analysis

The results of modeled trends and estimated precipitation frequencies have a large variability that can be attributed to the uncertainty inherent with GCMs and RCMs projections. The different climate models used for the example regions represent a significant component of future climate uncertainty in climate models. This uncertainty is represented by the range of climate futures indicated by the Coupled Model Intercomparison Project 6 (CMIP6) ensemble of projections (McSweeney and Jones, 2016; Masson-Delmotte et al., 2021).

The median of the twenty-six models shows an increase in mean annual temperature and mean annual precipitation (Figure 15.6). Temperature, in regard to daily maximum (frequency based) and monthly averages show an increase by 2100 for both the SSP-4.5 and SSP-8.5 projections (Figure 15.7 and Figure 15.8). Numeric values representing the change in temperature are shown in Table 15.2 and Table 15.3.

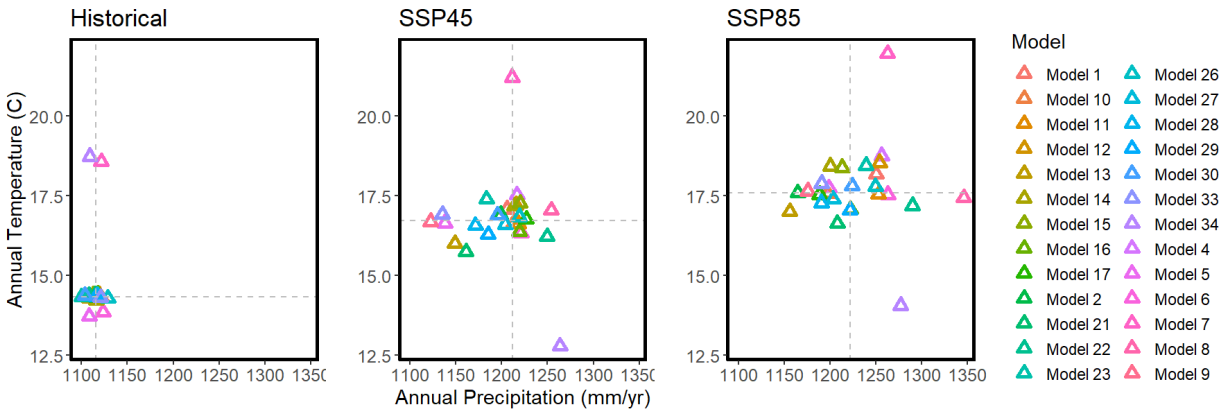

Figure 15.6: Comparison of mean annual temperature and mean annual precipitation for the three climate projection periods in Region 1

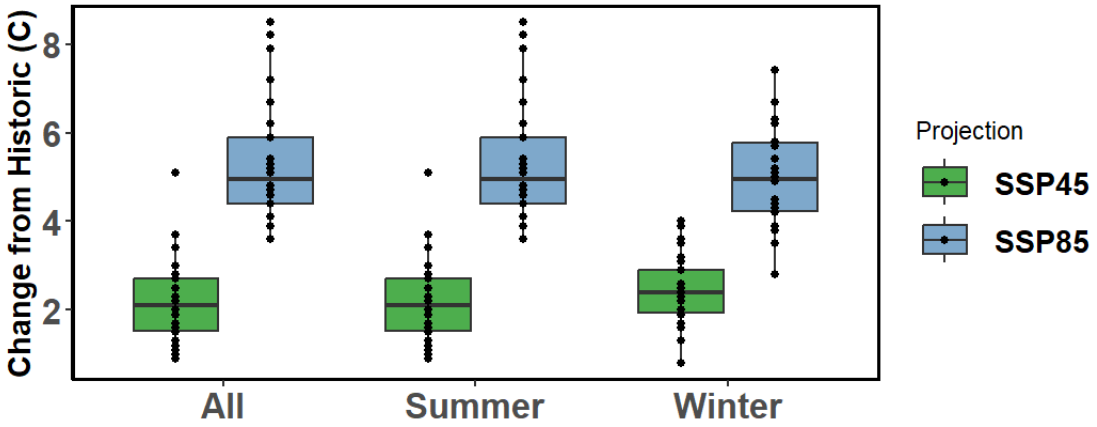

Figure 15.7: Change in daily average maximum temperatures from historic (1950-2014) climate conditions in Region1. Results are based on annual maximum frequency analysis.

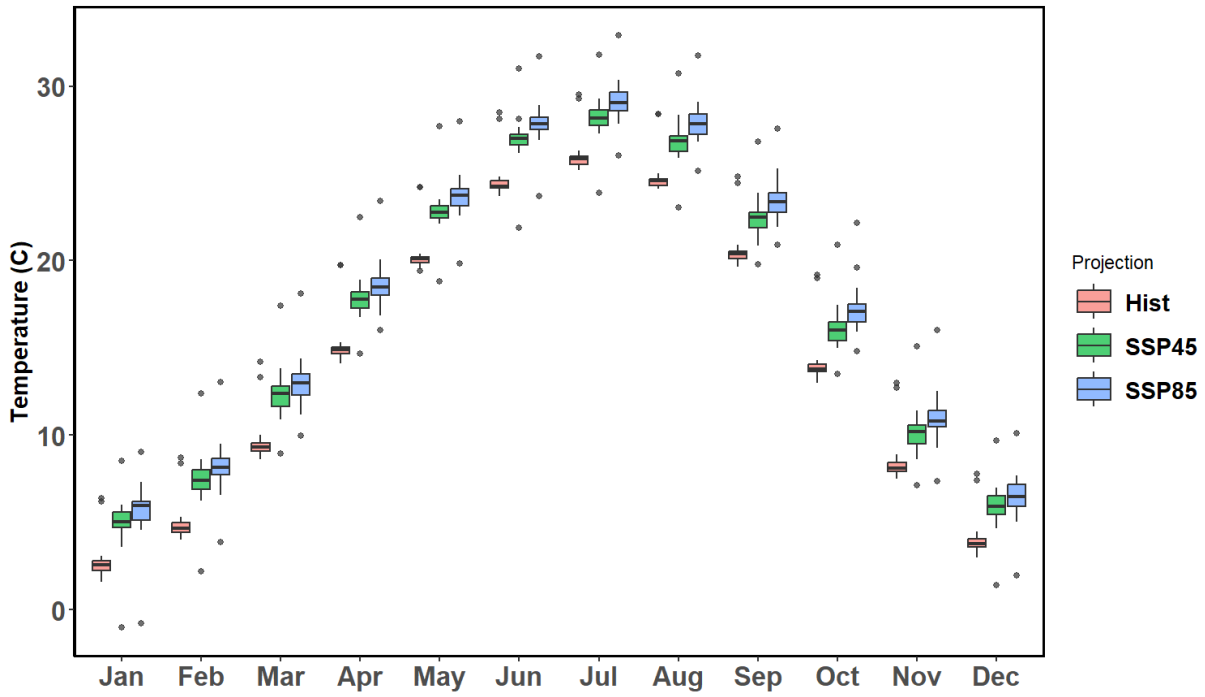

Figure 15.8: Monthly temperature normal compared for historical period (1950-2014) to climate change temperature normal period (2015-2100) for Region 1. Results are based on daily normal calculations.

Precipitation frequency analysis results are summarized below for 1-day, 3-day, and annual durations split into all seasons, the summer season, and the winter season. Results indicate a large range of change with the largest change occurring in the summer season for 1-day and 3-day durations (Figure 15.9). Numeric values representing the change in precipitation are shown in Table 15.2.

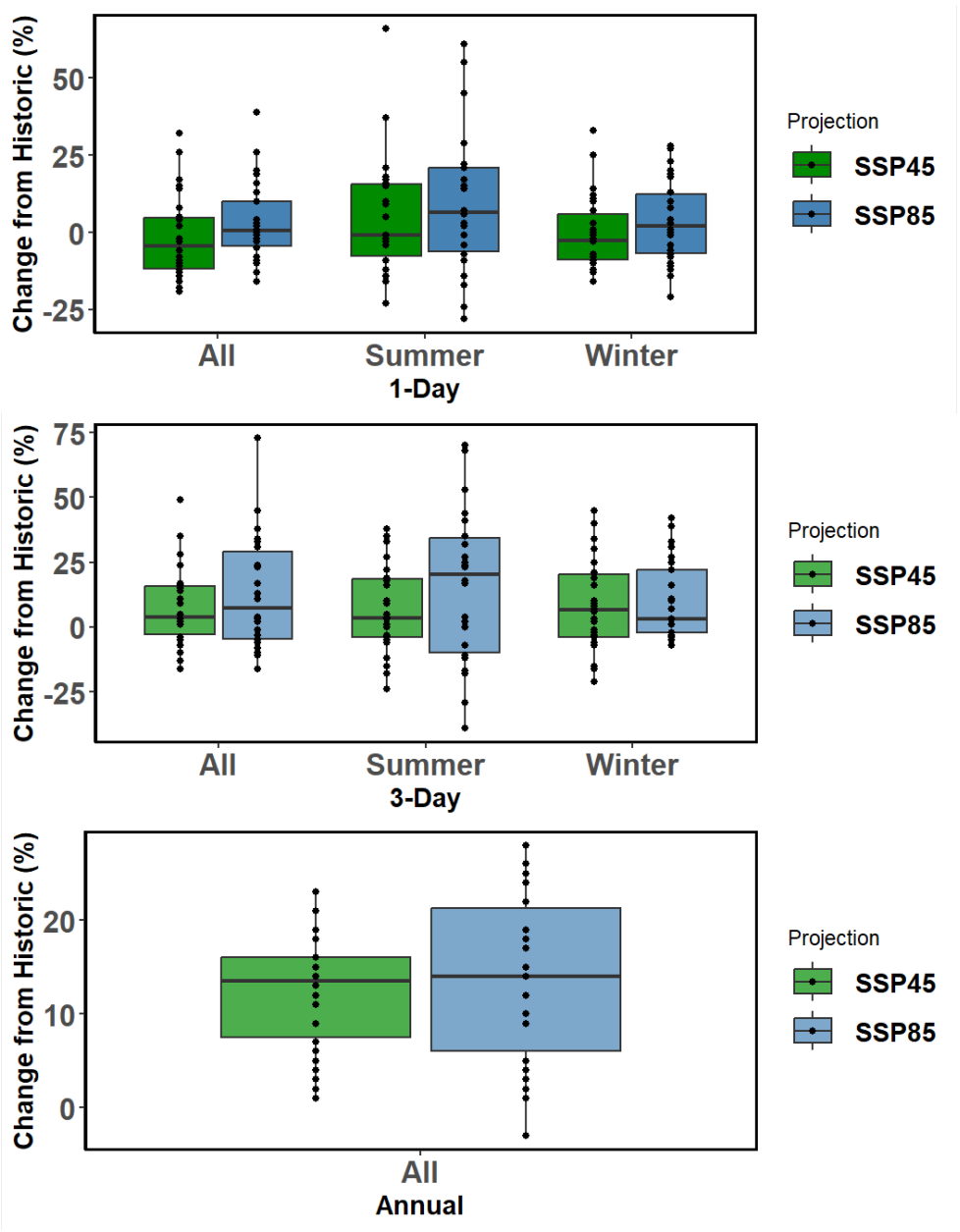

Figure 15.9: Change in maximum precipitation from current climate conditions for 1-day, 3-day, and annual durations in Region 1. Results are based on annual maximum frequency analysis.

Results indicate no change in precipitation and an increase in temperature by the year 2100. The analysis adequately captures the range of uncertainty and potential future outcomes. The most likely outcome regarding precipitation over the region going forward is that the mean annual and seasonal amount will increase, but the individual extreme events will stay within the range of uncertainty currently calculated.

This follows expected trends in the region under a warming climate scenario. In this case, more moisture would be available from an overall perspective, allowing for general increases in seasonal and annual scales. However, this same change is not reflected in the most extreme rainfall events that control PMP depths. This can be related to the variance in

atmospheric processes that convert moisture in the atmosphere to rainfall on the ground. These create both positive and negative feedback mechanisms where atmospheric instability at the most extreme levels are lessened in a warming environment because the thermal contrast between airmass is lessened. Therefore, there may be more frequent light rainfall events but less intense (PMP-type) rainfall events. Observational data of the storms which control PMP in the region confirm this as they do not show an increasing trend (Kappel et al. 2020a).

4 15.3.1 Application of Projections for Hydrologic Sensitivity

For hydrologic simulation and sensitivity, the recommended climate change adjustments and uncertainty values for temperature and precipitation are shown in Table 15.2. These are based on an evaluation of the rate of change from the current period through 2100 of each of the projections and taking an average of the outcomes. These values can be applied to a given period (i.e., 2050) by linear adjusting the climate change factors. For hydrologic simulation and sensitivity in Region 1, the recommended climate change adjustments and uncertainty values for monthly temperature are shown in Table 15.3 and precipitation in Table 15.4. An example of the scaling Region 1 results to the year 2050 is shown in Table 15.5. All four climate regions investigated had similar results to Region 1 and are shown in Tables 15.6 to Table 15.9. Additional details and results are provided in Appendix L.

Table 15.2: Maryland climate change projections for Region 1, change from historic period (1950-2014) to future period (2015-2100)

	SSP45				SSP85			
	Mean	**Median**	**10th**	**90th**	**Mean**	**Median**	**10th**	**90th**
Temperature 1-Day; C	**2.2**	**2.1**	1.0	3.2	**5.3**	**5.0**	4.0	7.5
Temperature 1-Day Summer; C	**2.2**	**2.1**	1.0	3.2	**5.3**	**5.0**	4.0	7.5
Temperature 1-Day Winter PF; C	**2.4**	**2.4**	1.6	3.5	**5.0**	**4.9**	3.8	6.3
Precipitation 1-Day PF; %	**-2**	**-5**	-17	16	**3**	**1**	-10	20
Precipitation 1-Day Summer PF; %	**5**	**-1**	-14	21	**9**	**7**	-16	37
Precipitation 1-Day Winter PF; %	**-1**	**-2**	-12	13	**4**	**2**	-11	21
Precipitation 3-Day PF; %	**8**	**4**	-12	26	**13**	**7**	-9	36
Precipitation 3-Day Summer PF; %	**7**	**4**	-13	33	**16**	**21**	-17	53
Precipitation 3-Day Winter PF; %	**9**	**6**	-11	32	**10**	**3**	-5	32
Precipitation Annual PF; %	**12**	**13**	3	19	**13**	**14**	1	25
1-Day Moisture Maximization; %	**No Change**				**No Change**			
3-Day Moisture Maximization; %	**No Change**				**Potential Change**			

* Climate Change Projections from 2015 through 2100

\+ Note, SSP8.5 represent the most extreme, the 95-percentile of all model forcing simulations

Table 15.3: Maryland monthly temperature (C) change from current climate (1950-2014) to 2015 through 2100 for Region 1

	Historical		SSP45		SSP85		Mean Delta		Median Delta	
	Mean	Median	Mean	Median	Mean	Median	SSP45	SSP85	SSP45	SSP85
January	2.7	2.6	4.9	5.1	5.6	6.0	*2.2*	*2.9*	*2.5*	*3.4*
February	5.0	4.7	7.4	7.4	8.2	8.2	*2.4*	*3.2*	*2.7*	*3.5*
March	9.6	9.3	12.4	12.4	13.0	13.0	*2.8*	*3.4*	*3.1*	*3.7*
April	15.2	14.9	17.8	17.8	18.6	18.5	*2.6*	*3.4*	*2.9*	*3.6*
May	20.3	20.1	22.8	22.8	23.7	23.7	*2.5*	*3.4*	*2.7*	*3.6*
June	24.6	24.3	26.9	27.0	27.8	27.9	*2.3*	*3.3*	*2.8*	*3.6*
July	26.1	25.9	28.1	28.2	29.1	29.1	*2.1*	*3.1*	*2.3*	*3.2*
August	24.8	24.6	26.8	26.9	27.9	27.8	*2.0*	*3.0*	*2.3*	*3.2*
September	20.6	20.4	22.4	22.5	23.5	23.4	*1.8*	*2.9*	*2.1*	*3.0*
October	14.2	13.8	16.1	16.0	17.2	17.1	*1.9*	*3.0*	*2.2*	*3.3*
November	8.5	8.1	10.1	10.2	11.0	10.8	*1.7*	*2.5*	*2.1*	*2.7*
December	4.0	3.8	5.9	5.9	6.5	6.5	*1.8*	*2.4*	*2.1*	*2.7*

Table 15.4: Maryland monthly precipitation (mm) change from current climate (1950-2014) to 2015 through 2100 for Region 1

	Historical		SSP45		SSP85		Mean Delta		Median Delta	
	Mean	Median	Mean	Median	Mean	Median	SSP45	SSP85	SSP45	SSP85
January	80.0	80.7	89.4	91.9	93.4	94.1	*1.12*	*1.14*	*1.14*	*1.17*
February	72.9	73.3	84.4	86.3	85.9	85.7	*1.16*	*1.18*	*1.18*	*1.17*
March	91.5	91.8	98.9	97.0	103.7	104.4	*1.08*	*1.06*	*1.06*	*1.14*
April	80.8	82.0	88.4	87.6	86.6	86.0	*1.09*	*1.07*	*1.07*	*1.05*
May	90.9	91.2	95.9	96.1	94.6	92.5	*1.06*	*1.05*	*1.05*	*1.01*
June	94.0	93.8	103.0	103.9	101.7	101.3	*1.09*	*1.11*	*1.11*	*1.08*
July	114.1	113.0	124.8	124.6	125.5	124.8	*1.09*	*1.10*	*1.10*	*1.10*
August	104.2	103.9	111.3	113.0	112.5	112.8	*1.07*	*1.09*	*1.09*	*1.09*
September	86.9	86.9	90.8	89.2	90.3	86.7	*1.04*	*1.03*	*1.03*	*1.00*
October	79.5	78.6	81.9	79.7	83.3	83.9	*1.03*	*1.01*	*1.01*	*1.07*
November	79.0	78.9	86.9	85.6	92.3	94.6	*1.10*	*1.09*	*1.09*	*1.20*
December	88.3	88.9	95.8	95.9	103.3	101.2	*1.09*	*1.08*	*1.08*	*1.14*

Table 15.5: Example of scaling Region 1 climate change results to 2050 from 2100

	2050	2100
1-Day Summer PF; %	0	-1
1-Day Winter PF; %	-1	-2
3-Day Summer PF; %	2	4
3-Day Winter PF; %	4	6

Table 15.6: Climate Change Projections for Region 1 from current climate (1950-2014) through 2100

Region 1	SSP45				SSP85			
	Mean	Median	10th	90th	Mean	Median	10th	90th
Temperature 1-Day; C	**2.2**	**2.1**	1.0	3.2	**5.3**	**5.0**	4.0	7.5
Temperature 1-Day Summer; C	**2.2**	**2.1**	1.0	3.2	**5.3**	**5.0**	4.0	7.5
Temperature 1-Day Winter PF; C	**2.4**	**2.4**	1.6	3.5	**5.0**	**4.9**	3.8	6.3
Precipitation 1-Day PF; %	**-2**	**-5**	-17	16	**3**	**1**	-10	20
Precipitation 1-Day Summer PF; %	**5**	**-1**	-14	21	**9**	7	-16	37
Precipitation 1-Day Winter PF; %	**-1**	**-2**	-12	13	**4**	**2**	-11	21
Precipitation 3-Day PF; %	**8**	**4**	-12	26	**13**	7	-9	36
Precipitation 3-Day Summer PF; %	7	**4**	-13	33	**16**	**21**	-17	53
Precipitation 3-Day Winter PF; %	**9**	**6**	-11	32	**10**	**3**	-5	32
Precipitation Annual PF; %	**12**	**13**	3	19	**13**	**14**	1	25
Moisture Maximization 1-Day, %	**No Change**				**No Change**			
Moisture Maximization 3-Day; %	**No Change**				**Potential Change**			

Table 15.7: Climate Change Projections for Region 2 from current climate (1950-2014) through 2100

Region 2	SSP45				SSP85			
	Mean	Median	10th	90th	Mean	Median	10th	90th
Temperature 1-Day; C	**2.4**	**2.3**	1.0	3.3	**5.7**	**5.1**	4.0	8.0
Temperature 1-Day Summer; C	**2.4**	**2.3**	1.0	3.3	**5.7**	**5.1**	4.0	8.0
Temperature 1-Day Winter PF; C	**2.5**	**2.4**	1.5	3.7	**5.3**	**5.3**	4.0	6.5
Precipitation 1-Day PF; %	**9**	**6**	-7	33	**10**	**6**	-10	36
Precipitation 1-Day Summer PF; %	**13**	**10**	-11	44	**9**	**3**	-17	45
Precipitation 1-Day Winter PF; %	**11**	7	-4	29	**14**	**13**	-1	32
Precipitation 3-Day PF; %	**12**	**16**	-5	26	**10**	**10**	-11	32
Precipitation 3-Day Summer PF; %	**9**	**3**	-17	45	7	**11**	-20	32
Precipitation 3-Day Winter PF; %	**15**	**15**	-5	36	**13**	**15**	-2	31
Precipitation Annual PF; %	**11**	**11**	5	20	**13**	**13**	3	23
Moisture Maximization 1-Day, %	**No Change**				**No Change**			
Moisture Maximization 3-Day; %	**No Change**				**No Change**			

Table 15.8: Climate Change Projections for Region 3 from current climate (1950-2014) through 2100

Region 3	SSP45				SSP85			
	Mean	Median	10th	90th	Mean	Median	10th	90th
Temperature 1-Day; C	**2.4**	**2.3**	1.0	3.3	**5.7**	**5.0**	3.8	8.2
Temperature 1-Day Summer; C	**2.4**	**2.3**	1.0	3.3	**5.7**	**5.0**	3.8	8.2
Temperature 1-Day Winter PF; C	**2.3**	**2.2**	1.5	3.6	**5.2**	**5.4**	3.9	6.7
Precipitation 1-Day PF; %	**8**	**6**	-9	28	**11**	7	-4	33
Precipitation 1-Day Summer PF; %	**10**	**9**	-10	31	**3**	**3**	-17	22
Precipitation 1-Day Winter PF; %	**10**	7	-6	28	**16**	**14**	5	32
Precipitation 3-Day PF; %	**11**	**14**	-10	28	**12**	**8**	-4	32
Precipitation 3-Day Summer PF; %	7	**4**	-15	31	**8**	**14**	-15	30
Precipitation 3-Day Winter PF; %	**12**	**12**	-3	28	**14**	**13**	0	30
Precipitation Annual PF; %	**12**	**10**	6	19	**13**	**13**	6	23
Moisture Maximization 1-Day, %	**No Change**				**No Change**			
Moisture Maximization 3-Day; %	**No Change**				**No Change**			

Table 15.9: Climate Change Projections for Region 4 from current climate (1950-2014) through 2100

Region 4	SSP45				SSP85			
	Mean	Median	10th	90th	Mean	Median	10th	90th
Temperature 1-Day; C	**2.4**	**2.3**	1.0	3.3	**5.7**	**5.0**	3.8	8.2
Temperature 1-Day Summer; C	**2.4**	**2.3**	1.0	3.3	**5.7**	**5.0**	3.8	8.2
Temperature 1-Day Winter PF; C	**2.3**	**2.2**	1.5	3.6	**5.2**	**5.4**	3.9	6.7
Precipitation 1-Day PF; %	**8**	**10**	-9	28	**12**	**8**	1	33
Precipitation 1-Day Summer PF; %	**10**	**9**	-10	31	**4**	**4**	-12	22
Precipitation 1-Day Winter PF; %	**9**	7	-6	28	**16**	**15**	5	32
Precipitation 3-Day PF; %	**12**	**15**	-10	28	**13**	**10**	-2	32
Precipitation 3-Day Summer PF; %	7	**4**	-15	31	**8**	**14**	-15	30
Precipitation 3-Day Winter PF; %	**13**	**13**	-3	29	**14**	**13**	0	30
Precipitation Annual PF; %	**11**	**10**	6	19	**13**	**13**	6	23
Moisture Maximization 1-Day, %	**No Change**				**No Change**			
Moisture Maximization 3-Day; %	**No Change**				**No Change**			

16. Uncertainty and Limitations

16.1 Sensitivity of Parameters

In the process of deriving PMP depths, various assumptions and meteorological judgments were made. Additionally, various parameters and derived values were used in the calculations, which are standard to the PMP development process. It is of interest to assess the sensitivity of PMP to assumptions that were made and to the variability of parameter values.

16.2 Saturated Storm Atmosphere

Atmospheric air masses that provide available moisture to both the historic storm and the PMP storm are assumed to be saturated through the entire depth of the atmosphere and to contain the maximum moisture possible for a given storm event based on the surface dew point or SST. This assumes moist pseudo-adiabatic temperature profiles for both the historic storm and the PMP storm. Limited evaluation of this assumption in the EPRI Michigan/Wisconsin PMP study (Tomlinson, 1993) and the Blenheim Gilboa study (Tomlinson et al., 2008) indicated that historic storm atmospheric profiles are generally not entirely saturated and contain somewhat less precipitable water than is assumed in the PMP procedure. More detailed evaluations were completed by Ben Alaya et al., (2018) utilizing an uncertainty analysis and modeling framework. This again demonstrated that the assumption of a fully saturated atmosphere in conjunction with maximum storm efficiency may not be valid. However, this assumption does produce the most conservative combination of factors and resulting PMP depths.

It follows that the PMP storm (if it were to occur) would also have somewhat less precipitable water available than the assumed saturated PMP atmosphere would contain. The *ratio* of precipitable water associated with each storm is used in the PMP calculation procedure. If the precipitable water values for each storm scenario are both slightly overestimated, the ratio of these values will be essentially unchanged. For example, consider the case where instead of a historic storm with a storm representative dew point of 70°F having 2.25 inches of precipitable water and assuming a saturated atmosphere, it actually had 90% of that value or about 2.02 inches. The PMP procedure assumes the same type of storm with similar atmospheric characteristics for the maximized storm but with a higher dew point, say 76°F. The maximized storm, having similar atmospheric conditions, would have about 2.69 inches of precipitable water instead of the 2.99 inches associated with a saturated atmosphere with a dew point of 76°F. The maximization factor computed, using the assumed saturated atmospheric values, would be 2.99/2.25 = 1.33. If both storms were about 90% saturated, the maximization factor would be 2.69/2.02 = 1.33. Therefore, any potential inaccuracy of assuming saturated atmospheres (whereas the atmospheres may be somewhat less than saturated) should have a minimal impact on storm maximization and subsequent PMP calculations.

16.3 Maximum Storm Efficiency

The assumption is made that if a sufficient period of record is available for rainfall observations, at least a few storms would have been observed that attained or came close to attaining the maximum efficiency possible in nature for converting atmospheric moisture to rainfall for regions with similar climates and topography. The further assumption is made that if additional atmospheric moisture had been available, the storm would have maintained the same

efficiency for converting atmospheric moisture to rainfall. The ratio of the maximized rainfall amounts to actual rainfall amounts would be the same as the ratio of precipitable water in the atmosphere associated with each storm.

There are two issues to be considered. The f irst relates to the assumption that a storm has a precipitation efficiency close to the maximum possible. Unfortunately, state-of-the-science in meteorology does not support a theoretical evaluation of storm efficiency. However, if the period of record is considered (generally over 100 years), along with the extended geographic region with transpositionable storms, it is accepted that there should have been at least one storm with dynamics that approached the maximum efficiency for rainfall production.

The other issue pertains to the assumption that storm efficiency does not change if additional atmospheric moisture is available. Storm dynamics could potentially become more efficient or possibly less efficient depending on the interaction of cloud microphysical processes with the storm dynamics. Offsetting effects could indeed lead to the storm efficiency remaining essentially unchanged. For the present, the assumption of no change in storm efficiency seems acceptable.

16.4 Storm Representative Dew Point/SST and Maximum Dew Point/SST

The maximization factor depends on the determination of storm representative dew points or SST, along with maximum historical dew point or SST values. The magnitude of the maximization factor varies depending on the values used for the storm representative dew point/SST and the maximum dew point/SST. Holding all other variables constant, the maximization factor is smaller for higher storm representative dew points/SSTs as well as for lower maximum dew point/SST values. Likewise, larger maximization factors result from the use of lower storm representative dew points/SSTs and/or higher maximum dew points/SSTs. The magnitude of the change in the maximization factor varies depending on the dew point/SST values. For the range of dew point/SST values used in most PMP studies, the maximization factor for a particular storm will change about 5% for every 1°F difference between the storm representative and maximum dew point/SST values. The same sensitivity applies to the transposition factor, with about a 5% change for every 1°F change in either the in-place maximum dew point/SST or the transposition maximum dew point/SST.

16.5 Judgment and Effect on PMP

During the process of PMP development several aspects involve professional judgment:

- Storms used for PMP development
- Storm representative dew point/SST value and location
- Storm transposition limits
- Use of precipitation frequency climatologies to represent differences in precipitation processes (including orographic effects) between two locations

Each of these processes were discussed and evaluated during the PMP development process internally within AWA and with the MDE and others involved in the project. The resulting PMP depths derived as part of the PMP development reflect the most defensible

judgments based on the data available and current scientific understanding. The PMP results represent defensible, reproducible, reasonable, and appropriately conservative estimates.

17. References

Alexander et al., 2015: The High-Resolution Rapid Refresh (HRRR): The operational implementation, in 95th Annual meeting of the American Meteorological Society.

Ben Alaya, M.A., F. Zwiers, and X. Zhang, 2018: Probable Maximum Precipitation: Its Estimation and Uncertainty Quantification Using Bivariate Extreme Value Analysis. *J. Hydrometeor.,* **19**, 679–694.

Bonnin, G., D. Martin, B. Lin, T. Parzybok, M. Yekta, and D. Riley, 2006: NOAA *Atlas 14 Volume 2, Precipitation-Frequency Atlas of the United States, Delaware, District of Columbia, Illinois, Indiana, Kentucky, Maryland, New Jersey, North Carolina, Ohio, Pennsylvania, South Carolina, Tennessee, Virginia, West Virginia*. NOAA, National Weather Service, Silver Spring, MD.

Bontà, V., 2003: Estimation of parameters characterizing frequency distributions of times between storms. Transactions of the ASAE. 46.

Corps of Engineers, U.S. Army, 1945-1973: Storm Rainfall in the United States, Depth-Area-Duration Data. Office of Chief of Engineers, Washington, D.C.

Corrigan, P., D.D. Fenn, D.R. Kluck, and J.L. Vogel, 1999: Probable Maximum Precipitation for California, Hydrometeorological Report Number 59, National Weather Service, National Oceanic and Atmospheric Administration, U. S. Department of Commerce, Silver Spring, MD, 392 pp.

Cudworth, A.G., 1989: Flood Hydrology Manual, Water Resources Technical Publication, United States Dept, of the Interior, United States Bureau of Reclamation, Denver office, 243pp.

Daly, C., R.P. Neilson, and D.L. Phillips, 1994: A Statistical-Topographic Model for Mapping Climatological Precipitation over Mountainous Terrain. J. Appl. Meteor., 33, 140–158.

Daly, C., Taylor, G., and W. Gibson, 1997: The PRISM Approach to Mapping Precipitation and Temperature, 10th Conf. on Applied Climatology, Reno, NV, Amer. Meteor. Soc., 10-12.

Dickens, J., 2003: On the Retrieval of Drop Size Distribution by Vertically Pointing Radar. American Meteorological Society 32nd Radar Meteorology Conference, Albuquerque, NM, October 2005

Draxler, R.R. and Rolph, G.D., 2013: HYSPLIT (HYbrid Single-Particle Lagrangian Integrated Trajectory) NOAA Air Resources Laboratory, Silver Spring, MD. Model access via NOAA ARL READY Website, http://ready.arl.noaa.gov/HYSPLIT.php

Dwight, B.W., 1822; An Account of a Remarkable storm which occurred at Catskill, July 26, 1819, *in* The American Journal of Science and Arts, Vol. IV, Articl XII.

England, J. F., Julien, P. Y., & Vellleux, M. L. (2014). Physically-based extreme flood frequency with stochastic storm transposition and paleoflood data on large watersheds. *Journal of Hydrology*, *510*, 228–245.

Environmental Data Service, 1968: Maximum Persisting 12-Hour, 1000mb Dew Points (°F) Monthly and of Record. *Climate Atlas of the United States*, Env. Sci. Srv. Adm., U.S. Dept of Commerce, Washington, D.C., pp 59-60.

Environmental Systems Research Institute (ESRI), ArcGIS Version 10.1 Computer Software, 2012.

Gelber, Ben, 1992: *Pocono Weather*, Uriel Publishing, Stroudsburg, New Jersey, 291 pp.

Goodyear, H.V., and J.T., Riedel, 1965: Probable Maximum Precipitation, Susquehanna River Drainage Above Harrisburg, PA *Hydrometeorological Report Number 40*,

Hydrometeorological Branch, Office of Hydrology, U.S. Weather Bureau, Washington, D.C., 78 pp.

GRASS (Geographic Resources Analysis Support System) GIS is an open source, free software GIS with raster, topological vector, image processing, and graphics production functionality that operates on various platforms. http://grass.itc.it/.

Guo, J.C.Y., 2012: Storm Centering Approach for Flood Predictions from Large Watersheds, Journal of Hydrologic Engineering.

Hansen, E.M, F.K. Schwarz, and J.T Reidel, 1977: Probable Maximum Precipitation Estimates. Colorado River and Great Basin Drainages. Hydrometeorological Report No. 49, NWS, NOAA, U.S. Department of Commerce, Silver Spring, MD, 161 pp.

Hansen, E.M, and F.K. Schwartz, 1981: Meteorology of Important Rainstorms in the Colorado River and Great Basin Drainages. Hydrometeorological Report No. 50, National Weather Service, National Oceanic and Atmospheric Administration, U.S. Department of Commerce, Silver Spring, MD, 167 pp.

Hansen, E.M., L.C. Schreiner and J.F. Miller, 1982: Application of Probable Maximum Precipitation Estimates – United States East of the 105th Meridian. Hydrometeorological Report No. 52, U.S. Department of Commerce, Washington, D.C., 168 pp.

Hansen, E.M, Fenn, D.D., Schreiner, L.C., Stodt, R.W., and J.F., Miller, 1988: Probable Maximum Precipitation Estimates, United States between the Continental Divide and the 103rd Meridian, Hydrometeorological Report Number 55A, National weather Service, National Oceanic and Atmospheric Association, U.S. Dept. of Commerce, Silver Spring, MD, 242 pp.

Hansen, E.M, Schwarz, F.K., and J.T. Riedel, 1994: Probable Maximum Precipitation- Pacific Northwest States, Columbia River (Including portion of Canada), Snake River, and Pacific Drainages. Hydrometeorological Report No. 57, National Weather Service, National Oceanic and Atmospheric Administration, U.S. Department of Commerce, Silver Spring, MD, 353 pp.

Hausfather, Zeke; Peters, Glen P., 2020: "Emissions – the 'business as usual' story is misleading". Nature. 577 (618–620). doi:10.1038/d41586-020-00177-3. Retrieved 2022-03-28.

Hershfield, D.M., 1961: *Rainfall frequency atlas of the United States for durations from 30 minutes to 24 hours and return periods from 1 to 100 years*. Weather Bureau Technical Paper No. 40, U.S. Weather Bureau, Washington, D.C., 115 pp.

Hicks, N. S., J. A. Smith, A. J. Miller, *and* P. A. Nelson, 2005: Catastrophic flooding from an orographic thunderstorm in the central Appalachians, Water Resour. Res., 41, *W12428*

Hipel, K.W. and McLeod, A.I., (2005): Time Series Modelling of Water Resources and Environmental Systems. Electronic reprint of our book originally published in 1994. http://www.stats. uwo.ca/faculty/aim/1994Book/.

Hosking, J.R.M, 2015a. L-moments. R package, version 2.5. URL: http://CRAN.R-project.org/package=lmom.

Hosking, J.R.M, 2015b. Regional frequency analysis using L-moments. R package, version 3.0-1. URL: http://CRAN.R-project.org/package=lmomRFA.

Hosking, J.R.M. and J.R. Wallis, 1997: "Regional Frequency Analysis, An Approach Based on L-Moments," Cambridge University Press, 224 pp.

Huff, F.A., 1967: Time Distribution of Rainfall in Heavy Storms, Water Resources Research.

Hultstrand, D.M., and Kappel, W.D., 2017: The Storm Precipitation Analysis System (SPAS) Report. Nuclear Regulatory Commission (NRC) Inspection Report No 99901474/2016-201, Enercon Services, Inc., 95pp.

IPCC, 2021: Climate Change 2021: The Physical Science Basis. Contribution of Working Group I to the Sixth Assessment Report of the Intergovernmental Panel on Climate Change [Masson-Delmotte, V., P. Zhai, A. Pirani, S.L. Connors, C. Péan, S. Berger, N. Caud, Y. Chen, L. Goldfarb, M.I. Gomis, M. Huang, K. Leitzell, E. Lonnoy, J.B.R. Matthews, Kappel, W.D., Hultstrand, D.M., Muhlestein, G.A., Steinhilber, K., McGlone, D., E.M. Tomlinson, and T. Parzybok. July 2013: Probable Maximum Precipitation Study for Arizona. Prepared for the Arizona Dept. of Water Resources, Dam Safety Division.

Kappel, W.D., Hultstrand, D.M., Muhlestein, G.A., Steinhilber, K., and D. McGlone, July 2014: Site-Specific Probable Maximum Precipitation (PMP) Study for the College Lake Basin, Colorado, prepared for Colorado State University.

Kappel, W.D., Hultstrand, D.M., Muhlestein, G.A., Steinhilber, K., McGlone, D., Parzybok, T.W, and E.M. Tomlinson, December 2014: Statewide Probable Maximum Precipitation (PMP) Study for Wyoming.

Kappel, W.D., Hultstrand, D.M., Muhlestein, G.A., Steinhilber, K., and McGlone, D., December 2015: Application of Temporal Patterns of PMP for Dam Design in Wyoming. Prepared for the Wyoming State Engineer's Office.

Kappel, W.D., Hultstrand, D.M., Rodel, J.T., Muhlestein, G.A., Steinhilber, K., McGlone, D., Rodel, J., and B. Lawrence, November 2015: Statewide Probable Maximum Precipitation or Virginia. Prepared for the Virginia Department of Conservation and Recreation.

Kappel, W.D., Hultstrand, D.M., Muhlestein, G.A., Steinhilber, K., and McGlone, D, February 2016: Site-Specific Probable Maximum Precipitation for Hebgen Dam, MT.

Kappel, W.D., Hultstrand, D.M., Muhlestein, G.A., Steinhilber, K., Rodel, J.T., McGlone, D., Parzybok, T.W., and B. Lawrence, September 2016: Statewide Probable Maximum Precipitation for Texas. Prepared for the Texas Commission of Environmental Quality.

Kappel, W.D., Hultstrand, D.M., Muhlestein, G.A., Rodel, J.T., Steinhilber, K., McGlone, D., and Lawrence, B., May 2017: Site-Specific Probable Maximum Precipitation and Annual Exceedance Probability Assessment for the Gross Reservoir Basin, Colorado. Prepared for Denver Water.

Kappel, W.D., Hultstrand, D.M., Muhlestein, G.A., Rodel, J.T., Steinhilber, K., and Lawrence, B., May 2018: Site-Specific Probable Maximum Precipitation and Annual Exceedance Probability Assessment for the Painted Rocks and East Fork Basins, Montana. Prepared for AECOM and Montana Dept. of Natural Resources.

Kappel, W.D., Rodel, J.T., Hultstrand, D.M., Muhlestein, G.A., Steinhilber, K., and McGlone, D, June 2018: Site-Specific Probable Maximum Precipitation and Annual Exceedance Probability Assessment for the Catawba Wateree Basin. Prepared for Duke Energy.

Kappel, W.D., Hultstrand, D.M., Muhlestein, G.A., Steinhilber, K., McGlone, D., and B. Lawrence, August 2018: Regional Probable Maximum Precipitation for the States of Colorado and New Mexico. Prepared for the Colorado Division of Water Resources and the New Mexico State Engineers Office.

Kappel, W.D., Hultstrand, D.M., Muhlestein, G.A., Rodel, J.T., Steinhilber, K., and Lawrence, B., October 2018: Site-Specific Probable Maximum Precipitation for Mayo Reservoir basin, North Carolina. Prepared for Duke Energy.

Kappel W.D., and Hultstrand, D.M., 2018: Hurricane Harvey, *Journal of Dam Safety*, Vol. 16, No. 1, 25-34.

Kappel, W.D., Hultstrand, D.M., Rodel, J.T., Muhlestein, G.A., Steinhilber, K., McGlone, D., and B. Lawrence, March 2019: Statewide Probable Maximum Precipitation for Pennsylvania. Prepared for the Pennsylvania Department of Environmental Protection.

Kappel, W.D., Hultstrand, D.M., Muhlestein, G.A., Steinhilber, K., Rodel, J., and B. Lawrence, August 2019: Regional Probable Maximum Precipitation for the states of Oklahoma, Arkansas, Louisiana, and Mississippi. Prepared for the Oklahoma Water Resources Board, Arkansas Dept. of Natural Resources, Louisiana Dept. of Transportation & Development, Mississippi Dept. of Environmental Quality.

Kappel, W.D., Hultstrand, D.M., Steinhilber, K., and J.T. Rodel, 2020: Climate Change and PMP: Are These Storms Changing? *Journal of Dam Safety*, Vol. 17, No. 3.

Kappel, W.D., Hultstrand, D.M., Muhlestein, G.A., Rodel, J.T., and. Steinhilber, K., November 2020: Site-Specific Probable Maximum Precipitation for the Mongaup System, New York. Prepared for Eagle Creek Renewable Energy.

Kappel, W.D., Hultstrand, D.M., Rodel, J.T., Muhlestein, G.A., and Steinhilber, K., June 2021: Statewide Probable Maximum Precipitation for North Dakota. Prepared for the North Dakota State Water Commission.

Kappel, W.D., Hultstrand, D.M., Rodel, J.T., Muhlestein, G.A., Venticinque, M, and Steinhilber, K., January 2022: Site-specific Probable Maximum Precipitation for the Lower Nelson River Basin, Manitoba, Canada. Prepared for Manitoba Hydro under subcontract to Hatch.

Kappel, W.D., Hultstrand, D.M., Rodel, J.T., Muhlestein, G.A., Venticinque, M, and Steinhilber, K., February 2022: Site-specific Probable Maximum Precipitation for the Loch Dornie Basin, North Carolina. Prepared for Grandfather Golf and Country Club under subcontract to Hazen and Sawyer.

Kappel, W.D., Hultstrand, D.M., Rodel, J.T., Muhlestein, G.A., Venticinque, M, and Steinhilber, K., March 2022: Site-specific Probable Maximum Precipitation for Faro Mine, Yukon Territory. Prepared for SRK.

Kappel, W.D. and Hultstrand, D.M., April 2022: Annual Exceedance Probability and Meteorological Evaluation and Climate Change Review for Solitude and Russell Gulch Mines, Arizona. Prepared for KCB and BHP.

Kappel, W.D., Hultstrand, D.M., Rodel, J.T., Muhlestein, G.A., Venticinque, M, and Steinhilber, K., August 2022: Site-specific Probable Maximum Precipitation for Seine River basin, Ontario, Canada. Prepared for Brookfield.

Kappel, W.D., Rodel, J., and Hultstrand, D.M., October 2022: Probable Maximum Precipitation, Annual Exceedance Probability and Meteorological Evaluation for the Lake Bronson Dam basin, MN. Prepared for BARR Engineering.

Kappel, W.D., Hultstrand, D.M., Rodel, J.T., Muhlestein, G.A., Venticinque, M, and Steinhilber, K., October 2022: Site-specific Probable Maximum Precipitation for Montreal, Magpie, Michipicoten, and Mississagi basins, Ontario, Canada. Prepared for Brookfield.

Kappel, W.D., Hultstrand, D.M., Rodel, J.T., Muhlestein, G.A., Venticinque, M, and Steinhilber, K., October 2022: Site-specific Probable Maximum Precipitation, Annual Exceedance Probability, and Climate Change Assessment for Kings Mountain, North Carolina. Prepared for SRK.

Kappel, W.D., Hultstrand, D.M., Muhlestein, G.A., Venticinque, M, Rodel, J.T., and Steinhilber, K., December 2022: Site-specific Probable Maximum Precipitation, Meteorological Characterization, and Climate Change Assessment for the KSM Mine Complex, British Columbia. Prepared for Seabridge Gold.

Kappel W.D., February 2023: How Much Rainfall Must a Dam Withstand?, *Hydro Leader*, Vol. 4, Issue 2, 24-27.

Kappel, W.D., Rodel, J.T., Hultstrand, D.M., Muhlestein, G.A., Venticinque, M., and Steinhilber, K., June 2023: Site-Specific Probable Maximum Precipitation for the Avonlea Dam Basin. Prepared for Water Security Agency in partnership with Hatch.

Kappel, W.D., Rodel, J.T., Hultstrand, D.M., Muhlestein, G.A., Venticinque, M., and Steinhilber, K., June 2023: Site-Specific Probable Maximum Precipitation for the Junction Dam Basin. Prepared for Water Security Agency in partnership with Hatch.

Kappel, W.D, Hultstrand, D.M., Rodel, J.T., Muhlestein, G.A., Venticinque, M, Cheke, D., and Steinhilber, K., July 2023: Statewide Probable Maximum Precipitation for New Jersey. Prepared for the New Jersey Dept. of Environmental Protection Dam Safety.

Kappel, W.D., Hultstrand, D.M., Muhlestein, G.A., Venticinque, M, Rodel, J.T., K., Steinhilber, and Cheke, D., December 2023: Site-specific Probable Maximum Precipitation, Meteorological Characterization, and Climate Change Assessment for the Nechako Mine Complex, British Columbia. Prepared for KCB and Rio Tinto.Keim, B. D., 1998: Record Precipitation Totals from the Coastal New England Rainstorm of 20-21 October 1996, *Bull. Amer. Meteo. Soc.*, **79**, 1061-1067.

Keim, B.D., R.A. Muller, and G.W. Stone, 2007: Spatiotemporal Patterns and Return Periods of Tropical Storm and Hurricane Strikes from Texas to Maine. *J. Climate*, **20**, 3498–3509.

Keim, B.D., Kappel W.D., Muhlestein, G.A, Hultstrand, D.M., Parzybok, T.W., Lewis, A.B., Tomlinson, E.M., and A.W., Black, October 2018: Assessment of the Extreme Rainfall Event at Nashville, TN and the Surrounding Region on May 1-3, 2010, *Journal of the American Water Resources Associates*, Vol. 54, No. 5, 1001-1010.

Kent, E.C, Woodruff, S. D., and D. I. Berry, 2007: Metadata from WMO Publication No. 47 and an Assessment of Voluntary Observing Ship Observation Heights in ICOADS. *J. Atmos and Ocean Tech.*, **24(2)**, 214-234.

Konrad, C.E., 2001: The Most Extreme Precipitation Events over the Eastern United States from 1950 to 1996: Considerations of Scale. *J. Hydrometeor.*, **2**, 309–325.

Kunkel, K.E., T.R. Karl, D.R. Easterling, K. Redmond, J. Young, X. Yin, and Hennon, P., 2013: Probable Maximum Precipitation and Climate Change*, Geophys. Res. Lett.*, **40**, 1402-1408.

Kunkel, K.E., T.R. Karl, H. Brooks, J. Kossin, J.H. Lawrimore, D. Arndt, L. Bosart, D. Changnon, S.L. Cutter, N. Doesken, K. Emanuel, P.Y. Groisman, R.W. Katz, T. Knutson, J. O'Brien, C.J. Paciorek, T.C. Peterson, K. Redmond, D. Robinson, J. Trapp, R. Vose, S. Weaver, M. Wehner, K. Wolter, and D. Wuebbles, 2013: Monitoring and Understanding Trends in Extreme Storms: State of Knowledge. *Bull. Amer. Meteor. Soc.,* **94**, 499–514.

Kunkel, K. E., and Champion, S. M., 2019: An assessment of rainfall from Hurricanes Harvey and Florence relative to other extremely wet storms in the United States. *Geophysical Research Letters*, 46, 13500– 13506. https://doi.org/10.1029/2019GL085034.

Letkewicz, C.E., M.D. Parker, 2010: Forecasting the Maintenance of Mesoscale Convective Systems Crossing the Appalachian Mountains. *Wea. Forecasting*, **25**, 1179–1195.

Mahoney, K., M. Alexander, J. D. Scott, and J. Barsugli, 2013: High-Resolution Downscaled Simulations of Warm-Season Extreme Precipitation Events in the Colorado Front Range under Past and Future Climates*. *J. Climate*, 26, 8671–8689.

Mahoney, K., 2016: Examining terrain elevation assumptions used in current extreme precipitation estimation practices: A modeling study of the 2013 Colorado Front Range floods. Amer. Meteor. Soc. 30th Conf. on Hydrology, January 2016, New Orleans, LA.

Mann, H.B., 1945: Nonparametric tests against trend, Econometric, 13, 245-259.

Martner, B.E, and V. Dubovskiy, 2005: Z-R Relations from Raindrop Disdrometers: Sensitivity to Regression Methods And DSD Data Refinements. 32nd Radar Meteorology Conference, Albuquerque, NM.

Masson-Delmotte, Valérie; Zhai, Panmao; Pirani, Anna; Connors, Sarah L.; Péan, Clotilde; Berger, Sophie; Caud, Nada; Chen, Yang; Goldfarb, Leah; Gomis, Melissa I.; Huang, Mengtian; Leitzell, Katherine; Lonnoy, Elisabeth; Matthews, J. B. Robin; Maycock, Tom K.; Waterfield, Tim; Yelekçi, Ozge; Yu, Rong; Zhou, Baiquan, eds., 2021: "Summary for Policymakers". Climate Change 2021: The Physical Science Basis. Contribution of Working Group I to the Sixth Assessment Report of the Intergovernmental Panel on Climate Change (PDF). IPCC / Cambridge University Press.

Miller, J.F., R.H. Frederick and R.S. Tracey, 1973: NOAA Atlas 2, Precipitation: Frequency Atlas of the Western United States. U.S. Dept. of Commerce, NOAA, National Weather Service, Washington DC.

Minty, L.J., Meighen, J. and Kennedy, M.R., 1996: Development of the Generalized Southeast Australia Method for Estimating Probable Maximum Precipitation, HRS Report No. 4, Hydrology Report Series, Bureau of Meteorology, Melbourne, Australia, August 1996.

National Climatic Data Center (NCDC). NCDC TD-3200 and TD-3206 datasets - Cooperative Summary of the Day

National Climatic Data Center (NCDC) Heavy Precipitation Page http://www.ncdc.noaa.gov/oa/climate/severeweather/rainfall.html#maps

National Oceanic and Atmospheric Association, Forecast Systems Laboratory FSL Hourly/Daily Rain Data, http://precip.fsl.noaa.gov/hourly_precip.html

Natural Resources Conservation Service (NRCS), Conservation Engineering Division. (2005, July). Earth Dams and Reservoirs, TR-60.

Ohara, N., Kavvas, M. L., Anderson, M. L., Chen, Z. Q., & Ishida, K., 2017: Characterization of extreme storm events using a numerical model based precipitation maximization procedure in Feather, Yuba, and American River watersheds in California. *Journal of Hydrometeorology*, *18*(5), 1413–1423.

Perica, S., Martin, D., Pavlovic, S., Roy, I., St. Laurent, M., Trypaluk, C., Unruh, D., Yetka, M., Bonnin, G., 2013: *NOAA Atlas 14 Volume 8 Version 2.0, Precipitation-Frequency Atlas of the United States, Midwestern States*. Tech. Rep., NOAA National Weather Service, Silver Spring, MD. http://hdsc.nws.noaa.gov/hdsc/pfds/

Perica, S. Martin, D., S. Pavlovic, I. Roy, C., Laurent, M.S., Trypaluk, D. Unruh, M. Yekta, and G. Bonnin, 2013: *NOAA Atlas 14 Volume 9 version 2, Precipitation-Frequency Atlas of the United States, Southeastern States* NOAA, National Weather Service, Silver Spring, MD.

Perica, S., Pavlovic, S., Laurent, M.S., Trypaluk, D. Unruh, Martin, D., and O. Wilhite, 2015: *NOAA Atlas 14 Volume 10 version 2, Precipitation-Frequency Atlas of the United States, Northeastern States,* NOAA, National Weather Service, Silver Spring, MD.

Pontrelli, M.D., Bryan, G., and J.M. Fritsch, 1999: The Madison County, Virginia, Flash Flood of 27 June 1995, *Weather and Forecasting.*, **14**, 384-404.

PRISM Mapping Methodology, http://www.ocs.oregonstate.edu/prism/index.phtml

Reynolds, R.W., T.M. Smith, C. Liu, D.B. Chelton, K.S. Casey, and M.G. Schlax, 2007: Daily High-resolution Blended Analysis for Sea Surface Temperature. *J. Climate.*, **20**, 5473-5496.

Riedel, J.T., Appleby, J.F., and R.W. Schloemer, 1956: Seasonal Variation of the Probable Maximum Precipitation East of the 105th Meridian for Areas from 10 to 1000 Square miles and Durations of 6, 12, 24, and 48 Hours, *Hydrometeorological Report 33*, US Department of Commerce, Weather Bureau, Washington, DC, 32pp.

Riedel, J.T., and L.C. Schreiner, 1980: Comparison of Generalized Estimates of Probable Maximum Precipitation with Greatest Observed Rainfalls, *NOAA Technical Report NWS 25*, US Department of Commerce, NOAA, Silver Spring, Md, 46 pp.

Robinson, D.A., I. Miyares, M. Pavlovskaya, G.A. Pope, 2001: Hurricane Floyd rainfall in New Jersey from the Hudson to the Hamptons: Snapshots of the New York Metropolitan Area.

Rolph, G., Stein, A., and Stunder, B., 2017: Real-time Environmental Applications and Display sYstem: READY. Environmental Modeling & Software, 95, 210-228.

Schaefer, M.G., B.L. Barker, G.H. Taylor and J.R. Wallis, 2006: *Regional Precipitation-Frequency Analysis and Spatial Mapping of Precipitation for 24-Hour and 2-Hour Durations in Eastern Washington*. Publication prepared for Washington State Department of Transportation, MGS Engineering Consultants.

Schreiner, L.C., and J.T. Riedel, 1978: Probable Maximum Precipitation Estimates, United States East of the 105th Meridian. Hydrometeorological Report No. 51, U.S. Department of Commerce, Silver Spring, Md, 242 pp.

Smith, J.A., M.L. Baeck, M. Steiner, and A.J. Miller, 1996: Catastrophic Rainfall from an Upslope Thunderstorm in the Central Appalachians: The Rapidan Storm of June 27, 1995. *Water Res. Research*, **32**, 3099-3113.

Smith, J. A., M. L. Baeck, G. Villarini, and W. F. Krajewski, 2010: The Hydrology and Hydrometeorology of Flooding in the Delaware River Basin. J. Hydrometeor, **11**, 841-859.

Smith, J A., Gabriele Villarini, and Mary Lynn Baeck, 2011: Mixture Distributions and the Hydroclimatology of Extreme Rainfall and Flooding in the Eastern United States. *J. Hydrometeor*, **12**, 294–309.

Smith, J A., M. L. Baeck, A.A., Ntelekos, G. Villarini, and M. Syeiner, 2011: Extreme Rainfall and Flooding from Orographic Thunderstorms in the Central Appalachians. *Water Res. Research*, **47**, W04514, 24pp.

Stein, A. F., R. R. Draxler, G. D. Rolph, B. J. B. Stunder, M. D. Cohen, and F. Ngan, 2015: NOAA's HYSPLIT Atmospheric Transport and Dispersion Modeling System. Bull. Amer. Meteor. Soc., 96, 2059–2077.

Thaler, J.S., 1996: *Catskill Weather*, Purple Mountain Press, Ltd., Fleischmanns, NY, 167 pp.

Thrasher, B., Wang, W., Michaelis, A. Nemani, R., 2021: NEX-GDDP-CMIP6. NASA Center for Climate Simulation, doi:10.7917/OFSG3345.

Thrasher, B., Wang, W., Michaelis, A., Melton, F., Lee, T., Nemani, R., 2022. NASA Global Daily Downscaled Projections, CMIP6. Nature Scientific Data

Tomlinson, E.M., 1993: Probable Maximum Precipitation Study for Michigan and Wisconsin, Electric Power Research Institute, Palo Alto, CA, TR-101554, V1.

Tomlinson, E.M., Kappel W.D., and Muhlestein, G.A., August 2007: Reevaluation of the Smethport, PA July 1942 Rainfall, Prepared for the St. Mary's Water Authority

Tomlinson, E.M., Kappel W.D., and Parzybok, T.W., February 2008: Site-Specific Probable Maximum Precipitation (PMP) Study for the Magma FRS Drainage Basin, Prepared for AMEC, Tucson, Arizona.

Tomlinson, E.M., Kappel W.D., Parzybok, T.W., Hultstrand, D., Muhlestein, G., and P. Sutter, December 2008: Statewide Probable Maximum Precipitation (PMP) Study for the state of Nebraska, Prepared for Nebraska Dam Safety, Omaha, Nebraska.

Tomlinson, E.M., Kappel, W.D., and Parzybok, T.W., February 2011: Site-Specific Probable Maximum Precipitation (PMP) Study for the Magma FRS Drainage Basin, Arizona.

Tomlinson, E.M., Kappel, W.D., and Parzybok, T.W., March 2011: Site-Specific Probable Maximum Precipitation (PMP) Study for the Tarrant Regional Water District, Texas.

Tomlinson, E.M., Kappel, W.D., Hultstrand, D.M., Muhlestein, G.A., S. Lovisone, and Parzybok, T.W., March 2013: Statewide Probable Maximum Precipitation (PMP) Study for Ohio.

U.S. Navy Marine Climate Atlas of the World (NAVAIR50-1C-65), 1981: Volume IX, Naval Oceanographic Command Detachment, Asheville, NC.

U.S. Weather Bureau, 1946: Manual for Depth-Area-Duration analysis of storm precipitation. *Cooperative Studies Technical Paper No. 1*, U.S. Department of Commerce, Weather Bureau, Washington, D.C., 73pp.

U.S. Weather Bureau, 1951: Tables of Precipitable Water and Other Factors for a Saturated Pseudo-Adiabatic Atmosphere. *Technical Paper No. 14*, U.S. Department of Commerce, Weather Bureau, Washington, D.C., 27 pp.

U.S. Weather Bureau, 1952: *Maximum 24-Hour Precipitation in the United States*. Technical Paper No. 16, U.S. Department of Commerce, Hydro-meteorological Section.

Weather Bureau, 1940: Maximum Possible Precipitation Over The Ompompasoosuc Basin Above Union Village, Vermont, A Study of Meteorological Causes of Record Storms and Quantitative Estimates of Critical Precipitation Rates, Hydrometeorological Report 1, pp205.

Weather Underground, http://www.wunderground.com/stationmaps/

Weiss, L.L., 1964: Ratio of True to Fixed Interval Maximum Rainfall, Journal Hydraulics, ASCE, 90(HY1), pp77-82.

World Meteorological Organization, 1986: Manual for Estimation of Probable Maximum Precipitation, Operational Hydrology Report No 1, 2nd Edition, WMO, Geneva, 269 pp.

World Meteorological Organization, 2009: Manual for Estimation of Probable Maximum Precipitation, Operational Hydrology Report No 1045, WMO, Geneva, 259 pp.

Worley, S.J., S.D. Woodruff, R.W. Reynolds, S.J. Lubker, and N. Lott, 2005: ICOADS Release 2.1 data and products. *Int. J. Climatol. (CLIMAR-II Special Issue)*, **25**, 823-842.

Young, B.C and B.M. McEnroe, 2003: Sampling Adjustment Factors for Rainfall Recorded at Fixed Time Intervals. Journal of Hydrologic Engineering, Vol8 (5).

Zehr, R.M. and V.A. Myers, 1984: NOAA Technical Memorandum NWS Hydro 40, *Depth-Area Ratios in the Semi-Arid Southwest United States*, Silver Spring, MD 55pp.